



Minute-Scale Wind Forecasting Using Lidar Inflow Measurements

Simon, Elliot

Link to article, DOI:
[10.11581/dtu:00000054](https://doi.org/10.11581/dtu:00000054)

Publication date:
2019

Document Version
Publisher's PDF, also known as Version of record

[Link back to DTU Orbit](#)

Citation (APA):
Simon, E. (2019). Minute-Scale Wind Forecasting Using Lidar Inflow Measurements. DTU Wind Energy. <https://doi.org/10.11581/dtu:00000054>

General rights

Copyright and moral rights for the publications made accessible in the public portal are retained by the authors and/or other copyright owners and it is a condition of accessing publications that users recognise and abide by the legal requirements associated with these rights.

- Users may download and print one copy of any publication from the public portal for the purpose of private study or research.
- You may not further distribute the material or use it for any profit-making activity or commercial gain
- You may freely distribute the URL identifying the publication in the public portal

If you believe that this document breaches copyright please contact us providing details, and we will remove access to the work immediately and investigate your claim.

Minute-Scale Wind Forecasting Using Lidar Inflow Measurements



Elliot Irving Simon

Technical University of Denmark
Risø Campus
March 2019

DOI:10.11581/dtu:00000054

PhD Student

Elliot Irving Simon
Department of Wind Energy
Meteorology and Remote Sensing Section (MES)
ellsim@dtu.dk

Supervisors

Michael Stephen Courtney, PhD
Senior Scientist, Department of Wind Energy
Test and Measurements Section (TEM)
mike@dtu.dk

Nicolaos Antonio Cutululis, PhD
Professor, Department of Wind Energy
Integration and Planning Section (INP)
niac@dtu.dk

Examiners

Rozenn Cecilie Pol Marie Wagner Fertil, PhD
Senior Scientist, Department of Wind Energy
Meteorology and Remote Sensing Section (MES)
rozn@dtu.dk

Lars Landberg, PhD
Director of Renewables: Strategic Research and Innovation, DNV GL
lars.landberg@dnvgl.com

Hannele Kristiina Holttinen, PhD
Docent, Aalto University and Senior Advisor, Recognis Ltd.
hannele.holttinen@recognis.fi

Technical University of Denmark**DTU Wind Energy****Department of Wind Energy**

DTU Risø Campus
Frederiksborgvej 399
4000 Roskilde, Denmark
www.vindenergi.dtu.dk

Summary

A key obstacle to the large scale adoption of wind power is the high variability of energy production caused by weather systems and the turbulent atmosphere. Forecast errors contribute a significant source of uncertainty for power system planning and operation when large shares of renewables constitute the supply mix. To address these issues, horizons for economic dispatch and financial settlement are being shortened from hourly to minute-scale operations across a growing number of markets.

Three key uses of wind forecasts on the minute scale include: Trading in intrahour wholesale electricity markets, supporting and managing grid balance actions, and collective wind farm control.

Wind and power forecasts on these very-short timescales are typically obtained by inferring patterns from past data (time series modelling) or by assuming unchanging conditions from the latest available measurements (persistence). Yet, these methods inevitably fail to perform under changing conditions where accurate forecasts are most needed.

Remote sensing instruments such as long-range pulsed Doppler lidars are able to measure the wind several kilometers away with high spatial and temporal resolution. By directing the lidar to measure upstream (inflow), preview information about wind patterns and structures which advect to some degree towards the site is gathered in real time. This information can be used together with models to generate site specific wind and power forecasts, either through the classification of anomalous events or in a regression approach which produces deterministic or probabilistic predictions.

To explore these possibilities, a series of experimental field campaigns have been conducted during the PhD project which build upon each other to provide high quality reference datasets used for model formulation and testing. Scanning lidar observations have been used to examine space-time correlations as a function of distance upstream. The results indicate a strong relationship particularly within the first 3 km upwind of the reference position which corresponds to an optimal forecasting window of up to 5-minutes ahead. Gains beyond this lead time have also been shown, which can be attributed to the effectively reduced forecast horizon as a function of distance ahead.

Three forecast methods have been implemented which range in complexity from simple time-of-flight shifting of reconstructed horizontal wind speeds, to a linear propagation

model which uses wind direction aligned wind speeds, to a machine learning computer vision approach which uses 2-D lidar scans in a convolutional LSTM neural network. In each case, the lidar based prediction models are able to fulfill the constraints of real time use, and are evaluated against common benchmarks and reflected upon.

Specific incidents captured during the experiments including wind ramps and the arrival of a weather front have also been examined to determine the ability of the lidar to detect and track their arrival to the site.

Overall conclusions of the PhD project are that forward looking lidar observations are useful in this context, particularly for detecting large scale events where the precise timing and location is not reliably captured by numerical weather prediction (NWP) models. Endeavors to produce multi-step time series forecasts and evaluate them statistically have been successful, especially compared with the persistence method. However the added value of these approaches remains ambiguous. Time series modelling techniques like ARIMA generally perform well, and the complexity and expense of installing and maintaining additional instrumentation may not prove to be cost effective. If these modest gains can be linked to significant economic impacts and users are able to capitalize on marginal improvements in the forecast accuracy, then an operational realization following the guidelines laid out in this thesis should be considered.

Dansk sammendrag

En væsentlig hindring for udbredelsen af vindkraft i stor skala er at der optræder store variationer i energiproduktion gennem tid grundet vekslende vejrsystemer og turbulens i atmosfæren. Fejl i vindprognoser udgør en væsentlig kilde til usikkerhed ved planlægning og drift af el systemet, især når de vedvarende energikilder udgør en stor del af forsyningen. For at løse dette problem er der i et stigende antal forsyningsmarkeder blevet ændret på tidsintervallet mellem el handelen og el leverancen. Tidsintervallet er blevet ændret fra timer til minutter.

Vindprognoserne på minutbasis anvendes i tre sammenhænge: Handel inden for en time på el markedet; styring af balancen i el systemet; og styring af en hel møllepark.

Vind- og elkraft-prognoser på disse meget korte tidsskalaer opnås typisk ved at anvende mønstre fra tidligere data (tidsserie-modellering) eller ved at antage uændrede forhold fra de seneste tilgængelige målinger (persistens). Begge metoder vil under vekslende vindforhold give unøjagtige prognoser, og netop på de tidspunkter kan prognoser være særligt betydningsfulde for planlægning og drift af el systemet.

Fjernmålings-instrumentet Doppler vind lidar kan måle vinden flere kilometer væk og give observationer med høj rumlig og tidsmæssig opløsning. Når lidaren måler op mod vinden i vindretningen vil de vindmønstre og strukturer som bevæges (advekteres) hen mod instrumentet blive indsamlet i realtid. Målingerne kan sammen med atmosfæriske modeller bruges til at generere stedspecifik vind- og elkraft-prognoser. Det kan udføres enten ved klassificering af uregelmæssige hændelser eller ved en regressionsmetode, der frembringer deterministiske eller statistiske forudsigelser.

For at udforske disse forskellige muligheder er der blevet gennemført en række eksperimentelle kampagner i løbet af ph.d.-projektet. Disse er udført i en sekvens, som har givet et referencedatasæt af høj kvalitet til anvendelse ved modelformulering og til testning. Mere specifikt er scanning vind lidar observationer blevet anvendt til at undersøge korrelationer i tid og rum som en funktion af afstanden opstrøms. Resultaterne viser meget høj korrelation især inden for de første 3 km opstrøms for instrumentet. Det svarer til at der findes et optimalt prognosevindue på op til 5 minutter. Der er også mulighed for at observere og forudsige vinden længere væk hvilket giver en længere tidshorisont for prognosen.

De tre prognosemetoder, som er blevet implementeret, inkluderer en relativ simpel

metode hvor vinden antages at bevæge sig med samme hastighed som den af lidaren målte horisontale vindhastighed; en lineær udbredelsesmodel, der bruger vindretningen og vindhastigheder som input; og en avanceret metode med machine learning computer vision, der anvender 2-D lidar-scanninger i et Long Short-Term Memory (LSTM) neuralt netværk. Alle tre lidar-baserede metoder opfylder kravene til at give en prognose, som kan anvendes i realtid. De er alle sammenlignet med en fælles benchmark.

Specielle vindforhold observeret under eksperimenterne såsom pludselige store ændringer i vindhastighed (ramps) og passage af vejrfroter er undersøgt nøje for at afklare vind lidarens evne til at opdage og spore disse specielle vindforhold og deres ankomst til målested.

Den overordnede konklusion af ph.d.-projektet er at vind lidar målinger er nyttige i forhold til at lave vind- og elkraft prognoser med. Det er især stor-skala vejrhendelser, som kan måles præcist i tid og sted, og hvor de numeriske modeller, der anvendes til vejrudsigter, ikke forudsiger vinden præcist. Forskningen har indeholdt flertrins tidsserier prognoser og disse er med gode resultater sammenlignet statistisk med persistens-metoden. Dog er fordelene af flertrins tidsserie prognoser tvetydige. Tidsserie modelleringsteknikker som ARIMA giver generelt gode resultater. Men kompleksiteten og omkostningerne ved at installere og vedligeholde supplerende instrumentering er muligvis ikke en fordel økonomisk set. I de tilfælde hvor der kan være en økonomisk gevinst ved at gøre brugerne i stand til at udnytte marginale forbedringer i prognosens nøjagtighed, så kan det overvejes at realisere korttids-prognoser med lidar-baseret måling efter de tekniske retningslinjer, som er beskrevet i denne afhandling.

Preface

This PhD thesis was prepared over a three year period at the Risø campus of the Department of Wind Energy at the Technical University of Denmark partially in fulfillment of the requirements for granting a PhD degree. Funding was provided through a departmental fellowship grant. An academic exchange to the École Polytechnique Fédérale de Lausanne (EPFL) in physics and energy systems took place in 2017. An external stay hosted in the Research Applications Laboratory (RAL) at the National Center for Atmospheric Research (NCAR) in Boulder, Colorado was conducted in 2018, focusing on artificial intelligence and computer vision methods.

DTU Wind Energy, Risø Campus

March 24, 2019

A handwritten signature in black ink, consisting of a stylized 'E' followed by a series of loops and a final flourish.

Elliot Irving Simon

Thesis outline and list of publications

This thesis consists of an introductory synopsis providing context for the work undertaken, a collaborative review paper of the state of the art in the field and two results papers which form the basis for the novel discoveries made during the PhD project. The papers are connected by various supporting chapters, addendums and case studies. In the end, a discussion and outlook chapter reflects on the key findings and recommends a practical approach for future work in the field. Following this, overall conclusions of the thesis are reiterated.

The following three articles are included, with permission from the copyright holders where applicable.

1. Würth, I., Valdecabres, L., **Simon, E.**, Möhrle, C., Uzunoğlu, B., Gilbert, C., Giebel, G., Schlipf, D., and Kaifel, A.: Minute-Scale Forecasting of Wind Power - Results from the collaborative workshop of IEA Wind Task 32 and 36, *Energies*, published, 2019.
2. **Simon, E.**, Courtney, M., and Vasiljevic, N.: Minute-Scale Wind Speed Forecasting Using Scanning Lidar Inflow Measurements, draft in preparation for submission, 2018.
3. **Simon, E.** and Courtney, M.: Minute-Scale Wind Vector Forecasting Using Scanning Lidar Inputs to a Convolutional LSTM Neural Network, draft in preparation for submission, 2019.

Other publications produced during the PhD period but outside the scope of this thesis are not considered.

Acknowledgements

Carrying out this PhD work has been both challenging and rewarding, and I have grown throughout it- both professionally and personally. This achievement would not have been possible without the immense amount of guidance and support I have received along the way. Firstly I would like to recognize my supervisor Mike, who has provided me with an outstanding level of encouragement complemented with productive mentorship of the highest standard. Similarly my co-supervisor Nikos for our many fruitful discussions, and for his services as PhD coordinator. My section leaders Hans and Poul, who have given me freedom and opportunity to pursue new ideas and for including me on equal terms within the institute. And all of my colleagues at DTU Wind Energy who I have exchanged ideas with and in many cases befriended. Working alongside fellow PhD students Tobias, Jonas, Pedro and Dominique has been especially gratifying in that regard. My hosts Sue and David-John and all the wonderful people I met during my stay at NCAR have also been extremely helpful and made my time in Boulder a real highlight. It was also a pleasure teaching together with Pierre in the Renewables in Electricity Markets course, and collaborating with the WFCT and WISDOM project partners. Further, I have greatly enjoyed the many conferences I attended, and would like to thank both the organizers and attendees I have interacted with for their valuable feedback.

The experimental component of this project has been greatly aided through the actions of a number of colleagues. I would like to sincerely thank Guillaume for everything he has taught me about how to design, build, and repair lidar systems, and for his invaluable assistance with the field campaigns. Likewise Nikola who has helped immensely in developing my knowledge and experience in the science of measurements. The technical staff at DTU have been an invaluable resource, and I would like to express my appreciation to Per, Steen and Hector. The coding and data analysis portion has heavily relied upon open-source software, and sincere thanks are due to all the contributing developers for their time and effort.

Funding for this PhD project has been generously provided by the department through the Danish taxpayers and industry partners. The Otto Mønsted Fund has also kindly financed a portion of the external research stay costs. I would also like to thank those who have had direct contributions to this thesis. Antoine for sharing his L^AT_EX template, Charlotte for translating the Danish summary, and the examination committee (Rozenn, Lars, and Hannele) for reading and evaluating this body of work.

Last but certainly not least, my eternal appreciation goes to my extraordinary family who have given me unbounded love and support and encouraged my drive to learn and experience the world.

Quote

“Of all the forces of nature, I should think the wind contains the largest amount of motive power- that is, power to move things. Take any given space of the earth’s surface- for instance, Illinois and all the power exerted by all the men, and beasts, and running-water, and steam, over and upon it, shall not equal the one hundredth part of what is exerted by the blowing of the wind over and upon the same space. And yet it has not, so far in the world’s history, become proportionably valuable as a motive power. It is applied extensively, and advantageously, to sail-vessels in navigation. Add to this a few wind-mills, and pumps, and you have about all. That, as yet, no very successful mode of controlling, and directing the wind, has been discovered; and that, naturally, it moves by fits and starts- now so gently as to scarcely stir a leaf, and now so roughly as to level a forest- doubtless have been the insurmountable difficulties. As yet, the wind is an untamed, and unharnessed force; and quite possibly one of the greatest discoveries hereafter to be made will be the taming and harnessing of the wind. That the difficulties of controlling this power are very great is quite evident by the fact that they have already been perceived, and struggled with more than three thousand years; for that power was applied to sail-vessels, at least as early as the time of the prophet Isaiah.”

Abraham Lincoln, Second Lecture on Discoveries and Inventions (1858)

Objectives of the PhD project

The following specific objectives were designed to encompass the overall goals of the PhD project. Each theme is incorporated in the thesis text and again addressed in the final conclusions (Section 5).

- Explore and document potential applications of minute-scale forecasts for wind energy
- Interface with forecast users and providers to survey existing practices and encourage community dialogue
- Perform field experiments to obtain observational data needed to build and evaluate remote sensing based forecast models
- Implement and test novel forecast methods using lidar observations which adhere to the constraints of real-time usage
- Benchmark the lidar forecast method's skill to other commonly used methods
- Reflect on the potential benefits and drawbacks of a real-world fulfillment of such a system

Table of Abbreviations

θ	Azimuth angle
ϕ	Elevation angle
ψ	Wind direction
ABL	Atmospheric boundary layer
AC	Alternating current
ACF	Autocorrelation function
AGL	Above ground level
AMSL	Above mean sea level
ANN	Artificial neural network
AR	Autoregressive
ARIMA	Autoregressive integrated moving average
ARMA	Autoregressive moving average
BA	Balancing authority
BRP	Balance responsible party
ConvLSTM	..	Convolutional long short-term memory
CNN	Convolutional neural network
CNR	Carrier to noise ratio
CW	Continuous-wave
DBS	Doppler beam swing
DTU	Technical University of Denmark
DWL	Doppler wind lidar
EPEX	European Power Exchange
FC	Fully connected
FIT	Feed in tariff
FWHM	Full width at half maximum

GPU	Graphics processing unit
Hz	Hertz
IEA	International Energy Agency
IQR	Interquartile range
ISO	Independent system operator
IVAP	Integrating velocity azimuth process
LCOE	Levelized cost of energy
LOS	Line of sight
LSTM	Long short-term memory
MA	Moving average
MAE	Mean absolute error
NEWA	New European Wind Atlas
NWP	Numerical weather prediction
OLS	Ordinary least squares
PACF	Partial autocorrelation function
PCA	Principal component analysis
PDF	Probability density function
PPA	Power purchase agreement
PPI	Plan position indicator
PSD	Power spectral density
R^2	Coefficient of determination
RBF	Radial basis function
RG	Range gate
RHI	Range height indicator
RMSE	Root mean square error
RNN	Recurrent neural network
RS	Remote sensing
s	Seconds
SCADA	Supervisory control and data acquisition
SDVR	Single Doppler velocity retrieval
SGDR	Stochastic gradient descent regression
SVR	Support vector regression
TSO	Transmission system operator

U	Scalar wind speed
u_r	Radial wind speed
u	Zonal (Easterly) horizontal wind component
USD	United States dollar
UTC	Coordinated universal time
v	Meridional (Northerly) horizontal wind component
VAD	Velocity azimuth display
VAR	Vector autoregressive
w	Vertical wind component
W	Watts
WRF	Weather research and forecasting
z	Height

Contents

Summary	i
Dansk sammendrag	iii
Preface	v
Thesis outline and list of publications	vi
Acknowledgements	vii
Quote	viii
Objectives of the PhD project	ix
Table of Abbreviations	x
Contents	xiii
1 Introduction	1
1.1 Energy generation from the wind	2
1.1.1 Motivation and global status	2
1.1.2 Intermittency of wind resource	4
1.1.2.1 Case study of wind turbine power variability	7
1.1.3 Wind farm control	10
1.1.4 Forecasting for wind energy	12
1.1.5 Power system and electricity markets	14
1.2 Remote sensing of winds	16
1.2.1 Doppler wind lidars	18
1.2.2 Measurement techniques	20
2 Minute-Scale Forecasting of Wind Power	22
2.1 Introduction and context	23
2.2 Results from the collaborative workshop of IEA Wind Task 32 and 36 . .	25
3 Experimental results	56
3.1 Structure of the results chapter	57
3.2 Initial investigation: WAFFLE experiment	58
3.3 Addendum: Key results and lessons learned	65

3.4	Introduction to second study: Østerild Balconies experiment	66
3.5	Minute-Scale Wind Speed Forecasting Using Scanning Lidar Inflow Measurements	67
3.6	Addendum 1: Case study of weather front event	102
3.7	Addendum 2: Key results and lessons learned	107
3.8	Introduction to third study: LASCAR experiment	108
3.9	Minute-Scale Wind Vector Forecasting Using Scanning Lidar Inputs to a Convolutional LSTM Neural Network	109
3.10	Addendum: Key results and lessons learned	138
4	Discussion and outlook	139
4.1	What remote sensing can be used for in the context of minute-scale wind forecasting	140
4.2	Recommended practical implementations	142
4.3	Opportunities for extension of work	145
5	Conclusions	146
A	Coauthor statements	151
	Bibliography for non-article texts	159

CHAPTER 1

Introduction

1.1 Energy generation from the wind

1.1.1 Motivation and global status

Global energy systems are currently undergoing a revolution. The production of electricity for household and industrial use has, until the recent past, relied almost entirely on non-renewable fuel sources including coal and petroleum derivatives which are burned to run steam turbine generators. A number of compelling motives exist which are precipitating change to the status quo.

The first motivation being the overwhelming scientific evidence of the impacts of large scale releases of air pollutants into the environment. Particulates have been closely linked to lung (Hamra et al., 2014) and heart disorders (Du et al., 2016). Carbon dioxide, a greenhouse gas, is also released through the combustion process and acts to increase the Earth's surface temperature through radiative forcing (Charlson et al., 1992), as well as acidify water bodies through the formation of carbonic acid and harming marine life (Doney et al., 2009). Other pollutants including sulfur oxides and nitrogen oxides contribute to smog and acid rain, and are similarly linked to acute health effects (Brunekreef and Holgate, 2002).

Realizing the urgency of these environmental concerns, authorities across the world have begun to enact agreements to curb their emissions contributions. These pacts can range from city and regional planning regulations, to national legislation and international treaties. Examples include the United Nations Kyoto Protocol and Paris Climate Agreement, European Commission's Clean Energy for all Europeans Framework (European Commission, 2019), China's Renewable Portfolio Standard (Patel, 2018) and Denmark's Energy Strategy (Danmarks Klima- og Energiministeriet, 2011). In conjunction with improvements in energy efficiency, large impacts can be made by the exchange and supplementation of low-carbon, renewable based generation including wind and solar.

Beyond commitments to avoiding the negatives associated with hydrocarbon based fuels, new opportunities have emerged with the maturation specifically of the wind energy industry. Rapid cost decreases have been demonstrated through experience, competition, and scaling which have brought the levelized-cost-of-energy (LCOE) of onshore wind power within reach and in many areas below that of traditional power plants without the need for subsidies. The IRENA renewable cost database reveals a 2017 average global LCOE for onshore wind at 60 and offshore wind at 140 USD/MWh, with projections for further decreases in the coming years (IRENA, 2018). The 2019 tender for Saudi Arabia's first installation, the 400 MW Dumat Al Jandal wind farm, resulted in a record power purchase agreement (PPA) of 21.3 USD/MWh (Masdar, 2019).

A final rationale for embracing renewable energy development in many areas is the opportunity for leveraging locally available resources instead of relying on imported fuels from territories which are often rife with geopolitical conflicts. Ensuring security of supply for the local population through greater self-sufficiency can lead to more a

balanced hegemony in regional and global politics.

While wind power only supplies about 4% of global electricity demand at present (14% in the European Union and 44% in Denmark), the aforementioned developments have resulted in a large and rapid expansion of planned and installed projects worldwide. Figure 1.1 presents a timeline of cumulative globally installed wind power, with the 2017 aggregate totalling over 539 GW. The growth rate is projected to remain near 10%, year on year (GWEC, 2017) with many large projects already approved and financed for construction in the coming years.

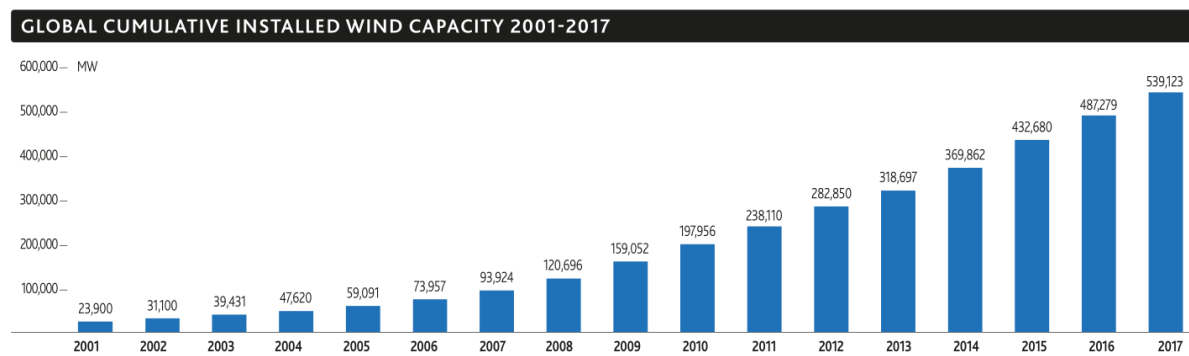


Figure 1.1: Cumulative worldwide installed wind power capacity from 2001-2017. The current value exceeding 539 GW. Source: GWEC, 2017.

1.1.2 Intermittency of wind resource

The reliable and efficient exploitation of wind power faces a unique set of challenges. Electrical energy produced by wind turbines is derived from the kinetic energy of the wind. Air flow generates a lift force on the blades causing them to rotate. This mechanical energy ultimately drives the generator, producing electricity which is collected and fed to the power grid. As the wind is not a controllable fuel source, the turbine's output will to a large extent be determined by atmospheric conditions.

Winds originate from differential heating of the Earth's surface and are transported by bulk motion. Within the boundary layer, they are largely influenced by the planet's surface (terrain and vegetation), human made obstacles, weather systems, and turbulent mixing.

Wind variability is defined as the fluctuations in energy content of the wind. These variations occur across a wide range of temporal and spatial scales. Contributions can include diurnal, seasonal, and interannual patterns, and physical processes including: gravity waves, cold fronts, storms, cellular convection, convective rolls, low level jets, and sea breezes (Vincent and Trombe, 2017). Combinations of these synoptic-, meso- and micro-scale influences lead to a high degree of intermittency in the wind, as shown in Figure 1.2 using measurements shown with a sampling rate of 1-second.

Because the amount of extractable power from the wind is proportional to the cube of the wind velocity, relatively small differences in wind conditions can result in large deviations in power output. Wind ramps, or large and sudden changes in a turbine or wind farm's output are notoriously difficult to forecast (both the scale and timing) and can cause (in the best case) energy to be wasted (through curtailment during up-ramps), or in the worst case system-level shortages (during down-ramps). To prevent these possible shortages during periods of expected variability, reserve wind power can be secured through down-regulation (curtailment) which is then available for activation through flexible dispatch mechanisms.

Power spectral density (PSD) plots illustrate the distribution of energies which contribute to the signal's variability, ordered by frequency. An example is shown in Figure 1.3 for wind speed and active power from a wind turbine using the same high-frequency dataset. This was obtained using Welch's method (Welch, 1967) with Hamming windowing to reduce noise in the spectra. The trends indicate that the variability decreases with decreasing time-scales in both cases.

Without system level storage, wind power variability is mostly addressed by spatial smoothing. Averaging occurs firstly on the turbine level, where the fastest (millisecond-second scale) fluctuations are to a large extent compensated for by the inertia and swept area averaging of the wind turbine's rotor. Although individual turbine outputs within a wind farm are strongly correlated, their collective power output is smoothed on the second-minute scale by the aggregation effect. Most substantially, entire wind farms

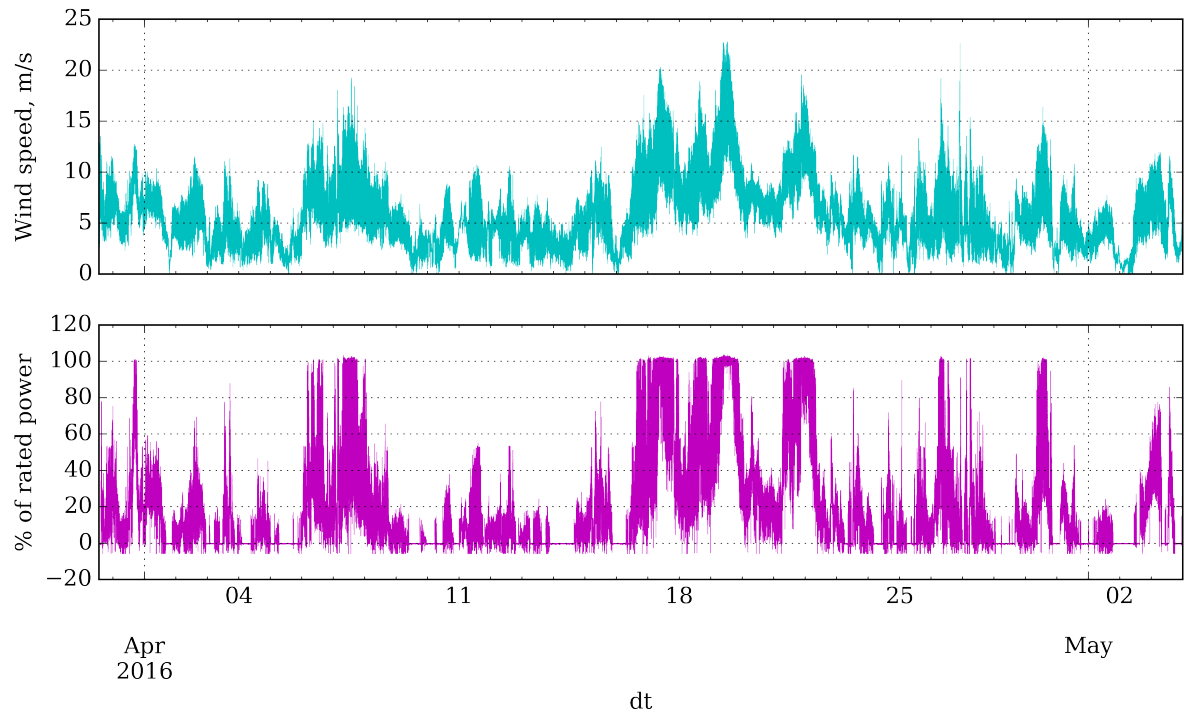


Figure 1.2: Time series example of wind speed (top) and wind power (bottom) variability from DTU's V52 research turbine.

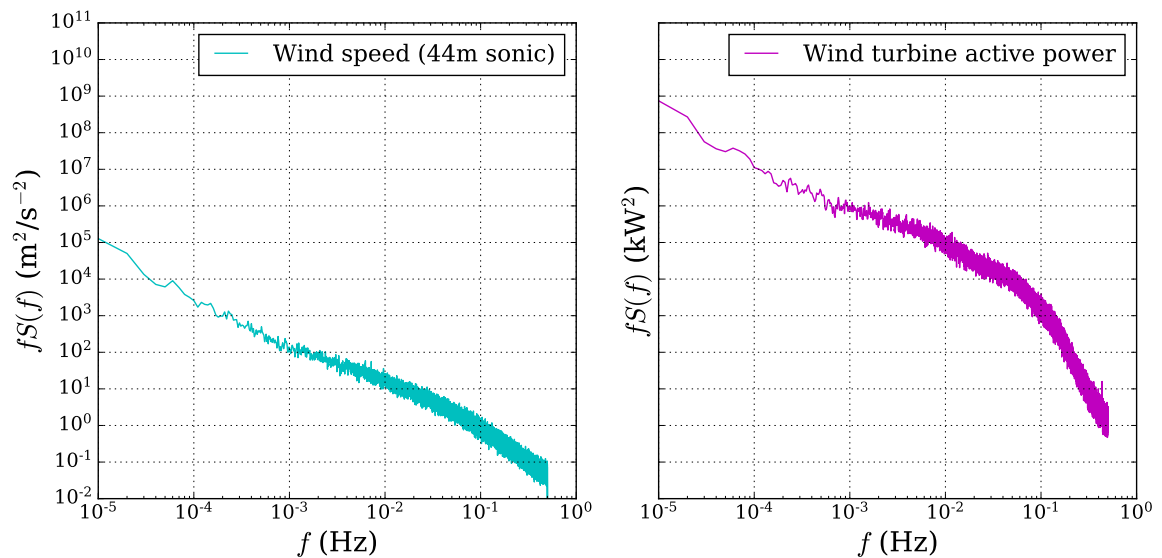


Figure 1.3: Power spectral density (PSD) of wind speed (left) and wind power (right) from DTU's V52 research turbine.

dispersed over large areas provide the largest impact towards reducing variability across all time scales due the low correlation of production between sites operating across different weather and geographic contexts.

An in-depth report on integrating large shares of wind generation into power systems is available in Holttinen et al., 2009, which provides further background and context for wind power variability in addition to relevant statistics and case studies.

1.1.2.1 Case study of wind turbine power variability

To further explore wind variability and its impact on power systems, a summary investigation was conducted to characterize changes in electrical power output from a real world wind turbine. The data consists of high-resolution SCADA measurements from DTU's Vestas V52 research turbine at Risø (DTU Wind Energy, 2019). This model is one of the most commonly sold turbines worldwide and has a rated capacity of 850 kW. The sourced data spans from March 30 to May 4th, 2016 (35 days) during a calibration period when the turbine's control systems were under normal operation and no aerodynamic modifications were present.

Measurements of the turbine's active power signal were down-sampled from 35 Hz to 1-second averages, and normalized with respect to rated power (where a value of 100 represents the generator's nameplate capacity). Note that it is possible to have both values below zero (during start up when drawing power from the grid) as well as values above 100 on the short term.

Statistics of absolute changes in the turbine's normalized power output within various time frames ranging from 1-second to 1-hour are presented in the following. Figure 1.4 presents a combined violin and boxplot across the selected time windows which illustrates statistical properties such as the shape and width of the distributions, quartile positions, median values, and spread of outliers. This is joined with Table 1.1 describing summary statistics.

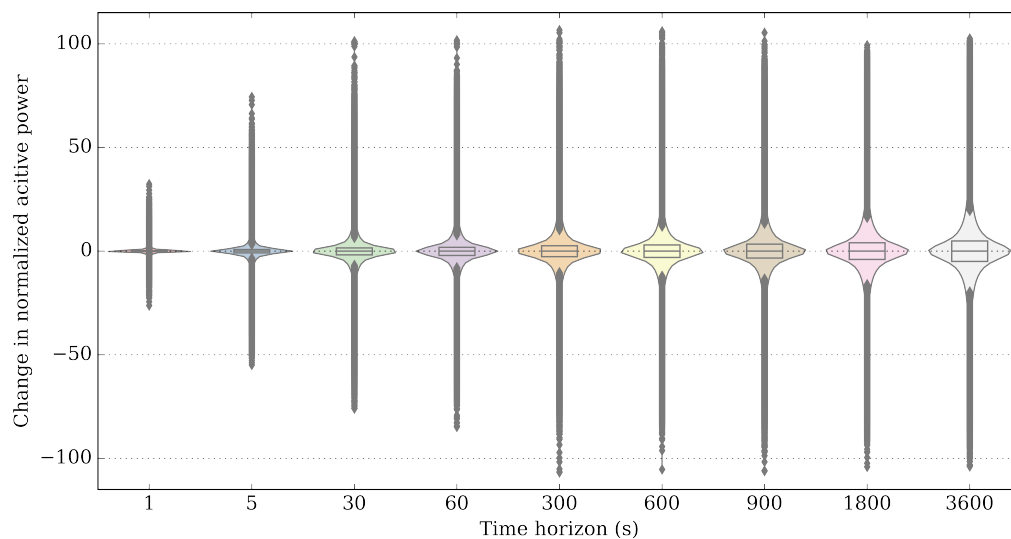


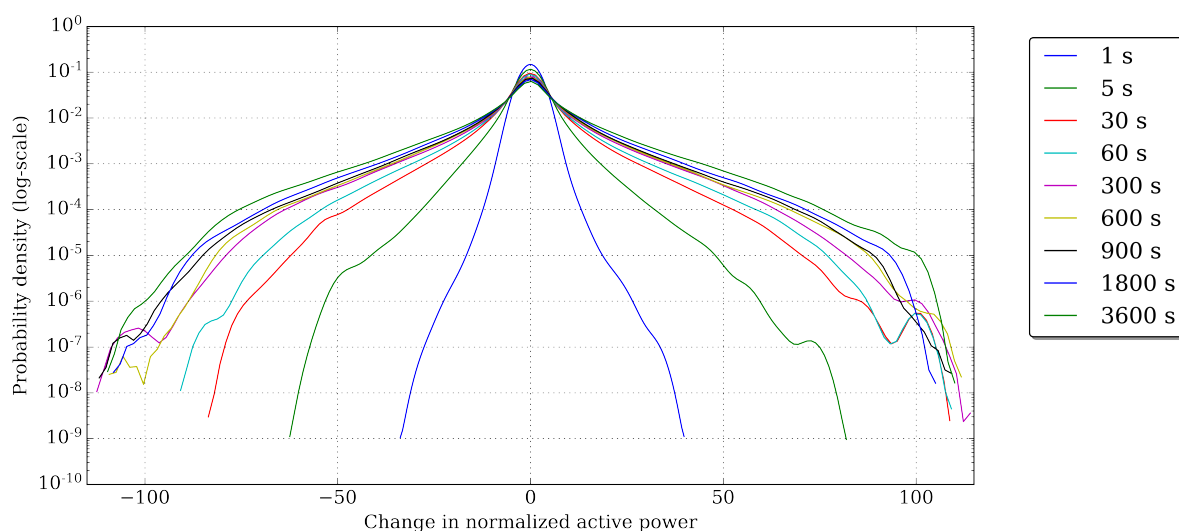
Figure 1.4: Combined violin and boxplot of normalized active power changes by various time windows from DTU's V52 research wind turbine.

Table 1.1: Table of statistics for V52 power output variability over selected time windows up to 1-hour.

	1 s	5 s	30 s	60 s	300 s	600 s	900 s	1800 s	3600 s
count	2976599	2976595	2976570	2976540	2976300	2976000	2975700	2974800	2973000
mean	0.000	0.000	0.000	0.000	0.002	0.003	0.004	0.008	0.009
std	1.209	4.387	8.133	9.536	11.362	11.976	12.532	13.674	15.485
min	-26.250	-54.907	-76.028	-84.816	-106.745	-105.303	-106.126	-104.044	-103.887
25%	-0.225	-0.888	-1.841	-2.103	-2.630	-3.075	-3.371	-4.049	-4.957
50%	0.000	0.000	0.000	0.000	0.000	0.000	0.000	0.000	0.000
75%	0.214	0.782	1.515	1.860	2.544	2.972	3.341	4.064	4.870
max	32.326	74.414	101.242	101.663	106.567	106.013	105.350	99.266	102.539

As expected, the variability grows with the length of the window. In all cases, the mean and median power output change is very close to zero and probability densities are symmetrical (normally distributed). On the very shortest timescales (1 and 5-seconds), the variations within the interquartile range (IQR) are small. However, from 30-seconds to 1-minute windows, the spread grows considerably. By the 5-minute case (300 s), the standard deviation approaches that of the longer timescales.

This is further shown in Figure 1.5, where the distributions are stacked atop each other for comparison (note the logarithmic y-axis scaling). Tail bumps present for certain time windows near the peripheries indicate periods of automatic start up (right tail) when the cut-in wind speed is reached and shut down (left tail) when the cut-out wind speed is exceeded.

**Figure 1.5:** Distribution of changes in normalized active power over various time horizons from DTU's V52 research wind turbine.

This simplified investigation has considered a single wind turbine and not collective wind farm output or otherwise geographically distributed generation which will act to some degree as a smoothing filter. Having said that, the case study has demonstrated that minute-scale variability of wind power is not insignificant and attention should also be focused on this timescale alongside the more commonly focused periods (e.g. 10-minutes and 1-hour).

1.1.3 Wind farm control

Utility scale wind power installations consist of multi-turbine arrangements known as wind farms. The layout is normally characterized by rows of turbines which affect each other through complex aerodynamic interactions. The most notable being wake induced power losses (through a reduction in the extractable energy of the wind by upstream turbines) and fatigue loading (by increased turbulence originating from the air-blade interaction of upstream turbines).

Modern wind turbines are designed with control systems which act to optimize their performance from an individual perspective. However, all together this greedy approach does not always result in the best coordination of the wind farm as a whole. The field of wind farm control aims to collectively optimize the power and loads of the entire wind farm in a collaborative manner by orchestrating control over each turbine's set-points. The overall objectives being to either maximize total active power or provide power control by following a reference signal, and to minimize fatigue loads (Knudsen, Bak, and Svenstrup, 2015). The two main mechanisms for dynamic wind farm control are induction control and wake steering.

Axial induction control reduces the velocity deficit of the downstream wake leading to larger amounts of recoverable energy available to downstream turbines. A wind turbine's power coefficient at its maximum operating point is much less sensitive to changes in pitch angle than its thrust coefficient (Annoni et al., 2016). Exploiting this relationship allows for small decreases in the upstream turbine's production to be more than made up for by increased production at the downstream turbines. This is accomplished by slightly pitching the rotor outwards (towards feathered position) and adjusting the generator torque which results in a decrease in the power and thrust coefficients and a reduction in the tip speed ratio. Normally this is performed by reducing the active power of the turbine (downrating), instead of manually interfacing with the turbine's pitch and torque set-points. P. M. O. Gebraad and Wingerden, 2015 establishes a 1.36% improvement in annual energy production (AEP) using dynamic induction control simulations at the Princess Amalia Wind Farm in the Netherlands. Induction control using static set-point optimization has demonstrated far less promise, with no net increase in wind farm efficiency during wind tunnel testing (Bartl and Sætran, 2016).

Wake steering is the intentional misalignment of an upstream turbine's rotor in order to redirect (steer) the wake away from downstream turbines. During normal operation, the turbine will orient its rotor perpendicularly to the wind direction. Applying wake redirection causes the turbine's yaw motor to re-orient itself to an angle relative to the wind direction (Fig. 1.6). This causes the wake to deflect away from downwind turbines, leading to a net increase in energy production for the overall wind farm. Positive yaw misalignment angles are normally used, as this results in a positive tilt angle which also directs the wake downwards. Simulations have indicated the potential for power gains using this approach while also avoiding significant load repercussions. The gains in AEP

are on the order of 5% through the reduction of wake losses (Knudsen, Bak, and Svenstrup, 2015, P. Gebraad et al., 2017). The concept has been successfully demonstrated in a recent field trial (Paul Fleming et al., 2017) which confirms the simulation estimates.

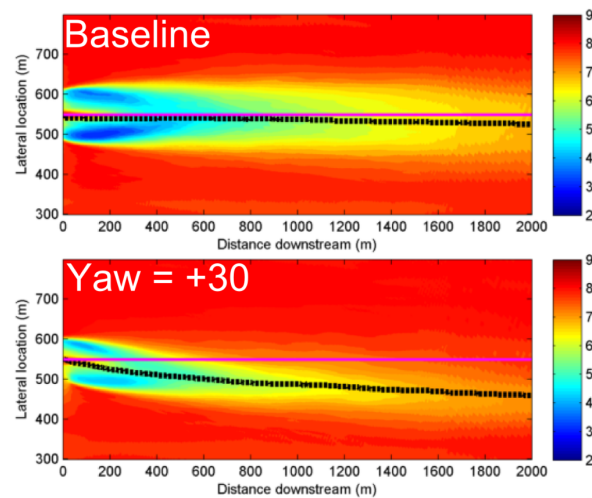


Figure 1.6: Comparison of the horizontal wake during normal operation (top panel) and under wake steering control (bottom panel, 30° yaw misalignment). The actual wake center-line is indicated in black, with the linear downstream reference in pink. Simulation using NREL’s SOWFA toolbox in OpenFOAM. Reproduced from: PA Fleming et al., 2014.

Wind farm control algorithms require estimates of the incoming wind speed and direction. These inputs are used in a wind farm flow model together with a delay factor to account for the wind field advection between turbine rows. The forecasts are applicable on the minute scale for preemptive optimization by the wind farm controller and for the individual turbines to adjust their configurations accordingly. Induction control is sensitive to accurate wind speed inputs, while wake steering is sensitive to accurate wind direction inputs. Improved forecast performance on this timescale therefore also enhances the benefits of dynamic wind farm control.

The field of individual turbine control (i.e. feed-forward and model predictive control) is largely irrelevant in the context of this project, as the timescales are in the order of seconds ahead where direct advection (frozen turbulence) models perform sufficiently well. There may be a case for individual turbine yaw control on the minute scale, however this is seen as a low priority application with limited relative benefits over existing solutions.

1.1.4 Forecasting for wind energy

The evolution of wind power together with advancements in computing and an improved understanding of atmospheric dynamics has established forecasting as a central element of operational research. An entire sub-industry is dedicated to developing and providing forecasting services to end users which include: wind farm owners and operators, power traders, asset managers, and transmission system operators (TSOs).

Wind prediction is conducted on a wide range of time scales, with lead times spanning from a few milliseconds up to one week or more. Prediction intervals can be described by a few broad categories, each with their own approaches and applications. Table 1.2 outlines the common forecast horizons relevant to wind energy and typical methods applied within them. Broad overviews of the field are also presented in Costa et al., 2008, Giebel et al., 2011 and Soman et al., 2010.

Forecasting techniques can be categorized into two fundamental classes- process driven physical models and data driven statistical approaches. Here general introductions are given for both. An extensive review is provided in Section 2.2.

Physical approaches such as numerical weather prediction (NWP) are based on well established physical and mathematical laws. Parameterizations of the atmosphere, where coarse input data (global or synoptic scale) is combined with mathematical modelling of atmospheric properties such as air, soil and sea temperature, pressure, land cover and surface obstacles to provide a local site forecast at varying temporal and spatial

Table 1.2: Overview of forecast intervals of interest for wind energy purposes.

Designation	Typical horizon	Example methods	Example applications
Immediate	Milliseconds to seconds	<ul style="list-style-type: none"> - Persistence - Wind field measurements using nacelle lidars [1] and/or upwind turbine SCADA [2] 	<ul style="list-style-type: none"> - Wind turbine control [1] - Grid regulation [3] (e.g. frequency, voltage support)
Very short-term (minute scale)	1-minute to 1-hour	<ul style="list-style-type: none"> - Persistence [4] - Statistical time series models [5] - Markov (regime switching) models [6] - Machine learning and artificial neural networks (ANN) [7,8] 	<ul style="list-style-type: none"> - Wind farm control - Ancillary services (e.g. reserve power) [2,9] - Intra-hour energy market trading [10] - Storage management (e.g. battery storage control)
Short-term	1 to 72 hours	<ul style="list-style-type: none"> - Statistical time series models [11,12] - Numerical weather prediction (e.g. WRF) [13] - Analogue ensemble prediction [13,14] - Kalman filter [11,15] 	<ul style="list-style-type: none"> - Intraday and day-ahead energy market trading [10] - Ancillary services - Storage management (e.g. battery, hydrogen and pumped storage control) [16] - Economic dispatch and generator planning - Operator portfolio management
Long-term	72 hours to 10 days or more	<ul style="list-style-type: none"> - Same as short term - Climatology 	<ul style="list-style-type: none"> - Reserve requirement decisions - Unit commitment decisions - Maintenance scheduling

References
<p>[1] D. Schlipf, D. J. Schlipf, and Kühn, 2012, [2] Göçmen, 2016, [3] Hansen, Altin, and Iov, 2016, [4] Hodge and Milligan, 2011, [5] Pierre Pinson, 2012, [6] Trombe, Pierre Pinson, and Madsen, 2012, [7] Potter and Negnevitsky, 2006, [8] Niu et al., 2018, [9] Mackenzie and Dyson, 2017, [10] Bathurst, Weatherill, and Strbac, 2002, [11] Liu, Tian, and Li, 2012, [12] Torres et al., 2005, [13] Mahoney et al., 2012, [14] Delle Monache et al., 2013, [15] Bossanyi, 1985, [16] Castronuovo et al., 2013</p>

resolutions. Optionally, through data assimilation the model states can be iteratively adjusted using real-time observations to adapt the simulation and correct for biases. These systems generally run on large supercomputers and require significant time and computational power to generate their forecasts. Further, they have not sufficiently demonstrated their ability to predict local microscale events that are of greatest relevance for real-time wind farm control. Therefore they are not considered appropriate in the context of minute-scale wind forecasting as they are ill-suited to be used operationally with today's computing technology.

Statistical approaches use empirical methods to model relationships between historical observations. The models are then used with real-time inputs to extrapolate future outcomes. Meteorological data is normally given as a time-series, where samples are highly correlated, non-independent and naturally ordered in time. The high temporal autocorrelation of wind measurements lends itself well to the simplest statistical approach called persistence. Persistence simply forecasts the future value of the series to be the same as the most recent observation, or a moving average of it. This method is widely used on horizons from the immediate to short-range, and is a common benchmark for evaluating more complex techniques. Autoregressive (AR) models are also appropriate, and are widely employed, often in conjunction with moving average (MA) models. In cases where the target signal is non-stationary, a number of transformation steps can be taken to impart stationarity (e.g. differencing, trend removal, seasonal and cyclical adjustments). Formulations which have demonstrated particularly adept skill are autoregressive integrated moving average (ARIMA) models. Further details on ARIMA modelling are given in Section 3.9. The flexibility of statistical approaches empower their suitability for minute-scale forecasting applications. This thesis work therefore exists within this research topic.

1.1.5 Power system and electricity markets

The vast majority of wind power installations are grid connected and offer the sale of their production through either long term power purchase agreements (PPA) or via wholesale electricity spot markets.

The modern electrical grid is a network of providers and consumers of electrical energy, interconnected via transmission and distribution lines used to transport supply from generation facilities to homes and businesses. Electrical appliances are designed to operate within a narrow range of the design frequency and voltage of the local AC power grid. Deviations can result in malfunctions or damage, or even in cascading failures as devices such as pumps, fans, motors, and power electronics drift from their intended output or stop functioning completely. For this reason, the supply and demand of electricity must be kept in constant balance. Variability occurring on both sides of the equation (load and generation) drives a need for accurate forecasts, which are used in system planning and generator dispatch. Deviations from the equilibrium between generation and consumption requires real-time adjustments, directed by the balancing authority (BA) through the activation of a suite of ancillary services to ensure stable frequency and voltage levels. Traditionally, wind power plants have not participated in these ancillary services. Grid codes are beginning to allow such involvement, for example tertiary regulation and deviation management in Spain (de la Fuente, 2016), and minute-scale reserves in Germany through the intentional down-regulation of wind farms (Regelleistung, 2016).

Energy markets attempt to provide the optimum allocation of resources through the minimization of pricing while fulfilling balance constraints. This is enacted through an auction style clearing process, where utilities place bids to cover the forecasted demand of their customers, and generators place bids to offer their production into the market. The market price is then set at the intersection of the supply and demand offers, which is calculated for each region (i.e. zone or node). The market is subdivided geographically to account for constraints in transmission capacity, with import/export links considered. Once offers are accepted, participants are balance responsible (BRP) for delivering their scheduled quota within the given trading block. If any deviations occur, they may incur financial penalties depending on the effect of their imbalance (i.e. helping or hurting the system). It is common for market operators (e.g. in NordPool's two-price system) to discourage gaming tactics by preventing revenues from exceeding initial market payouts through exploiting up- and down-regulation price movements.

Market design is highly dependent on location, but exchanges often operate day-ahead and intraday markets with trading segments in one hour blocks, and with long lead times between bid placement and delivery. These lengthy intervals create issues for variable renewables such as wind. Market operators in regions with high penetrations of renewables are moving to shorten these horizons, in certain cases to continuous intraday markets with 5, 15, and 30 minute contracts (EPEX SPOT SE, 2019, AEMC, 2017)

where minute-scale wind forecasts become relevant and necessary for traders.

1.2 Remote sensing of winds

For centuries wind measurements in the atmospheric boundary layer (ABL) have been performed using a variety of in situ techniques, where instruments including cup anemometers and wind vanes are mounted on towers to measure the local flow at the sensor's position. These methods are often employed within wind energy for resource assessment and site suitability studies, and for turbine power performance testing.

The increasing scale of modern wind turbines (e.g. the 9.5 MW Vestas V164 and GE's upcoming 12 MW Haliade-X) has resulted in rotor tip heights approaching 300 m, which represents both a financial and technical challenge when relying on mast based measurements, particularly in offshore environments.

Remote sensing (RS) is a measurement process in which observations are made at a distance (i.e. without being physically present at the target position). This provides a number of advantages in the flexibility and cost of running a measurement campaign, and in enabling new ways to measure.

For performing wind measurements, active RS devices are designed to utilize the Doppler effect to obtain velocity information. This is done by emitting an electromagnetic or sound wave of a known frequency which backscatters off of objects within the measurement volume and is acquired again by the receiver (e.g. telescope, parabolic dish, microphone). The returned signal is analyzed (either directly or using coherent detection methods) and the radial velocity is determined through its proportionality to the frequency shift using spectral estimation. The obtained radial velocity represents the wind velocity projected along the beam's path (line of sight, LOS). In the case of atmospheric measurements, the target objects are aerosols- particles such as dust, water vapor, and particulate matter (pollutants) which are suspended in the air and are assumed to be moving together with the wind.

Relevant RS devices represent a wide class of technologies such as Doppler radar, Doppler sodar, and Doppler lidar which can be ground based, nacelle mounted, on fixed or floating platforms, or on space-borne satellites. Each tool has its own advantages and disadvantages. Operational pulse Doppler radar systems typically have large antennas and high powered transmitters which enable them to measure at far distances (e.g. up to 300 km for S-band Nexrad systems in the US observation network). However, they require precipitation for reflectivity and the range resolution is insufficient for detecting small scale motion, especially at further distances. Ka-band Doppler radars have been developed which are more compact and are able to measure in clean air up to 30 km (Hirth et al., 2012). These devices show potential for providing real-time microscale wind field measurements, however initial reports on data availability have been disappointing. In this thesis we will focus solely on Doppler wind lidar systems due to their portable size, commercial availability, well established performance, and capability of measuring in diverse atmospheric conditions. Compact pulsed lidar variants have a typical maximum

range on the order of 10 km, which corresponds to advection occurring up to 30-minutes ahead, depending on wind speed.

1.2.1 Doppler wind lidars

Doppler wind lidars are active remote sensing instruments which use laser light in the near-infrared band as their medium. The laser source is in most cases a $1.5 \mu\text{m}$ all-fiber laser, which corresponds to the spectral absorption line of atmospheric water vapor and carbon dioxide while also satisfying eye safety requirements (Cariou, Augere, and Valla, 2006). An added benefit is that this application overlaps with fiber optic components used in the telecommunications industry. This has resulted in affordable and widely available hardware options for manufacturing the lidar's optical systems.

Doppler wind lidars are built commercially in a variety of configurations depending on the mounting location and measurement setup. The simplest systems have fixed telescopes which stare or switch between predetermined beam positions and are commonly used in nacelle lidars. Units with a rotating platform and offset mirror or prism perform repeating conical scans along a fixed path and are commonly used in certain lidar wind profilers. Scanning lidars are equipped with a dual-axis scanner head which allows the beam to be pointed arbitrarily in space, with little restrictions on the path, timing, and geometric complexity of the scanning trajectory (subject to the kinematic constraints imposed by the mechanical design). Fig. 1.7 presents a look at some of the most common commercially available lidar systems.



Figure 1.7: Selection of commercially available lidar systems, grouped by main function. Images sourced from the manufacturer's respective product brochures.

Two main diverging classes of lidar technology exists- pulsed and continuous-wave (CW) systems, which differ greatly in their spatial and temporal resolutions. CW lidars emit a continuous focused beam, which must be re-focused for different measurement ranges. The spatial resolution of a CW lidar is directed by the aperture of the telescope, which results in an increase in the probe length as a function of the square of the range.

This implies that CW lidar technology is only suitable for close ranges, up to a few hundred meters away. In contrast, pulsed lidars emit a collimated beam using a series of short pulses on the order of nanoseconds. This allows all distances along a pulsed lidar's laser path to be measured at once, using time-of-flight calculations to discern the appropriate distances into range gates (RG) without any change in spatial resolution with distance (i.e. the probe length is fixed, but the intensity of the returned signal is reduced by the square of the range). Coherent pulsed Doppler lidars equipped with high powered optical amplifiers are capable of measuring up to 30 km, although compact units are usually limited to between 5-12 km. For these reasons, pulsed lidar variants show the most promise in terms of suitability towards applications which cover large spatial scales, including minute-scale forecasting.

1.2.2 Measurement techniques

As introduced in Section 1.2.1, application specific lidar systems normally follow preset scanning strategies, while scanning lidars allow for more complex measurement techniques. A brief synopsis of available measurement configurations for a coherent pulsed scanning Doppler lidar is given in the following:

- LOS (staring mode) — The beam position remains fixed and measurements are acquired continuously at the target point.
- DBS (Doppler beam swing) — A technique used to measure vertical wind profiles by measuring at typically four orthogonal positions around a cone and optionally including a fifth central beam to directly measure the vertical wind component. The conical radial speed observations exhibit a cosine function. Fitting techniques are then used to produce estimates of the wind vector components by assuming the wind is frozen and horizontally homogeneous between the discrete sampling points.
- VAD (velocity azimuth display) — Also used primarily for vertical wind profiling, but in certain cases is rotated for horizontal use. The elevation angle is held constant while sweeping across the full range of azimuths. This performs a full conical scan which can be fit similarly to the DBS technique.
- PPI (plan position indicator) — Closely related to the VAD method, PPI scans use fixed, low (or flat) elevation angles and sweep across a full or partial range of azimuths. This results in conical arc slices over a large horizontal distance. The radial speed signals similarly follow a cosine function, with the peak and trough corresponding to the azimuth position aligned into and away from the wind direction. When the beam is perpendicular to the wind, the observed radial speed is zero. PPI scans produce cross-sections of the horizontal wind structure and are processed using retrieval or fitting methods by assuming horizontal homogeneity and by not taking vertical effects into account.
- RHI (range height indicator) — The counterpart to PPI scanning, RHI scans vary the elevation axis while keeping the azimuth fixed. This produces cross-sections of the vertical wind structure along an arc.
- User defined — Complex trajectories which are custom tailored for the particular application are also possible. An example of this is the ridge transect scan used in the Perdigão field campaign which follows the site's topography along a fixed height (Menke, Mann, and Vasiljevic, 2018).
- Dual and triple Doppler — Beams from multiple separated lidars can be intersected in space (and ideally time) to measure either two or all three of the wind velocity components with any of the above-mentioned scan patterns. The independent measurements are then combined together when performing the wind field reconstruction. Dual Doppler approaches have shown to slightly improve wind retrieval results in simple terrain compared to single Doppler techniques (E. Simon and

Courtney, 2016, Floors et al., 2016), while forgoing the assumption of horizontal homogeneity. However, this advantage is offset by the increased cost of the additional systems and reliance on data availability with all systems.

- Dynamic — The previously described scan types are normally configured in advance and set to repeat continuously, or to cycle through a predetermined set of scans along a schedule. Dynamic scanning adapts the lidar's trajectory to real-time inputs, chiefly those derived from the measurements themselves such as wind speed and direction. An example includes Wildmann, Vasiljevic, and Gerz, 2018 which adjusts parameters of the scan to follow the downstream turbine wake through changes in the wind direction.

These scanning strategies can be configured and combined to suit the measurement objective and take site-specific particularities into account. This allows for ultimate flexibility in the placement of devices, measurement range and spatial resolution, sampling rate of the data, and spatial

CHAPTER 2

Minute-Scale Forecasting of Wind Power

2.1 Introduction and context

The International Energy Agency (IEA) was established in the wake of the 1973 oil crisis in order to ensure and regulate security of supply for energy resources in the OECD countries. The wind energy specific sub-programme of the IEA provides a venue for information sharing, research collaboration, and policy review in the form of Research Tasks.

Two relevant Research Tasks were followed as a contributing member during the PhD project. Task 32 focuses on the maturation and acceptance of wind lidars for various applications in wind energy, including operational control. Task 36 brings together users and creators of wind power forecasts to improve the scientific standards of forecast methods and recommend best practices in the usage of forecast products.

Due to the relevance of both working groups to the PhD project objectives, a goal of merging the two communities for a collaborative workshop was pursued. The workshop was organized alongside fellow researchers in the field Ines Würth and Laura Valdecabres Sanmartin, together with the operating agents of Task 36 (Gregor Giebel) and Task 32 (David Schlipf).

The workshop was held at Risø in June of 2018, and brought together 40 attendees from across the world representing the entire chain of wind energy services. This includes commercial forecast providers, wind farm operators, research scientists and academics, transmission system operators, wind turbine manufacturers, national meteorological institutes, power trading companies, and lidar manufacturers.

The workshop was structured with presentations of recent work on the topic, and discussion sessions aimed at collecting inputs from the various perspectives. These included fruitful exchanges on the needs for wind power forecasts on the minute-scale, potential relevant methods to generate them, and possible barriers to adopting them.

An important objective of the meeting was to agree on common terminology for forecast lead times below one hour. 'Minute-scale' was decided upon as it denotes a clear interval and avoids the ambiguity of nonspecific verbage (e.g. very-short-term).

The workshop presentations were live-streamed and are available in the IEA Task 36 video archive (IEA Wind Task 36, 2018).

It was recognized that the recent prominence of the field has led to a distinct gap in knowledge, particularly on a broad level. One of the outcomes of the workshop was the formation of a working group to distill key information into a publicly available document which presents a state of the art review of the field, together with suggestions on future directions to pursue, reached through a consensus approach.

The contributions of the PhD student towards this work include envisioning and

co-organizing the workshop and leading discussion groups where the framework and direction of the review paper was decided. Significant writing contributions were made in the sections focusing on intrahour wind variability (Section 2), remote sensing and lidar methods (Sections 5.1 and 5.1.1), statistical time series models (Section 5.2), and the overall comparison of methods (Section 5.5). The portions on data assimilation theory and practices are largely outside the scope of expertise.

The resulting open access journal article is presented in Section 2.2.

2.2 Results from the collaborative workshop of IEA Wind Task 32 and 36

Article

Minute-Scale Forecasting of Wind Power—Results from the Collaborative Workshop of IEA Wind Task 32 and 36

Ines Würth ^{1,*}, Laura Valldecabres ², Elliot Simon ³ , Corinna Möhrle ⁴ , Bahri Uzunoğlu ^{5,6}, Ciaran Gilbert ⁷ , Gregor Giebel ³ , David Schlipf ⁸  and Anton Kaifel ⁹ 

¹ Stuttgart Wind Energy, University of Stuttgart, Allmandring 5b, 70569 Stuttgart, Germany

² ForWind-University of Oldenburg, Institute of Physics, K pkersweg 70, 26129 Oldenburg, Germany; laura.valldecabres@forwind.de

³ DTU Wind Energy (Ris  Campus), Technical University of Denmark, Frederiksborgevej 399, 4000 Roskilde, Denmark; ellsim@dtu.dk (E.S.); grgi@dtu.dk (G.G.)

⁴ WEPROG, Willemoesgade 15B, 5610 Assens, Denmark; com@weprog.com

⁵ Department of Engineering Sciences, Division of Electricity, Uppsala University, The  ngstr m Laboratory, Box 534, 751 21 Uppsala, Sweden; bahriuzunoglu@computationalrenewables.com

⁶ Department of Mathematics, Florida State University, Tallahassee, FL 32310, USA

⁷ Department of Electronic and Electrical Engineering, University of Strathclyde, 204 George St, Glasgow G11XW, UK; ciaran.gilbert@strath.ac.uk

⁸ Wind Energy Technology Institute, Flensburg University of Applied Sciences, Kanzleistra e 91–93, 24943 Flensburg, Germany; david.schlipf@hs-flensburg.de

⁹ Zentrum f r Sonnenenergie- und Wasserstoff-Forschung Baden-W rttemberg, Meitnerstra e 1, 70563 Stuttgart, Germany; anton.kaifel@zsw-bw.de

* Correspondence: wuerth@ifb.uni-stuttgart.de; Tel.: +49-711-685-68285

Received: 14 December 2018; Accepted: 14 February 2019; Published: 21 February 2019



Abstract: The demand for minute-scale forecasts of wind power is continuously increasing with the growing penetration of renewable energy into the power grid, as grid operators need to ensure grid stability in the presence of variable power generation. For this reason, IEA Wind Tasks 32 and 36 together organized a workshop on “Very Short-Term Forecasting of Wind Power” in 2018 to discuss different approaches for the implementation of minute-scale forecasts into the power industry. IEA Wind is an international platform for the research community and industry. Task 32 tries to identify and mitigate barriers to the use of lidars in wind energy applications, while IEA Wind Task 36 focuses on improving the value of wind energy forecasts to the wind energy industry. The workshop identified three applications that need minute-scale forecasts: (1) wind turbine and wind farm control, (2) power grid balancing, (3) energy trading and ancillary services. The forecasting horizons for these applications range from around 1 s for turbine control to 60 min for energy market and grid control applications. The methods that can be applied to generate minute-scale forecasts rely on upstream data from remote sensing devices such as scanning lidars or radars, or are based on point measurements from met masts, turbines or profiling remote sensing devices. Upstream data needs to be propagated with advection models and point measurements can either be used in statistical time series models or assimilated into physical models. All methods have advantages but also shortcomings. The workshop’s main conclusions were that there is a need for further investigations into the minute-scale forecasting methods for different use cases, and a cross-disciplinary exchange of different method experts should be established. Additionally, more efforts should be directed towards enhancing quality and reliability of the input measurement data.

Keywords: wind energy; minute-scale forecasting; forecasting horizon; Doppler lidar; Doppler radar; numerical weather prediction models

1. Introduction

In the past years, minute-scale forecasting of wind power has become an important research topic in the wind energy community. Whereas traditional forecasting techniques provide a forecasting horizon in the hour or day range [1], new methods allow us to predict the power output of wind turbines or wind farms on a minute scale. Due to the increasing penetration of renewable energy power systems into the grid, there is a demand for minute-scale wind power forecasts, as grid operators need to ensure grid stability in spite of the highly fluctuating power sources. The forecasts become even more important with increasing sizes of wind farms of several 100 MW and especially if those wind farms conglomerate geographically as is the case for offshore sites. The objective of this paper is to provide a summary of the needs of minute-scale forecasting and an overview of the developed methods and the possible solutions to the barriers that prevent end users from adopting them.

The results presented in this paper are based on the outcome of the collaborative IEA Wind Task 32 and 36 workshop “Very Short-Term Forecasting of Wind Power” held in Roskilde, Denmark in June 2018. IEA Wind Task 32: “Wind lidar Systems for Wind Energy Deployment” is an international open platform with the objective of bringing together experts from the academic and industrial communities to identify and mitigate barriers to the use of lidar for wind energy applications. IEA Wind Task 36: “Forecasting of Wind Power” is focused on improving the value of wind energy forecasts to the wind energy industry. Details of the Tasks can be found in supplementary materials. During the workshop, 39 participants from academia, forecasting service providers, wind farm operators as well as the lidar and wind turbine manufacturers discussed the future needs of minute-scale forecasting, the advantages and barriers of different forecasting techniques and strategies for overcoming those barriers.

This paper is organized as follows: Sections 2 and 3 discuss the need for minute-scale forecasting and explain target forecasting horizons for different applications. In Section 4 state-of-the-art forecasting methods and the need for new methods in the minute-scale is explained. Section 5 gives a review of methods for minute-scale forecasting. In Section 6 challenges for the implementation and commercialization of the new methods are discussed and the paper is finalized with conclusions in Section 7.

2. Intra-Hour Variability of Wind Power Generation

In 2017, Denmark was the country with the highest wind power penetration rate (44% of the annual consumption of electricity), followed by Portugal (24%) and Ireland (24%). In the case of Denmark, the maximum hourly penetration rate was over 140%. With a total net installed capacity of 169 GW, the power generation capacity of wind power in Europe increased by almost 300% in the last 10 years [2]. Given the expected rising penetration levels of wind power and the increasing size of on- and especially offshore wind farms feeding power into the grid at a single point [3], it becomes crucial to have more precise forecasts of wind power generation with lead times of few minutes ahead and temporal resolutions of seconds or minutes.

When generating a forecast, one useful practice is to consider the power spectral density (PSD) of the measured physical process to understand which time frequencies contribute to the variance of the signal. Peaks in the spectra correspond to larger relative fluctuations which are traditionally more difficult to capture and predict. This type of analysis is demonstrated in Larsen et al. [4] using long-term site measurements from Høvsøre test station and Horns Rev offshore wind farm in Denmark. Boundary layer wind spectra were resolved across cycles ranging from 0.1 s (10 Hz) to 1 year. Figure 1 presents a main result of that work which compares full scale wind PSDs at 50 m height both on- and offshore [4]. Apt [5] presents a similar PSD analysis of wind turbine output using 1-second power data for a single wind turbine as well as a 6-turbine wind farm. Attributes of the PSD signal will vary by location, time, sensor type, and physical property being measured. Still, from the results in Figure 1, a strong local peak can be detected around 1 min, indicating the strong variability of the wind at that temporal scale. This variability of the wind is associated to atmospheric phenomena like open cellular convection, gravity waves, sea breezes or low level jets, among others [6]. At frequencies

$f > 0.02$ Hz, i.e., periods below one minute, the PSD signal strongly decreases and, as reported in [7], wind power fluctuations of large wind farms are not considered an issue due to the smoothing effect of aggregated power.

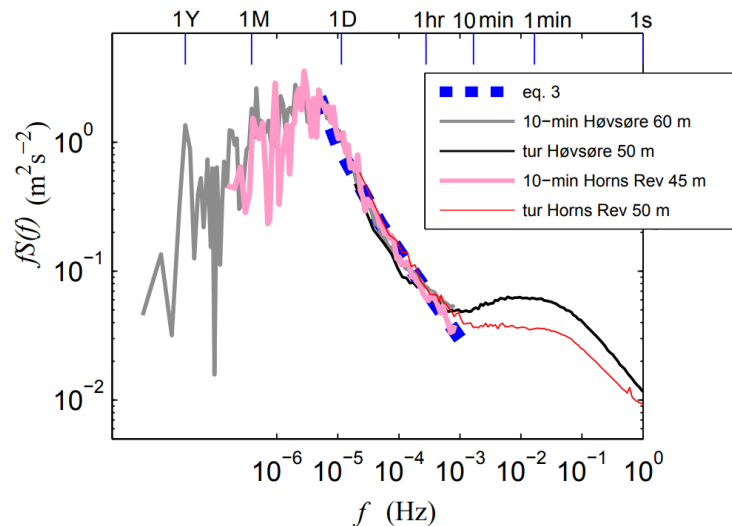


Figure 1. Power spectral density (PSD) of wind speed with corresponding timescales denoted atop. High frequency sonic measurements are used to devise the onshore (black) and offshore (red) lines. Reproduced with modifications from Larsen et al. [4] with permission from Springer Nature.

Yet, the intra-hour variability of wind power not only depends on the variability of the wind itself but on the size of the wind farm, the number of wind turbines and their geographic dispersion. Indeed, it has been shown by several authors that for offshore wind farms, the small geographic dispersion of the wind turbines results in an increased power variability in the minute scale, compared to widely dispersed onshore wind turbines [8].

One of the main challenges for the integration of large amounts of wind power into the grid is the occurrence of rapid and strong changes in wind power generation (ramp events). These unexpected events are mainly caused by extreme changes in wind speed and/or direction in a very short period of time, and are frequently associated with the passage of weather fronts. However, the most critical ramp event can occur even for small changes in wind speed. When the wind speed reaches the wind turbine's cut-out speed, wind turbines shut down automatically for safety reasons, resulting in a large loss of generated power. Despite being critical for the management of the grid, the dynamic allocation of reserves and the stability of the system [9,10] there is no standard definition of a ramp event. It is an individual process of the end-user to define critical ramps and thereby ramp events. A recent publication on the history of wind power ramp forecasting [11] gives an overview of the definitions used in ramp event detection, the meteorological conditions associated to those events and the current forecasting techniques. For most wind power forecasting applications however, the definition of what is critical for an end-user is very individual and dependent on the application as well as the available reserves. For example, a system operator on an island grid or badly interconnected grid needs to have all reserves available within the control zone in order to prevent a critical ramp from causing security issues. A trader may also be very interested in ramp forecasts, as just one event with a large error may cause 95% of the imbalance costs in a month.

Ramp events are often classified into ramp-up and ramp-down events, according to the direction of the power gradient. As an example, the time-series in Figure 2 illustrates a number of steep ramps in both directions. While ramp-up events can always be handled in the very short term with curtailments, ramp-down events can become extremely critical due to the sudden missing generation. This enhances the importance of generating accurate minute-scale forecasts of wind power.

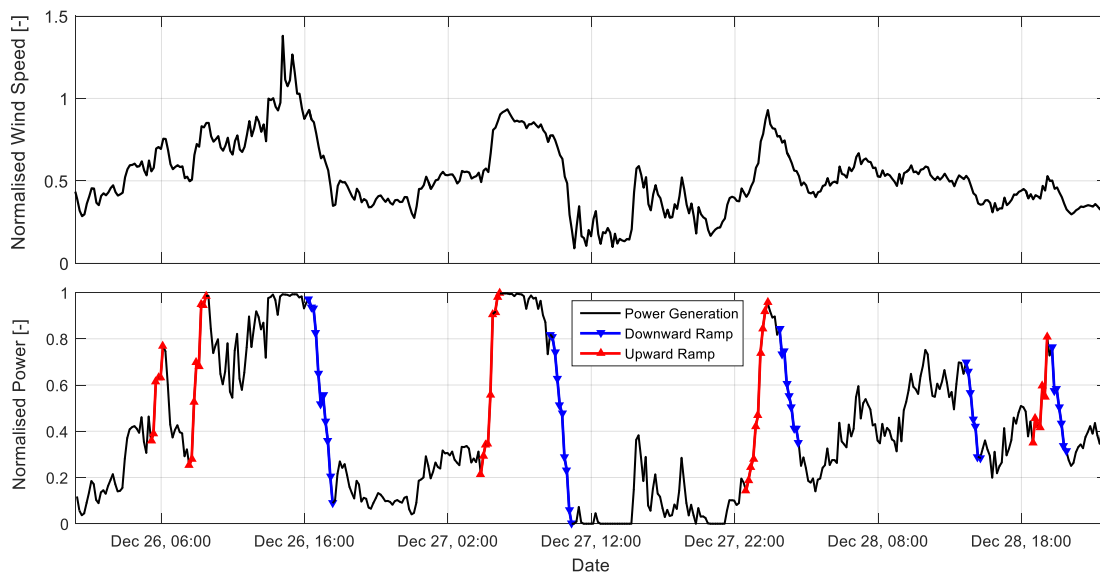


Figure 2. Example time series of wind speed and generated power of a single wind turbine with wind ramps marked for a time window of 60 min and a change of power of 40%. Each data point in the time series corresponds to a 10-minute average. Reproduced without modifications from Würth et al. [12].

3. An Overview of Different Applications for Minute-Scale Forecasting in the Wind Industry

The forecast horizon and the parameters that are needed to be forecasted depend on the application of the forecast. Three applications have been identified where minute-scale forecasts of wind speed or power are needed.

1. Wind farm control: Wind turbine and wind plant controllers need the information to optimize, e.g., the power output of the turbines.
2. Physical balancing: They are required by the Transmission System Operator (TSO) in order to optimally operate reserves for the continuous balance of the power system and grid constraint management.
3. Economic balancing: Trading and balancing of wind power in the intra-day or rolling power markets require minute-scale updates of the forecasts with real power output in order to reduce imbalance costs and increase incomes.

It is expected that a next step in the evolution will be storage system planning and optimization in the real-time markets, where the bulk of the energy production will come from renewable energy sources. However, this paper focuses on the applications listed above. In the following each application is discussed in more detail.

3.1. Wind Turbine and Wind Farm Control

Preview information of the wind field is helpful for the control of wind turbines and wind plants. Wind turbine and wind farm controllers need to continuously adjust the operation of the controlled system due to the stochastic changes in the wind inflow. However, traditional controllers are mostly based on feedback and are only able to react to wind changes after the changes already have impacted the turbine dynamics and farm operation. Lidar-assisted control algorithms can use the preview information of the wind to proactively adjust and thus improve the wind turbine and wind farm operation by increasing the energy production and reducing structural loads.

Regarding the required preview time for lidar-assisted wind turbine control, the following classification is useful:

1. around 1 s: Feed forward control is used to compensate wind changes to reduce structural loads. For example, the blade pitch, the rotor-effective wind speed is needed only a short time before the wind reaches the rotor to overcome the pitch actuator dynamics [13,14].
2. around 10 s: For Model Predictive Control, the control inputs are optimized to get a chosen compromise of load reduction, energy production, and actuator wear [15,16]. Here, a short time horizon of wind characteristics such as wind speed, direction, and shears is used, typical 5–10 s.
3. around 1–10 min: For yaw control, a wind direction estimation is used to align the wind turbine with the mean wind direction. Yaw control is generally done in the minute scale. In this time scale [17], the yaw signal of lidar systems provides good agreement [18,19].

Active wind farm control is a promising technology to increase the energy production of wind farms [20]. However, flow models are still an important research topic, and the validation of flow models and control strategies are still ongoing. Wind previews for flow control is mainly used in induction control and wake steering for higher energy capture and management of fatigue loading.

Regarding the required preview time for lidar-assisted wind farm control, following classification is useful:

1. around 10 s to 10 min for induction control: Usually the blade pitch angle is used to reduce the power and thus the thrust to weaken wake effects on downstream turbines, which increase the overall production. At partial load this is done by adjusting the “fine pitch” settings which is usually based on a filtered wind speed estimate. Wind previews might help to better adjust the power balancing [21].
2. around 1–10 min for wake steering: The yaw misalignment is used to deflect wakes away from downstream turbines and thus similar preview times compared to the conventional yaw control is useful [22]. A preview of the wind direction might help to better adjust the yaw misalignment in a wind farm.

Table 1 summarizes the preview times for the different applications.

Table 1. Helpful wind preview times for various wind turbine and wind farm applications.

Application	Preview Time
Single turbine blade pitch feed forward control	≈1 s
Single turbine model predictive control	≈10 s
Wind farm control via induction control	≈10 s to 10 min
Single turbine yaw control and wind farm control via wake steering	≈1 to 10 min

3.2. Power Grid Balancing, Frequency Control and Power Quality in Reserve Market

The focus in this section is on grid balancing, frequency control and power quality embedded in reserve market while the energy market and ancillary services are discussed in the following Section 3.3. The balancing term can be employed in a much broader sense in the context of balancing longer time scales. However, in these time scales of mainly energy and reserve market, where balancing actions are scheduled before real time, there are several other means of observations with lower resolutions available [23–25]. However, these are not within the time scales of minute-scale forecasting which is the focus of this section. It should be noted that there are differences in terminology between countries for the same and slightly different balancing actions. In this section, the EU terminology is adopted.

To guarantee the stability of the grid, supply and demand always have to be balanced in spite of the fluctuating power sources. Power quality is achieved if the grid frequency stays within a certain range of a rated value. An imbalance between supply and demand impacts voltage stability and grid frequency, hence there is a need for power balancing [23,26–28].

The volatility of wind resources creates volatility in the supply and as a result, balancing control actions are needed. One can distinguish between different time scales in this phase of controls

embedded in the reserve market, which are known as primary, secondary, and tertiary controls. The autonomous response of the system to supply/demand imbalances is automatically addressed with primary controls, which is in the scale of microseconds to a few minutes mainly in the scale of seconds. In secondary controls, there are automatic actions and manual actions in scales of seconds to several minutes mainly in the scale of minutes. In tertiary control, both manual and automatic controls are in action from minutes to quarter of an hour to half an hour scales. These are summarized in Table 2. All of these actions of balancing are carried out in order to ensure power system quality.

From a market perspective primary, secondary and tertiary reserves are handled differently. Primary reserve is contracted on bi-lateral contracts due to the high-availability requirements. Secondary and tertiary reserves are in some countries traded by auction. The periods range from daily to several days or weeks. Common for or all three reserve products is that the reimbursement is split up into a price for the availability of a specific generation capability and a price for the actual utilization [29].

Wind power and other renewable energy sources create low levels of rotational inertia since these energy conversion systems do not normally act on rotational inertia which has impacts on the power grid frequency. Moreover modern variable-speed turbines are disconnected by inverters from the rotating mass of inertia. Suppliers have started to make changes to create synthetic inertia that can emulate inertia synthetically [30]. Synthetic inertia is about acting to AC frequency, possibly after the loss of a big power plant which makes the grid under-supplied and will result with the AC frequency beginning to fall. This makes accurate short-term forecasting even more important since all of these emulations are dependent on accurate estimation of wind speeds. Hence automatic control for primary and/or secondary controls will certainly benefit from more accurate forecasting on the short-time scales of minutes in control applications.

On another note for the data that is available in the context of this research, any forecast data that is available on scale of microseconds to minutes can be automatically employed in the state estimator of the controller [23,26–28]. The state estimator corrects the state of the system with observational data.

Table 2. Activation of the reserves after an imbalance.

Application	Approximate Range of Operation	Overlap with Other Balancing
Primary control	≈0 to 2 min	Transition overlaps secondary control
Secondary control	≈2 min to 15 min	Transition overlaps tertiary control
Tertiary control	≈15 min to hour scales	

3.3. Energy and Ancillary Services Markets

Electricity markets need to be balanced in order to match the supply and demand of energy. This physical balancing of the transmission grid is carried out by the transmission system operators (TSO) or by an independent system operator (ISO). Given the increased integration of power generation from variable sources of energy like wind and solar, the physical balancing has become more complicated. Therefore, electricity markets with such intermittent and variable sources have to become more flexible and introduce either rolling markets (e.g., in the UK and Australia) or introduce shorter intra-day auctions, additional to the day-ahead auction, which have become very popular in Europe. Among the intra-day market platforms, one can distinguish between discrete auctions or continuous intra-day markets. In intra-day auction markets like in Italy, Spain or Portugal, intra-day bids are restricted to a few established auctions. By contrast, in continuous intra-day markets, counter parties match the bids using a trading platform that operates continuously. Those continuous intra-day balancing markets operate in Europe with different lead times ranging from 5 to over 90 min and most of the countries work with trading blocks of 15 min. Table 3 includes the lead times and smallest trading blocks for several countries in Europe and for Turkey. A more detailed description of the

electricity markets and their time lines can be found in [31]. Hence, the importance of the use of updated available minute-scale forecast of wind power has arrived to stay.

Table 3. Lead times and smallest trading blocks for different countries. Sources: Epex [32], Nordpool [33], Energy Exchange Istanbul (EXIST) [34], and BSP South Pool [35].

Country	Lead Time (Minutes)	Trading Blocks (Minutes)	Market
Austria and Germany	5	15	EPEX Spot
Bulgaria, Denmark, Estonia, Finland, Lithuania, Norway and Sweden	60	15	NordPool
Belgium, France and the Netherlands	5	60	EPEX Spot
Slovenia	60	15	BSP Southpool
Switzerland	30	15	EPEX Spot
Turkey	90	60	EXIST

In light of this, the forecast process can be split into three components: (1) production of a smooth day-ahead forecast tuned for economic adjustment via the intra-day market, (2) targeting intra-day forecasts for the predictable part of the day-ahead forecast errors and (3) application of forecasts on the minute-scale to manage the wind power generation after gate closure of the intra-day. The two first components correspond to current practices in long-term and short-term processes with some enhancements. The third component is a process running on minute-scale with 1 or 2 h look ahead (e.g., [36]).

Minute-scale forecasts are also necessary when applying to provide ancillary services, secondary or tertiary reserve or balancing capacity for the pool of large utilities. For instance, a recent pilot project in Germany allows wind power generators to participate in the reserve market by down-regulating their production. The possible or available power produced by the wind farms needs to be calculated in one-minute intervals. Furthermore, the standard deviation of the percentage error of the possible or available wind farm power, during the pilot phase, should be less than 5% [37].

4. State-of-the-Art of Wind Power Forecasting

State-of-the-art wind power forecasting methodologies utilize wind speeds from weather forecasts and on-site real-time measurements to compute wind power.

Figure 3 shows qualitatively the forecast error levels of a day-ahead, hours-ahead and minutes-ahead forecast compared to a persistence error, where the persistence forecast is the most recent available measurement. The qualitative visualization of the forecast errors in the different time scales shall be seen in the light of their starting point and forecast error growth over time. For example the day-ahead forecast has an almost linear error growth and is typically responsible for approximately 1/3 of the forecast error [38]. The day-ahead forecast also starts with an inherent error at forecast time zero due to a number of aspects. In [38] these are described as for example (i) the initial weather conditions; (ii) sub grid scale weather activity; (iii) coordinate transformations; (iv) the algorithm used to compute the wind power; (v) imperfection of turbines and measurement errors. For Pahlow et al. [38] one question remained: which fraction of this background error is caused by imperfect initial conditions of the weather forecast and which fraction is due to erroneous wind power parameterizations. They extrapolated the linear forecast error growth from 9–45 h down to the 0 h forecast and thereby estimated the background mean absolute error (MAE) just under 4% of installed capacity. Part of that gap of approximately 4% error at the initial time can be reduced by the hours-ahead forecast with knowledge about the real power production. Pahlow et al. [38] characterized this inherent error at the initial time to a mix of unknown technical and non-technical constraints at the forecast location. These can be wind farm specific constraints, such as unknown non-availability of wind turbines, but also errors due to the computation of the wind power at the site. The hours-ahead forecasts are steeper in error growth than the day-ahead and reach this level

typically around 4–8 h ahead in time. This time span is the typical temporal influence radius of a measurement [38]. The minute-scale and persistence forecasts are both starting at the zero error in their initialization. This is what characterizes this forecasting time scale, where the current state of the power plant is fully known. The steepness of the error growth is also highest for these two forecast techniques due to the decreasing influence of the measurement at the power plant over time. A general industry experience is that a persistence forecast is at the same level as a hour-ahead forecast after around one hour. A minute-ahead forecast should ideally be below the hour-ahead forecast for about 3 h as a thumb rule when evaluating the usefulness of the technique. The time between 1 h and 3 h into the forecast is where the persistence forecast typically reaches the day-ahead forecast error level and loses forecast skill.

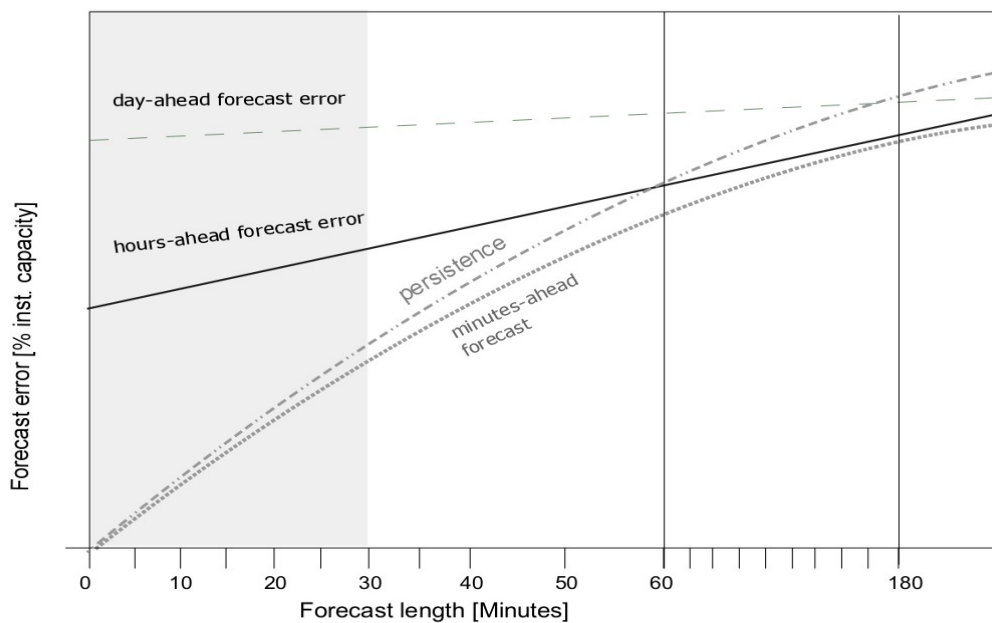


Figure 3. Qualitative visualization of the forecast error development over the first hours of a forecast for different temporal forecast techniques.

Figure 3 illustrated nicely that the margin of possible improvements by minutes-ahead forecasts in the first 30 min of the forecast is rather small in comparison to persistence. Additionally, the average error growth of up to 2% of the installed capacity of a short-term forecast of 15 minute time resolution is rather steep (see Figure 3). It is therefore fair to say that the improvement over persistence, which is the objective in the very short time ranges of minutes and hours, is therefore rather modest. This is often used as a reason not to base decisions on forecasts, but rather use persistence, even during ramping, where the persistence forecast is a poor approximation. If the previous 15-min forecast already appears to be off track, then the forecast user cannot be justified in trusting the forecast. Also, the similarity between the average error of a short-term forecast and persistence over the next 15 min strongly indicates whether the short-term forecast performs better or worse than persistence.

Forecast providers are continuously looking for enhancements, which can improve the hour-ahead and minute-scale forecast in the less good quality periods, because these result in the most significant power system benefits. Use of wind speed measurements in addition to wind power measurements is therefore a key to improve forecasts in periods, where the wind speed is in the flat ranges of the power curve (<5 m/s or >12 m/s). Without wind speed measurements, the minute-scale forecast is in fact unable to correct the weather forecast for phase errors in periods, where the generation is zero or at full capacity.

A forecast of the steady increase in wind speed from 15 m/s to above the high-speed shutdown point at 25 m/s can also be improved by using wind speed measurements in short-term algorithms. At the high-speed shutdown points (>25 m/s), the wind speed forecast uncertainty is at least 2 m/s even in highly predictable events. The timing of the shutdown is therefore uncertain, even a few minutes before it happens. Wind speed measurements from wind farms reduce this uncertainty significantly. The timing of a high speed shutdown is important for grid security, because there are potentially many Megawatts instantly ramping down. In combination with forecasting on the minute-scale, such wind speed measurements can help to bridge the gap between actual generation and both short-term and long-term forecast.

For wind speeds below the cut-in level there are similar considerations. Mostly, low aggregated wind power generation occurs at low wind speeds. Nevertheless, a large and strong low pressure centre may have near-zero wind speeds from different directions. Both the changes in wind direction and wind speed are better identified by wind speed measurements than wind power measurements. Thus information about wind speeds below cut-in can be crucial for the forecast accuracy near a low pressure system center with highly aggregated wind power generation. During periods of moderate and high generation, wind speed measurements can be used to calculate current potential turbine available generation power or validate the signal of current available power generation sent by the wind generation plant. To conclude, measurements of low, medium and high wind speeds all add value to forecasting, while measurement signals in the steep range of the power curve are least important.

From a technical perspective of the instrumentation, one of the most reported gaps for forecasting hours-ahead and minutes-ahead is the quality of the measurement signals. While wind farm developers have to use calibrated instrumentation and standardized methodologies in order to obtain a bankable level of siting accuracy in the first planning and commissioning phase of a wind project, in the following operational phase the use of meteorological measurements is mostly not defined, documented or standardized. Although the measurements are important in many ways, e.g., situational awareness in extreme events, scheduling and dispatch of generation on power system level, the balancing of large forecast errors, maintenance of instrumentation, there are no standards for the quality of the signals in real-time environments today. For example, if a measurement stops working correctly and sends constant values, a persistence forecast that uses only this data will benefit in performance assessment, while a more advanced minute-ahead forecast that uses other data or models is penalized for providing a more realistic view of the situation. Dependent on the amount of such periods with constant values, this can easily lead to an overestimation of the performance of a persistence forecast in comparison to minutes-ahead forecasts and thereby prevent use and application of minutes-ahead forecasts.

Due to such missing standards and industry guidelines, the main gaps for the use of and collection of meteorological measurements and thereby advances in minute-scale forecasting can be summarized as:

- lack of requirements in the grid codes
- lack of strategy for handling of missing or constant signals from measurements in real-time
- lack of quality of measurements in real-time

5. Review of Methods for Minute-Scale Forecasting

In the previous section we discussed the state-of-the-art in minute-scale forecasting. In this section we investigate instrumentation that can improve forecasting with current techniques and we outline which and how new types of instrumentation and models can be used to improve forecasting on minute scales when persistence can no longer provide a correct picture of the weather conditions.

5.1. Minute-Scale Forecasting Based on Preview Data From Remote Sensing Devices

Remote sensing techniques are a new technology development in wind energy applications, which have their roots in the desire to find alternative measurements for the expensive and at times

difficult installation of meteorological masts. With increasing experience and technical advances in technology, remote sensing devices have become viable alternatives. This has also been reflected in the IEC 61400-12-1 2017 standard [39], where such devices have been incorporated as possible instruments to carry out measurements for wind energy applications. A new application for remote sensing devices is forecasting. Especially scanning devices such as scanning lidars and radars which offer the possibility to carry out minute-scale forecasts by delivering high resolution temporal and spacial previews of the upstream wind field of a wind turbine or wind farm. Therefore, the next subsections give an overview of using those devices for forecasting purposes and finally lessons learned with remote sensing instruments in real-time forecasting projects are summarized.

5.1.1. Scanning Lidar-Based Propagation Models

Doppler wind lidars measure the wind speed in direction of the laser beam, also referred to as line of sight (LOS). Depending on the system, the measurement range varies from a few centimeters to several kilometers [40]. Commercial lidars were first used for wind energy applications in the early years of this millennium [41]. Nowadays they have become accepted as an alternative to meteorological masts (met masts) due to cost and ease of installation. Ground based systems are used for site assessment and power performance testing and are now included in international standards [39]. Nacelle-based lidars that can measure upstream of operating turbines, are used for feed-forward control of wind turbines [42]. These systems measure the wind speed several hundred meters upwind, thus forecasting the rotor effective wind speed seconds before it hits the rotor just in time to pitch the rotor blades and reduce loads. A new application for scanning lidars is within wind power forecasting. Commercial lidar manufacturers have increased the range of their systems and compact pulsed scanning wind lidars may now measure the wind speed up to a distance of 10 km over an entire site from one location (see, e.g., [43,44]). There are also systems on the market that measure 30 km and more, but these systems are bigger in size and therefore less suitable for flexible measurement campaigns. The basic idea is to use the spatial and temporal high resolution wind field information measured several kilometers upwind of a wind turbine or wind farm to forecast the power output ahead in time.

The forecast process (Figure 4) is the same for both applications—control and power grid balancing. First the raw lidar data is filtered and the horizontal wind speed and direction is reconstructed from the measured LOS wind speeds. Depending on the number of synchronized lidar measurements, different assumptions need to be made in order to resolve both horizontal wind speed and direction. For instance, a velocity-azimuth display (VAD) retrieval technique is used to resolve both wind speed and direction when only one lidar measurement is available [45]. This method assumes a homogeneous wind field and should only be used in flat terrain where the assumption generally holds true. Then the wind speed in the distance is propagated towards the site by means of a propagation model. The simplest model is based on Taylor's hypothesis which claims that turbulent structures, so called eddies, are transported with the mean flow without changing their properties. With this assumption the time can be calculated that the wind speed measured in a certain distance needs to reach the turbine or wind farm. Thus the farthest measured distance determines the forecast horizon. The forecasted wind speed at the turbine or farm location is then used either to forecast the power output by means of a power curve model, or as an input to the wind turbine controller.

As mentioned, the forecast horizon is determined by the measurement distance of the lidar and the magnitude of the wind speed (Figure 5). For wind speeds at rated power of a typical turbine, the maximum forecast horizon with a state-of-the-art long-range scanning lidar that ideally measures up to 10 km is around 15 min. The maximum horizon increases to around 40 min for a wind speed of 4 m/s that corresponds to a typical cut-in wind speed.

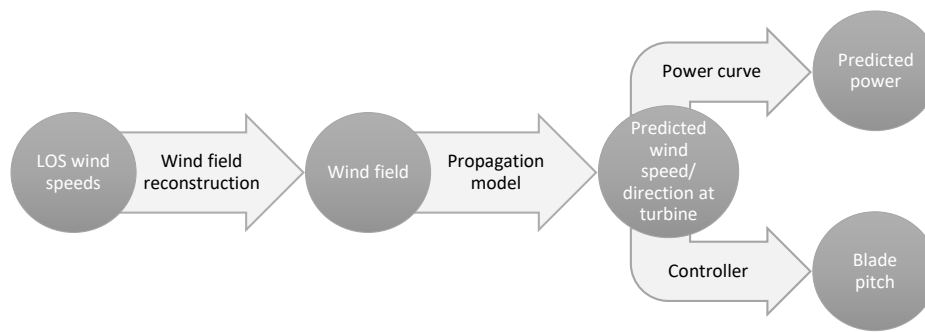


Figure 4. Forecast process using scanning lidar data.

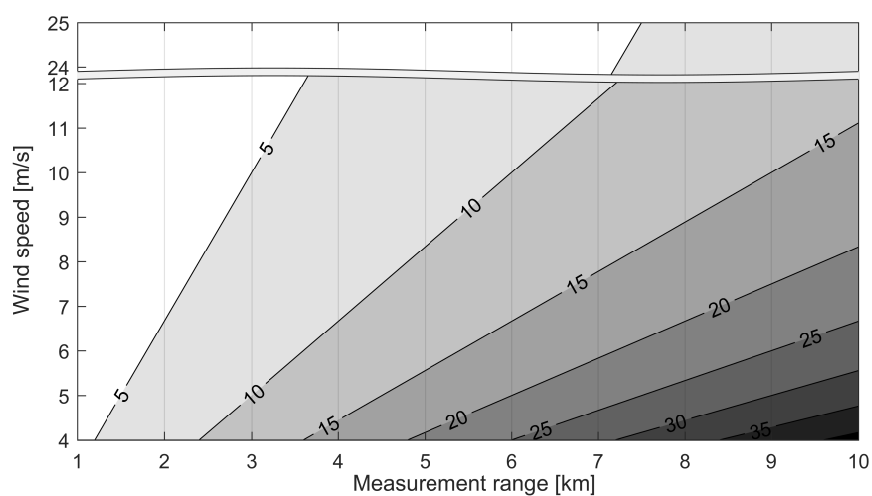


Figure 5. Forecast-horizon calculated based on Taylor for different wind speeds and measurement ranges; the horizon is given in minutes.

The advantage of scanning lidars is that they offer the possibility to directly measure the wind speed upstream of a turbine. All long-range scanning lidars are pulsed devices, which means that the wind speed information is gathered simultaneously at different measurement distances. Thus the wind flow can be tracked over the span of the measurement and local changes in the wind speed are captured. Modern lidars have compact dimensions of around one cubic meter which allows for flexible measurement campaigns and the installation for instance on the nacelle of a wind turbine or other elevated points such as an offshore substation. Then the scanning of the area on, e.g., a horizontal arc leads to the desired horizontal wind speed information after reconstruction without having to take into account shear effects. When installing the lidar on the nacelle of a wind turbine behind the rotor, it should be noted that due to the blade passage the available data will be reduced, and nacelle vibrations and the tilt angle from the rotor thrust might introduce disturbances in the measurement range and height.

Recent investigations have shown that lidar-based forecasting models were able to predict near-coastal winds better than the benchmarks persistence and ARIMA for a forecasting horizon of 5 min [46]. Another relevant study is Simon et al. (2018) [47] which explores space-time correlations of upwind lidar observations measured on a flat horizontal plane. The study also shows results of a 1–60 min ahead forecast method utilizing the lidar inflow scans which significantly outperforms the persistence method.

However, there are some drawbacks when using lidar data for forecasting. One of the major barriers to overcome is the availability of the measurements. The lidar measures the wind speed by

sending out laser pulsed that are back-scattered from particles suspended in the air. The wavelength of the back-scattered light shifts relative to the speed of the aerosols according to the Doppler principle [48]. Therefore the device records a noisy signal if not enough or too many aerosols are in the air. It also means that the measurement range fluctuates due to environmental conditions such as fog or rain showers [49]. And as the measurement range determines the forecast horizon, minute-scale forecasts are not possible if the lidar is blind. As a consequence, a fallback solution should be implemented in case the lidar does not provide measurements. Data from other sensors such as radar or drone measurements could be one solution. Using statistical models (cf. Section 5.2) or the coupling of the measurements with NWP models (cf. Section 5.3) could be another solution. More investigations have to be carried out to determine the optimum conditions for good range measurements of lidars.

Another drawback of lidars so far have been the high costs and the inaccuracies of wind field reconstruction in complex terrain. According to the white paper of the Deutsche Windguard [50,51], especially “in complex terrain sites, influence of the relatively large scanning volume of today’s lidar and SODAR must be carefully considered in terms of its influence on the measurement accuracy...”. This has been a general observation and an ongoing research topic (see, e.g., [41,43,52–55]). In one recent large scale measurement campaign, the Land-Atmosphere Feedback Experiment (LAFE), measurements were setup with multiple synchronized scanning lidars that enable the direct measurements of wind field components (see, e.g., [44,56]). Their instrument setup configuration addressed “the required combination of measurements for advanced studies of the land-atmosphere feedback” with a combination of instrumentation of scanning lidars and surface and airborne in situ measurements that provided the necessary overlap of measured data signals to fill gaps in the instrument’s measurement ranges. This strategy could directly be transferred to the minute-scale forecasting problem in real-time environments and in complex terrain and is also widely applied in the data assimilation of NWP models (see Section 5.3).

Another significant obstacle for the application of lidars in the wind power industry is the lack of standard or recommended practices for the use of scanning lidars for wind speed forecasting. More research is needed to find out what the ideal measurement setup looks like, in particular how many lidars are needed and where to place those devices within a wind farm or within a control zone of a system operator. Also, optimal measurement strategies need to be established and transferred to different problem areas and sizes. To that end, different use cases have to be investigated to find out what the best campaign setup and measurement strategy is. Such use cases should include on- and off-shore wind farms of different scales. Recommended practices then need to be consolidated so that the widespread use of lidar for forecasting becomes possible on a commercial level.

5.1.2. Radar-Based Density Models

Radars are remote sensing systems which can determine the position, angle or motion of objects and are being used in multiple applications including traffic control, ocean surveillance, weather monitoring, flight control systems and antimissile systems. Similarly to wind lidars, Doppler radars can be used for wind power forecasting as they are able to determine the velocity of the objects. The working principle is the same as for lidars, but rather than sending light waves, they emit radio waves. Thus, in an environment where meteorological particles with high humidity such as water droplets or ice crystals are present, radars are able to measure the wind speed by determining the motion of the hit particles.

The maximum range that radars can measure is given by the wavelength of the signal emitted, but in this paper we only focus on radars which work on wavelengths that are of interest for minute-scale forecasting of wind power. Thus, we limit our review to radars working between the C-Band and the Ka-band radars, or with a wavelength of 3.2 cm to 8.6 mm.

Doppler-radars working in the Ka-band (35 GHz) are optimal candidates for wind power forecasting (Figure 6). The short wavelength employed allows for high temporal and spatial resolution

of the measured wind fields. As with lidars, Doppler radars measure the LOS wind speed. Thus, measuring with one Doppler radar over a defined Plan Position Indicator (PPI) trajectory, the horizontal wind speed can be determined by applying a VAD retrieval technique in the same manner as lidar. To derive the two horizontal wind speed components, two synchronized Doppler radars are needed [57]. The number of publications on the use of Doppler radars for wind energy applications has grown in the last years. Hirth et al. coupled wind farm operational data with wind fields measured by two synchronized Doppler radars (dual-Doppler radar) to further investigate wind farm wake effects [58]. Dual-Doppler measurements of the wake behind an offshore wind farm were also reported by Nygaard et al. [59]. The performance of wind turbines was also validated with dual-Doppler measurements in [60].

First evidence of the promising application of Doppler radar systems for forecasting purposes was documented by Hirth et al. [61]. An extreme wind ramp event observed by the Texas Tech University Ka-band radars at a wind farm in Oklahoma was presented. The authors merged dual-Doppler wind fields with operational data from 32 wind turbines to document the observed transient wind event and its effect on the wind turbines' performance. They also coupled data from a meteorological tower to analyze the weather conditions that originated the transient event.

Recently, it was shown that Doppler radar observations can be employed to derive minute-scale density forecasts of wind power. In [62] the authors proposed a methodology that uses dual-Doppler radar observations of wind speed and direction in front of a wind turbine to forecast the power generated in a probabilistic framework. In a case study, they predicted the power generated by seven turbines "free-wake" wind turbines in an offshore wind farm. Predictions were generated with a temporal resolution of one minute and with a lead time of five minutes. With their study, the authors showed that the radar-based forecasting model is able to outperform the persistence and climatology benchmarks in terms of overall forecasting skill and generate reliable density forecasts in the case of optimized trajectories.



Figure 6. One of the two Doppler radar units deployed for the BEACon project [59,62].

One of the main advantages of Doppler radars is the extended range they can measure (over 30 km). Additionally, the optimal trade-off between the temporal (one minute) and spatial (50 m) resolution of dual-Doppler radar measurements, compared to that of typical wind measurements from met masts or satellites, makes them promising candidates for minute-scale forecasting of wind power.

As with lidars, the same wind power forecasting process can be implemented to derive a wind power forecast. Besides, the fact that they can perform volumetric measurements (wind field measurements at multiple heights), allows to infer further information such as horizontal and vertical wind shear.

However, as with lidars, one of the main obstacles to the adoption of radar as a forecasting tool is the availability of the measurements. The radar measurement principle lies in the backscattering of particles in the air containing high humidity such as water droplets or ice crystals. Therefore, the quality of the measurements relies on the concentration of these particles in the air [57]. Besides, the relatively large dimensions of Doppler radars complicate their installation and reduces the range of possibilities for placing them, especially in offshore environments. The advantage of Doppler radar with respect to lidars is the maximum range that they can measure. However, compared to lidars, the wider beam width of radar results in larger beam spread at large ranges.

5.1.3. Weather Radars for Prediction of Strong Wind Power Fluctuations

Although we have mainly focused on the use of Doppler radars for forecasting applications, weather radars have been also identified as promising candidates for very short-term power forecasting of offshore wind power. Modern weather radars working in the C and X-band measure the intensity of precipitation. They are consequently able to anticipate precipitation fields associated with severe wind speed and power fluctuations with lead times of minutes to few hours, as they can measure up to few hundreds of kilometers, depending on the radar type. The capabilities of anticipating strong wind power fluctuations in offshore wind farms using local weather radars was introduced in [63,64]. In their work the authors were able to track the arrival of precipitation events to the surroundings of an offshore wind farm. These events were highly correlated with the strong observed power fluctuations. The authors also identified shortcomings of the use of weather radars for wind power forecasting, which included: interception of radar waves (cluttering), beam attenuation due to intense precipitation, anomalous propagation of the radar waves during specific atmospheric conditions, underestimation of precipitation reflectivity (beam filling) during convective events, and overshooting at long ranges due to the curvature of the Earth.

5.1.4. Lessons Learned With Remote Sensing Instruments in Minute-Scale Forecasting Projects

Several research projects have been conducted with the goal of integrating remote sensing measurement into real-time forecasting projects. For this purpose not only were scanning devices deployed, but also ground-based profiling devices. In the largest and longest measurement campaigns targeted towards real-time forecasting of wind energy in recent years were two projects funded by the United States Department of Energy. In the Wind Forecasting Improvement Project (WFIP I and II) [65] there were 12 wind profiling radars, 13 sodars and three lidars amongst other meteorological sensors used. Lidars as well as sodars are basic equipment used in meteorological data assimilation today and have been quality checked following meteorological standards through the Meteorological Assimilation Data Ingest System (MADIS) [66]. This was a necessary step in order to integrate the simulations into real-time model forecast systems [67]. In the second project, “Distributed Resource Energy Analysis and Management System (DREAMS) Development for Real-time Grid”, a number of sodars and lidars were used to enhance the Hawaiian system operator’s EMS (Energy Management System) tools for situational awareness of critical events [68]. Here, the instruments were used for the first time as part of an operational management system at a system operator in real-time.

From the above described studies and experimental measuring campaigns as well as real-time testing it can be concluded that remote sensing instruments need to be serviced and maintained similarly to any other real-time instrument. Skilled personnel are required in order for the the devices to run continuously and reliably.

The following list presents the major findings and recommended technical requirements from these studies and real-time tests towards ensuring high quality data during long-term real-time operation:

- Lightning protection and recovery strategy after lightning should be ensured.
- Instruments must be serviced and maintained by skilled staff.
- Version control must be maintained for signal processing.
- Measurements must be the originally measured values or technical requirements must include maintenance and software updates.
- Wind data should be measured at a height appropriate for the wind farm, either at hub height or preferable at both hub height and the lowest possible measuring height (e.g., 30 m).
- Remote sensing devices in complex terrain require special consideration.

From studied projects and measurement campaigns, it can be concluded that in active weather conditions, i.e., at the flat range of the power curve as well as under strong precipitation events, it must be expected that met-mast anemometers are more reliable than sodar or lidar devices. From a forecasting and operational monitoring perspective, conditions outside of the instrument's operating conditions are some of the most critical conditions for grid operation, such as storms with precipitation or high winds. Sodars are more prone to data delivery failures than lidar. In general, however, both devices suffer under non accessibility of measurement information in—for the grid operator—critical situations.

5.2. Statistical Time Series Models

Statistical approaches to forecasting problems mainly rely on deducing patterns from past observational data and extrapolating these relationships to predict future values over a desired time step. With wind energy applications in mind, in this section we consider the task of forecasting a one dimensional time series signal such as a wind speed measurement, or a SCADA source such as wind turbine or wind farm active power signal. The chosen forecast horizon should relate to the time resolution of available input data, and at minimum be one sample (time step) ahead to avoid errors introduced by interpolation. Statistical forecasting methods used on the minute scale are largely identical to techniques employed for longer horizons. The main differences being the temporal resolution of the data and the variability of the physical process being predicted (see Section 2).

Data acquisition systems are ordinarily capable of sampling and saving data at high frequency, although historically this data has not always been used nor recorded. For the purposes of minute-scale forecasting, 10-minute or hourly averaged data sets are not sufficient for capturing signal characteristics needed to construct and validate a well performing statistical model. For this reason we recommend that all data generators ensure that they have access to and are logging their high frequency data (both turbine and meteorological sources), and that the instruments are properly maintained. The lower bound of the recorded sampling rate should be at minimum twice the highest frequency in the analog signal you wish to capture, in order to avoid aliasing in the discrete signal transformation (Nyquist sampling theorem). In practice, 1 Hz (1 sample per second) is proposed as a compromise between functionality and transmission/storage considerations. This will allow for future model building and testing which can resolve fluctuations on the minute-scale.

Time series data contrasts to cross-sectional data in that it is naturally ordered in time. Samples which are closer together will normally express a higher correlation than those further apart. This temporal link should be explored through inspection of the autocorrelation and partial autocorrelation function of the time series before beginning any attempts to build a model.

There are often a number of characteristic sub-components embedded in the time series which can be obtained through decomposition techniques in order to normalise samples across time. Examples include differencing an integrated series, removing an overall trend (usually by either mean subtraction or model fitting to obtain the residuals), accounting for cyclic fluctuations, and adjusting for seasonal variations.

A common assumption made by statistical forecasting methods is that of stationarity. Stationary processes comprise of data where the mean, variance, and autocorrelation structure do

not change over time. By implementing the techniques described above, it is possible to transform a non-stationary time series into a stationary one which can be used with traditional forecasting methods.

Benchmarking in any forecasting exercise is crucial. Commonly for forecasting at these short timescales the persistence and climatology models are employed; these simple methods assume that the forecast for the target variable is the most recent available measurement or summary statistics of historical measurements, respectively. Statistical methods for wind speed and power forecasting are typically based on time-series models such as autoregressive [69] (AR) and autoregressive moving average (ARMA) [70,71] models as well as other soft computing techniques such as neural networks [72].

Purely AR models are formulated as a weighted combination of past observations (lags) where the coefficients are normally estimated via ordinary least squares regression. The order of the AR model, or maximum lag, is crucial and can be chosen most simply by inspection of the auto-correlation and partial auto-correlation functions of the signal. Cross-validation or an information criterion provide an alternative method for defining the model order. Domain knowledge of the local meteorological conditions can also be used to extend these simple models. For example, in certain regions the wind/power time series may exhibit strong diurnal trends which would necessitate the inclusion of time-of-day into the model.

Beyond time series models, machine learning techniques also are widely employed. These techniques can be more flexible than classic time series models in terms of easily allowing for more explanatory variables and are typically more naturally able to capture non-linear relationships. It should be noted that this comes at the expense of additional model tuning to optimize algorithm specific hyper-parameters and possible overfitting of the data unless careful cross-validation procedures are followed. Examples include artificial neural networks [72], hybrid multi-models with blending [73] together with feature selection [74], and penalized regression [75].

Artificial neural networks, particularly recurrent neural networks (RNN), have been widely applied for sequence prediction including time-series data. Long short-term memory (LSTM) networks are explicitly designed to capture data patterns of arbitrary lags, and assimilate long-term temporal dependencies [76]. This has led to numerous applications in energy forecasting which outperform traditional time-series modeling approaches. Wu et al. [77] demonstrates such a probabilistic 4-h ahead wind power forecast model employing a LSTM network architecture.

Statistical forecasting models can also be made dependent on the current behaviour of the target time-series or on exogenous variable(s). These are termed regime-switching models and can be based on unobserved regimes [78,79] or by observed regimes like atmospheric conditions [80,81]. It follows that these regimes can be derived from lidar/radar measurements [64]. The benefit of regime switching is that the statistical models can react faster to changing conditions, as opposed to having a fixed coefficient models or by tracking slower changes in behaviour via for instance an online update of the coefficient estimates.

Concurrent information from spatially distributed wind farm or met mast measurements also provide a route for improvements in forecast skill [82]. Multivariate forecasts which encode information on the spatio-temporal dependency of neighbouring sites can be tackled via a vector autoregressive models (VAR) at these time horizons. With an increasing number of sites, making sparse estimates of the coefficient matrices becomes more important, as does estimating them via efficient numerical procedures [83–85].

Forecast uncertainty at these horizons can also be accounted for via probabilistic density forecasts, quantiles, or prediction intervals [86]. These may be generated using parametric assumptions of the forecast distribution shape [69,83] or non-parametric techniques [87,88]. Uncertainty forecasts enable the user to manage risk in decision making and leverage more actionable information from their data, if information content is communicated properly [89].

These discussed statistical methods have been widely proven to increase forecast skill over persistence at time-horizons generally at a minimum of 10 min ahead. Further research is required

to evaluate the suitability of statistical methods below this time horizon and at what time range forward facing lidar/radar based systems or hybrid statistical and radar/lidar systems are a more suitable choice.

5.3. Statistical Data Assimilation Based on Physical Models

Data assimilation performs an essential role in the forecasts of wind power systems. While the concept is very inclusive, meaning assimilation of any data with any model, in this section, the term is used in more exclusive sense without addressing statistical time series models. Time series models are a special case of data assimilation where usually non-physical models are taken into consideration. This was discussed in the previous section. The concept is inherent from the fact that neither the model nor the observations are perfect. In order to have an accurate state of the system, the numerical model itself is not sufficient and therefore guidance from observations is required. This is even more so for weather forecast systems, where the system itself is very sensitive to initial conditions and boundary conditions. Data assimilation was first employed in engineering; however, today it is more than an engineering tool.

In summary, in the context of this review article, data assimilation is a technique to adopt multiple measurements and observations of different types into a 3-dimensional model space. In meteorology it is used to generate an initial state of the atmosphere from observations, i.e., an input field, together with boundary conditions to any numerical weather prediction (NWP) model.

Also for the renewable energy production, data assimilation and/or state estimation has an important role, for example in the assimilation of data into the control system on wind turbine or even wind farm level. System operators and wind farm operators require advanced knowledge of ramp-up and ramp-down events [90–92]. In a ramp/extreme event forecasting you want to analyze and use outliers in order to assess the risk of a critical ramp/event that is about to occur, while some data assimilation algorithms can dismiss outliers. The increased frequency of assimilation can address this challenge. The frequency of assimilation is important for ramp prediction, while the challenge comes from the model size and assimilation method chosen for the task; however, simplified models with higher frequencies can be adapted for the applications discussed here.

The work on data assimilation spans many disciplines and several decades in which many different methods have been developed to adapt the state of the atmosphere in numerical weather prediction models to large sets of measurements [93,94]. The initial development of data assimilation has started as an objective analysis (e.g., [95,96]), which is also referred to as successive correction methods.

This work was followed by optimum interpolation (OI) (e.g., [93,97]). Optimal Interpolation (OI) methods have led to development of variational methods in data assimilation, where constraints were introduced in variational data assimilation methods. These methods are namely 1DVAR, 2DVAR, 3DVAR (e.g., [98,99]) and 4DVAR (e.g., [100,101]) where D stands for Dimension. Variational approaches can be also formulated in the context of a Bayesian problem.

In parallel Kalman filter based approaches were developed (e.g., [102,103]). The Kalman filter is a sequential data assimilation technique and was introduced as an observer feedback control system. The main difference between 4DVAR and Kalman filters are the way that they address the mode and mean when the distributions are non-normal. There are several existing methods used in state estimation and/or data assimilation. Most of those methods build on the filtering theory introduced by Kalman and Bucy [104]. For the state estimation of linear Gaussian systems the original form of the Kalman filter has been widely applied. However, as it is linear it is not preferred for non-Gaussian and nonlinear systems [105,106]. Therefore techniques such as extended Kalman filter (EKF), ensemble Kalman filter (EnKF), unscented Kalman filter (UKF) and particle filter (PF) algorithms were developed [105,106] and applied to a wide range of use cases from low to high dimensional systems. EnKF method employs the linearization of the non-linearities with a Jacobian matrix, and also

employs Monte-Carlo methods to estimate the background covariance errors to introduce nonlinearities to Kalman filter (e.g., [102,107–109]).

Möhrlen et al. [36] found that some of the Kalman filter limitations in a meteorological context are, however, not a limitation in the wind power context, because the area of observational distribution is rather small, even if the area spans over an entire country. In atmospheric data assimilation the measurement data used is spread widely in space (globally), but is mostly sparse in time. In a wind power context, observations are concentrated in small areas with high time resolution. A classical KF approach would not make sense as models would have to generate forecasts in a small area, which is undesired, or it would require unrealistically many computing resources and observational input of meteorological variables [36]. The physical based ensemble prediction methods, especially the multi-scheme approach, has been found as the most efficient method due to its ability to generate spread that has a physical/meteorological meaning in any time step with a much smaller ensemble size [110].

One non-exclusive approach that can address the above approximations on linearities and Gaussianity is particle filter (PF); however, it brings computational cost with it [111]. The computational cost is also related to ensemble size; however, this can be addressed adaptively with careful selection of ensembles introduced by Uzunoğlu [112,113]. The computational complexity in the above summarized methods can be addressed in the subspace of ensembles that was one of the focuses of the Maximum Likelihood Ensemble Filter (MLEF) that employs ensembles in the pre-conditioner. The computational time is reduced by optimizing a nonlinear cost function in low dimensional sampling space for Hessian information through maximum likelihood practice which also addresses the stochasticity and the discontinuity. This method has been applied to many disciplines such as power systems as well as to the wind energy industry [27,114]. In the workshop, the successful application of this method to second scales were presented.

5.4. Extreme Event Forecasting Models

Extreme events in a meteorological sense are events that deviate from the mean and exceed beyond specific threshold limits. In the power system, extreme events can occur under meteorological average conditions as well and not be considered extreme, when meteorological threshold values, such as wind speed, are exceeded. The differences are mainly due to constraints in the transmission lines and the supply and demand relationship. Only in areas where wind turbines shut down due to high wind speeds- so called high-speed shutdowns, can such wind speeds challenge both life and the ability to safely control the grid.

The way to deal with extreme events in both meteorology and the power industry is by applying uncertainty forecasts that provide an objective measure of the possible extreme. Deterministic forecasts cannot serve such situations, as they are tuned for best average conditions, i.e., in the setup, statistical training and model output statistics, outliers and extremes are filtered out. While statistical approaches can be used in many life science applications, in power system applications it is crucial to employ an approach that provides a valid uncertainty of the forecast inclusive of extremes in every hour of the forecast. Such extreme forecasts must be established based on probabilities computed from a probabilistic prediction system that can take the spatial and temporal scales into consideration in order to capture the temporal evolution and spatial scale of, e.g., low pressure systems that contain wind speeds leading to large scale shut-down of wind farms.

This can for example be provided by a physical approach based on a NWP ensemble that ideally contains all extreme values inherent in the approach without the requirement of statistical training such as the multi-scheme method. Alternative solutions may exist from statistical approaches by employing an extreme event analysis to a statistical ensemble (e.g., [89]). However, statistical approaches are always limited to past climatology and require large amounts of data. The requirement for such forecasts is that they must be able to provide probabilities of extreme events, where each forecast or “forecast member” provides a valid and consistent scenario of the event. The probabilities need to be

suitable solutions for a decision process. They can be computed for very critical and less critical events, depending on the end-users' requirements.

In meteorology the use of sophisticated observational instrumentation for data assimilation problems is an ongoing transformation throughout the last decades. As new technologies become available that in some way are able to reflect some part of the atmospheric system, where the model systems require parameterizations, such instrumentation is usually tested in research campaigns and then deployed at specific locations (e.g., [110,115–118]). Transferring this knowledge to the assimilation of wind power observations that are irreversible in their nature is more complex. Nevertheless, a unified methodology that is able to decide on the value of an observational signal and its impact on the total system is required to solve this task.

In Section 5.1.2 we learned that radar measurements can be used for forecasting, but require transformation algorithms to be useful for the forward propagation of the data signals. The Kalman Filter techniques are practical approaches that have inherent capabilities to transform such data signals and use them in convective-scale data assimilation tasks (see, e.g., [117,118]).

With ensemble Kalman filter techniques, the input ensemble data can also be used to deal with the uncertainty of different types of measurements, also in the transformation phase of more advanced data signal technologies if the signals are in relation with the target parameter [36]. The example in Figure 7 shows the functionality of an inverted Kalman Filter approach for the assimilation of point measurements in (wind and solar) power space with a multi-scheme ensemble approach described in [36]. In this schematic, power signals from wind and/or solar generating units and other related meteorological observation are assimilated with the help of a so-called multi-scheme ensemble, a physical based ensemble approach [36]. The ensemble contains 75 members with 13 different parameterisation schemes, 10 from the physical part of the model and 3 dynamical parameterization schemes. Details of this system can be found in [38,119]. By applying physically possible outcomes from a 3-dimensional simulation of the atmosphere and transforming this into a vector in direct relation to the observation, a physically consistent data assimilation is possible. This approach is a major improvement and enhancement in energy meteorology as it opens the door to resolutions in time and space with minimal computational requirements for short-term or minute-scale forecasting, as the computational expensive work resides in the 6-hourly forecasting cycle of the ensemble. The assimilation of local measurements can be done on minute basis [36].

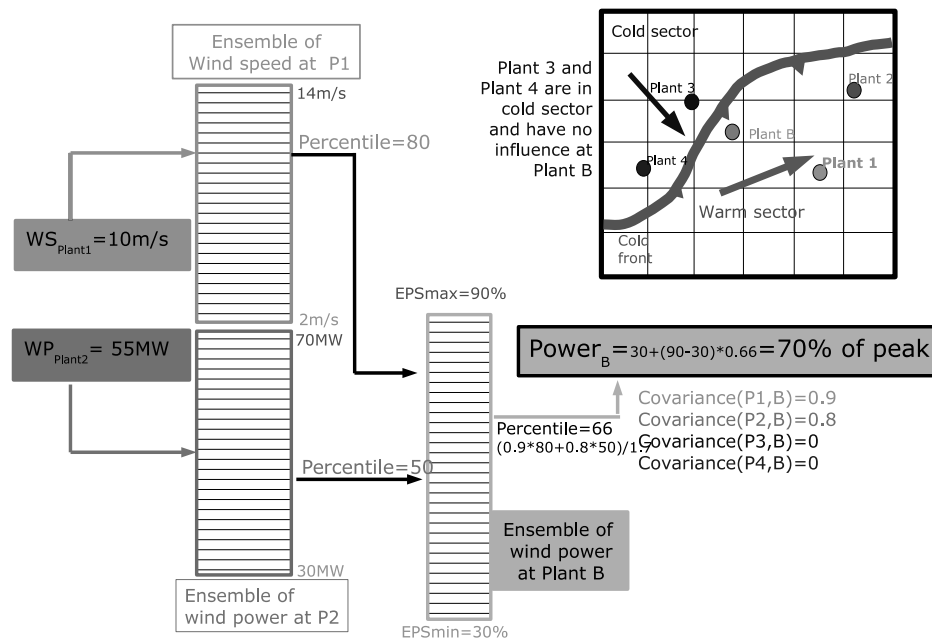


Figure 7. Functionality of the inverted Ensemble Kalman Filter when using different kind of measurements. P stands for Plant.

5.5. Overview of Methods for Minute-Scale Forecasting

Table 4 provides an overview and summary of the different minute-scale prediction methods, their forecasting horizons as well as advantages and limitations to the adoption of the methods. It also lists next steps that are suggested as a way to overcome the limitations.

During the discussions at the workshop and also whilst writing this paper, it became clear that as of now we are not in a position to recommend a minute-scale forecasts method that performs well in all conditions and for all use cases. Depending on the data input and the method, there are certain advantages and limitations that are inherent to the respective forecast types and methods. Remote sensing-based models for example work with preview data of the wind field several kilometers upstream of a wind turbine, but rely on the data availability of the remote sensing device which strongly depends on atmospheric conditions. Time series models are flexible in terms of input data, have a proven track record in power forecasting and have been used to a great extent across multiple disciplines. However, they rely on historical data and are therefore not likely to perform well for events outside of normal conditions. Data assimilation models have a wide range of applicability and can incorporate different types of measurements, but there is a lack of experience in the wind power industry.

What we propose as next steps for all methods are further investigations of the methods for different use cases, and also a cross-disciplinary exchange of different method experts. Remote sensing and NWP experts for example have to work together to see what the benefit in assimilating scanning-lidar data into a physical model is. Neural-network experts could implement real-time preview data from radar devices and investigate the possibility to forecast wind ramps when not only relying on historical data. The solution to minute-scale forecasting will possibly lie in the diversity of available input data and a forecasting method, that is tailored to the end user's needs.

Table 4. Overview of methods for minute-scale forecasting.

Type	Method	Input Data	Forecast Horizon	Advantages	Limitations	Next steps	Ref.
Remote sensing based models	Scanning lidar-based propagation models	Lidar data	1 s–30 min	<ul style="list-style-type: none"> - Comprehensive knowledge of wind field several kilometres upstream - Scanning of vertical wind profiles for, e.g., detection of low level jets - Compact size → flexible measurement campaigns, cost-competitive to met masts 	<ul style="list-style-type: none"> - Fluctuating measurement range and forecast horizon due to environmental conditions - Ideal measurement setup for forecasting not clear, no standard available - Need for post processing is challenging in a real-time environment 	<ul style="list-style-type: none"> - Need for a reliable fallback method if no data available - Investigation of different lidar cases to find best campaign setup → standards definition. - Regular service and calibration → decreases risk of faulty signal processing but increases costs. 	[14,42,43,45,46,49,50]
	Radar-based density models	Doppler radar data	1 min–<1 h	<ul style="list-style-type: none"> - Extended maximum measurement range (up to 35 km) - Reconstructed wind fields with high temporal (1-min) and spatial (50 m) resolution - Volumetric measurements allow us to resolve information over the whole rotor area 	<ul style="list-style-type: none"> - Data availability highly depends on the meteorological conditions - Large beam spread at large ranges → increased uncertainty - Large dimensions of the radar → complex installation 	<ul style="list-style-type: none"> - Explore deeply and define the conditions and locations for optimal measurements - Investigate added value of installing a radar system for ramp event prediction in a wind farm cluster 	[61,62]
	Radar-based power fluctuation forecast	C and X-band weather radar data	10 min–2 h	<ul style="list-style-type: none"> - Precipitation data highly correlates with strong fluctuations - Extended maximum measurement range → 60–240 km - Spatial resolution: 0.5–2 km/Temporal resolution: 1–15 min 	<ul style="list-style-type: none"> - Clutter due to: wind turbine interference, meteorological targets - Measurement uncertainty increases with precipitation intensity - Underestimation of precipitation reflectivity during convective events 	<ul style="list-style-type: none"> - Further development of pattern recognition techniques is required - Investigation on new wind turbine clutter detection and mitigation techniques - Improve cooperation between weather radars and wind energy communities 	[63,64]
Time series models	AR AR(I)MA	SCADA, met-mast data, remote sensing	30 s–24 h	<ul style="list-style-type: none"> - Easy to implement and demonstrates higher skill than persistence for most lead times - Proven track record in power forecasting and a large volume of reference work across quantitative disciplines on how to design, build, and validate models 	<ul style="list-style-type: none"> - Relies on historical data, therefore not likely to perform well for events outside of normal conditions - Data quality concerns for, e.g., sensor faults 	<ul style="list-style-type: none"> - Collect, store, and label high-frequency data for building and testing statistical models at the 1 s–10 min horizons - Utilize statistical model benchmarks in all minute-scale forecasting trials for comparison 	[69–71,80,120]
	Neural networks	Same as above	15 s–24 h	<ul style="list-style-type: none"> - Ability to learn complex non-linear relationships - Flexible model construction in terms of inputs/outputs compared to ARIMA methods 	<ul style="list-style-type: none"> - Computationally demanding, large datasets required for training and validation - Requires significant background knowledge to understand and implement, added complexity not always an improvement 	<ul style="list-style-type: none"> - Continue monitoring developments as the field is rapidly evolving - Leverage this power and flexibility to extract value from high dimensional data (e.g., from remote sensing instruments) 	[72,73,77,120]
Data assimilation models	VAR models		look ahead time	<ul style="list-style-type: none"> - Methods have a wide range of applicability and can incorporate different types of measurements 	<ul style="list-style-type: none"> - Lack of use cases in power industry to prove the value of such information 	<ul style="list-style-type: none"> - Setting up measurement campaigns with open data access for research and development 	
	Kalman filters	lidar, radar, sodar, cup / sonic anemometers	3 h–12 h for analysis, forecast	<ul style="list-style-type: none"> - Extreme event analysis benefits from a diversity of observations 	<ul style="list-style-type: none"> - Lack of standards and transparency of data exchange in power markets 	<ul style="list-style-type: none"> - Increased collaborative research between meteorology and wind power forecasting community 	[27,36,67,68,110]
	Ensemble Kalman filters		1 min–12 h	<ul style="list-style-type: none"> - Expensive ensemble computations not required on minute scale, but, e.g., 6 h-schedule—inverted EnKF: first weather dependent short-term algorithm for wind power apps 		<ul style="list-style-type: none"> - Development of standards in power industry for instrumentation and measurement accuracies for real-time usage 	

6. Challenges for the Implementation of Minute-Scale Forecasting in Large Energy Systems

There are several use cases for predictions shorter than 1 to 2 h. In Australia, the system runs on a 5-min schedule [121] and requires renewable energy and load forecasts on those time scales. In Germany, renewable energy plants can be pre-qualified to participate in the reserve market, and need to predict their possible power with less than 5% error in the pilot phase and less than 3.3% in the implementation phase. This is calculated in one-minute intervals. In Denmark, with hourly wind penetrations of over 140%, the grid is run proactively in hourly steps, predicting the imbalance and reacting accordingly on the basis of spatio-temporal forecasts [122]. So the use cases for minute scale forecasts are present, and the best forecasts require upstream information in real time.

In a large energy system with moderate penetration from wind sources, a system operator can choose to outsource balancing of wind. This is the approach chosen widely in central Europe. A major reason behind the liberalized strategy in Europe is a wish to make the market more competitive which has happened faster than anybody expected in both Denmark (2009) and Germany (2012) [123] with the result of lower spot market prices in the NordPool market and the German-Austrian component of EPEX.

The difference between a TSO and a power trader's prioritized optimization lies in the target horizon. The trader is looking up to several weeks ahead, while the TSO's optimization horizon is over the entire year. In particular once the power trading is privatized and handled by private balance responsible parties, then the TSO lacks information about the generation and must rely on the information from the trading companies. In Germany, the TSOs have today little control of renewable energy generation and rely on out-sourced solutions for critical system information to a large degree which has not been considered acceptable for many years from a system security perspective.

Although Germany has the highest capacity of wind and solar generation in Europe, it is apparent that the system lacks information for optimization. This is seen in frequent downregulation of wind farms during day-time and recovery during the middle of the night, often many hours after the wind has dropped again. This process has become highly inefficient in recent years, because there are no requirements for wind farms to provide real-time data to the system operator.

The German experience shows that wind energy loses efficiency and value unless there are obligations for wind farms to provide data required by various forecasting and system operation processes.

Based on this experience, it is crucial to define standards regarding the setup and maintenance of instrumentation, collection and provision of data, as well as required quality of data. Beside the standards, in transparent markets the grid codes should also contain a clear definition about the rights on the use and the obligation to provide the data. Without such regulations, the required quality is hard to achieve in order to improve forecasts. Corrupt and wrongly calibrated instrumentation can do more damage to a forecast than not having data. This is one of the greatest challenges at present and the reason for slow progress on minute-scale forecasting. Especially in large systems such as Germany with many thousands of individual wind turbines and small wind farms, this is a difficult challenge to overcome. Nevertheless, the need to make appropriate changes to the grid codes is the same for all markets.

7. Conclusions

Minute-scale forecasting of wind power is a discipline that is becoming crucial to accomplish in globally transitioning power systems with increasing amounts of variable generating power sources from renewables. The participants of the collaborative IEA Wind Task 32 and 36 workshop have established a framework for forecasting at the minute scale and have discussed new techniques that will push the limits of state-of-the-art forecasting methods.

Three applications were identified that can benefit from minute-scale forecasting and their respective forecasting horizons. Wind turbine and wind farm controllers need wind speed forecasts with the shortest horizon to optimize the turbine and farm operation. The task of balancing the power grid, and finally optimizing energy markets which rely heavily on precise wind power forecasts on a slightly longer time scale as well.

To carry out forecasts that range from 1 second to 60 min, forecasters have the choice between different methods (Figure 8). In our discussions at the workshop and this review paper we differentiate between using preview data from remote sensing devices, time series models that deduce patterns from observational data to predict future values and finally methods that are based on data assimilation into physical models. These assimilated data can originate both from remote sensing devices or other existing observational data sources i.e., meteorological masts and wind turbine data.

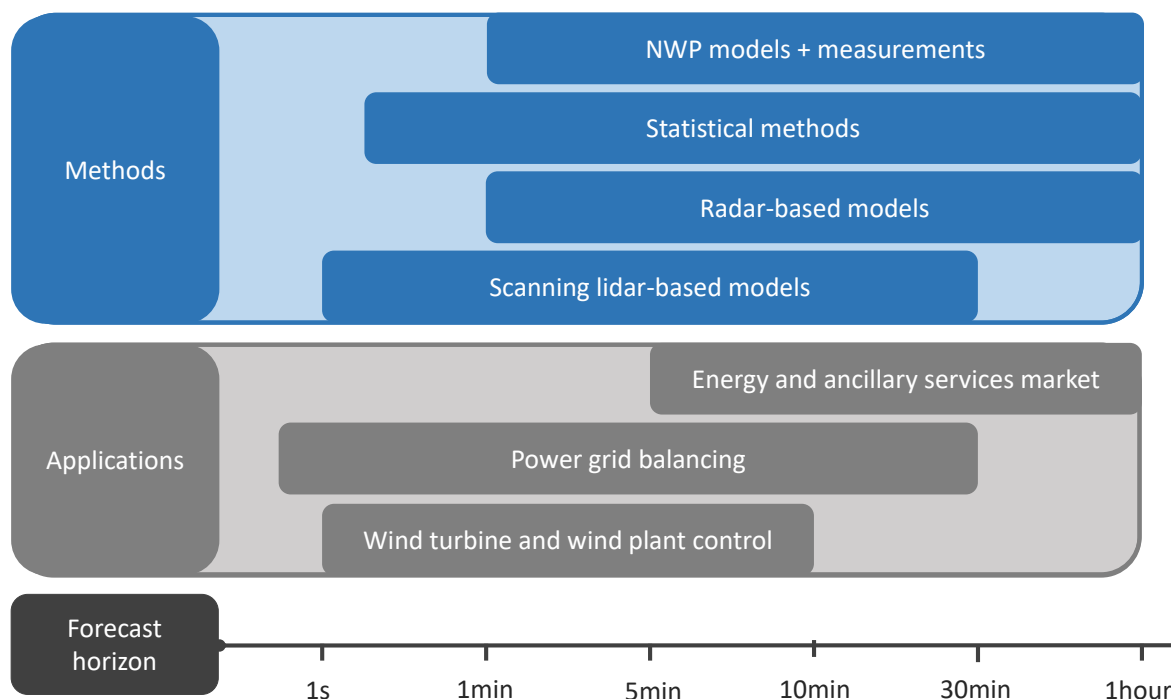


Figure 8. Overview of forecast horizons of different wind energy applications and forecast methods in the second and minute scale.

By investigating more deeply the respective methods it became clear that they all have advantages, but also limitations that need to be overcome in order to achieve reliable forecasts for commercial use. The following list provides an overview of focus areas for the near future to advance further with minute-scale forecasting:

- **Research requirements.** At this point, many methods are still under development. There are several open questions to solve and the optimal forecasting techniques for the different applications have not been concluded. It is also not sufficiently demonstrated that all methods add value. More research and especially more measurement campaigns using different types of instrumentation (lidars, radars, sodars and in situ measurements such as cup and sonic anemometers etc.) to compare their benefits and disadvantages as individual inputs but also as combinations of inputs is required. Both measurement experts and weather modelers need to collaborate closely to find solutions.

- Data requirements. All forecasting methods rely on data. This might sound obvious, but what is needed is high resolution, high quality data delivered in real-time to forecast systems. Wind turbine or wind farm operators often only log 10-min averages of their operational data. However, to train and validate models, high frequency data is necessary.
- Requirement for standards. End users have more confidence in data when the collection and use of the data is supported by Recommended Practices and standards. Community-driven recommended practices are available for some applications of wind lidar, but not in the context of forecasting.
- Expert training. As with any emerging technology, there are a limited number of experts that know how to carry out a remote sensing measurement campaign, feed data into neural networks or are capable of assimilating data into a NWP model. This forms a barrier to the widespread commercialization of minute-scale forecasting. IEA Wind Tasks provide an ideal platform for the international exchange and dissemination of knowledge order to establish more widespread training in the above mentioned areas.

Supplementary Materials: IEA Wind Task 32 is operated by the Chair of Wind Energy at the Institute of Aircraft Design at the Faculty of Aerospace Engineering at the University of Stuttgart. More details about IEA Wind Task 32, including minutes from the workshops and other documents, can be found at www.ieawindtask32.org. IEA Wind Task 36 Forecasting is operated by Gregor Giebel of DTU Wind Energy at Risø, Denmark. See www.ieawindforecasting.dk for more information. General information about IEA Wind can be found at www.ieawind.org. IEA Wind TCP functions within a framework created by the International Energy Agency. Views, findings, and publications of the IEA Wind TCP do not necessarily represent the views or policies of the IEA Secretariat or of all its individual member countries. IEA Wind TCP is part of IEA's Technology Collaboration Programme (TCP).

Author Contributions: I.W. was a co-organizer of the workshop, led the paper and wrote the abstract, introduction, Section 5.1.1, conclusion, some section introductions, and edited all sections. L.V. Sanmartin was a co-organizer of the workshop, was a co-editor of this paper, led Sections 2, 3.3 and 5.1.2 and contributed to Sections 5.1 and 5.1.1. E.S. was a co-organizer of the workshop, led Section 5.2, and contributed in Sections 2, 5.1, 5.1.1 and 5.5. C.M. led and wrote Sections 4 and 5.1.4, contributed to Sections 3.3, 5.2, 5.1 and 6 and wrote Sections 5.3 and 5.4 together with B.U. who also wrote Section 3.2. C.G. contributed to Section 5.2. G.G. contributed to Section 4. D.S. led Section 3.1. A.K. and all other co-authors participated in the paper review and revision process.

Funding: This publication was supported by the Open Access Publishing Fund of the University of Stuttgart and has received funding from the European Union's Horizon 2020 research and innovation program under the Marie Skłodowska-Curie Grant No. 642108 and the Danish EUDP project Wind Task 36 Forecasting Danish Consortium under the contract no. 2015-II-64015-0559.

Acknowledgments: We would like to thank DTU Wind Energy (Risø campus) for graciously hosting the workshop, and all of the workshop participants who contributed their ideas and knowledge.

Conflicts of Interest: The authors declare no conflict of interest.

References

1. Giebel, G.; Brownsword, R.; Kariniotakis, G.; Denhard, M.; Draxl, C. *The State-Of-The-Art in Short-Term Prediction of Wind Power*; Technical Report; Technical University of Denmark (DTU): Roskilde, Denmark, 2011.
2. Fraile, D.; Mbistrova, A. *Wind in Power 2017: Annual Combined Onshore and Offshore Wind Energy Statistics*; Technical Report; WindEurope: Brussels, Belgium, 2018.
3. Fraile, D.; Komusanac, I. *Wind energy in Europe: Outlook to 2022*; Technical Report; WindEurope: Brussels, Belgium, 2018.
4. Larsén, X.; Larsen, S.; Lundtang Petersen, E. Full-Scale Spectrum of Boundary-Layer Winds. *Bound.-Layer Meteorol.* **2016**, *159*, 349–371. [[CrossRef](#)]
5. Apt, J. The spectrum of power from wind turbines. *J. Power Sources* **2007**, *169*, 369–374.
6. Vincent, C.L.; Trombe, P.J. 8—Forecasting intrahourly variability of wind generation. In *Renewable Energy Forecasting*; Kariniotakis, G., Ed.; Woodhead Publishing Series in Energy; Woodhead Publishing: Cambridge, UK, 2017; pp. 219–233.

7. Sørensen, P.; Cutululis, N.A.; Viguera-Rodríguez, A.; Madsen, H.; Pinson, P.; Jensen, L.E.; Hjerrild, J.; Donovan, M. Modelling of power fluctuations from large offshore wind farms. *Wind Energy* **2008**, *11*, 29–43. [[CrossRef](#)]
8. Akhmatov, V.; Abildgaard, H.; Pedersen, J.; Eriksen, P. Integration of Offshore Wind Power into the Western Danish Power System. In Proceedings of the 2005 Copenhagen Offshore Wind International Conference and Exhibition, Copenhagen, Denmark, 26–28 October 2005.
9. van Kooten, G.C. Wind power: The economic impact of intermittency. *Let. Spat. Resour. Sci.* **2010**, *3*, 1–17. [[CrossRef](#)]
10. Ela, E.; Kirby, B. *ERCOT Event on February 26, 2008: Lessons Learned*; Technical Report; National Renewable Energy Laboratory: Golden, CO, USA, 2008.
11. Gallego-Castillo, C.; Cuerva-Tejero, A.; Lopez-Garcia, O. A review on the recent history of wind power ramp forecasting. *Renew. Sustain. Energy Rev.* **2015**, *52*, 1148–1157. [[CrossRef](#)]
12. Würth, I.; Ellinghaus, S.; Wigger, M.; Niemeier, M.J.; Clifton, A.; Cheng, P.W. Forecasting wind ramps: Can long-range lidar increase accuracy? *J. Phys. Conf. Ser.* **2018**, *1102*, 012013. [[CrossRef](#)]
13. Dunne, F.; Pao, L.Y.; Schlipf, D.; Scholbrock, A.K. Importance of lidar measurement timing accuracy for wind turbine control. In Proceedings of the 2014 American Control Conference, Portland, OR, USA, 4–6 June 2014; pp. 3716–3721. [[CrossRef](#)]
14. Schlipf, D. Lidar-Assisted Control Concepts for Wind Turbines. Ph.D. Thesis, University of Stuttgart, Stuttgart, Germany, 2015.
15. Gros, S. An economic NMPC formulation for wind turbine control. In Proceedings of the Conference on Decision and Control, Florence, Italy, 10–13 December 2013.
16. Schlipf, D.; Schlipf, D.J.; Kühn, M. Nonlinear model predictive control of wind turbines using LIDAR. *Wind Energy* **2013**, *16*, 1107–1129. [[CrossRef](#)]
17. Hau, E. *Wind Turbines: Fundamentals, Technologies, Application, Economics*; Springer: Berlin, Germany, 2006.
18. Kragh, K.A.; Hansen, M.H.; Mikkelsen, T. Improving Yaw Alignment Using Spinner Based LIDAR. In Proceedings of the 49th AIAA Aerospace Sciences Meeting Including the New Horizons Forum and Aerospace Exposition, Orlando, FL, USA, 4–7 January 2011.
19. Schlipf, D.; Kapp, S.; Anger, J.; Bischoff, O.; Hofsaß, M.; Rettenmeier, A.; Smolka, U.; Kühn, M. Prospects of Optimization of Energy Production by LiDAR Assisted Control of Wind Turbines. In Proceedings of the European Wind Energy Association Annual Event, Amsterdam, The Netherlands, 29 November–1 December 2011.
20. Bossanyi, E. Combining induction control and wake steering for wind farm energy and fatigue loads optimisation. *J. Phys. Conf. Ser.* **2018**, *1037*. [[CrossRef](#)]
21. Ela, E.; Gevorgian, V.; Fleming, P.; Zhang, Y.; Singh, M.; Muljadi, E.; Scholbrook, A.; Aho, J.; Buckspan, A.; Pao, L.; et al. *Active Power Controls From Wind Power: Bridging the Gaps*; Technical Report; National Renewable Energy Laboratory: Golden, CO, USA, 2014.
22. Gebraad, P.M.O. Data-Driven Wind Plant Control. Ph.D. Thesis, Delft University of Technology, Delft, The Netherlands, 2014.
23. Momoh, J.A. *Smart Grid: Fundamentals of Design and Analysis*; John Wiley & Sons: Hoboken, NJ, USA, 2012; Volume 63.
24. Menin, M.; Uzunoglu, B. Parametric Sensitivity Study for Wind Power Trading through Stochastic Reserve and Energy Market Optimization. In Proceedings of the 2015 Seventh Annual IEEE Green Technologies Conference, New Orleans, LA, USA, 15–17 April 2015; pp. 82–87. [[CrossRef](#)]
25. Uzunoglu, B.; Bayazit, D. A generic resampling particle filter joint parameter estimation for electricity prices with jump diffusion. In Proceedings of the 2013 10th International Conference on the European Energy Market (EEM), Stockholm, Sweden, 27–31 May 2013; pp. 1–7. [[CrossRef](#)]
26. Uzunoglu, B.; Akifülker, M.; Bayazit, D. Particle filter joint state and parameter estimation of dynamic power systems. In Proceedings of the 2016 57th International Scientific Conference on Power and Electrical Engineering of Riga Technical University (RTUCon), Riga, Latvia, 13–14 October 2016; pp. 1–7. [[CrossRef](#)]
27. Uzunoglu, B.; Ülker, M.A. Maximum Likelihood Ensemble Filter State Estimation for Power Systems. *IEEE Trans. Instrum. Meas.* **2018**, *67*, 2097–2106. [[CrossRef](#)]

28. Ülker, M.A.; Uzunoğlu, B. Simplex optimization for particle filter joint state and parameter estimation of dynamic power systems. In Proceedings of the IEEE EUROCON 2017-17th International Conference on Smart Technologies, Ohrid, Macedonia, 6–8 July 2017; pp. 399–404. [CrossRef]
29. Eriksson, R.; Modig, N.; Elkington, K. Synthetic inertia versus fast frequency response: A definition. *IET Renew. Power Gener.* **2018**, *12*, 507–514. [CrossRef]
30. Díaz-González, F.; Haub, M.; Sumper, A.; Gomis-Bellmuntac, O. Participation of wind power plants in system frequency control: Review of grid code requirements and control methods. *Renew. Sustain. Energy Rev.* **2014**, *43*, 551–564. [CrossRef]
31. Mazzi, N.; Pinson, P. 10 - Wind power in electricity markets and the value of forecasting. In *Renewable Energy Forecasting*; Kariniotakis, G., Ed.; Woodhead Publishing Series in Energy; Woodhead Publishing: Cambridge, UK, 2017; pp. 259–278.
32. EPEX Spot SE. *Intraday Continuous: Intraday Lead Times*. Available online: https://www.epexspot.com/en/product-info/intradaycontinuous/intraday_lead_time (accessed on 10 December 2018).
33. NordPool. *Intraday Trading*. Available online: <https://www.nordpoolgroup.com/trading/intraday-trading/> (accessed on 10 December 2018).
34. Energy Exchange Istanbul (EXIST). *Intra-day Market*. Available online: <https://www.epias.com.tr/en/intra-day-market/phases> (accessed on 10 December 2018).
35. BSP South Pool. *Intraday Continuous Market*. Available online: <https://www.bsp-southpool.com/intraday-continuous-market.html> (accessed on 10 December 2018).
36. Möhren, J.J. *A New Algorithm for Upscaling and Short-Term Forecasting of Wind Power Using Ensemble Forecasts*; Energynautics GmbH: Bremen, Germany, 2009.
37. 50Hertz.; Amprion.; Tennet.; TransnetBW. *Leitfaden zur Präqualifikation von Windenergieanlagen zur Erbringung von Minutenreserveleistung im Rahmen einer Pilotphase / Guidelines for Prequalification of Wind Turbines to provide Minute Reserves during a Pilot Phase*; Technical Report; German Transmission System Operators: Berlin, Germany, 2016.
38. Pahlow, M.; Möhrlein, C.; Jørgensen, J. Application of cost functions for large-scale integration of wind power using a multi-scheme ensemble prediction technique; In *Optimization Advances in Electric Power Systems*; NOVA Publisher: Hauppauge, NY, USA, 2008.
39. IEC. *Wind Energy Generation Systems—Part 12-1: Power Performance Measurements of Electricity Producing Wind Turbines*; Standard; International Electrotechnical Commission: Geneva, Switzerland, 2017.
40. Clifton, A.; Clive, P.; Gottschall, J.; Schlipf, D.; Simley, E.; Simmons, L.; Stein, D.; Trabucchi, D.; Vasiljevic, N.; Würth, I. IEA Wind Task 32: Wind Lidar - Identifying and mitigating barriers to the adoption of wind lidar. *Remote Sens.* **2018**, *10*, 413–433. [CrossRef]
41. Emeis, S.; Harris, M.; Banta, R.M. Boundary-layer anemometry by optical remote sensing for wind energy applications. *Meteorol. Z.* **2007**, *16*, 337–347. [CrossRef]
42. Simley, E.; Pao, L.Y.; Frehlich, R.; Jonkman, B.; Kelley, N. Analysis of light detection and ranging wind speed measurements for wind turbine control. *Wind Energy* **2014**, *17*, 413–433. [CrossRef]
43. Clifton, A.; Boquet, M.; Burin Des Roziers, E.; Westerhellweg, A.; Hofsass, M.; Klaas, T.; Vogstad, K.; Clive, P.; Harris, M.; Wylie, S.; et al. *Remote Sensing of Complex Flows by Doppler Wind Lidar: Issues and Preliminary Recommendations*; Technical Report TP-5000-64634; National Renewable Energy Laboratory: Golden, CO, USA, 2015.
44. Vasiljević, N.; Palma, J.M.; Angelou, N.; Carlos Matos, J.; Menke, R.; Lea, G.; Mann, J.; Courtney, M.; Frölen Ribeiro, L.; Gomes, V.M. Perdigoão 2015: Methodology for atmospheric multi-Doppler lidar experiments. *Atmos. Meas. Tech.* **2017**, *10*, 3463–3483. [CrossRef]
45. Courtney, M.; Simon, E. *Deploying Scanning Lidars at Coastal Sites*; DTU Wind Energy: Roskilde, Denmark, 2016.
46. Valldecabres, L.; Peña, A.; Courtney, M.; von Bremen, L.; Kühn, M. Very short-term forecast of near-coastal flow using scanning lidars. *Wind Energy Sci.* **2018**, *3*, 313–327. [CrossRef]
47. Simon, E.; Courtney, M.; Vasiljevic, N. Minute-Scale Wind Speed Forecasting Using Scanning Lidar Inflow Measurements. *Wind Energy Sci. Discuss.* **2018**. [CrossRef]
48. Kokhanovsky, A. *Aerosol Optics: Light Absorption and Scattering by Particles in the Atmosphere*; Springer: Berlin/Heidelberg, Germany, 2008.

49. Würth, I.; Brenner, A.; Wigger, M.; Cheng, P.W. How far do we see? Analysis of the measurement range of long-range lidar data for wind power forecasting. In Proceedings of the German Wind Energy Conference DEWEK, Bremen, Germany, 17–18 October 2017.
50. *Performance Verification of Galion*; Technical Report Report 13001; Deutsche Windguard: Varel, Germany, 2013.
51. Bradley, S. Wind speed errors for LIDARs and SODARs in complex terrain. *IOP Conf. Ser. Earth Environ. Sci.* **2008**, *1*, 012061. [[CrossRef](#)]
52. Bradley, S.; Perrott, Y.; Behrens, P.; Oldroyd, A. Corrections for wind-speed errors from Sodar and Lidar in complex terrain. *Bound.-Layer Meteorol.* **2012**, *143*, 37–48. [[CrossRef](#)]
53. Bradley, S.; von Hünenbein, S.; Mikkelsen, T. A bistatic Sodar for precision wind profiling in complex terrain. *J. Atmos. Ocean. Technol.* **2012**, *29*, 1052–1061. [[CrossRef](#)]
54. Kindler, D.; Oldroyd, A.; MacAskill, A.; Finch, D. An eight month test campaign of the Qinetiq Zephyr system: Preliminary results. *Meteorol. Z.* **2007**, *16*, 479–489. [[CrossRef](#)]
55. Yang, Q.; Berg, L.; Pekour, M.; Fast, J.; Newsom, R. Evaluation of WRF-Predicted Near-Hub-Height Winds and Ramp Events over a Pacific Northwest Site with Complex Terrain. *J. Appl. Meteorol. Climatol.* **2013**, *52*, 1753–1763. [[CrossRef](#)]
56. Wulfmeyer, V.; Turner, D.D.; Baker, B.; Banta, R.; Behrendt, A.; Bonin, T.; Brewer, W.A.; Buban, M.; Choukulkar, A.; Dumas, E.; et al. A New Research Approach for Observing and Characterizing Land–Atmosphere Feedback. *Bull. Am. Meteorol. Soc.* **2018**, *99*, 1639–1667. [[CrossRef](#)]
57. Hirth, B.D.; Schroeder, J.L.; Gunter, W.S.; Guynes, J.G. Measuring a Utility-Scale Turbine Wake Using the TTUKa Mobile Research Radars. *J. Atmos. Ocean. Technol.* **2012**, *29*, 765–771. [[CrossRef](#)]
58. Hirth, B.D.; Schroeder, J.L.; Gunter, W.S.; Guynes, J.G. Coupling Doppler radar-derived wind maps with operational turbine data to document wind farm complex flows. *Wind Energy* **2015**, *18*, 529–540. [[CrossRef](#)]
59. Nygaard, N.G.; Newcombe, A.C. Wake behind an offshore wind farm observed with dual-Doppler radars. *J. Phys. Conf. Ser.* **2018**, *1037*, 072008. [[CrossRef](#)]
60. Marathe, N.; Swift, A.; Hirth, B.; Walker, R.; Schroeder, J. Characterizing power performance and wake of a wind turbine under yaw and blade pitch. *Wind Energy* **2016**, *19*, 963–978. [[CrossRef](#)]
61. Hirth, B.D.; Schroeder, J.L.; Irons, Z.; Walter, K. Dual-Doppler measurements of a wind ramp event at an Oklahoma wind plant. *Wind Energy* **2016**, *19*, 953–962. [[CrossRef](#)]
62. Valldecabres, L.; Nygaard, N.G.; Vera-Tudela, L.; von Bremen, L.; Kühn, M. On the Use of Dual-Doppler Radar Measurements for Very Short-Term Wind Power Forecasts. *Remote Sens.* **2018**, *10*, 1701. [[CrossRef](#)]
63. Trombe, P.J.; Pinson, P.; Vincent, C.; Bøwith, T.; Cutululis, N.A.; Draxl, C.; Giebel, G.; Hahmann, A.N.; Jensen, N.E.; Jensen, B.P.; et al. Weather radars—The new eyes for offshore wind farms? *Wind Energy* **2014**, *17*, 1767–1787. [[CrossRef](#)]
64. Trombe, P.; Pinson, P.; Madsen, H. Automatic Classification of Offshore Wind Regimes With Weather Radar Observations. *IEEE J. Sel. Top. Appl. Earth Observ. Remote Sens.* **2014**, *7*, 116–125. [[CrossRef](#)]
65. Freedman, J.M.; Manobianco, J.; Schroeder, J.; Ancell, B.; Brewster, K.; Basu, S.; Banunarayanan, V.; Hodge, B.M.; Flores, I. *The Wind Forecast Improvement Project (WFIP): A Public/Private Partnership for Improving Short Term Wind Energy Forecasts and Quantifying the Benefits of Utility Operations—The Southern Study Area*; AWS Truepower Tech. Rep. DOE-AWST-04420, U.S. DOE Office of Energy Efficiency and Renewable Energy (EERE); Wind and Hydropower Technology Program (EE-2B); Washington, DC, USA, 2014. [[CrossRef](#)]
66. Meteorological Assimilation Data Ingest System (MADIS). Available online: <https://madis.ncep.noaa.gov/> (accessed on 10 December 2018).
67. Wilczak, J.; Finley, C.; Freedman, J.; Cline, J.; Bianco, L.; Olson, J.; Djalalova, I.; Sheridan, L.; Ahlstrom, M.; Manobianco, J.; et al. The Wind Forecast Improvement Project (WFIP): A Public–Private Partnership Addressing Wind Energy Forecast Needs. *Bull. Am. Meteorol. Soc.* **2015**, *96*, 1699–1718. [[CrossRef](#)]
68. Nakafuji, D. *Distributed Resource Energy Analysis & Management System (DREAMS) Development for Real-time Grid Operations*; Technical Report DOE-EE0006331-FTR1; Hawaiian Electric Company to U.S. Department of Energy: Honolulu, HI, USA, 2016.
69. Pinson, P. Very-short-term probabilistic forecasting of wind power with generalized logit-normal distributions. *J. R. Stat. Soc. Ser. C Appl. Stat.* **2012**, *61*, 555–576. [[CrossRef](#)]
70. Torres, J.; García, A.; Blas, M.D.; Francisco, A.D. Forecast of hourly average wind speed with ARMA models in Navarre (Spain). *Sol. Energy* **2005**, *79*, 65–77. [[CrossRef](#)]

71. Erdem, E.; Shi, J. ARMA based approaches for forecasting the tuple of wind speed and direction. *Appl. Energy* **2011**, *88*, 1405–1414. [[CrossRef](#)]
72. Li, G.; Shi, J. On comparing three artificial neural networks for wind speed forecasting. *Appl. Energy* **2010**, *87*, 2313–2320. [[CrossRef](#)]
73. Feng, C.; Cui, M.; Hodge, B.M.; Zhang, J. A data-driven multi-model methodology with deep feature selection for short-term wind forecasting. *Appl. Energy* **2017**, *190*, 1245–1257. [[CrossRef](#)]
74. Niu, T.; Wang, J.; Zhang, K.; Du, P. Multi-step-ahead wind speed forecasting based on optimal feature selection and a modified bat algorithm with the cognition strategy. *Renew. Energy* **2018**, *118*, 213–229. [[CrossRef](#)]
75. Pinson, P. Introducing distributed learning approaches in wind power forecasting. In Proceedings of the 2016 International Conference on Probabilistic Methods Applied to Power Systems (PMAPS), Beijing, China, 16–20 October 2016; pp. 1–6. [[CrossRef](#)]
76. Hochreiter, S.; Schmidhuber, J. Long Short-Term Memory. *Neural Comput.* **1997**, *9*, 1735–1780. [[CrossRef](#)] [[PubMed](#)]
77. Wu, W.; Chen, K.; Qiao, Y.; Lu, Z. Probabilistic short-term wind power forecasting based on deep neural networks. In Proceedings of the 2016 International Conference on Probabilistic Methods Applied to Power Systems (PMAPS), Beijing, China, 16–20 October 2016; pp. 1–8. [[CrossRef](#)]
78. Ailliot, P.; Monbet, V. Markov-switching autoregressive models for wind time series. *Environ. Model. Softw.* **2012**, *30*, 92–101. [[CrossRef](#)]
79. Pinson, P.; Madsen, H. Adaptive modelling and forecasting of offshore wind power fluctuations with Markov-switching autoregressive models. *J. Forecast.* **2012**, *31*, 281–313. [[CrossRef](#)]
80. Browell, J.; Drew, D.R.; Philippopoulos, K. Improved very short-term spatio-temporal wind forecasting using atmospheric regimes. *Wind Energy* **2018**, *21*, 968–979. [[CrossRef](#)]
81. Browell, J.; Gilbert, C. Cluster-based regime-switching AR for the EEM 2017 Wind Power Forecasting Competition. In Proceedings of the 2017 14th International Conference on the European Energy Market (EEM), Dresden, Germany, 6–9 June 2017; pp. 1–6. [[CrossRef](#)]
82. Hering, A.S.; Genton, M.G. Powering Up With Space-Time Wind Forecasting. *J. Am. Stat. Assoc.* **2010**. [[CrossRef](#)]
83. Dowell, J.; Pinson, P. Very-Short-Term Probabilistic Wind Power Forecasts by Sparse Vector Autoregression. *IEEE Trans. Smart Grid* **2016**, *7*, 763–770. [[CrossRef](#)]
84. Messner, J.W.; Pinson, P. Online adaptive lasso estimation in vector autoregressive models for high dimensional wind power forecasting. *Int. J. Forecast.* **2018**. [[CrossRef](#)]
85. Cavalcante, L.; Bessa, R.J.; Reis, M.; Browell, J. LASSO vector autoregression structures for very short-term wind power forecasting. *Wind Energy* **2017**, *20*, 657–675. [[CrossRef](#)]
86. Zhang, Y.; Wang, J.; Wang, X. Review on probabilistic forecasting of wind power generation. *Renew. Sustain. Energy Rev.* **2014**, *32*, 255–270. [[CrossRef](#)]
87. Jeon, J.; Taylor, J.W. Using Conditional Kernel Density Estimation for Wind Power Density Forecasting. *J. Am. Stat. Assoc.* **2012**, *107*, 66–79. [[CrossRef](#)]
88. Wan, C.; Xu, Z.; Pinson, P.; Dong, Z.Y.; Wong, K.P. Probabilistic Forecasting of Wind Power Generation Using Extreme Learning Machine. *IEEE Trans. Power Syst.* **2014**, *29*, 1033–1044. [[CrossRef](#)]
89. Bessa, R.J.; Möhrlein, C.; Fundel, V.; Siefert, M.; Browell, J.; Haglund El Gaidi, S.; Hodge, B.M.; Cali, U.; Kariniotakis, G. Towards Improved Understanding of the Applicability of Uncertainty Forecasts in the Electric Power Industry. *Energies* **2017**, *10*, 1402. [[CrossRef](#)]
90. Yıldırım, N.; Uzunoglu, B. Data Mining via Association Rules for Power Ramps Detected by Clustering or Optimization. In *Transactions on Computational Science XXVIII: Special Issue on Cyberworlds and Cybersecurity*; Springer: Berlin/Heidelberg, Germany, 2016; pp. 163–176.
91. Yıldırım, N.; Uzunoglu, B. Spatial Clustering for Temporal Power Ramp Balance and Wind Power Estimation. In Proceedings of the 2015 Seventh Annual IEEE Green Technologies Conference, New Orleans, LA, USA, 15–17 April 2015; pp. 214–220. [[CrossRef](#)]
92. Yıldırım, N.; Uzunoglu, B. Association Rules for Clustering Algorithms for Data Mining of Temporal Power Ramp Balance. In Proceedings of the 2015 International Conference on Cyberworlds (CW), Visby, Sweden, 7–9 October 2015; pp. 224–228. [[CrossRef](#)]

93. Dey, C.H. The Evolution of Objective Analysis Methodology at the National Meteorological Center. *Weather Forecast.* **1989**, *4*, 297–312. [[CrossRef](#)]
94. Ide, K.; Courtier, P.; Ghil, M.; Lorenc, A.C. Unified Notation for Data Assimilation: Operational, Sequential and Variational. *J. Meteorol. Soc. Jpn. Ser. II* **1997**, *75*, 181–189. [[CrossRef](#)]
95. Cressman, G.P. An operational objective analysis system. *Mon. Weather Rev.* **1959**, *87*, 367–374. [[CrossRef](#)]
96. Gandin, L. *Objective Analysis of Meteorological Fields*; Translated from the Russian; Israel Program for Scientific Translation: Jerusalem, Israel, 1965.
97. Kanamitsu, M. Description of the NMC Global Data Assimilation and Forecast System. *Weather Forecast.* **1989**, *4*, 335–342. [[CrossRef](#)]
98. Courtier, P.; Andersson, E.; Heckley, W.; Vasiljevic, D.; Hamrud, M.; Hollingsworth, A.; Rabier, F.; Fisher, M.; Pailleux, J. The ECMWF implementation of three-dimensional variational assimilation (3D-Var). I: Formulation. *Q. J. R. Meteorol. Soc.* **1998**, *124*, 1783–1807. [[CrossRef](#)]
99. Wu, W.S.; Purser, R.J.; Parrish, D.F. Three-Dimensional Variational Analysis with Spatially Inhomogeneous Covariances. *Mon. Weather Rev.* **2002**, *130*, 2905–2916. [[CrossRef](#)]
100. Courtier, P.; Thépaut, J.N.; Hollingsworth, A. A strategy for operational implementation of 4D-Var, using an incremental approach. *Q. J. R. Meteorol. Soc.* **1994**, *120*, 1367–1387. [[CrossRef](#)]
101. Zupanski, D. A General Weak Constraint Applicable to Operational 4DVAR Data Assimilation Systems. *Mon. Weather Rev.* **1997**, *125*, 2274–2292. [[CrossRef](#)]
102. Evensen, G. Sequential data assimilation with a nonlinear quasi-geostrophic model using Monte Carlo methods to forecast error statistics. *J. Geophys. Res. Oceans* **1994**, *99*, 10143–10162. [[CrossRef](#)]
103. Turner, M.; Walker, J.; Oke, P. Ensemble member generation for sequential data assimilation. *Remote Sens. Environ.* **2008**, *112*, 1421–1433. Remote Sensing Data Assimilation Special Issue. [[CrossRef](#)]
104. Kalmann, R.; Bucy, R.S. New Results in Linear Filtering and Prediction Theory. *ASME. J. Basic Eng.* **1961**, *83*, 95–108. [[CrossRef](#)]
105. Jazwinski, A. *Stochastic Processes and Filtering Theory*; Mathematics in Science and Engineering; Elsevier Science: Amsterdam, The Netherlands, 1970.
106. Ristic, B.; Arulampalam, S.; Gordon, N. *Beyond the Kalman Filter: Particle Filters for Tracking Applications*; The Artech House Radar Library, Artech House, Incorporated: Boston, MA, USA 2004.
107. Todling, R.; Cohn, S.E.; Sivakumaran, N.S. Suboptimal Schemes for Retrospective Data Assimilation Based on the Fixed-Lag Kalman Smoother. *Mon. Weather Rev.* **1998**, *126*, 2274–2286. [[CrossRef](#)]
108. Anderson, J.L. An Ensemble Adjustment Kalman Filter for Data Assimilation. *Mon. Weather Rev.* **2001**, *129*, 2884–2903. [[CrossRef](#)]
109. Houtekamer, P.L.; Mitchell, H.L. A Sequential Ensemble Kalman Filter for Atmospheric Data Assimilation. *Mon. Weather Rev.* **2001**, *129*, 123–137. [[CrossRef](#)]
110. Meng, Z.; Zhang, F. Tests of an Ensemble Kalman Filter for Mesoscale and Regional-Scale Data Assimilation. Part II: Imperfect Model Experiments. *Mon. Weather Rev.* **2007**, *135*, 1403–1423. [[CrossRef](#)]
111. Xiong, X.; Navon, I.M.; Uzunoglu, B. A Note on the Particle Filter with Posterior Gaussian Resampling. *Tellus A Dyn. Meteorol. Oceanogr.* **2006**, *58*, 456–460. [[CrossRef](#)]
112. Uzunoglu, B.; Fletcher, S.J.; Zupanski, M.; Navon, I.M. Adaptive ensemble reduction and inflation. *Q. J. R. Meteorol. Soc.* **2007**, *133*, 1281–1294. [[CrossRef](#)]
113. Uzunoglu, B. Adaptive observations in ensemble data assimilation *Comput. Methods Appl. Mech. Eng.* **2007**, *196*, 4207–4221. [[CrossRef](#)]
114. Zupanski, M. Maximum Likelihood Ensemble Filter: Theoretical Aspects. *Mon. Weather Rev.* **2005**, *133*, 1710–1726. [[CrossRef](#)]
115. Houtekamer, P.L.; Mitchell, H.L.; Pellerin, G.; Buehner, M.; Charron, M.; Spacek, L.; Hansen, B. Atmospheric Data Assimilation with an Ensemble Kalman Filter: Results with Real Observations. *Mon. Weather Rev.* **2005**, *133*, 604–620. [[CrossRef](#)]
116. Hamill, T.M.; Snyder, C. Using Improved Background-Error Covariances from an Ensemble Kalman Filter for Adaptive Observations. *Mon. Weather Rev.* **2002**, *130*, 1552–1572. [[CrossRef](#)]
117. Snyder, C.; Zhang, F. Assimilation of Simulated Doppler Radar Observations with an Ensemble Kalman Filter. *Mon. Weather Rev.* **2003**, *131*, 1663–1677. [[CrossRef](#)]
118. Zhang, F.; Snyder, C.; Sun, J. Impacts of Initial Estimate and Observation Availability on Convective-Scale Data Assimilation with an Ensemble Kalman Filter. *Mon. Weather Rev.* **2004**, *132*, 1238–1253. [[CrossRef](#)]

119. Möhrle, C. Uncertainty in Wind Energy Forecasting. Ph.D. Thesis, National University of Ireland, Cork, Ireland, 2004.
120. Simon, E. Minute-Scale Wind Forecasting Using Lidar Inflow Measurements. Ph.D. Thesis, Danmarks Tekniske Universitet, Roskilde, Denmark, 2019, to be submitted for publication.
121. DISPATCH; Technical Report; Australia Electricity Market Operator (AEMO): Melbourne, Australia, 2018.
122. Borup, L. IEA Wind Task 36 Forecasting Webinar: How to Run 40% RE in the Danish System. Available online: <https://www.youtube.com/watch?v=IGhUasWctUM> (accessed on 3 December 2018).
123. Bundesnetzagentur, *EEG in Zahlen 2016*; Bundesnetzagentur: Bonn, Germany, 2016.



© 2019 by the authors. Licensee MDPI, Basel, Switzerland. This article is an open access article distributed under the terms and conditions of the Creative Commons Attribution (CC BY) license (<http://creativecommons.org/licenses/by/4.0/>).

CHAPTER 3

Experimental results

3.1 Structure of the results chapter

This chapter contains the novel scientific research carried out during the PhD project. The studies are formulated as a series of continuing works which build upon lessons learned from the previous investigation(s). In each case, the field campaign is described in detail, along with processing steps of the dataset and a description of the methodology used for generating the forecasts with sufficient detail to be reproduced. In the end, results of each technique are evaluated and conclusions are presented.

The first portion (Sections 3.2 and 3.3) relates to the initial feasibility study (WAFFLE campaign). The next segment (Sections 3.4, 3.5, 3.6, and 3.7) contains work within the full-scale Østerild Balcony campaign. Finally, the third component (Sections 3.8, 3.9, and 3.10) relate to the terminal LASCAR campaign.

The main results from the two comprehensive experiments are presented in manuscript form, which are intended for publication. The former is currently under review at the journal *Wind Energy Science*, while the latter is in draft form targeted to *Atmospheric Measurement Techniques*.

All work contained herein (research and writing) has been performed by the PhD student under counsel of the supervision team and exchange hosts. Cooperation with technical staff during the experimental periods has been attributed in the relevant sections and in the published datasets.

3.2 Initial investigation: WAFFLE experiment

Introduction

As a first step towards assessing the feasibility of the project goals, a short measurement campaign was conducted to gather data for performing exploratory analysis and for investigating the core assumption of advection based flow transport.

Work contained in this section is an expanded version of a poster presentation given at the 3rd International Conference on Future Technologies in Wind Energy (WindTech 2017 in Boulder, Colorado).

A 3-week field experiment named 'WAFFLE' took place between March 23rd and April 6th, 2017 at DTU-Risø campus. A single long-range scanning lidar (Leosphere WindCube 400S) was deployed at ground level in the field of DTU's research wind turbines.

The dataset has been made publicly available in DTU's data repository (E. Simon and Lea, 2019b) and a subset was also utilized in an applied workshop with data and code examples available in E. Simon, 2018.

The lidar was set to perform scans facing west to measure the dominant wind inflow to the test site. A PPI (sector scan) configuration was used with a sampling rate of 23 seconds, maximum range of 9.6 km, and scanning elevation of 3 degrees (see depiction in Figure 3.1).



Figure 3.1: Left: Photo of scanning lidar taken during experiment. Right: Aerial view of measurement setup. The radius of the arc is 9.6 km.

The elevation angle was necessary in order for the beam to clear the vegetation and other infrastructure present at the site. This however, resulted in a height change as a function of range at a relationship of 52 meters per kilometer. During the data analysis stage, it was determined that this elevation gradient caused a significant issue, both due

to the probe volume averaging being affected by wind shear and the lack of correlation of winds at higher heights- the furthest range gate (9.6 km) being at 500 m AGL while the first (288 m) corresponding to 15 m AGL.

Methods

A rudimentary but accepted method to normalize the height differences was applied using the wind profile power law. This is a simple engineering model based on empirical relationships between wind speeds at two heights. During periods of neutral atmospheric conditions, this approach has been well demonstrated to perform similarly to the logarithmic wind profile law above the surface layer and up to the height of the boundary layer. This approach is also favoured because it requires no information about the friction velocity or surface roughness which would normally originate from met-mast observations.

$$u = u_r \left(\frac{z}{z_r} \right)^\alpha \quad (3.1)$$

Where u and z are the target wind speed and height, u_r and z_r are the reference wind speed and height, and α is an empirically derived coefficient, often given as $1/7 \approx 0.143$ for neutral atmospheric stability over open land. A sensitivity analysis of the α value has not been performed. Peterson and Hennessey, 1978 has however investigated this at the Risø site, and concluded that the $1/7$ value provides conservative but reasonable results and that the total mean wind power density estimate is not particularly sensitive to the choice of α .

A 2-day period with westerly winds and neutral/near-neutral stability was chosen and two range gates (RG) were selected which were spaced reasonably far apart but within a range of heights relevant for wind energy purposes. Measurements at the 1200 m RG distance (62 m AGL) and the 1800 m RG distance (93 m AGL) were reconstructed into horizontal wind vector components using the IVAP (integrating velocity azimuth process) algorithm from Liang, 2007 which are given in Equations 3.2 and 3.3. From there, the scalar horizontal wind speeds and directions were obtained (Equations 3.4 and 3.5).

$$u = \frac{\sum_{\theta_{start}}^{\theta_{stop}} (U_r * \cos \theta) * \sum_{\theta_{start}}^{\theta_{stop}} (\sin^2 \theta) - \sum_{\theta_{start}}^{\theta_{stop}} (U_r * \sin \theta) * \sum_{\theta_{start}}^{\theta_{stop}} (\cos \theta * \sin \theta)}{\sum_{\theta_{start}}^{\theta_{stop}} (\cos^2 \theta) * \sum_{\theta_{start}}^{\theta_{stop}} \sin^2 \theta - \sum_{\theta_{start}}^{\theta_{stop}} (\cos \theta * \sin \theta)^2} \quad (3.2)$$

$$v = \frac{\sum_{\theta_{start}}^{\theta_{stop}} (U_r * \sin \theta) * \sum_{\theta_{start}}^{\theta_{stop}} (\cos^2 \theta) - \sum_{\theta_{start}}^{\theta_{stop}} (U_r * \cos \theta) * \sum_{\theta_{start}}^{\theta_{stop}} (\cos \theta * \sin \theta)}{\sum_{\theta_{start}}^{\theta_{stop}} (\cos^2 \theta) * \sum_{\theta_{start}}^{\theta_{stop}} (\sin^2 \theta) - \sum_{\theta_{start}}^{\theta_{stop}} (\cos \theta * \sin \theta)^2} \quad (3.3)$$

$$U_h = \sqrt{u^2 + v^2} \quad (3.4)$$

$$\psi = \arctan2(v, u) \quad (3.5)$$

Where θ are the range of azimuth angles of the PPI scan, U_r are the corresponding radial velocity measurements, U_h is the scalar horizontal wind speed, and ψ is the wind direction.

Measurements spanning April 7-8 (7226 23-second samples or approximately 46 hours) were used for the following investigation. The methods utilize reconstructed lidar data at two positions which have been height corrected to 93 m AGL relative to the lidar's telescope: The further upwind position (1800 m RG), and the closer downwind position (1200 m RG). The downwind position is treated as a reference, and three forecasting methods have been performed.

The lead time for the forecasts was set at 70-seconds. This is derived from the theoretical mean advection time by considering the average wind speed (8.55 m/s) during the period together with the horizontal travel distance between the two points (600 m).

The first method is a persistence benchmark, which simply assumes that the wind speed will remain unchanged over the forecast horizon from the last available measurement. For this, only the reference signal is used (i.e. not the upwind measurements).

The second method, called 'scan-shifting', uses measurements at the upwind position (with no additional modelling) from the current time to predict wind speeds for the downwind position at a given time in the future (current time + forecast length). As the scan rate of the lidar is fixed at 23-seconds, a shift of 3 scans (69-seconds) was used to match the chosen forecast length.

A demonstration of the scan-shift method is shown in Figure 3.2 from April 8th of the WAFFLE experiment. When comparing the two signals in real time, a phase error is apparent. After shifting the upwind signal as a function of scan-times, the signals converge to a large degree.

As a further sanity check of the scan-shift method, upwind measurements were shifted by a range of scan-times and cross-correlated with the reference values to determine if a peak is present at the number of scans corresponding to our mean advection rate and chosen forecast length. Figure 3.3 shows this result, where a clear correlation peak can be seen at the number of scan-times corresponding with the theoretical position.

The final method constitutes building a regression model which takes the upwind measurements as an input to predict the downwind wind speed at the same forecast length. As the number of samples is small, the support vector regression (SVR) method from Drucker et al., 1996 with radial basis function (RBF) kernel was used. This was implemented using the scikit-learn library using recommended parameter values given in the documentation (Scikit-learn, 2018). The model was trained on 40% of the available

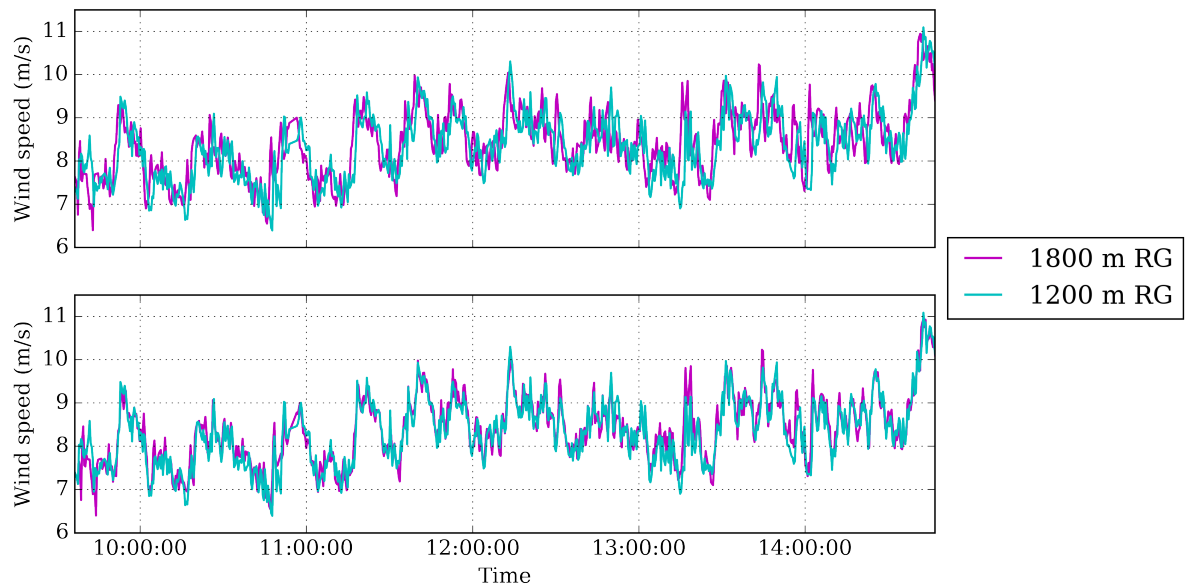


Figure 3.2: Time series example of the scan-shift method. Top: Reconstructed wind speeds at the two range gates in real time. Bottom: Upwind signal shifted by 3 scan-times to demonstrate agreement with downwind signal.

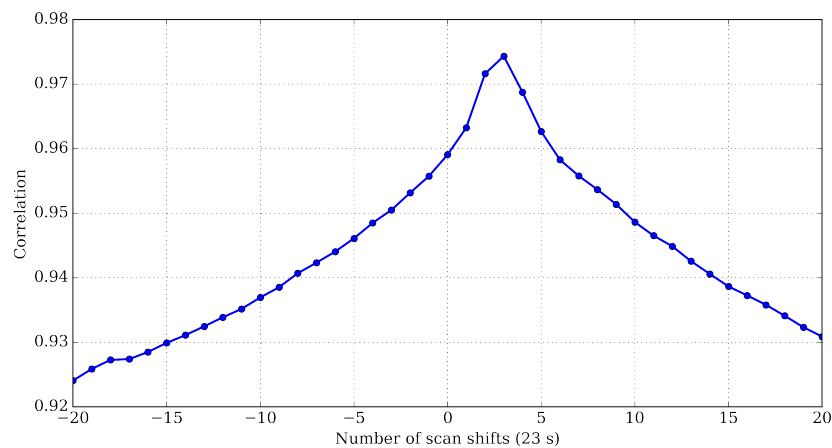


Figure 3.3: Cross-correlation function for a range of scan-shifts between the upwind and downwind measurements. A peak exists at the expected location corresponding to the mean advection time.

data. After fitting to the in-sample data, the model was used to make predictions for the remaining 60% of the dataset. The model was also applied to the entire dataset. This approach is not endorsed as it evaluates the model on data which it has already been optimized on. Since accuracy metrics were similar in both the train and test datasets, it was done anyway to allow for comparison with the other methods by generating the same number of samples.

In addition to evaluating forecast performance on wind speeds, a transformation to wind power was made using a power curve model (Figure 3.4). This illustrates a generic turbine model where units are expressed such that a value of one represents the wind turbine generator's rated power. The nonlinear power curve perverts forecast error impacts at different wind speeds, so it is pertinent to also inspect errors in the power domain.

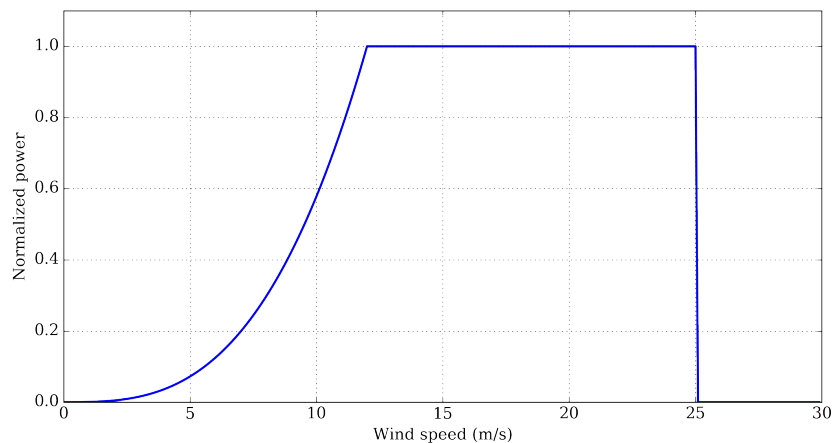


Figure 3.4: Power curve of generic wind turbine. Normalized such that a value of one represents the turbine's full rated power.

Results

An overall results comparison of the three methods is presented in Figure 3.5, both for wind speed and wind power. The two lidar approaches have improved significantly over the persistence method, with a reduction in root-mean-squared-errors (RMSE) of 20% for wind speed and 30% for wind power. Persistence performs well at very low wind speeds (below 5 m/s), but displays larger amounts of scatter at higher speeds. A possible explanation for this is that lower wind speeds are often associated with the presence of a stable boundary layer which is composed of lower levels of ambient turbulence. There does not appear to be a marked difference in performance between the scan-shift and SVR methods.

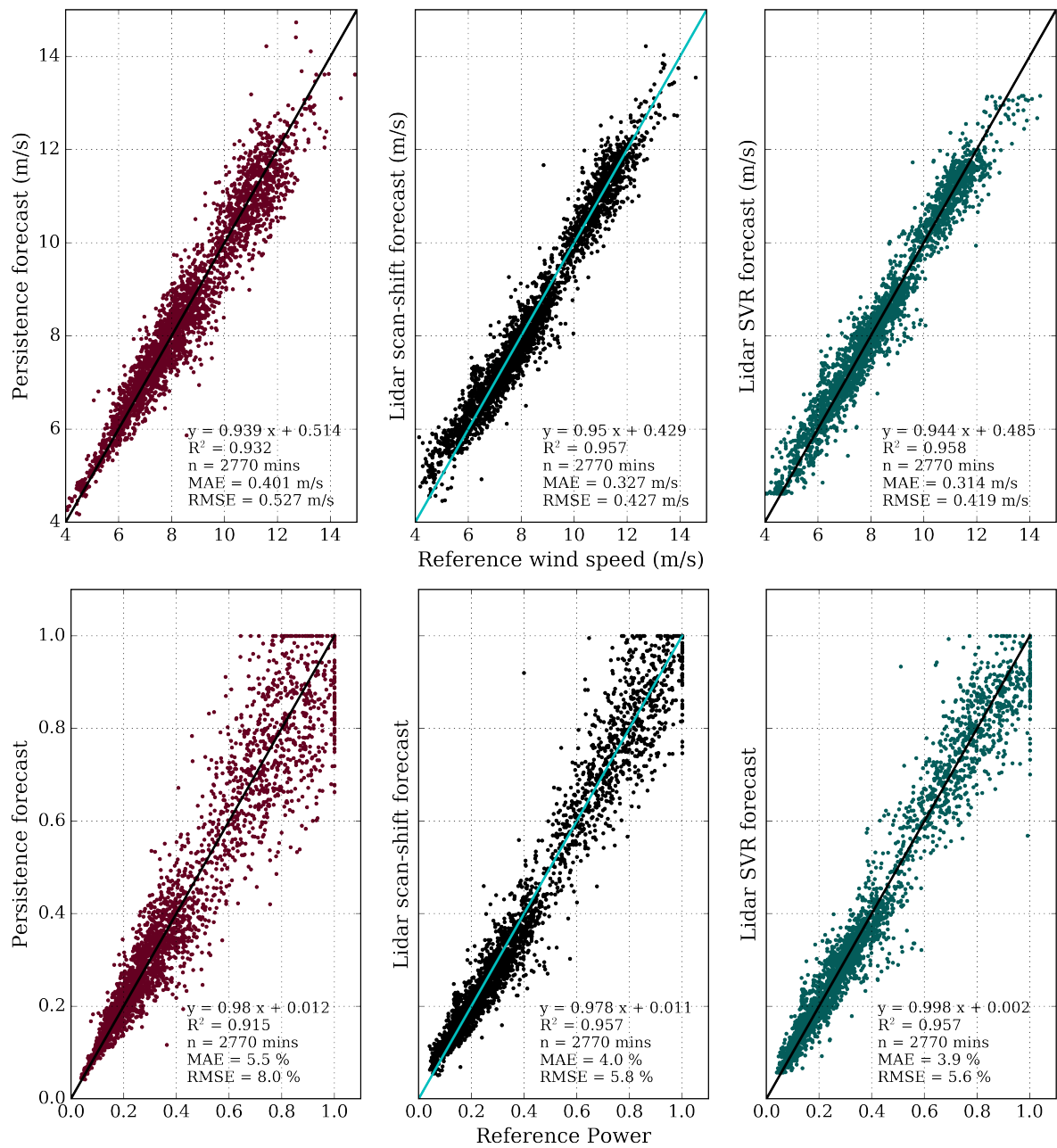


Figure 3.5: Comparison of three approaches with line $y=x$ also shown. The top row presents the wind speed results, while the bottom row is in the normalized wind power domain. The left panes are persistence, middle panes are the lidar scan-shift method, and right panes are the lidar SVR approach. General linear model fit parameters and error metrics between the forecast and reference values are annotated.

Conclusions

In summary, two novel forecasting methods have been applied using upwind lidar measurements to generate 1-minute (actually 69 s) ahead wind speed and power forecasts which significantly outperform the persistence benchmarks. The promising results achieved promote further development of the concept. Adjustments to the measurement setup are strongly recommended in future field campaigns, in order to avoid issues arising from sampling horizontal winds across a sloped plane. For this reason, the extended measurement range of the 400S scanning lidar was not capitalized upon in this particular study.

3.3 Addendum: Key results and lessons learned

- A short pilot experiment was carried out to investigate the use of upwind lidar measurements for minute-scale forecasting.
- The inclined measurement plane resulted in difficulties relating positions that were spaced kilometers apart due to the height difference between range gates.
- The empirical space-time correlation function between upwind and downwind measurements matched well to the theoretical approximation using the mean speed advection of the horizontal winds.
- Two novel forecasting methods using upwind lidar measurements were implemented to predict 1-minute ahead wind speeds at the downwind reference position. A persistence benchmark was also performed.
- The two lidar methods have demonstrated superior performance against the persistence benchmark, with similar error metrics between each other (both reducing RMSE wind speed errors by 20%).
- Forecast performance has also been evaluated in the wind power domain by applying a wind turbine power curve model. The lidar methods have also outperformed the benchmark by a 30% reduction in RMSE.

3.4 Introduction to second study: Østerild Balconies experiment

Building upon the methods and results of the initial investigation, a full scale experiment was planned in conjunction with the New European Wind Atlas (NEWA) project. A primary objective of the campaign was to collect data for the purpose of developing a minute-scale wind forecasting system using upwind observations from the scanning lidars. The resulting Østerild Balconies experiment provides cross-sectional scans of the horizontal wind by performing PPI scans at a height raised above the ground. This avoids the wind shear and height difference problems revealed in the initial investigation.

An in-depth report of the experiment and research results are presented in the open access journal article Section 3.5, which is expanded upon in Addendum 1 (Section 3.6).

The data set and campaign metadata have been published on DTU's data repository (E. Simon and Vasiljevic, 2018).

3.5 Minute-Scale Wind Speed Forecasting Using Scanning Lidar Inflow Measurements

Minute-Scale Wind Speed Forecasting Using Scanning Lidar Inflow Measurements

Elliot Simon, Michael Courtney, and Nikola Vasiljevic

Technical University of Denmark, Department of Wind Energy (Risø Campus), Roskilde, Denmark

Correspondence: Elliot Simon <ellsim@dtu.dk>

1 Abstract

Wind turbines and wind farms lack information about upstream wind conditions which are ultimately converted into electricity. Remote sensing instruments such as compact pulsed scanning wind lidars can observe the incoming wind field at large distances (up to 10 km) ahead of a wind farm and provide spatial and temporal information about the inflow on operational timeframes
5 not feasible with numerical weather models. On very-short horizons (below 1-hour lead times), the persistence method is commonly used, which fails to capture the unsteady state of the atmosphere and can introduce costly errors into the power system by means of imbalances.

A method of measuring, processing, and predicting site-specific 1-60 minute ahead wind speeds is proposed using machine learning methods applied to lidar observations from a field experiment in western Denmark. A direct multi-step forecast strategy
10 is implemented using Stochastic Gradient Descent Regression (SGDR) with model weights updated following each repeating lidar scan. Overall, the proposed method demonstrates improved skill over persistence, with a reduction of root-mean-squared (RMS) wind speed errors ranging from 21 % (1-min ahead), to 10.9 % (5-mins ahead), 9.2 % (10-mins ahead), 7.1 % (30-mins ahead), and 6.2 % (60-mins ahead) while maintaining normally distributed errors.

2 Introduction

15 As the share of variable generation increases in a power system, reducing forecast errors becomes crucial in maintaining power grid balance and stable electricity pricing through minimizing supply shocks and reserve requirements. Numerical weather prediction (NWP) models such as Weather Research and Forecasting (WRF) are standard tools used by meteorologists for forecasting both general weather conditions as well as energy production from wind turbines. However for very-short time scales (< 1 hour) these methods are generally not applicable due to their coarse temporal and spatial resolutions, and long
20 initialization times (Giebel et al. (2011)). Site measurements combined with statistical models offer a promising approach to

forecasting for these lead times. Here we will explore various uses of intrahour forecasts and example methods used to generate them.

2.1 Uses of minute-scale wind forecasts

Predictions of the wind on very-short (minute) time scales have numerous applications both within and beyond the wind energy field. Concerning grid connected utility scale wind farms, the main uses lie in controls, grid support and participation in electricity markets. Consider the following use cases:

1. Forecasts of the incoming wind field near wind turbines and wind farms on this time scale allow for predictive control towards achieving optimum operation (both for energy production and loads). Currently, turbine and farm controllers react to what is experienced real-time by the turbine, which can delay or prevent ever reaching ideal performance. By anticipating changes in the incoming wind (such as speed and direction changes), a controller can configure set points to take better advantage of the impending conditions. This can be achieved for example by preemptively yawing the turbine so that its rotor axis is aligned to the wind direction, and/or by pitching the turbine blade flaps to achieve an optimal aerodynamic efficiency and avoid certain extreme loads. This concept has been demonstrated using feed-forward control on single wind turbines with continuous-wave nacelle lidars in Bossanyi et al. (2014) with look ahead times of 5 seconds. With longer-range pulsed Doppler lidar or radar systems, the spatial coverage is much larger and thus could potentially be applied to a controller covering an entire wind farm.
2. Electricity market participation horizons are shortening to better accommodate an increase in variable renewable energy generation. In the Northern European day-ahead market (NordPool Elspot), balancing costs paid by wind power producers not under support schemes such as the feed-in-tariff (FIT) can be large due to market structures and difficulties in making accurate predictions of wind power output within the defined (hourly) trading segments. As balance responsible parties (BRP), market participants are liable for financial penalties, mainly enacted through trading in regulating power markets to cover deviations between accepted bids and delivered quantities. Holttinen (2006) assesses that on average, 30-40 % of wind power estimates in day-ahead markets need to later be corrected through the intraday and regulating power markets. Additionally, integration costs also apply to the transmission system operators (TSOs) mainly in the form of increased reserve requirements associated with wind power's variability and uncertainty of production. Estimates of EU-wide system balancing costs to TSOs are between 1-4.5 EUR per MWh of production at 20 % penetration levels (EWEA (2015)), which are quickly being surpassed. In Denmark during 2017, this corresponds to between 3 and 15 % of electricity prices on the wholesale market.

Elbas (NordPool's intraday market) has, in selected markets as of 2018, introduced 15 and 30-minute gate closures alongside the traditional hourly contracts in an effort to better accommodate wind power forecast adjustments from day-ahead offerings (NordPool (2019)). Similarly, in June 2017 the European Power Exchange (EPEX) announced 5-minute ahead lead times in their German continuous intraday markets (EPEX SPOT (2017)). Bids for trading within

each of Germany's 4 control zones (described in Fraunhofer (2016)) can be placed up to 5-minutes before delivery. Otherwise the gate closure is 30 minutes for cross-zonal trades in Germany (EPEX SPOT (2018)). Australia has also announced plans to enact 5-minute dispatch and financial settlements beginning in 2021 (AEMC (2017)). We can expect that Denmark and the rest of Europe, along with other countries with a similar high penetration of renewables to soon follow suit by reducing lead times to delivery. This will make predicting the wind on very-short time scales more relevant for participating in these markets.

3. A systematic decrease in wind power forecast errors can allow for reducing the capacity requirements for real-time balancing by grid operators. The Danish transmission system operator (TSO, Energinet) operates a number of ancillary service markets to support grid operation (Energinet (2018)). The shortest response time currently in effect is 5 seconds for 50 % of available power response in frequency-controlled disturbance reserves (FCR-D). The longest response time at present is 15 minutes for secondary automatic frequency restoration reserves (aFRR) and its manual counterpart (mFRR). These response times are consistent with the very-short term prediction interval and can further enable wind power plants to contribute to grid support actions. A recent pilot study in Germany demonstrates the willingness of TSOs to allow this type of reserve market participation by wind power producers (Regelleistung (2016)).

2.2 Brief background of relevant forecasting methods

The simplest prediction method, known as persistence, is a naïve predictor which forecasts the wind speed at time $t + \Delta t$ to be equal to the most recent observation t , where Δt represents the forecast interval. Customarily, a moving average of the most recent observations (usually 10-minutes) is used in order to smooth the signal and reduce noise. This method is commonly used operationally on very-short time scales and in many cases outperforms complex physical and statistical methods (Potter and Negnevitsky (2006)). Therefore, it is regularly used as a benchmark in testing and validating more elaborate methods. This study also considers the persistence approach as a control in this manner, in order to determine improved skill of the lidar prediction method.

Statistical methods such as time series models utilize patterns from past observations to predict future outcomes. Auto-Regressive-Moving Average model-sets (ARMA) are widely used in this context. The Auto-Regressive component involves regressing the variable on its own time-lagged values, while the Moving Average term models the linear combination of error terms which accumulate over the prediction steps. This combination results in both long and short-term memory of variable trends (Whittle (1951)).

Because ARMA-family models assume that the univariate time series input is stationary (mean and variance being constant over time), a common processing step involves modelling the difference of the signal between time steps instead of the signal itself. This may be done one or more times until stationarity can be assumed. This differenced model is referred to as Auto-Regressive Integrated Moving-Average (ARIMA).

Observational based forecasting methods have been demonstrated before, both from in-situ measurements as well as using remote sensing data. Utilizing meteorological and wind power data from nearby areas (1-30km) has been shown to improve short-term forecasts by between 10-25 % over persistence using genetic algorithms (GA) in Damousis et al. (2004) for lead times between 30 mins and 2 hours. Alexiadis et al. (1999) has also demonstrated a 20-40 % wind power forecast improvement over persistence through an ANN spatial correlation approach used to predict wind speed and power over 15 min windows from 1 min to 2 hours ahead using upwind observations from sites spaced between 12 and 40 km apart.

Utilizing lidar observations to improve short-term wind forecasts is suggested in Frehlich (2012), which considers possibilities for assimilation of long-range lidar measurements into numerical weather models. The first demonstration of a purely observationally driven approach appears in Magerman (2014), where a Lockheed Martin WindTracer lidar was deployed in a site with complex terrain. Spatial variances in the wind were tracked as they advected towards a point representing a simulated wind turbine. Another relevant study includes Valldecabres et al. (2017), which combines advection of coastal lidar observations with additional model refinements based on atmospheric processes in order to make a 5-minute ahead wind speed prediction which outperforms both ARIMA and persistence during neutral atmospheric conditions.

In the context of this existing knowledge, we propose a local observation system which uses long-range inflow measurements from a scanning Doppler lidar to generate a site-specific wind speed forecast up to 1-hour ahead with a time resolution of 49 seconds (corresponding to the configured sampling rate of the lidar system used in the field experiment presented in Section 3).

2.3 Brief introduction to wind measurements with pulsed scanning Doppler lidars

Doppler lidars are active remote sensing instruments which probe the atmosphere with laser light in the near infrared band. Light pulses emitted by the lidar are reflected off of particles suspended in the air which are assumed to be moving with the speed of the wind. When interacting with these moving aerosols, the wavelength of the light shifts according to the Doppler principle. The lidar system receives the backscattered pulses and through spectral analysis is able to determine the Doppler (frequency) shift and thus the radial speed (projection of the wind speed along the laser's path). Time of flight calculations allow for measurements at multiple distances along the line-of-sight, known as range gates. The addition of a steerable scanner head (usually dual-axis) allows the lidar to measure arbitrarily in space within its mechanical and optical limits, as long as the target is within a clear line of sight (i.e. not blocked by an object). A detailed overview of the hardware and software measurement chain of a typical pulsed scanning wind lidar can be found in Vasiljevic (2014).

2.4 Motivations and research questions

The following questions represent the core aims that this research work sets out to answer:

- How is a horizontal wind field correlated in time and space at relatively high heights over fairly uniform terrain?

- At what distance upwind of the reference sensor do the lidar observations correlate?
 - Does the observed horizontal wind field advect with its mean speed?
 - Can an improvement be made over persistence by utilizing long-range lidar measurements as a model input for very-short term forecasting (1-60 minutes ahead)?
- 5 – Is it possible to track coherent events with a lead time that can be utilized for turbine/farm control (1-min), or in market actions (5-mins)?

3 Field experiment

3.1 Site description

The Technical University of Denmark (DTU Wind Energy) operates two test stations for very large wind turbines in western Denmark (Høvsøre and Østerild). The field experiment for this study took place at Østerild test center, located near the town of Thisted with the following coordinates: 57° 2'55.94"N latitude, 8°52'51.00"E longitude.

The site is located on a coastal plain between Limfjord (6 km south) and the Vigsø Bay in the North Sea (7.5 km north). The vegetation is mostly grasslands with scattered forestlands to the south and north-west and the presence of sand dunes along the coastline. A terrain and vegetation map is presented in Fig. 3. Surface information is obtained using the Danish Geodata Agency's digital height model (DHM) with a spatial resolution of 0.4 m (Kortforsyningen (2018)).

There are 7 turbine test stands running north-south, enclosed by two 250 m guyed aircraft warning towers equipped with meteorological instruments. The tower positions are indicated with star markers in Fig. 3.

3.2 Measurement characteristics, configuration and calibration

3.2.1 Lidar instruments

20 In the Balconies experiment, two scanning wind lidars (with specifications set according to Table 1) were deployed at Østerild test center. The two instruments together form a time synchronized multi-lidar apparatus known as the Long-Range WindScanner system (LRWS). The system is described fully in Vasiljevic et al. (2016).

The overall measurement goal of the experiment was to observe the 2-dimensional incoming wind field on a horizontal plane. This necessitates that the lidar instruments be situated at the desired measurement height, and be set to scan with an elevation angle of zero degrees. Purpose-built platforms were constructed and attached to the 250 m tall masts at the north and south



Figure 1. Location of Østerild test center in Denmark, with Risø also denoted

ends of the site (see Fig. 3). The lidars were then raised by truck mounted winch and lifted into place. Photos of one of the platforms being lifted can be seen in Fig. 2. A video of the lifting procedure is available in Vasiljevic (2016).



Figure 2. Photos of the lidar platform during the lifting procedure

The lidars were first installed at 50 m above ground level (AGL) during the first phase of the experiment (April 12 – June 17, 2016). They were later raised to 200 m AGL in the second phase of the experiment (June 29 – August 12, 2016).

Table 1. Lidar specifications used in the field experiment

Manufacturer/Model	DTU Long-Range WindScanner (Now commercially available as Leosphere Windcube 200S)
Laser source	Er-Yb silica fiber laser (pulsed)
Mean emission power	1 W
Laser emission wavelength	1543 nm
Telescope diameter	100 mm
Pulse length	400 ns (long pulse)
Pulse energy	100 μ J (long pulse)
Pulse repetition frequency (PRF)	10 kHz (long pulse)
Photodetector sampling rate	4 ns (250 MHz)
Eye safety	IEC/EN 60825-1 & ANSI-Z136.1-2007 compliant
Radial wind speed range	-30 m/s to 30 m/s
Dimensions	1.5 x 0.55 x 0.65 m
Weight	150 kg
Operating conditions	IP65 and ISO9227 compliant

The multi-lidar system was configured to scan in one of two mirrored configurations (east or west facing as shown in Fig. 4), depending on the incoming wind direction. The direction changes were performed manually by the operator throughout the campaign. The scan pattern was created such that the range gate positions measured by both lidars were collocated in space. Points along the central intersecting line were synchronized in both space and time. This allows for a dual-Doppler reconstruction of the wind field at all points where the beams intersect. The reconstructed points not along the time synchronized transect will be averaged over the time it takes to complete one scan (49 seconds).

For the purposes of this study, only measurements taken during phase two of the experiment are used (200 m AGL). This is due to the desire to have wind conditions as similar to offshore as possible by minimizing the effects of terrain and vegetation on the measured winds. Further, although two lidars were deployed in the field campaign, this study only utilizes observations from the unit ‘Sirocco’ mounted on the south tower, while it was operating the westerly scanning pattern depicted in Fig. 4. This was decided in order to avoid data loss (since both systems would require sufficient measurement range for a dual Doppler reconstruction), and to avoid turbine wake effects which are present in the east. These decisions ultimately act to simplify the system so that only one lidar would be required to demonstrate the forecasting system- as we expect would be typical of an operational setup. This solution is further supported by the result presented in Simon and Courtney (2016) which shows excellent agreement between both single and dual Doppler wind retrieval approaches on 10-minute averages.

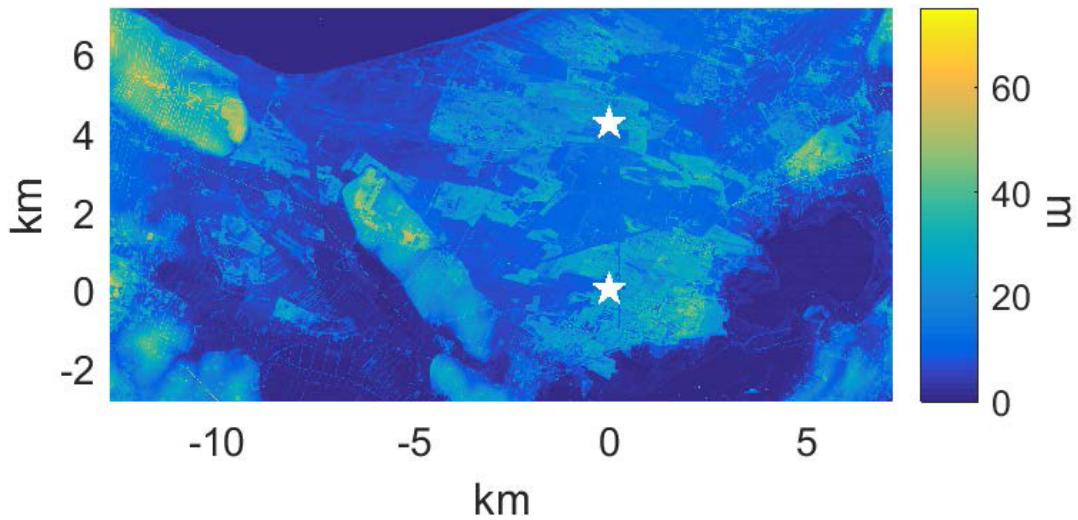


Figure 3. Combined terrain and vegetation (tree) height map of the experiment site with met-masts locations indicated with stars (Created by Ebba Dellwik and available in Simon et al., 2017)

Table 2 describes the measurement setup for the lidar used in this study.

Following installation of the two lidars on their mast-attached platforms, they were levelled according to their dual-axis inclinometer readouts. The static pointing accuracies of the instruments were assessed by mapping the Carrier-to-Noise Ratio (CNR) of targeted landmarks, including e.g. met-masts (see Fig. 5). The north instrument “Vara” had its dual-axis inclinometer previously calibrated for another campaign, thus the mapped and referenced positions of the landmarks matched well (difference of 0.05° in azimuth, θ , and elevation, ϕ). However, the dual-axis inclinometer of the south instrument “Sirocco” had not been previously calibrated which resulted in its imperfect levelling. Figure 6 demonstrates this imperfect levelling through a full (360°) PPI scan obtained at supposedly zero degrees elevation. The ground reflection of the laser beam appearing along with the expected reflection from the targeted landmarks indicates that the lidar is inappropriately levelled.

10 Assuming that the static pointing error originates only from the lidar’s imperfect levelling and home position offset, Vasiljevic and Courtney (2017) demonstrates that the elevation error follows a sine curve for the full range of azimuth angles. Therefore, by deducing the elevation error for several well distributed azimuth positions, finding the sine curve that defines the elevation error is possible. The sine curve can then be encoded in the motion controller to compensate the imperfect levelling and home position offset and thus improve the pointing accuracy.

15 To implement this for the south instrument (Sirocco), the surrounding terrain was profiled with the lidar’s laser beam. It was found that the terrain at θ (azimuth) = 255° and $\theta = 286^\circ$ from the instrument was increasing in height from approximately 5 m to 23 m at 3.75 km and from 5 m to 44 m at 5.29 km respectively. Two RHI (range height indicator) scans with fixed azimuth

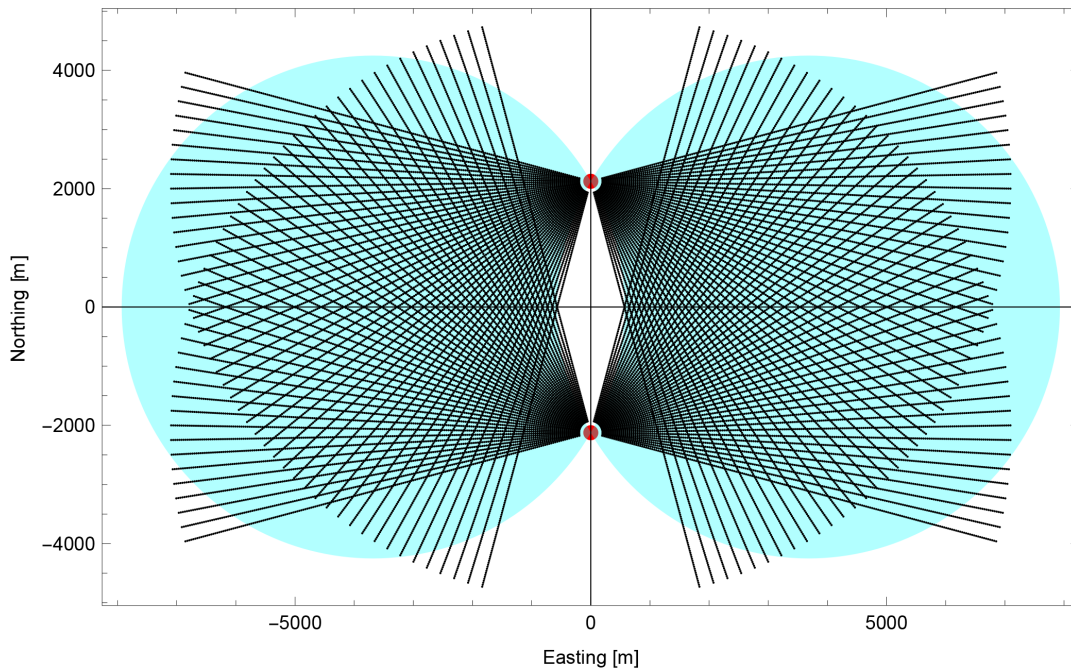


Figure 4. Merged scanning pattern of the lidars (red dots). Switches between east/west to measure inflow. The northing coordinate is relative to the time and space synchronized transect line. Blue areas represent regions where the beam intersecting angle is larger than 30 degrees. (Modified figure created by Jakob Mann and available in Simon et al. (2017))

and varying elevation angles were configured to profile the terrain along these two azimuth positions. The elevation angle ranged from 0° to 1° with steps of 0.01° . Using the RHI scans it was possible to deduce the elevation angle up to which the laser beam was still reflected by the terrain. Since the terrain height with respect to the distance from the lidar and the height of the instrument were known, it was then possible to calculate the elevation angle at which the laser beam would be reflected back from the ground if the lidar was properly levelled. Using the mapped and calculated elevation angles, the elevation error was computed. Two values for the elevation error were derived for two different azimuth positions of the scanner head, relatively close to each other (approximately 30° apart). Next, the north met-mast, a chimney and a wind turbine located at the azimuth positions of 355° , 50° , and 120° respectively were mapped and the corresponding elevation errors were calculated. These five points were then used to perform a sinusoidal fit, shown in Fig. 7, which was then implemented in the motion controller of the south WindScanner “Sirocco”. Succeeding this procedure, the lidar’s static pointing accuracy is considered to be within 0.5° on its elevation axis.

Table 2. Measurement setup for lidar ‘Sirocco’ mounted on the south mast and scanning north-west

Scan type	Plan position indicator (PPI)
Azimuth angle range	255-345 degrees
Elevation angle	0.05 degrees
Accumulation time	1000 ms
FFT size	128 bins
Measurement range	105-7000 m
Range gate spacing	35 m
Scanner head motion	2 degrees / second
Reversing?	No. Scanner head resets to initial position after completing each scan
Scan rate	45 s per scan, plus 4 s to reset position
Probe length full-width half maximum (FWHM)	75 m
Number of lines-of-sight (LOS)	45
Number of range gates (RG)	198

3.2.2 Mast instruments

The 250 m tall masts are equipped with a range of meteorological instruments. This study utilizes the following sensors, both mounted on the southern mast where the lidar Sirocco is deployed.

- Cup anemometer, with top of instrument situated at 210 m AGL. Type RISØ/WindSensor-P2546A with P3118A support pole. Boom length of 4.8 m. Wind speed data is logged at 10 Hz.
- Sonic anemometer (3-D), with top of instrument situated at 244 m AGL. Type Metek USA-1/P2901 with P4023A support pole. Boom length of 4.8 m. 3D velocity data is logged at 20 Hz, which is projected into vector components (u, v, w) . Note that only wind direction data from this instrument was used in this study, and that the cup and sonic sensors are not collocated at the same height.

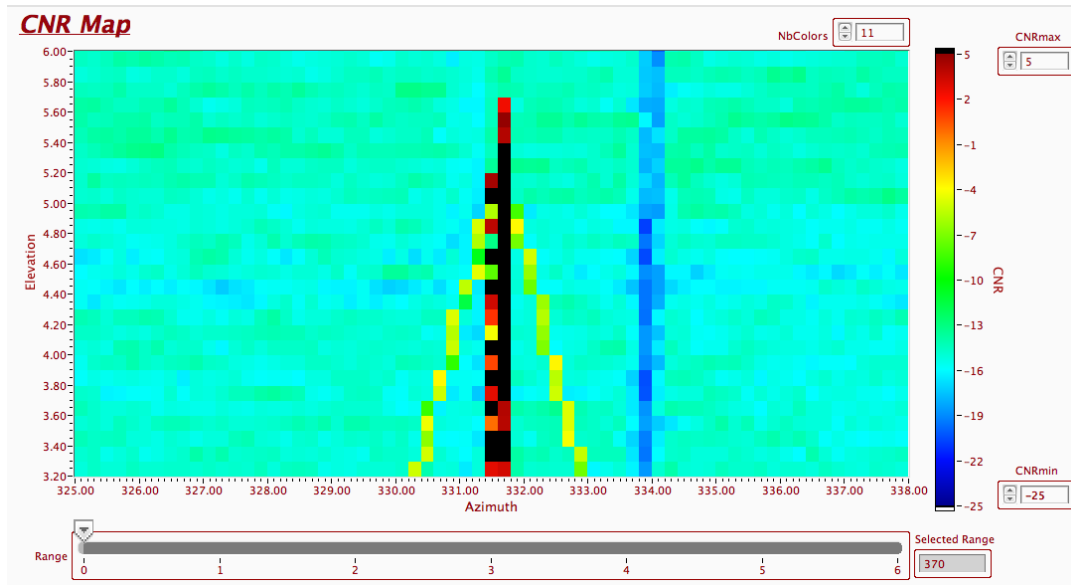


Figure 5. CNRMapper example, mapping met-mast in order to determine the static pointing error

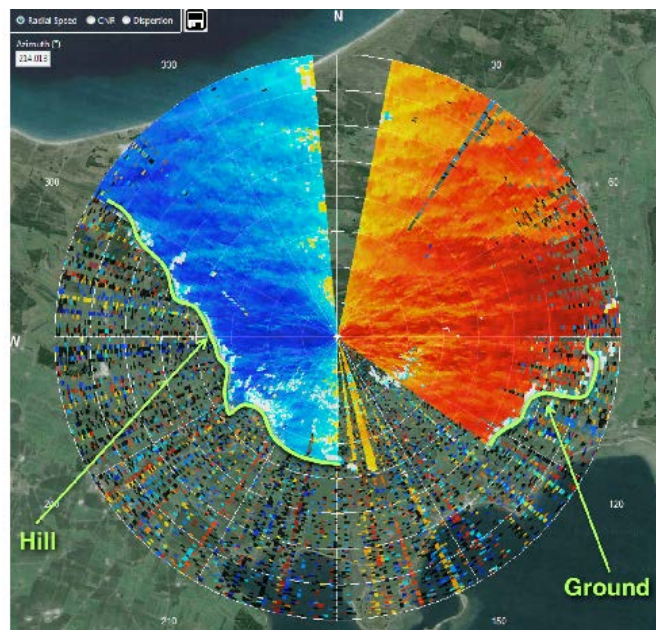


Figure 6. Uncalibrated PPI scan at 0 degree elevation from Sirocco, demonstrating the imperfect levelling of the instrument

3.3 Data filtering and processing

An overview of the dataset preparation and filtering steps are presented in Fig. 8.

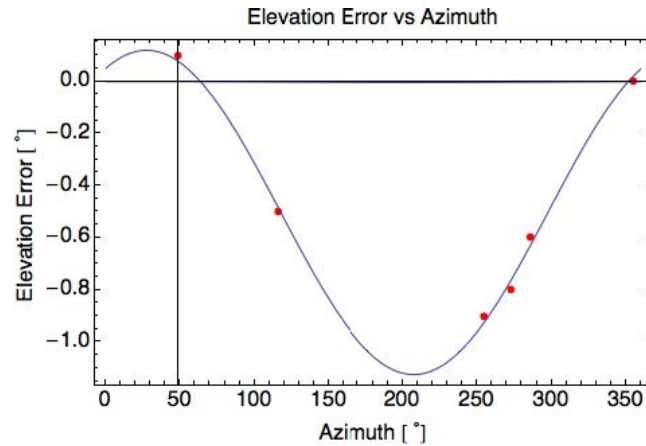


Figure 7. Sinusoidal fit of elevation error by azimuth angle for Sirocco (lidar positioned on the south met-mast)

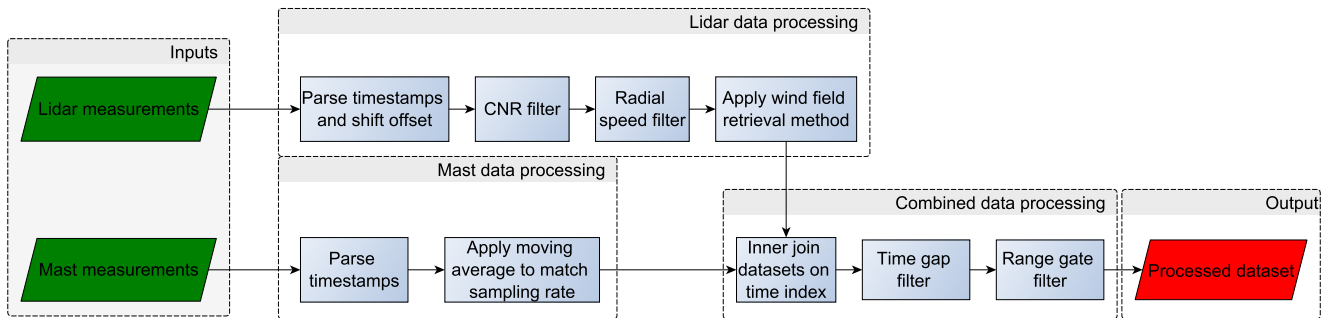


Figure 8. Flowchart of dataset filtering and preparation steps

Measurements from the met-mast were expressly not used for filtering purposes of the lidar data. This is to demonstrate real-world usage where such instrumentation is not available, for example at an offshore wind farm where costs of mast installation alone can exceed 10 million euros (4C-Offshore (2017)).

Measurements from the lidar were filtered according to the following steps:

- 5 1. Carrier to noise ratio (CNR) threshold. Signal quality must be above -25 dB to be considered valid
2. Inflow only conditions. Radial speeds must have the correct sign (negative in WindScanner convention)
3. Sparse data (data point are filtered if more than a 10-minute gap exists between them and the previous or subsequent valid observation)

A plot demonstrating effective lidar range over the experiment is shown in Fig. 9. The figure is presented such that the range
10 representation is aligned with the lidar beam (horizontally). Purple data is valid, while yellow data has been removed according

Table 3. Data filtering timeline (n = number of 49-second samples)

Original data	After CNR and RadSpeed filter	After time gap filter
n = 67932 (925 hours)	n = 36363 (495 hours)	n = 35058 (477 hours)

to the filtering procedure described above. Due to low availability of data at ranges beyond 6 km, we have decided to only include measurements from 105 to 5950 m into the forecast model. Note that only periods where the lidar was operating using the westerly pattern are considered. Therefore, we do not consider data to be missing if the winds are from the east and the lidar is configured to scan eastwards. Such periods are simply omitted from the dataset.

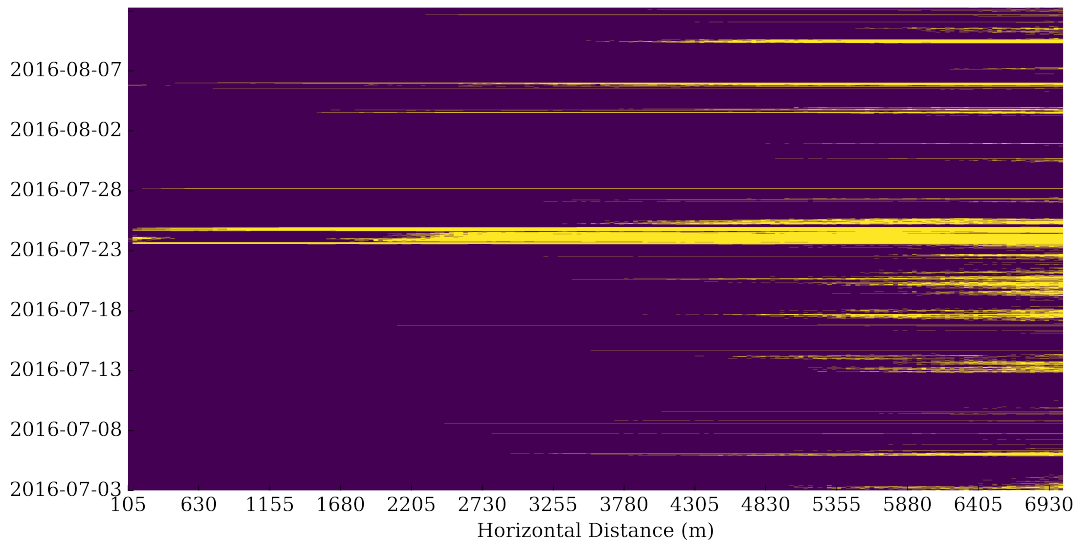


Figure 9. Availability of lidar measurements. Horizontal range from left (105 m) to right (7 km). Filtered data in yellow

- 5 Implications of the filtering steps can be seen in the wind roses (Fig. 10), which indicate wind direction representativeness as well as corresponding wind speed distributions included in the dataset.

Fig. 11 presents the scan area of the filtered lidar data (dashed lines) on top of the terrain and vegetation height map. Note that these angles do not correspond to the entire scanned measurement area (shown in Fig. 3). This is done for ease of interpretation of the results.

- 10 Following the outlined filtering procedure, the lidar observations were processed according to the retrieval method presented in the methodology (Section 4.1), and matched in time to the met-mast measurements. This was achieved by converting both time-series to datetime format (millisecond precision) and cross-correlating the first lidar range gate to the cup anemometer signal in order to determine if a time offset was present. The time offset was determined to be very close to 1-hour. This is

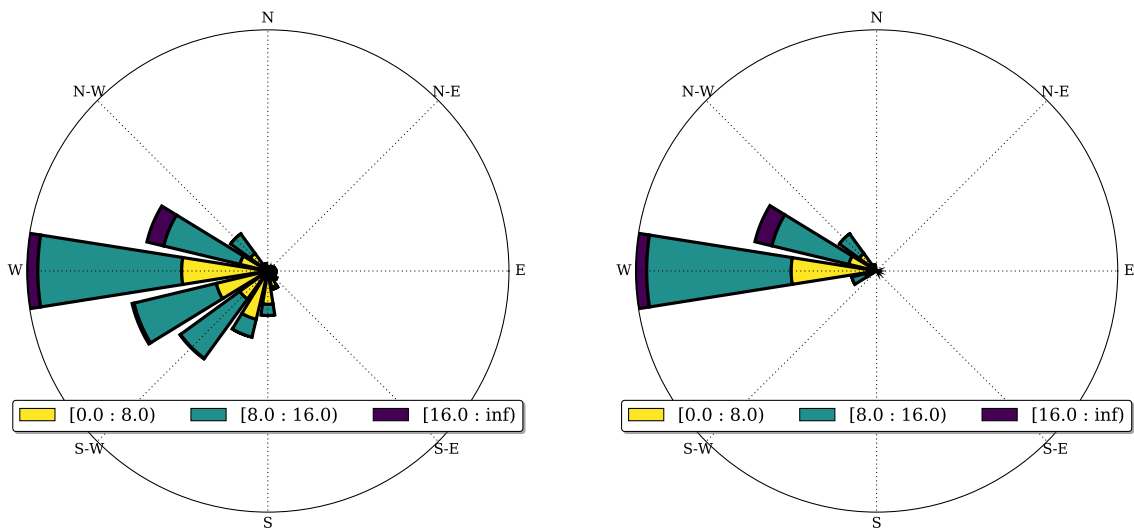


Figure 10. Wind rose before (left) and after (right) data filtering

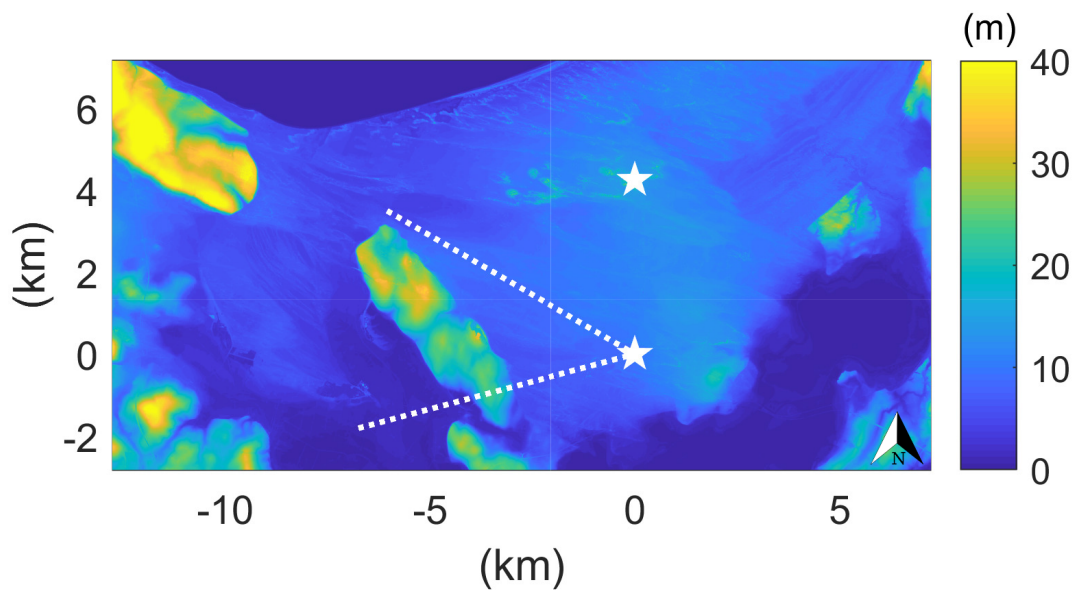


Figure 11. Terrain and vegetation height map of the lidar scan area (dashed lines) after filtering. Stars represent the 250 m tall met-mast positions. Created by Ebba Dellwik

due to the lidar recording data in UTC format whereas the mast was set to local time (Central European Time, UTC+1). The offset was then corrected for by shifting the lidar timestamps (by 1-hour) so that the measurements are matched in time. The

empirical time offset was found not exactly at 1-hour due to the fact that the first lidar range gate was 105 m horizontally upstream of the cup anemometer. A 49-second moving average was applied to all mast observations before being joined with the coinciding lidar measurements. This was done to match the sampling rate of the mast data to that of the lidar.

4 Methodology

5 4.1 Wind field retrieval method

The radial speed obtained by the lidar is described by Eq. 1, when the unit is calibrated such that its azimuth angle is oriented to the geographic direction ($0^\circ = \text{North}$), and the laser beam is parallel to the ground (i.e. zero degree elevation angle).

$$u_r(m.s^{-1}) = U * \cos(\beta - \theta) \tag{1}$$

where u_r is the radial speed, U is the horizontal wind speed, β is the wind direction angle, and θ is the azimuth angle.

10 Therefore, the true wind speed is equal to the absolute value of the radial wind speed when measuring directly into and away from the wind. When scanning perpendicularly, the lidar will measure zero radial speed.

Commonly when processing PPI scans, a fitting function is used on a range of radial speed inputs in order to obtain the u and v (horizontal) vector components of the wind speed. This approach was first introduced in Lhermitte and Atlas (1961) and demonstrated in Browning and Wexler (1968) as the velocity azimuth display (VAD) method using steep elevation angles (up to
15 30°). Horizontal “sector” scanning at lower elevation angles builds upon this principle using e.g. the IVAP (integrating velocity azimuth process) reconstruction method demonstrated in Liang (2007). These fitting methods have the benefit of performing even when measuring at angles relative to the wind, where the maximum (or minimum) radial speed is not measured directly. However, as they assume homogeneity within the scan volume and fit a function to the measurements, there are inherent errors introduced by these methods.

20 Contrary to traditional fitting algorithms- by ensuring that our lidar scan crosses into (or away from) the oncoming wind direction, we can utilize the lidar observations of radial speed directly. This entails finding the maximum absolute magnitude of the radial speed within each scan, and recording both the speed value itself, as well as the azimuth position of the lidar scan head where the maximum occurs. At this point we will obtain the wind direction aligned wind speed, and corresponding wind direction for each range gate at each completed scan time. The method also assumes that the wind is frozen (homogeneous)
25 during each PPI scan (here 49 seconds) but has the benefit of significant computational speed and memory improvements over the traditional fitting approaches along with the avoidance of errors introduced by the fitting function. However it should also be noted that this method can introduce a slight positive bias as points with the maximum positive perturbation are chosen. It is

important that the peak selection be done in conjunction with the filtering steps, considering that it is possible to filter out the local minima or maxima if filtering is done beforehand. As this wind retrieval method is not well established in the literature, a validation has been included in the results (Section 5.1).

4.2 Model training and prediction

5 4.2.1 Overview of stochastic gradient descent (SGD) training

Stochastic gradient descent (SGD) training is a process which aims to minimize an objective (cost function) by using iterative stochastic approximation of a gradient descent function (convex minimization) (Scikit-learn (2018a)). By design it is a fast algorithm suitable for very large training sets, and can be implemented out-of-core (i.e. datasets too large to fit in memory).

The algorithm begins with initial input conditions (step size and learning rate), and stochastically manipulates coefficient weights of the inputs to follow the decrease (sign) in the objective function until approaching a minimum. The end result is a fitted linear model with weights optimized to achieve the best metric of the loss function (e.g. mean-squared-error (MSE), mean-absolute-error (MAE), etc.). This method can be applied both to regression (SGDR) and classification problems. By using a convex cost function such as MSE for linear regression, it is guaranteed to approach close to the global minima (and avoid being trapped at a local minima if the number of iterations is too few). The SGD method also incorporates a regularization penalty which can be used to counteract overfitting and perform feature selection.

SGD models are particularly sensitive to feature scaling (also called data normalization). This step can significantly increase model performance and training speed. Feature scaling normalizes input variables in terms of their mean, minimum, maximum, variance, and distribution. The recommended scaling method will depend on characteristics of the input data together with assumptions made within the algorithm itself.

The mathematical formulation of the SGDR algorithm is presented in Scikit-learn (2018a) and further elaborated in Zhang (2004).

4.2.2 Forecast model implementation details

The scikit-learn implementation of SGDR does not accept sparse (missing) data as inputs, so a strategy to fill or remove them from the dataset was needed. We have chosen to fill missing data using the mean value along the line of sight using the scikit-learn preprocessing imputer (Scikit-learn (2018b)).

In order to ensure proper compartmentalization of past and future data, and to simulate real-world usage, a walk-forward training and prediction architecture is implemented. At each point in time (here every 49 seconds which corresponds to the lidar scan rate in the experiment), in-sample data is used to train and predict wind speeds from 1 to 73 scan-times ahead (corresponding to 0.8-60.4 minute ahead lead times). Subsequently, 49 seconds later, the latest measurements are assimilated

into the training data, which is then updated and used to predict another set of wind speeds over the prediction interval. The model does not know how well it has performed until the proper amount of time has elapsed and the corresponding data is then included in the updated training set.

The model training begins with an initial 500 sample spin-up, which corresponds to 6.8 hours of training data before the first prediction is made. Separate models are trained for each prediction length, in order to fully capture the spatio-temporal correlations present in the observations. Training data for models with lead times 0.8 to 3.27 minutes (1-4 steps) include all available past data, while training data for subsequent models (4.08 – 60.4 minutes or 5-74 steps) represents a rolling window of the last 1000 observations (13.6 hours). The main practical difference is that in the incremental approach new observations are partially fit to the already trained model from the previous time step, while in the rolling window approach a new model is trained at each time step. This hybrid approach leads to an increase in robustness, overall skill, and computational speed. The two data architectures are presented in Fig. 12 and the two process flowcharts are presented in Fig. 13 and 14 respectively.

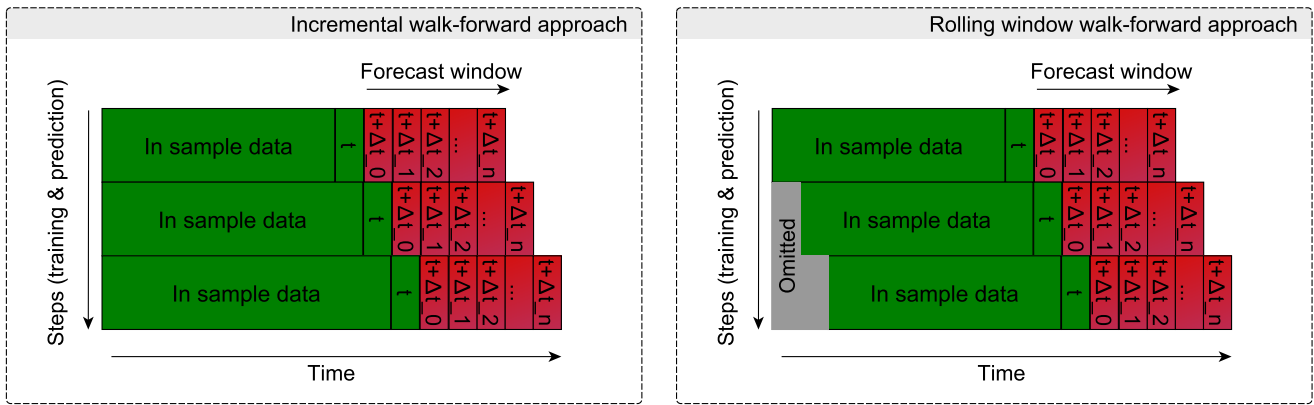


Figure 12. Walk-forward training and prediction architecture. Incremental (left) and rolling window (right)

Input features consist of wind direction aligned radial wind speeds from 105 m to 5950 m horizontal distance (upwind) from the lidar. This corresponds to the 35 m range gate spacing of the measurement setup. As mentioned in Section 3.3, data from 5985 m-7000 m are not included as inputs due to poor availability during the experiment after signal quality filtering. Model predictions are the 0.8-60.4 minute ahead cup anemometer measurements at 210 m AGL from the southern mast where the lidar is mounted. As previously mentioned, SGD training requires feature scaling for optimum performance. Since our wind speed time series is neither stationary nor normally distributed, and contains outliers which would otherwise influence the sample mean and variance, we have chosen to use the robust scaling method to transform our data using the interquartile range (IQR) of each feature. Following model prediction, we inverse transform our scaled outputs back into familiar wind speed values. The robust scaling method is described in Eq. 2.

Table 4. Scikit-learn SGDR model parameters

Parameter	Value	Note
Loss function	squared_loss	Ordinary least squares (OLS) fitting using mean-squared error (MSE)
Learning rate	constant	Used to frame our model as an online learning problem, where new data is being assimilated as time passes
Shuffle	FALSE	Prevents shuffling of the training data since the observations are naturally ordered in time
Initial learning rate (eta0)	0.0001	A small learning rate is chosen based on hyper parameter tuning
Maximum iterations (training epochs)	1	Only one full training cycle is performed as the data is not shuffled

$$x_s = \frac{x_i - Q_1(x)}{Q_3(x) - Q_1(x)} \tag{2}$$

where x_s represents the scaled variable, x_i represents the unscaled input, and $Q_n(x)$ represents the n^{th} quartile of the input data distribution.

The model is trained using scikit-learn’s SGDRRegressor class (Scikit-learn (2018c)) with parameters according to Table 4. If the parameter is not explicitly mentioned, then the default values listed in the referenced documentation are used.

While the walk-forward execution runs on the dataset, the 0.8-60.4 minute ahead predictions at each time step are saved in memory along with the last (49 s averaged) wind speed observation from the met-mast (last value persistence). A 10-minute moving average of the mast observations (10-minute average persistence) is also included as a benchmark. After all predictions are made, the reference wind speed from the mast is joined to the predictions in order to calculate performance metrics of the three forecast methods.

Figs. 13 and 14 present a flowchart overview of the two methods used to produce the forecasts.

4.3 Forecast evaluation

When evaluating a regression model’s skill on (continuous) time series data, there are a multitude of metrics available. The choice should be context driven and related to the cost function used in the model’s training/optimization. Two of the most common standards are the mean-absolute-error (MAE) and root-mean-square error (RMSE). The root-mean-square metric penalizes larger errors disproportionately to smaller errors. Thus it is a good fit for evaluating forecasts of wind speed for the

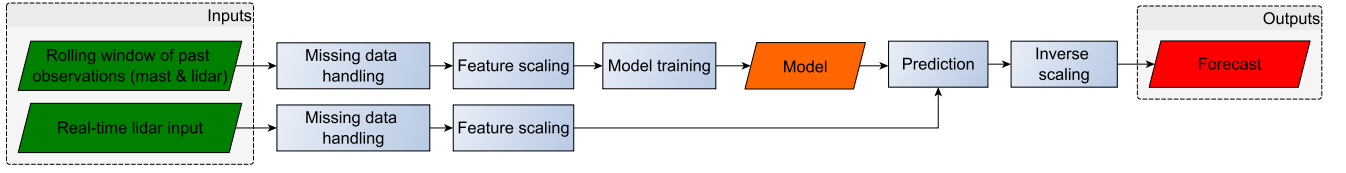


Figure 13. Forecast procedure for models with lead times between 1-4 steps ahead (0.8 - 3.27 minutes)

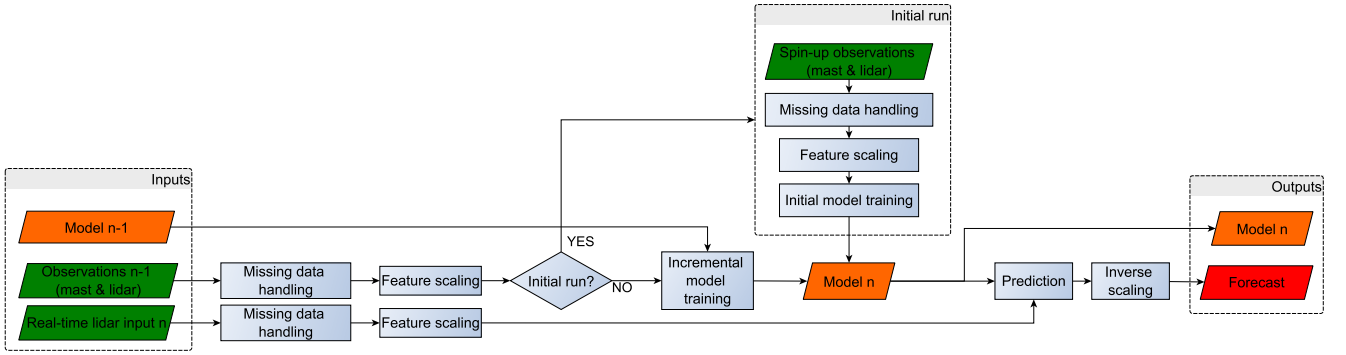


Figure 14. Forecast procedure for models with lead times between 5-74 steps ahead (4.1 - 60.4 minutes)

purposes of wind power prediction, since errors are amplified or attenuated by nonlinearities in the wind turbine's power curve. Further, the RMSE metric is sensitive to large errors which have the most detrimental effects on the power system. MAE and RMSE units are the same as the input variable (here ms^{-1}).

$$MAE(y, \hat{y}) = \frac{1}{n} \sum_{i=0}^{n-1} |y_i - \hat{y}_i| \quad (3)$$

$$5 \quad RMSE(y, \hat{y}) = \sqrt{\frac{1}{n} \sum_{i=0}^{n-1} (y_i - \hat{y}_i)^2} \quad (4)$$

Where y is the known value and \hat{y} is the predicted value at point i over all samples n . A simple general linear model between the predictions and observations is also used to determine systematic bias (y-intercept), goodness of fit (coefficient of determination, R^2) and proportion (slope) between the two time-series.

5 Results

5.1 Validation of wind field retrieval method

The following figures demonstrate the performance of the simple wind field retrieval method by comparing time-series plots and 2-D histograms of the first lidar range gate with the met-mast observations. Note that the measurements are not collocated in space. The lidar measurements are taken 105 m upwind of the met-mast, also with a height difference of 10 m for the cup anemometer, and 44 m for the sonic anemometer (wind direction).

It is clearly demonstrated that the retrieval method performs well for wind speed, with an ordinary least squares (OLS) coefficient of determination (R^2) of 0.97, slope of 0.96 ms^{-1} and constant offset of 0.28 ms^{-1} .

However, the wind direction result is distinctly mediocre in comparison. There are noticeably larger errors and an overall higher level of scatter. Because the method utilizes the lidar measurements directly, its resolution is limited by the angular separation between the lines of sight (here 2 degrees between each LOS). This is the cause of the striping pattern observed in Fig. 16 (right panel). A linear regression (OLS) between the two wind direction signals produces an R^2 of 0.64, slope of 0.71 degrees, and offset of 80.44 degrees. By forcing the regression through the origin, the slope of the linear model becomes 0.99. This indicates that the wind direction errors are normally distributed around the one-to-one line.

5.2 Spatio-temporal correlations

To demonstrate the core utility of exploiting upwind measurements for the purposes of wind speed forecasting, Figs. 17 and 18 present the spatio-temporal relationships present in the processed dataset. Here the cross-correlation between the lidar obtained wind speed signal (across all range gates) and the time synchronized cup anemometer measurements are shown.

Fig. 17 presents the correlation coefficient as a function of scan lags (49 s shifts) of the upwind lidar observations relative to the cup anemometer. A distinct maximum peak is observed at the closest distance (105 m) at lag index zero. The peak then shifts forward (to the right) as the upwind distance increases, demonstrating the temporal link as the wind field advects downwind towards to the mast sensor. In addition, the peak also broadens as upwind distance increases and turbulent mixing decorrelates the measured winds between both positions.

Fig. 18 shows the same space-time correlation result as a 2-dimensional heat map. As expected, the correlation is highest for shorter scan lags and closer distances upwind. Observations within 30-mins of each other exhibit the highest temporal correlation.

Using these space-time correlations, it is possible to construct a relationship between the distance upwind measured by the lidar and the temporal lag until it reaches the mast's cup anemometer. This is done empirically by choosing the peak of each cross-correlation by range. Knowing the distance and average time of flight then gives a mean advection speed, which is presented in blue in Fig. 19.

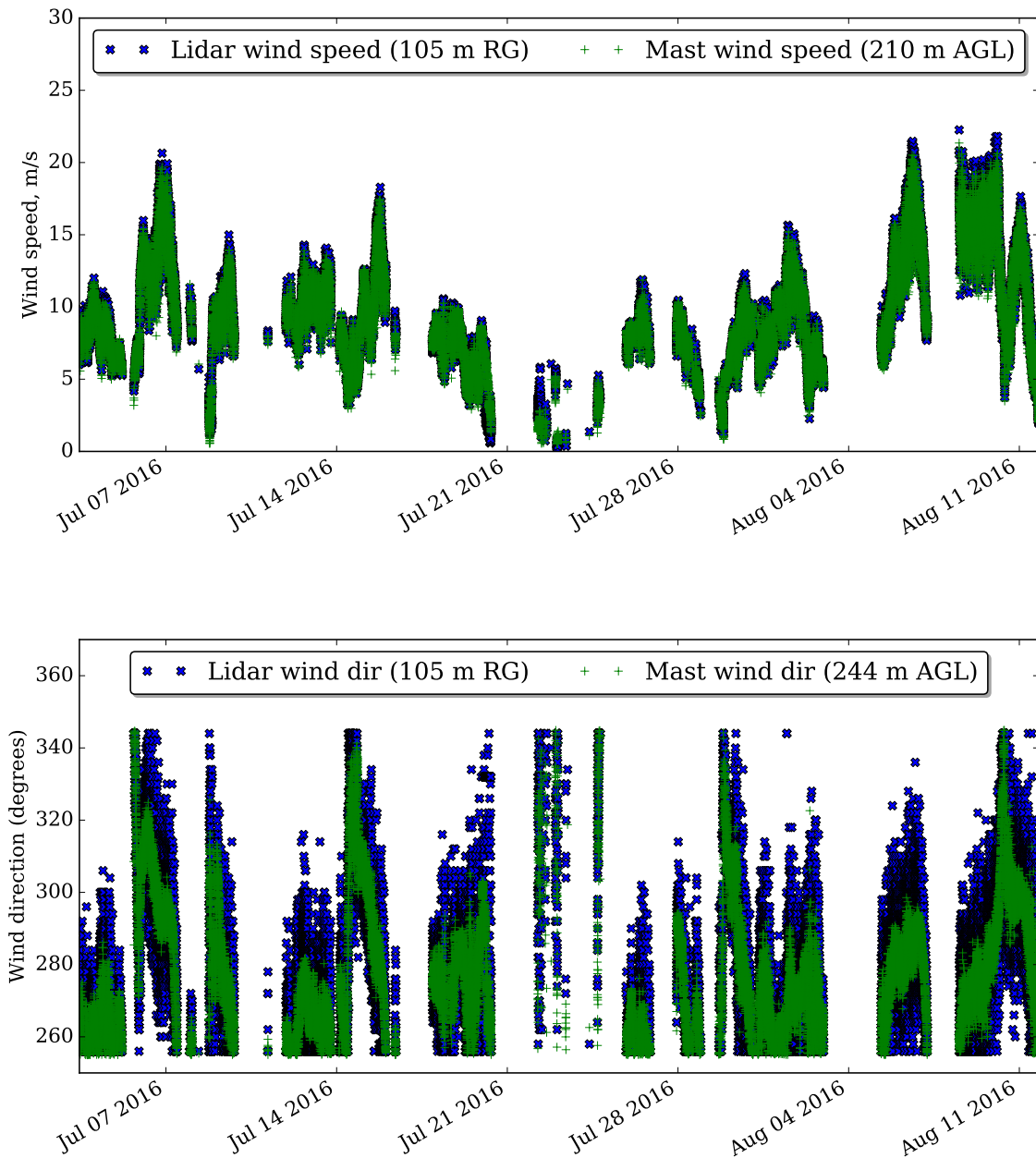


Figure 15. Time series comparison between closest lidar and mast measurement, wind speed (top) and wind direction (bottom)

Taylor’s frozen turbulence hypothesis states that the wind field advects with its mean speed (Taylor (1938)). This allows for a theoretical derivation which can be compared with the empirical approach. An average wind speed over the entire experiment is taken (9.8 ms^{-1}) which is used to construct the same relationship as shown in green in Fig. 19.

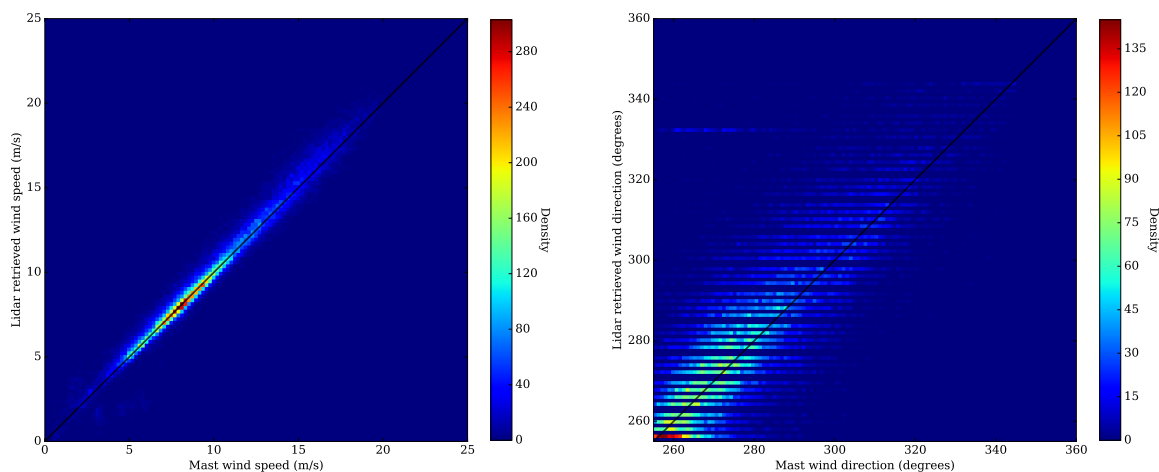


Figure 16. 2-D histogram comparisons between closest lidar and mast measurement, wind speed (left) and wind direction (right). Also showing the ideal relationship $y=x$ with a black line

Although the trends do follow, there is a disparity between the forecast horizons related by the two methods, particularly at further distances upwind. A linear model fit to the empirical data (dashed blue line) suggests a mean advection rate of 14.5 ms^{-1} compared to its mean speed (9.8 ms^{-1}). This result suggests that Taylor's hypothesis does not hold over all distances observed and that features present in the wind field do not simply advect downwind. At shorter distances (up to about 2 km) both approaches show good agreement which implies that advection is the primary transport mechanism up to about 3-minutes ahead.

5.3 Coherent structure tracking

Using the processed lidar measurements, it is also possible to visualize coherent structures as they approach the reference position (met-mast). This is achieved by plotting a 2-dimensional heat map of the upwind measurements over space and time. The slope of the feature represents its mean advection speed. Many such events are present in the dataset, which occur particularly during periods with stable atmospheric conditions (low turbulence), for example during night time. An example is presented in Fig. 20 where a 5-minute sustained wind ramp can be detected advecting towards the mast position over a period of 15 minutes. The subsequent abatement of the event can also be tracked over the same timescale.

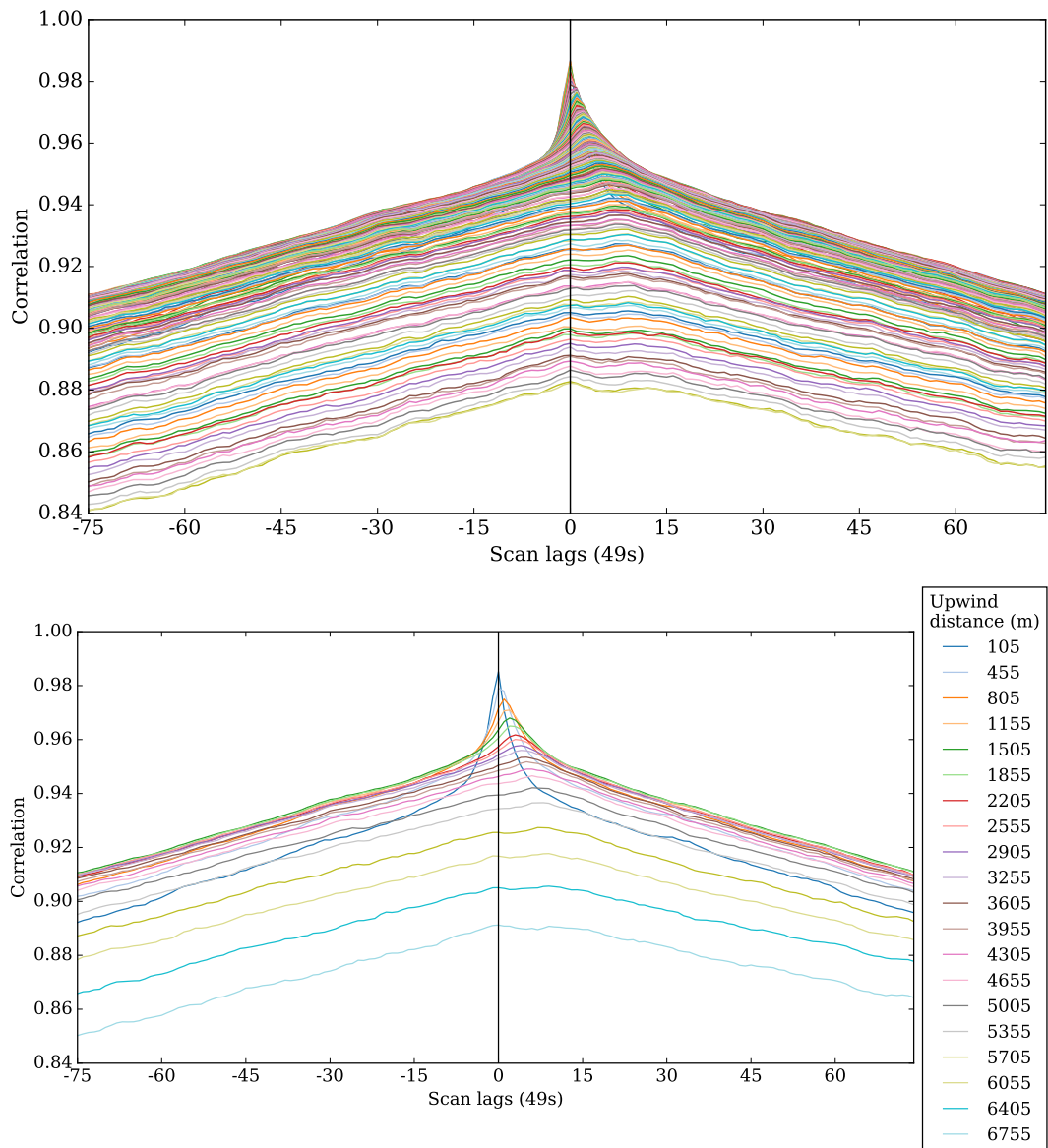


Figure 17. Cross-correlation function between the lidar and mast wind speed signals by 49 s scan lags for each upwind distance (35 m spacing, top) and a magnified version for every 10th range gate (350 m spacing, bottom)

5.4 Overall forecast model results (wind speed prediction)

Root-mean-square errors (RMSE) as a function of lead time for the three forecasting methods are presented in Figure 21.

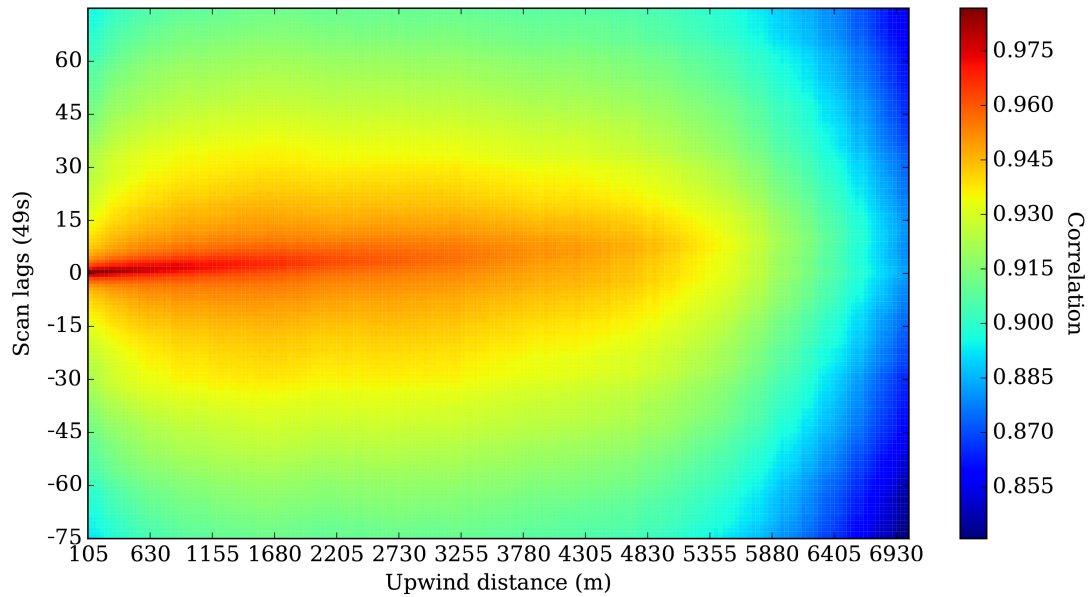


Figure 18. Cross-correlation function between the lidar and mast wind speed signals by 49 s scan lags

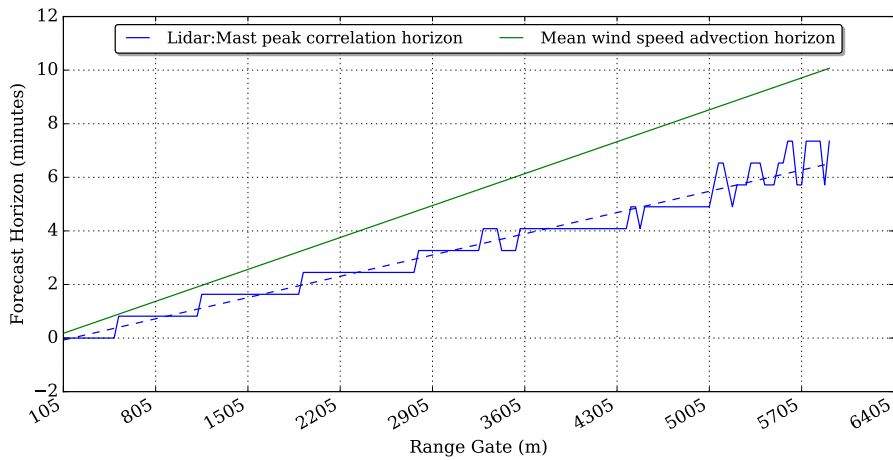


Figure 19. Theoretical and empirical ideal forecast horizon as a function of measurement range

Note that although the forecasts are generated in multiples of 49 s (corresponding to the lidar sampling rate), for ease of discussion in the text, the time horizons are rounded to the nearest minute (e.g. the 6 step ahead forecast which is 294 s ahead is reported as the 5-min model).

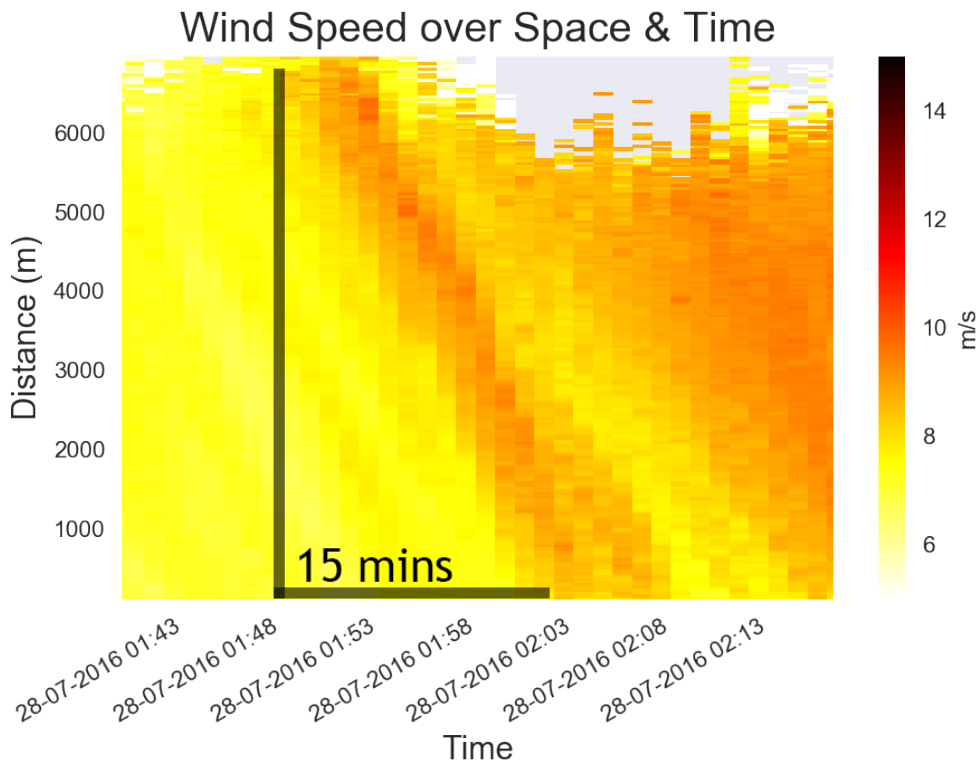


Figure 20. Coherent structure tracking example with 15-minute ahead detection. Plot is wind speed over space and time upstream of the reference met-mast

The lidar method is demonstrated to outperform both the last-value and 10-minute averaged persistence methods. The improved model performance is most significant from 1-3 minutes ahead, and continues up to 20-minutes ahead. After this point the performance advantage represents a near-constant reduction in root-mean-square errors (7 %). This is consistent with the results obtained in Section 5.2 relating to the upwind space-time correlations. The improvement upon persistence demonstrated

5 by the lidar method at longer lead times could be explained as a shift in the persistence lead time as a function of distance measured by the lidar.

When relying on the persistence method, it is almost always better to use a 10-minute smoothed signal instead of the singular most recent observation. Only for the 1-minute ahead predictions does the last instantaneous value approach outperform a 10-minute moving average, and then only marginally.

10 An example time-series of the lidar prediction and reference signal is shown in Fig. 22 for the 5-minute model.

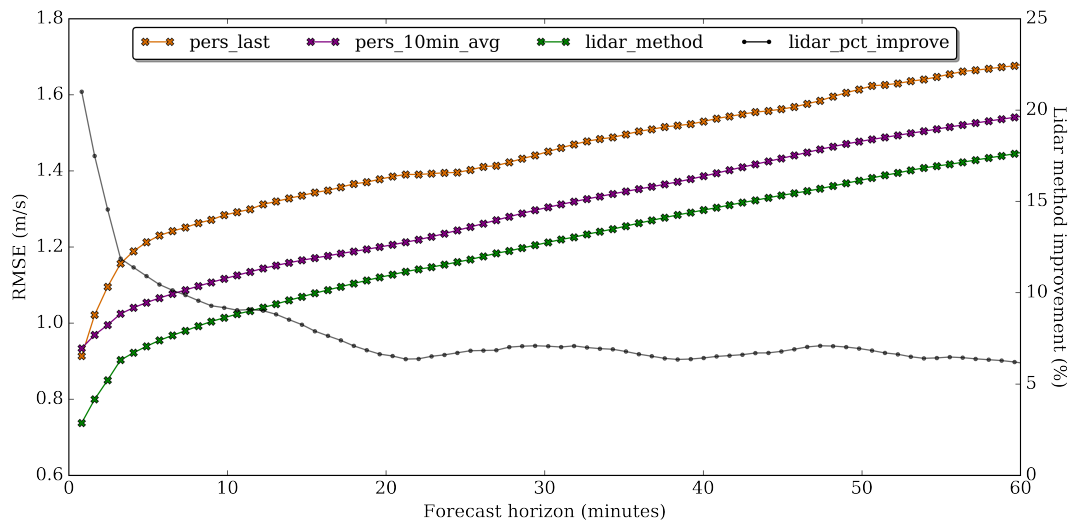


Figure 21. Comparison of overall RMSE results for the three approaches by forecast lead time. Also included is the lidar method percent improvement over the 10 minute moving average persistence forecast (right side y-scale)

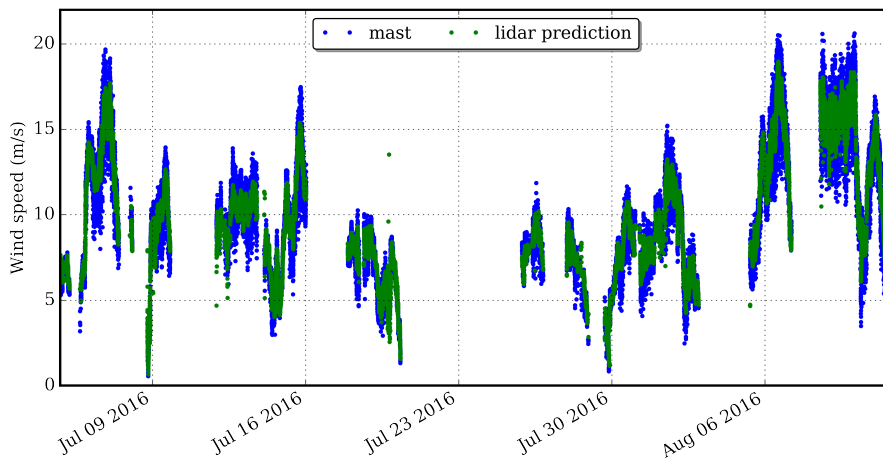


Figure 22. Time series of lidar method predictions with mast measurement for 5-min horizon

From comparing the two signals, we observe that the lidar forecast tracks the reference measurement well with only a few major errors. However, there is significantly reduced variability in the lidar forecast, which is smoothed relative to the turbulent anemometer readings.

5.5 Coefficients of the fitted models

Coefficient weights of two linear models (1-min and 10-min ahead) used in the lidar prediction method are shown in Fig. 23. The iterations show how the model weights change while progressing through time. Note that as conditions are constantly changing, we do not expect the weights to converge to any particular range of values.

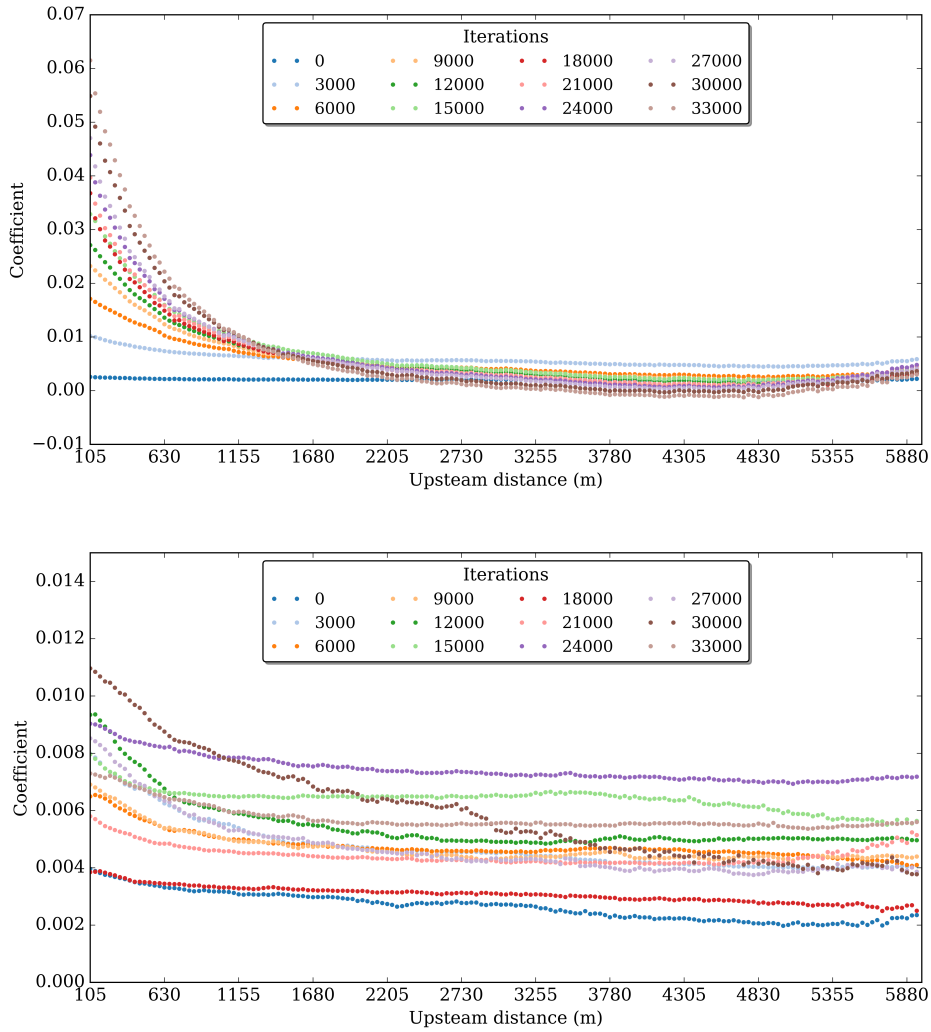


Figure 23. Coefficient weights of the lidar forecast model at selected points in time (iterations, i.e. batch number). 1-minute ahead model (top) and 10-minute ahead model (bottom). Note that the y-scales differ

- 5 We observe that for both models, the nearest observations are assigned the highest weights. The 1-min ahead model mainly relies on observations within 1 km upwind of the met-mast, while the 10-minute model weighs further distances more equally.

Between approximately 2.5 km to 5.5 km, the 1-minute model assigns near-zero coefficients to the upwind measurements. This can be through means of the regularization penalty L1 (Lasso) incorporated in the optimization, as this region does not correlate to the wind which reaches the mast sensor along this timescale. However, inputs at the edge of the measurement range are once again positive (non-zero). The reasons for this are not well understood, however we can speculate that this information is not already accounted for in the other model terms and as such has relevance for predicting changes.

5.6 Performance statistics for various time steps

Table 5 presents performance results of the three forecast methods for selected lead times. Fitted parameters using ordinary least squares (OLS) between forecast model predictions and the reference (cup anemometer) measurements are also included.

Fig. 24 presents the probability density functions (PDFs) of absolute forecast errors (prediction minus reference) across the three methods for the same selected lead times as described in Table 6.

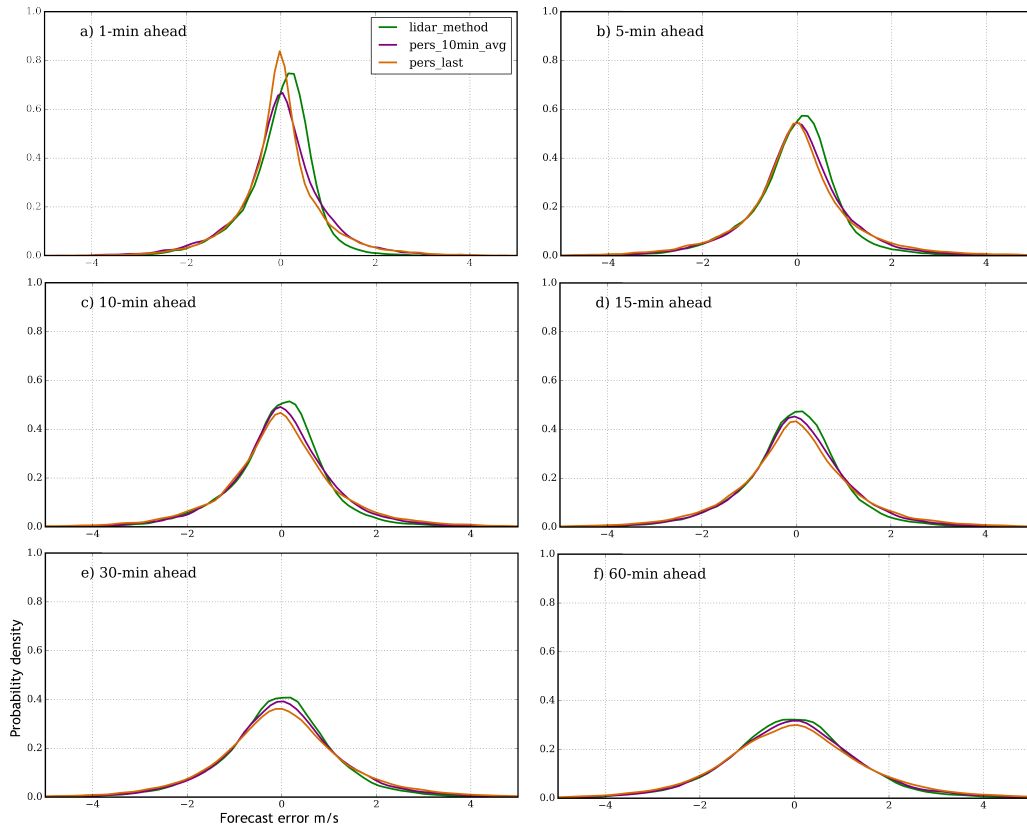


Figure 24. Forecast error distributions for 1-min (a), 5-min (b), 10-min (c), 15-min (d), 30-min (e), and 60-min (f) predictions

Table 5. Performance statistics for various time steps

Horizon	Method	MAE (ms ⁻¹)	RMSE (ms ⁻¹)	y-intercept	coefficient	R ²
1-min	Lidar input to SGDR	0.535	0.737	0.503	0.95	0.958
	Last value persistence	0.615	0.913	0.322	0.967	0.936
	10-min average persistence	0.656	0.934	0.536	0.946	0.933
5-min	Lidar input to SGDR	0.678	0.938	0.732	0.931	0.934
	Last value persistence	0.838	1.212	0.557	0.944	0.892
	10-min average persistence	0.754	1.054	0.619	0.938	0.917
10-min	Lidar input to SGDR	0.737	1.013	0.791	0.925	0.923
	Last value persistence	0.911	1.284	0.627	0.938	0.88
	10-min average persistence	0.811	1.116	0.675	0.933	0.907
15-min	Lidar input to SGDR	0.783	1.068	0.838	0.92	0.914
	Last value persistence	0.958	1.335	0.681	0.932	0.87
	10-min average persistence	0.852	1.165	0.722	0.928	0.899
30-min	Lidar input to SGDR	0.886	1.204	0.966	0.908	0.891
	Last value persistence	1.056	1.441	0.803	0.92	0.85
	10-min average persistence	0.954	1.297	0.855	0.915	0.875
60-min	Lidar input to SGDR	1.071	1.445	1.225	0.882	0.845
	Last value persistence	1.235	1.676	1.099	0.891	0.799
	10-min average persistence	1.138	1.541	1.136	0.887	0.826

We observe from Fig. 24 that the error distributions across the three forecast approaches are similarly shaped (normally distributed around a zero mean). Note that the figure data represents the simple difference which considers all errors to have equal

weights (unlike the RMSE metric). The lidar method lead times up to 15-mins tend to have slightly negative (left) skew, while exhibiting fewer over-prediction errors greater than 1 ms⁻¹. This evidences why for example the 1-minute ahead lidar model outperforms the last value persistence method in RMSE, while the PDF of the persistence forecast error appears to exhibit smaller errors on average.

5 5.7 Model changes which did not improve the overall result

Numerous efforts to evaluate changes in model inputs were tested, without leading to an improved result. Such attempts included transformation of the processed wind speed data into principal components (PCA). This procedure attempts to detect correlation between variables and reduce the dimensionality of the data by finding the directions of maximum variance and re-projecting these into a smaller dimensional subspace while preserving the patterns between the remaining (principle) components. Further attempts to reduce data dimensionality by thinning the input data by selecting every n -range gates where: $n \in (2, 3, \dots, 10)$ also led to reduced model performance. This could be due to the regularization component of the SGDR training where non-contributing inputs are automatically removed from the model (their coefficients set to zero) without needing to do so manually.

Auto-Regressive (AR) lags of all input variables were also tested in order to further increase sample weights of the more recent observations and include short-term memory of the inputs. These were tested with lags ranging from 1 step backwards (49 seconds) up to 73 steps (60.4 minutes) included in the test data used for training and prediction. Each AR lagged model performed less favorably compared to the model presented in the methodology (Section 4.2.2).

5.8 Future extensions of work

The forecast models presented are deterministic by design (single point predictions). Commercial providers and forecast users are beginning to move towards probabilistic approaches which also contain information about the uncertainty of the prediction (Pinson et al. (2007)). Further, this study focuses on generating scalar wind speed predictions, and neglects the obvious utility of wind direction forecasts, or in forecasting the vector components themselves. These are recommended directions to consider for future work in this topic.

6 Conclusions

A novel field experiment was successfully conducted where horizontal wind fields were observed by scanning Doppler lidars situated alongside in-situ mast sensors. A simple lidar wind retrieval method was demonstrated which performs excellently for wind speed but less favorably for wind direction.

Space-time correlations between upwind lidar observations and reference cup anemometer measurements were investigated, which reveal a distinct peak which shifts in time and broadens as a function of distance upwind. The highest correlations occur up to around 2-3 km upwind, which indicates the region where advection transport dominates. An example of gust tracking is also presented, which follows the structure as it advects downwind over a 15-min period.

5 Overall, the forecasting model utilizing these upwind lidar observations outperforms both benchmark persistence methods in all aspects of importance for wind speed predictions: RMSE, MAE, general linear fit and overall level of scatter. This is true across all lead times, however the improvements are most significant for the 1-3 minute ahead forecasts corresponding to the upwind distances with the strongest spatio-temporal wind speed correlations.

10 At the 1-minute horizon, RMSE wind speed predictions are reduced by 21 % compared to the benchmark (10-min moving average persistence for the same horizon). This skill improvement continues for: 5-min (10.9 %), 10-min (9.2 %), 30-min (7.1 %) and 60-min (6.2 %). Moving beyond 20-min ahead predictions, the model settles to consistently demonstrate approximately 6-9 % improved skill. This can be explained as a shift (decrease) in the persistence lead-time by the distance upstream visible by the lidar.

15 The model training algorithm with walk-forward execution was implemented in a way which emulates an operational real-time forecast system and is able to adapt to changing conditions. The regularization penalty inside the SGD fitting is able to perform feature selection, making the system robust to a large number of highly correlated input features which do not need to be expertly chosen.

20 This research work has applicability towards reducing forecast errors within and below 60-minute ahead lead times. This acts to increase knowledge and reduce risk for stakeholders in countries which currently or plan to operate generator dispatch and market clearing on very-short intervals such as Germany, Australia, and the countries which will follow.

Data availability. The Østerild Balconies experiment was funded as part of the New European Wind Atlas project. Data access is restricted to project participants until after the embargo period, after which time it will be released to the public. The dataset is published in Simon and Vasiljevic (2018).

25 *Author contributions.* E.S. conducted the research work and drafted the manuscript. E.S. and N.V. participating in the design, monitoring, and data collection of the experiment. E.S. prepared the data and executed the in-depth data analysis. M.C. supervised the overall research work and made contributions to the scientific direction. All co-authors participated in discussing and revising the paper.

Competing interests. The authors declare that they have no conflicts of interest.

Acknowledgements. Feedback and guidance towards finalizing this research work with Sue Ellen Haupt and David John Gagne II at NCAR are greatly appreciated.

The authors would like to recognize the efforts of Guillaume Lea along with the technical staff at Østerild test station for their assistance throughout running the field experiment.

5 Ebba Dellwik has created the terrain maps of the experiment site, presented in Figures 3 and 11.

Jakob Mann has created the lidar scanning depiction, presented in Figure 4.

The field experiment was funded by the European Union grant NEWA ERA-NET Plus, topic FP7-ENERGY.2013.10.1.2 as part of the New European Wind Atlas project, including financing towards purchase and deployment of the lidar systems. The scientific work relating to formulating a lidar based forecasting method is funded by the Department of Wind Energy at the Technical University of Denmark.

References

- 4C-Offshore: LiDAR is a cost effect alternative to met masts claim industry experts - 4C Offshore, <http://www.4coffshore.com/windfarms/lidar-is-a-cost-effect-alternative-to-met-masts-claim-industry-experts-nid6131.html>, 2017.
- AEMC: Five Minute Settlement, <https://www.aemc.gov.au/rule-changes/five-minute-settlement>, 2017.
- 5 Alexiadis, M. C., Dokopoulos, P. S., and Sahsamanoglou, H. S.: Wind speed and power forecasting based on spatial correlation models, *IEEE Transactions on Energy Conversion*, 14, 836–842, <https://doi.org/10.1109/60.790962>, 1999.
- Bossanyi, E. A., Kumar, A., and Hugues-Salas, O.: Wind turbine control applications of turbine-mounted LIDAR, *Journal of Physics: Conference Series*, 555, 012 011, <https://doi.org/10.1088/1742-6596/555/1/012011>, <http://stacks.iop.org/1742-6596/555/i=1/a=012011>, 2014.
- Browning, K. A. and Wexler, R.: The Determination of Kinematic Properties of a Wind Field Using Doppler Radar, *Journal of Applied Meteorology*, 7, 105–113, [https://doi.org/10.1175/1520-0450\(1968\)007<0105:TDOKPO>2.0.CO;2](https://doi.org/10.1175/1520-0450(1968)007<0105:TDOKPO>2.0.CO;2), [http://journals.ametsoc.org/doi/abs/10.1175/1520-0450\(1968\)007%3C0105%3ATDOKPO%3E2.0.CO%3B2](http://journals.ametsoc.org/doi/abs/10.1175/1520-0450(1968)007%3C0105%3ATDOKPO%3E2.0.CO%3B2), 1968.
- 10 Damousis, I. G., Alexiadis, M. C., Theocharis, J. B., and Dokopoulos, P. S.: A fuzzy model for wind speed prediction and power generation in wind parks using spatial correlation, *IEEE Transactions on Energy Conversion*, 19, 352–361, <https://doi.org/10.1109/TEC.2003.821865>, 2004.
- 15 Energinet: Rules and regulations in the Danish electricity market, <https://en.energinet.dk:443/Electricity/Rules-and-Regulations>, 2018.
- EPEX SPOT: EPEX SPOT SE: Details, https://www.epexspot.com/en/press-media/press/details/press/Exchange_Council_approves_the_introduction_of_15-minute_contracts_on_the_Dutch_market_, 2017.
- EPEX SPOT: EPEX SPOT SE: Germany, <https://www.epexspot.com/en/product-info/intradaycontinuous/germany>, 2018.
- EWEA: Balancing Responsibility and Costs of Wind Power Plants, <http://www.ewea.org/fileadmin/files/library/publications/position-papers/EWEA-position-paper-balancing-responsibility-and-costs.pdf>, 2015.
- 20 Fraunhofer: The four grid control areas in Germany, http://windmonitor.iec.fraunhofer.de/windmonitor_en/2_Netzintegration/2_netzbetrieb/1_Die_vier_Regelzonen/, 2016.
- Frehlich, R.: Scanning Doppler Lidar for Input into Short-Term Wind Power Forecasts, *Journal of Atmospheric and Oceanic Technology*, 30, 230–244, <https://doi.org/10.1175/JTECH-D-11-00117.1>, <https://journals.ametsoc.org/doi/abs/10.1175/JTECH-D-11-00117.1>, 2012.
- 25 Giebel, G., Brownsword, R., Kariniotakis, G., Denhard, M., and Draxl, C.: The State-Of-The-Art in Short-Term Prediction of Wind Power, *ANEMOS.plus*, <https://doi.org/10.11581/DTU:00000017>, <https://doi.org/10.11581/DTU:00000017>, 2011.
- Holttinen, H.: Handling of wind power forecast errors in the Nordic power market, in: 2006 International Conference on Probabilistic Methods Applied to Power Systems, pp. 1–6, DOI: 10.1109/PMAPS.2006.360288, <https://doi.org/10.1109/PMAPS.2006.360288>, <https://ieeexplore.ieee.org/document/4202300>, 2006.
- 30 Kortforsyningen: DHM/Overflade (0,4 m grid), <https://download.kortforsyningen.dk/content/dhmoerflade-04-m-grid>, 2018.
- Lhermitte, R. and Atlas, D.: Precipitation motion by pulse Doppler radar, in: Proc. Ninth Weather Radar Conf., Boston, Amer. Meteor. Soc, pp. 218–223, 1961.
- Liang, X.: An Integrating Velocity–Azimuth Process Single-Doppler Radar Wind Retrieval Method, *Journal of Atmospheric and Oceanic Technology*, 24, 658–665, <https://doi.org/10.1175/JTECH2047.1>, <https://journals.ametsoc.org/doi/abs/10.1175/JTECH2047.1>, 2007.
- 35 Magerman, B.: Short-Term Wind Power Forecasts using Doppler Lidar, Ph.D. Thesis, <http://adsabs.harvard.edu/abs/2014PhDT.....314M>, 2014.
- NordPool: Trading on our intraday markets., <http://www.nordpoolgroup.com/trading/intraday-trading/>, 2019.

- Pinson, P., Chevallier, C., and Kariniotakis, G. N.: Trading Wind Generation From Short-Term Probabilistic Forecasts of Wind Power, *IEEE Transactions on Power Systems*, 22, 1148–1156, <https://doi.org/10.1109/TPWRS.2007.901117>, 2007.
- Potter, C. W. and Negnevitsky, M.: Very short-term wind forecasting for Tasmanian power generation, *IEEE Transactions on Power Systems*, 21, 965–972, <https://doi.org/10.1109/TPWRS.2006.873421>, 2006.
- 5 Regelleistung: Leitfaden zur Präqualifikation von Windenergieanlagen zur Erbringung von Minutenreserveleistung im Rahmen einer Pilotphase, <https://www.regelleistung.net/ext/download/pqWindkraft>, 2016.
- Scikit-learn: 1.5. Stochastic Gradient Descent — scikit-learn 0.19.1 documentation, <http://scikit-learn.org/stable/modules/sgd.html>, 2018a.
- Scikit-learn: 4.3. Preprocessing data — scikit-learn 0.19.1 documentation, <http://scikit-learn.org/stable/modules/preprocessing.html#preprocessing-scaler>, 2018b.
- 10 Scikit-learn: sklearn.linear_model.SGDRegressor — scikit-learn 0.19.1 documentation, http://scikit-learn.org/stable/modules/generated/sklearn.linear_model.SGDRegressor.html#sklearn.linear_model.SGDRegressor, 2018c.
- Simon, E. and Courtney, M.: A Comparison of sector-scan and dual Doppler wind measurements at Høvsøre Test Station – one lidar or two?, Technical Report, DTU Wind Energy, [http://orbit.dtu.dk/en/publications/a-comparison-of-sectorscan-and-dual-doppler-wind-measurements-at-hoevsore-test-station--one-lidar-or-two\(bfb41f11-ddac-474c-acc4-6e79739f\)](http://orbit.dtu.dk/en/publications/a-comparison-of-sectorscan-and-dual-doppler-wind-measurements-at-hoevsore-test-station--one-lidar-or-two(bfb41f11-ddac-474c-acc4-6e79739f))
- 15 .html, 978-87-93278-69-1, 2016.
- Simon, E. and Vasiljevic, N.: Østerild Balconies Experiment (Phase 2), <https://doi.org/10.11583/DTU.7306802>, <http://doi.org/10.11583/DTU.7306802>, 2018.
- Simon, E., Courtney, M., Vasiljevic, N., Lea, G., Dellwik, E., Karagali, I., and Mann, J.: Lidars Lifted: The Østerild Balconies Experiment, 2017.
- 20 Taylor, G. I.: The Spectrum of Turbulence, *Proceedings of the Royal Society of London A: Mathematical, Physical and Engineering Sciences*, 164, 476–490, <https://doi.org/10.1098/rspa.1938.0032>, <http://rspa.royalsocietypublishing.org/content/164/919/476>, 1938.
- Valdecabres, L., Peña, A., Courtney, M., Bremen, L. v., and Kühn, M.: Very short-term forecast of near-coastal flow using scanning lidars, *Wind Energy Science Discussions*, pp. 1–22, <https://doi.org/https://doi.org/10.5194/wes-2017-48>, <https://www.wind-energ-sci-discuss.net/wes-2017-48/>, 2017.
- 25 Vasiljevic, N.: A time-space synchronization of coherent Doppler scanning lidars for 3D measurements of wind fields - DTU Orbit, PhD Thesis, DTU Wind Energy, [http://orbit.dtu.dk/en/publications/a-timespace-synchronization-of-coherent-doppler-scanning-lidars-for-3d-measurements-of-wind-fields\(e2519d99-5846-4651-947d-38c287452366\).html](http://orbit.dtu.dk/en/publications/a-timespace-synchronization-of-coherent-doppler-scanning-lidars-for-3d-measurements-of-wind-fields(e2519d99-5846-4651-947d-38c287452366).html), PhD Thesis, 2014.
- Vasiljevic, N.: WindScanner Balcony Experiment - Phase 1, <https://www.youtube.com/watch?v=ZnkCuZG22YU>, 2016.
- 30 Vasiljevic, N. and Courtney, M.: Accuracy of dual-Doppler lidar retrievals of near-shore winds, in: *WindEurope Resource Assessment Workshop 2017*, [http://orbit.dtu.dk/en/publications/accuracy-of-dualdoppler-lidar-retrievals-of-nearshore-winds\(b9afd697-54f3-4d16-8d39-046946a8d8fb\).html](http://orbit.dtu.dk/en/publications/accuracy-of-dualdoppler-lidar-retrievals-of-nearshore-winds(b9afd697-54f3-4d16-8d39-046946a8d8fb).html), 2017.
- Vasiljevic, N., Lea, G., Courtney, M., Cariou, J.-P., Mann, J., and Mikkelsen, T.: Long-Range WindScanner System, *Remote Sensing*, 8, 896, <https://doi.org/10.3390/rs8110896>, <https://www.mdpi.com/2072-4292/8/11/896>, 2016.
- 35 Whittle, P.: *Hypothesis testing in time series analysis.*, Almqvist & Wiksells boktr., Uppsala, oCLC: 22153644, 1951.
- Zhang, T.: Solving Large Scale Linear Prediction Problems Using Stochastic Gradient Descent Algorithms, in: *ICML 2004: Proceedings of the Twenty-First International Conference on Machine Learning*. Omnipress, pp. 919–926, 2004.

3.6 Addendum 1: Case study of weather front event

This section expands upon an oral presentation titled "Lidars Lifted: The Østerild Balconies Experiment" given at the 97th American Meteorological Society (AMS) conference in Seattle (E. I. Simon et al., 2017).

During the first phase of the Balconies experiment while the scanning lidars were deployed at 50 m above ground level (AGL), a weather event was encountered with a potentially high impact for an operational wind turbine or wind farm.

At approximately 6PM UTC on the 6th of June 2016, the arrival of a cold front drastically changed the wind regime at the test site. Although it did not cause a significant wind speed ramp, the wind directions of the two air masses were diametrically opposed. The result was a near instant 180 degree shift in wind direction (from 130 to 310 degrees) as the frontal advection displaced the formerly presiding conditions.

This example of sudden and extreme veer has undesired and potentially damaging effects for a wind turbine. From an energy production perspective by requiring significant time and control adjustments to adapt to the new conditions, and from a loads perspective by introducing a sudden and extreme loading of the rotor and tower structure which is outside of normal operating conditions.

Figure 3.6 presents a meteorological look into the event using measurements from the northern aircraft warning tower at Østerild, which is located at (57°5'13.34" N latitude, 8°52'50.42" E longitude).

The event is clearly visible in the lidar observations from the Sirocco unit, shown in Figure 3.7. The frontal boundary is located where the sign of the radial speeds switch from positive (outflow) to negative (inflow). It is first detected 7 km away from the mast position, and the propagation can be tracked over a 2-hour period as it approaches the test site.

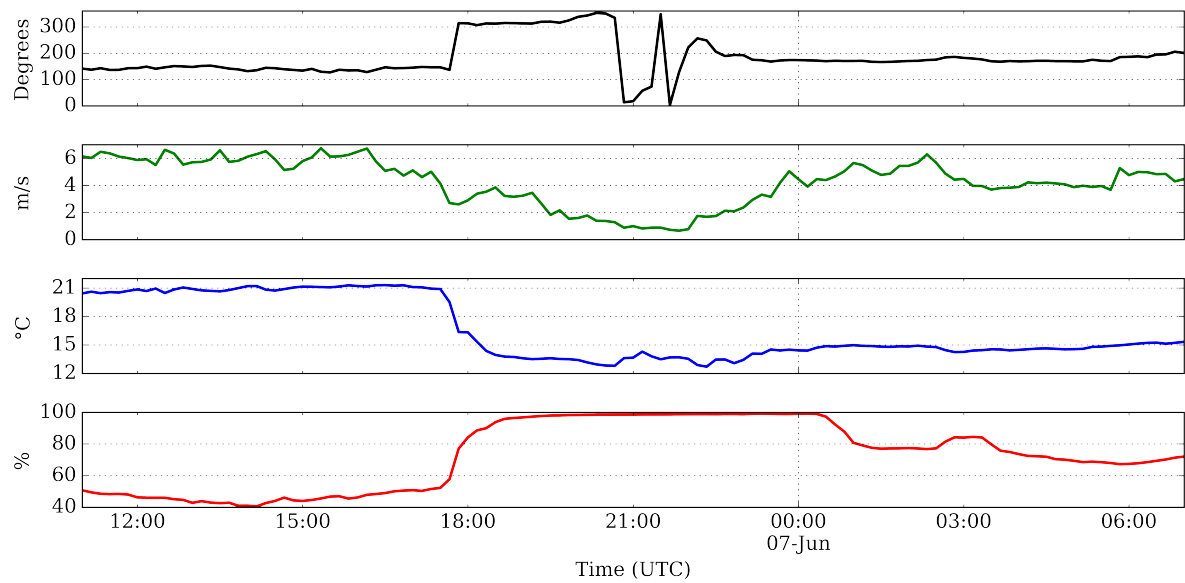


Figure 3.6: Mast measurements during a passing cold front at Østerild test center on June 6-7, 2016. Top panel: Wind direction at 40 m AGL. Second panel: Wind speed at 40 m AGL. Third panel: Temperature at 37 m AGL. Bottom panel: Relative humidity at 7 m AGL.

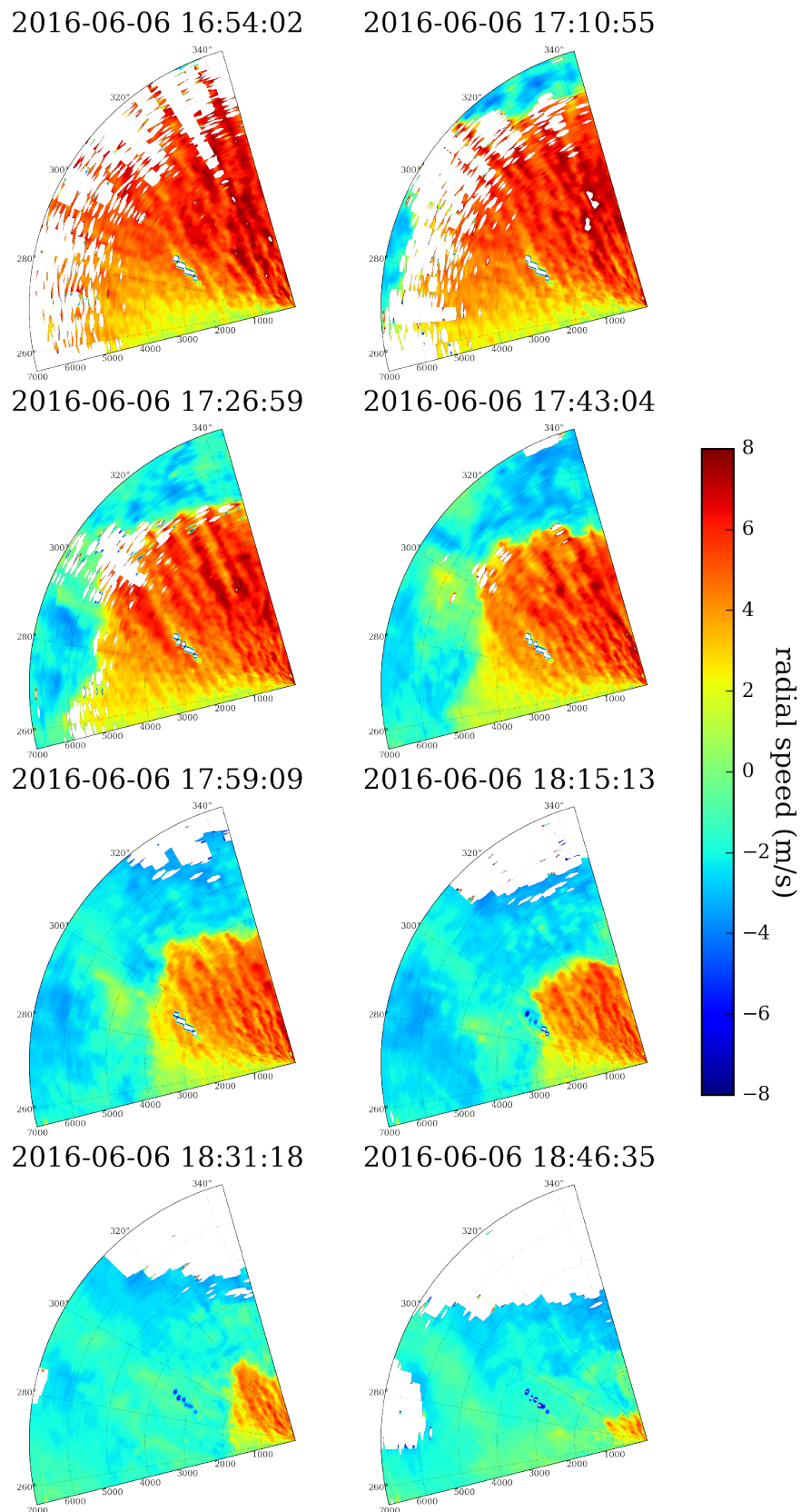


Figure 3.7: Lidar observations of the frontal passage event from the Sirocco unit. Images are single PPI scans spaced 15-minutes apart. Timestamps are in UTC format.

This event is an example of a very difficult to forecast phenomenon. Statistical methods including persistence and autoregressive (AR) models will fail spectacularly as there is no connection between the recent past and impending conditions. While physical approaches including numerical weather prediction (NWP) models are in many cases able to predict the existence of a passing weather front, correctly predicting the precise timing is notoriously difficult (phase error).

To further examine the usefulness of the upwind lidar system in capturing the event, predictions from an NWP model were compared with the local site measurements. Weather Research and Forecasting (WRF) version 3.5.1 model outputs at 2 km spatial resolution and 1 hour temporal resolution were obtained from Andrea Hahmann at DTU Wind Energy. The domain is shown in Figure 3.8 along with the grid cell nearest to the met-mast. The distance from the met-mast position to the nearest grid cell is 1.16 km.

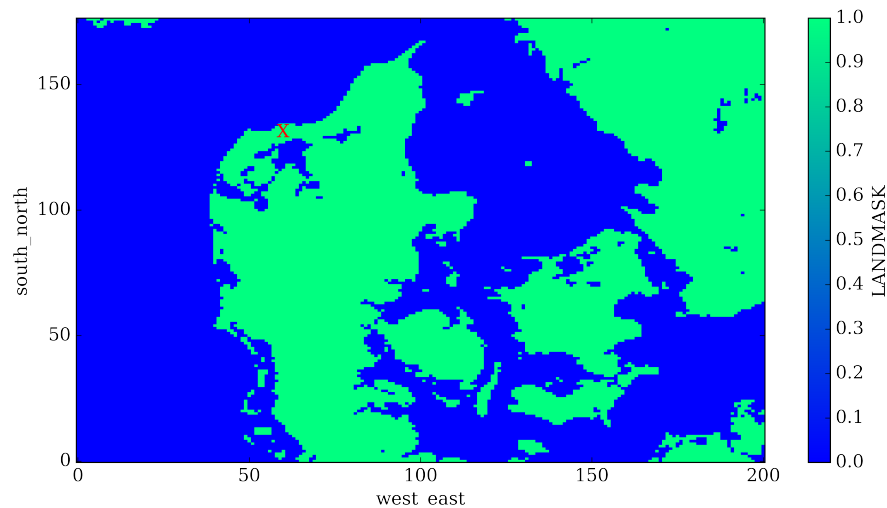


Figure 3.8: Domain for WRF simulation, with a red X denoting the chosen grid cell nearest to the met-mast.

Four runs: two initialized on June 5th at 0Z (midnight UTC) and 12Z (noon UTC), and two initialized on June 6th (0Z and 12Z) were used to make comparisons between wind speed and direction predictions and the reference site measurements. Note that in an operational context, the NWP results will not be available until some time after the model is initialized. In this case, the computation time is on the order of 8 hours. The met-mast measurements have been converted to UTC time for synchronization with the WRF model outputs.

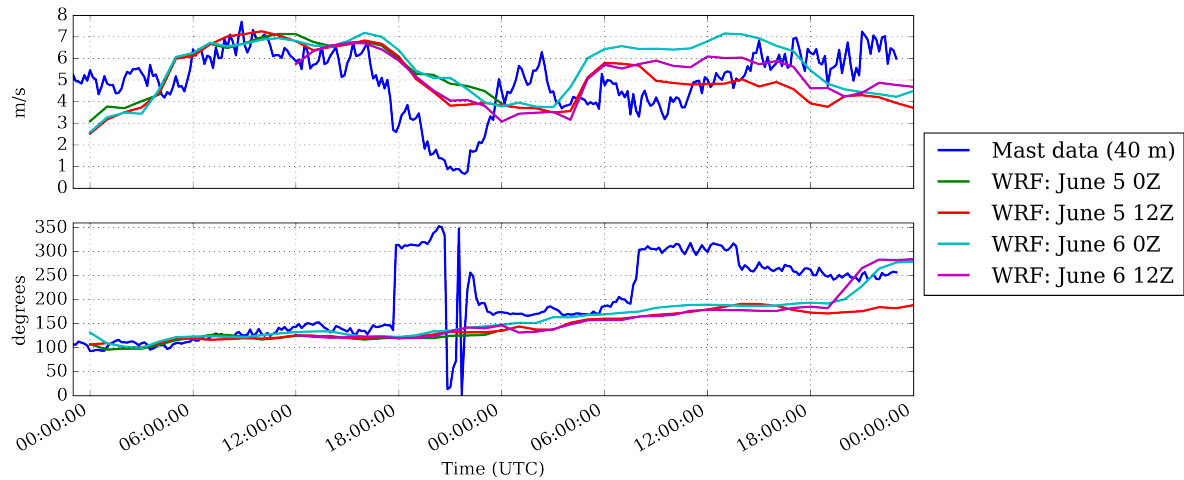


Figure 3.9: Comparison of four WRF model predictions with reference met-mast measurements.

WRF results are largely consistent across the four runs. Predictions between midnight and 6 PM UTC appropriately match the observational data from the met-mast. However, after this time the forecast does not capture the direction change which is a result of the event observed by the lidar. A further example of a timing (phase) error can be seen in the second direction veer occurring at 8 AM but forecasted to occur 12 hours later.

In summary, the lidar observations have demonstrated a clear value in capturing and tracking a weather event of potential concern as it approaches a wind turbine or wind farm. The event was not predicted by the WRF NWP approach, but was detected 2 hours beforehand by the scanning lidar and its propagation was tracked until arriving to the met-mast position.

This result supports the use of upwind lidar data for detecting and forecasting the arrival of large scale events at a local site. Particularly for sites with recurring localized weather patterns, this application carries promise when used as a classification and warning system to the operator or automated control systems.

3.7 Addendum 2: Key results and lessons learned

- An extensive field campaign was conducted using an improved lidar configuration for measuring long-range inflow of horizontal winds.
- A simple wind retrieval method was demonstrated which works well for wind speed but less favorably for wind direction
- Space-time correlations between a met-mast and upwind lidar positions were investigated, which indicate a sharp discernible peak up to 2-3 km distance upstream.
- The average advection behavior was compared between theoretical (Taylor's frozen turbulence hypothesis) and empirical (lidar retrieved winds) which shows agreement at the same scales as the space-time correlation result.
- A direct multi-step wind speed forecast model was implemented which emulates real-time scanning lidar inputs to predict 1-60 minute ahead wind speeds at the met-mast position.
- A rolling (walk-forward) training and prediction approach was used which assimilates the last observations to update model weights used in subsequent predictions.
- Root-mean-square wind speed forecast errors were reduced by 21% (1-min ahead), 10.9% (5-mins ahead), 9.2% (10-mins ahead), 7.1% (30-mins ahead), and 6.2% (60-mins ahead) compared to a 10-minute moving average of persistence.
- Gust events were detected upstream, which were able to be tracked up to 15-minutes before arriving to the met-mast position.
- A weather event (frontal boundary pass-through) was captured and tracked with a lead time of 2-hours which was not predicted by numerical weather models.

3.8 Introduction to third study: LASCAR experiment

After achieving promising results in the preceding investigation (Section 3.5), an augmented study was planned which would utilize the 2-Dimensional upwind lidar scans directly, in lieu of processing them into 1-Dimensional time series through a wind retrieval algorithm.

Arising from the space-time correlations observed in the Balconies experiment, a new field campaign was designed and conducted which focused on the 3-4 km spatial scale and 5-minute temporal scale. The LASCAR experiment built upon the measurement lessons learned so far to trade maximum range and angular resolution for scanning speed in order to better track spatial patterns as they advect downwind.

Additionally, the importance of accurately forecasting wind direction has been made clear by recent work in the field of wind farm control. Therefore the design criteria has been expanded to include both wind speed and direction forecasts.

The resulting study is presented in Section 3.9.

The data set and campaign metadata have been published on DTU's data repository (E. Simon and Lea, 2019a).

3.9 Minute-Scale Wind Vector Forecasting Using Scanning Lidar Inputs to a Convolutional LSTM Neural Network

Minute-Scale Wind Vector Forecasting Using Scanning Lidar Inputs to a Convolutional LSTM Neural Network

Elliot Simon and Michael Courtney

Technical University of Denmark, Department of Wind Energy (Risø Campus), Roskilde, Denmark

Correspondence: Elliot Simon <ellsim@dtu.dk>

Abstract.

The increasing share of wind power in energy systems leads to integration challenges for real time grid balancing and electricity market participation. As energy services move towards faster decision-action timeframes, improving the accuracy of wind power forecasts becomes crucial for ensuring system reliability and stable pricing. Forecasts on the minute-scale are traditionally based on statistical approaches using historical data. Remote sensing instruments such as pulsed scanning Doppler lidars are able to measure at long distances upwind of a wind turbine or wind farm and provide a preview of the approaching wind resource. Recent developments in machine learning have produced a convolutional-recurrent neural network unit called ConvLSTM. This enables models to learn from spatiotemporal patterns present in 2-Dimensional image sequences and use them to predict future outcomes.

To explore the possibilities of lidar-based wind forecasting, an artificial neural network (ANN) has been developed which utilizes lidar scans of the upstream horizontal wind field to predict downstream horizontal wind vectors in a multi-output fashion up to 5-minutes ahead. The results of the ANN-lidar model have been benchmarked against three common statistical approaches (persistence, AR, and ARIMA). The ANN-lidar approach has demonstrated skill below the 4-minute horizon, but has also highlighted challenges towards advancing the state of the art.

1 Introduction

1.1 Minute-scale forecasting of winds

Meteorological forecasts with time resolutions on the minute-scale are becoming increasingly useful in the wind energy field. The underlying variability of the wind resource, together with constraints from the power system and energy markets drives a need for accurate site-specific forecasts of impending conditions, particularly at large wind power plants. To date, the state of the art for producing such forecasts is normally based on time series modelling of past observational data (Giebel et al. (2011)). Another advanced approach is to adapt the output from previously computed ensemble numerical weather prediction

(NWP) models to real-time measurements (Moehrlen (2004)). The inclusion of local measurements in this manner has shown potential towards improving the inability of NWP models to correctly predict the timing, magnitude and duration of wind ramps- that is, large and sudden changes in the extractable energy in the wind (Mahoney et al. (2012)). However, in light of these developments, the most widely used technique by the wind power industry on timescales below 1-hour remains the persistence method.

Persistence assumes that short-run future conditions will remain unchanged from the recent past. Due to the high temporal autocorrelation of winds on very-short timescales, this method has performed acceptably well to date. Yet by design, the persistence method fails to predict changes (such as weather fronts and ramp events) which results in undesired discrepancies in expected and actual production, as well as imperfect information being fed to control systems.

As energy systems across the world transition to higher shares of variable renewable generation, these forecast errors become increasingly problematic for maintaining stable frequency control and limiting financial risk for imbalances in the energy markets. Owners of wind power assets have historically been supported by agreements such as the feed-in-tariff (FIT) or other power purchase agreements (PPA) which disregard the timing of their production. As these programmes phase out, operators will face financial consequences for forecast errors as balance responsible parties (BRP).

To date, a number of national and regional grid operators support trading of energy in markets with delivery times on the minute-scale (EPEX SPOT (2019)), with others expected to follow suit as their share of renewable generation increases. Minute-scale wind forecasts are also an integral component of wind turbine and farm control applications, which aims to maximize energy production while minimizing fatigue and extreme loading of the structures.

1.2 Remote sensing of winds

With the advent of remote sensing technologies, it is now possible to measure winds at a distance, without the expense and limitations of tower based in situ sensors. Lidar technology in particular has benefitted from rapid cost decreases partly due to hardware overlaps with optical fiber components used in the telecommunications industry. Doppler wind lidars have found applicability in wind energy and proven their practicality within areas including: wind resource assessment (Brower (2012)), power performance verification (Wagner et al. (2014)), independent sensor (Ahsbahs et al. (2017)) and model (Veiga Rodrigues et al. (2016), Mann et al. (2018), Vollmer et al. (2015)) validation, NWP data assimilation, operational turbine control (Schlipf et al. (2012)), among others.

In this paper we will solely refer to coherent pulsed scanning Doppler lidar technology. These instruments are active remote sensing devices which use shaped pulses of laser light, typically with a wavelength of 1.54 μm to probe the atmosphere. This wavelength was chosen as it corresponds to the absorption line of atmospheric water vapour and CO₂, meets eye safety standards, and is compatible with hardware components developed in the telecom industry (Cariou et al. (2006)). Laser pulses are emitted in a collimated beam from the lidar's telescope which backscatter off of aerosols (particles suspended in the air) and in turn shift their frequency according to the Doppler principle. A small portion of the backscattered pulses are received by the

lidar's optical chain and through spectral processing a radial velocity is obtained. This radial velocity represents the projection of the wind velocity along the beam angle (line-of-sight, LOS). As pulsed lidars do not focus their beam, measurements at multiple distances (range gates, RG) are taken simultaneously. The values are calculated by range weighting of the spectra and discerned through a time-of-flight calculation based on the fixed speed of light. It is important to note that the lidars do not
5 measure at discrete points in space, but rather a volume-average of the backscattered pulses.

Scanning lidars are equipped with a movable scanner head with two degrees of freedom used to steer the beam along a given trajectory. This is achieved through control of the system's azimuth and elevation motors, while range gating accounts for the third degree of freedom. These capabilities allow for measuring in 1D (staring), 2D (plane), and 3D (volumetric) modes. In this study, we will employ the following two scan types:

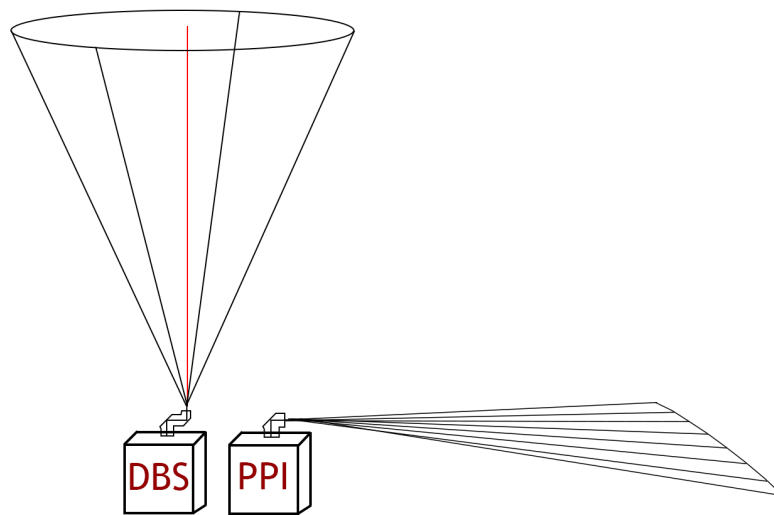


Figure 1. Depiction of Doppler beam swinging (DBS, left) and plan position indicator (PPI, right) scanning trajectories

- 10 – Doppler beam swinging (DBS) scans. Skyward facing DBS scans are used to measure the vertical wind profile by sampling at normally four orthogonal directions in addition to a vertical beam (Strauch et al. (1987)). Under the assumption of horizontal homogeneity and sampling concurrency, the horizontal wind vector is deduced with the vertical component being directly measured.
- 15 – Plan position indicator (PPI) scans. PPI scans are conducted by sweeping across a range of azimuths while holding the elevation angle constant. At zero degrees elevation this follows an arced horizontal plane representing a cross-section of horizontal winds projected along the azimuth of each beam direction.

Traditionally, radial velocity measurements from PPI scans are used to obtain horizontal wind vectors through single-Doppler velocity retrieval (SDVR) techniques such as the integrating Velocity Azimuth Process (IVAP) (Liang (2007)). This method

treats the line-of-sight measurements as different perspectives of the same homogeneous wind which reduces the data dimensionality to a time series of the horizontal wind components (u,v) at each range gate.

Wind patterns are discernable in the 2D scans themselves and contain spatial information which is largely lost using the classic SDVR techniques. By treating the PPI scans as a 2-dimensional image, we are able to employ techniques from the fields of image processing and computer vision to make use of the spatial patterns contained within the scan. This is the chosen direction of this study.

1.3 Concept of lidar based forecasting

Remotely measured wind fields present the potential for improving these very-short term forecasts by integrating wind patterns measured upwind of a wind turbine or wind farm's position into a prediction model. The observed winds advect to some degree downstream and the motion of coherent structures such as gusts, weather fronts, and turbulent eddies can provide forward looking information about conditions which arrive in the order of minutes ahead.

Pulsed scanning Doppler lidars are well suited for this application due to their high spatial and temporal resolution, extended field of vision (up to 10 km (Leosphere (2018)), 12 km (Halo Photonics (2018)) or 30 km (Mitsubishi Electric (2018))), configurable scan patterns, and ability to measure throughout diverse environmental conditions.

A number of studies have been conducted to date concerning forecasting for wind energy purposes using lidar observations directly. Carpenter (2013) demonstrates an advection based method which propagates wind fields of a site-specific ramp phenomenon downstream to produce a forecast up to 45 minutes ahead which significantly improved upon persistence while achieving peak performance at the 10 minute ahead forecast horizon. Magerman (2014) tracks spatial variances of turbulence and extractable energy content in the upstream wind to produce a wind power forecast several minutes ahead, and also tracks a ramp event occurring due to a frontal passage over a one hour timescale. Valdecabres et al. (2017) demonstrates a lidar based advection approach to generate 5-minute ahead wind speeds of near-coastal flow. Another work by Valdecabres et al. (2018) applies a similar advection based methodology to dual Doppler radar measurements for producing probabilistic wind power forecasts up to 5-minutes ahead. A recent work by Simon et al. (2018) utilizes horizontally scanning lidars mounted alongside a met-mast to make wind speed predictions up to 1-hour ahead.

1.4 Artificial neural networks (ANN)

Artificial neural networks (ANNs) are computing systems which take inspiration from the structure of the cerebral cortex. That is, they are designed to simulate the way the human brain processes and analyzes information. ANNs are capable of both self-learning and generalization, and have demonstrated their prowess for modelling complex non-linear relationships (Ogunmolu et al. (2016)). Core applications of this technology include natural language processing (Kim (2014)), pattern recognition (Taigman et al. (2014)), and sequence prediction (i.e. forecasting) (Laptev et al. (2017)). Supervised learning tasks use labelled

training data (known inputs and outputs) to refine model weights through the forward activation of outputs and the backwards propagation of errors. Once a model is fit to a set of known observations, it can then be used as an analytical tool for predicting out-of-sample data.

Recommended background readings for further general context in the field include Goodfellow et al. (2016), Google Developers (2019) and Li (2018).

The tracking of wind patterns from real-time 2D lidar scans applied as a forward prediction engine represents a spatiotemporal sequence forecasting problem. There are two classes of neural networks which are relevant for different elements of this application. Convolutional neural networks (CNN) apply a sliding kernel to an input image, which extracts features from the image while preserving the spatial relationships. CNNs are widely applied to computer vision and object tracking tasks, and use a feed-forward architecture which only allows signals to travel in one direction (input to output). The second class are recurrent neural networks (RNNs), which in contrast to feed-forward designs, include loops to allow signals to travel in both directions of the network. Computations from past inputs are fed back into the network which imparts the ability for memory of sequences of inputs. As time series signals contain a high degree of temporal autocorrelation, RNNs are routinely applied to forecasting tasks. Today's state of the art RNNs mainly comprise of long short-term memory (LSTM) units (Hochreiter and Schmidhuber (1997)) which were designed to use gating rather than activation functions to avoid the vanishing or exploding gradient problem (Greff et al. (2017)).

Shi et al. (2015) has introduced a combination of both classes which aims to capture spatiotemporal correlations by designing a model where the input-to-state and state-to-state transitions are convolutional (i.e. the input and recurrent transformations). The ConvLSTM unit is well suited for problems where both the spatial features and their correlations in time are fundamental features of the phenomenon. In the seminal work, Shi et al. applied the ConvLSTM approach to precipitation nowcasting using radar reflectivity images as inputs which significantly outperforms fully connected (FC) LSTMs. The ConvLSTM units will similarly be applied here using the Doppler lidar scans together with pooling layers to extract the dominant features.

2 Motivations and research questions

The following questions represent the core aims that this research work sets out to answer:

- How do 2-dimensional lidar scans correlate to each other? Can the advection of winds be tracked?
- Can 2D lidar scans be utilized as images in a convolutional LSTM neural network for generating minute-scale predictions?
- Can such a model forecast wind vectors at a reference position minutes ahead with higher skill than relevant benchmark methods?

- Can this be accomplished in real-time so that the predictions can be put to practical use?

3 Field experiment

3.1 Site description

The field experiment for this study took place at the Risø Campus of the Technical University of Denmark, situated at the following coordinates: 55° 41' 21.2604" N latitude, 12° 6' 1.6632" E longitude. The site is located along the shore of Roskilde fjord, a predominately shallow inland body of water containing a number of small islands (see Fig. 2). Winds are measured both over land and water. The onshore topography is characterized by mostly flat terrain rising upwards from the shoreline at an average slope of 5 degrees. Onshore background surface roughness is estimated at 0.05 m. Trees and shelter belts exist nearby, along with small patches of forest. The small low-lying island wholly included in the measurement area is Elleore, a self-proclaimed independent Kingdom (Mislán and Streich (2019)). The western bank of the water is the peninsula Bognæs, a mainly forested area used for hunting and recreation.

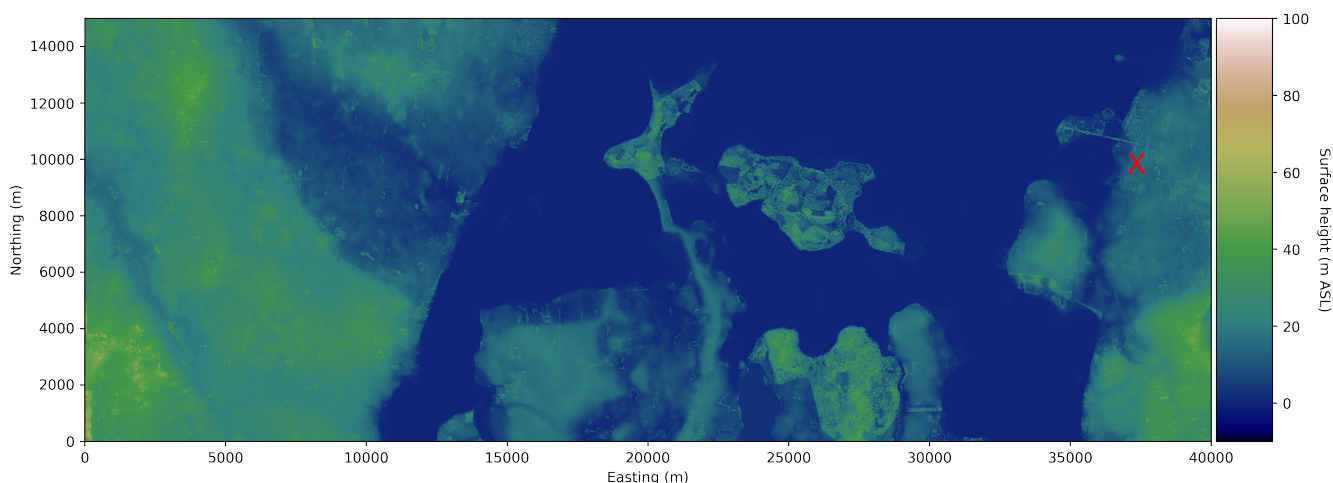


Figure 2. Digital surface model of the surrounding area. The lidar deployment area is denoted with a red X. Heights are relative to mean sea level

3.2 Measurement characteristics, configuration and pre-processing

3.2.1 Experiment overview

A field experiment involving a total of six scanning wind lidars was conducted during the autumn and winter of 2017-18 (October 12, 2017 – February 27, 2018). The goal of the experiment (designated LASCAR) was to obtain detailed measurements of the wind particularly for westerly inflows which develop over Roskilde fjord. Observations were made across flat horizontal and vertical planes, together with vertical profiles of the horizontal winds. In this study, we utilize data from two of the lidar systems deployed in the experiment.

All lidar instruments are of the DTU Long-Range WindScanner variety (Vasiljevic et al. (2016)). Key parameters of the measurement scenario are presented in Table 1 and Table 2 for each scanner respectively.



Figure 3. LASCAR experiment overview, with positions of the two scanning lidars and the met-mast denoted. The radius of the arc is 4 km

10 3.2.2 Sirocco unit – Plan position indicator (PPI)

In order to measure winds at the same height across all distances, the Sirocco unit was raised above ground with its elevation axis set to zero degrees. The lidar was deployed on the rooftop of Risø building 313, as shown in Fig. 3. This was accomplished

Table 1. Lidar specifications for the ‘Sirocco’ unit

Pulse length	200 ns (middle pulse)
Pulse energy	50 μ J
Pulse repetition frequency (PRF)	20 kHz
Probe length (FWHM)	35 m
Scan type	Plan position indicator (PPI)
Azimuth angle range	250 ° - 280 ° (30 ° sector size)
Elevation angle	0 °
Accumulation time	400 ms
FFT size	64 bins
Measurement range	80 – 4000 m
Range gate (RG) spacing	20 m (197 RGs)
Scanner head motion	2.5° / s
Reversing?	No. Scanner head resets to initial position following each scan
Number of lines-of-sight (LOS)	30 (1° LOS spacing)
Scan rate	13 s / scan (including reversing)

using a crane truck which lifted the device from the ground onto the roof, which was then carried manually into its position at the edge of the flat rooftop. The lidar’s height above mean-sea-level (AMSL) was measured at 22.07 m using a Leica Geosystems CS15 field controller and GS15 GPS receiver which has a 15 mm vertical static root-mean-square (RMS) accuracy (Leica Geosystems (2012)). Several points at the base of the building and coastline were also measured, leading to a determined height above ground-level (AGL) of 8.53 m and height above water-level (AWL) of 20.65 m at the time of measurement during typical conditions. The water level is subject to change, particularly during storms and under presiding northerly winds when water is transported into the fjord.

The system was levelled along both axes of the telescope using a digital level along with the system’s internal inclinometer. Standard procedures were followed to map multiple objects (hard targets) spaced across a range of positions in order to perform a static pointing calibration. Once the system’s position and orientation were known, offsets were hardcoded into the motion controller such that the zero degrees azimuth reference matched to north.

The lidar was configured according to Table 1 and set to perform repeating PPI scans as depicted with the red outline in Fig. 3. This entails keeping the elevation angle fixed while scanning over a range of azimuths to produce an arc slice through the horizontal wind.

Table 2. Lidar specifications for the ‘Brise’ unit

Pulse length	100 ns (short pulse)
Pulse energy	25 μ J
Pulse repetition frequency (PRF)	40 kHz
Probe length (FWHM)	25 m
Scan type	Doppler beam swinging (DBS)
Number of lines-of-sight (LOS)	5 beam method
Half cone angle	15 °
Accumulation time	1 s
FFT size	64 point
Measurement range	50 – 1000 m
Range gate (RG) spacing	10 m (96 RGs)
Scan rate	15 s / scan

3.2.3 Brise unit – Doppler beam swinging (DBS)

The Brise unit was deployed at ground level in the lee of the same building as Sirocco. Using the Leica controller, the height of Brise relative to Sirocco was found to be -7.8 m with a total Pythagorean distance between the two system’s telescopes equaling 31.86 m. The relative height difference differs from Sirocco’s height AGL as the terrain slopes down around the building. The same levelling and calibration procedures were performed on Brise as Sirocco. The lidar was configured according to Table 2 and set to perform repeating DBS scans. This entails measuring along 4 fixed positions along a cone, followed by a central vertical beam which provides a direct measure of the vertical wind component.

3.2.4 Other instrumentation

Conventional (in situ) measurements from a nearby meteorological mast are used as an independent reference for validation purposes. The source of the data is the meteorological mast 400 m directly southwest of the lidar deployment location (indicated in Fig. 3). The mast is an IEC compliant reference for DTU’s Vestas V52 research turbine. Ultrasonic anemometer measurements from 44 m AGL are used, as this is the closest instrumented height to Brise’s 50 m AGL range gate.

3.3 Data filtering and processing

A 12-hour continuous subset of the experiment has been selected for this study. Measurements obtained between November 14th at 16:45 and November 15th at 04:45 represent a population size of 3270 13-second samples (corresponding to the lidar’s

scan rate). The criteria used for selecting this period was for both lidar systems to be operational and the winds to originate broadly from the west (inflow to the experimental setup).

3.3.1 Sirocco unit (PPI scans)

A flowchart overview of the data processing steps for Sirocco is presented in Fig. 5.

5 Processing of the PPI scans from Sirocco began with reading in the radial speed measurements produced by the lidar system from all scenarios within the given time period. Timestamps were parsed from LabVIEW epoch time into datetime objects, with time zone conversion from UTC to local time (Central European Time, or UTC+1) in order to match the met-mast data logger convention.

10 Filtering steps included the removal of partial scans which can exist at the partition between scenario files. A carrier to noise ratio (CNR) threshold filter was applied which discarded measurements below -26 dB (low signal quality) and above 0 dB (hard target contamination). A radial speed filter was then applied which ensures that only periods of inflow, when the wind direction was approaching the lidar were considered. Next, a line-of-sight (LOS) filter was applied to reduce the angular width of scan from 30° to 21°. This was required as the azimuth range between 250° and 258° was contaminated by turbulence generated by a small patch of wooded trees. Finally, a range gate (RG) filter was applied which reduced the maximum distance
15 included to 3 km. This was due to low data availability at the opposite bank of the fjord due to the presence of sloped terrain and vegetation blocking the lidar's beam.

Using the filtered dataset, each scan was projected from radial dimensions (azimuth, range) to Cartesian coordinates (x, y) on a 10 m resolution meshgrid, and filled using nearest-neighbor interpolation. This approach was chosen to allow the use of standard loss functions, instead of needing to redefine spherical implementations for training the model. As a side effect, this
20 step also increases the magnitude of the data represented in memory.

The 2-D lidar scan images were then scaled to values between zero and one. This acts to normalize the feature range of the scans when input to the neural network. A custom method was applied which prevents outliers from significantly affecting the scaling of the data. First, the mean, minimum and standard deviation across both dimensions were calculated. Next, the maximum values were determined as four standard deviations above the mean (Eq. 1). The scaling was then applied following
25 Eq. 2. Any values above four standard deviations over the mean were then set to one. An example of a processed scan is given in Fig. 4. Note that the scaling range was determined for each scan independently, and therefore does not use any past or future information.

$$X_{\max} = \bar{X} + 4\sigma_X^2 \quad (1)$$

$$X_{\text{scaled}} = \frac{X - X_{\min}}{X_{\max} - X_{\min}} \quad (2)$$

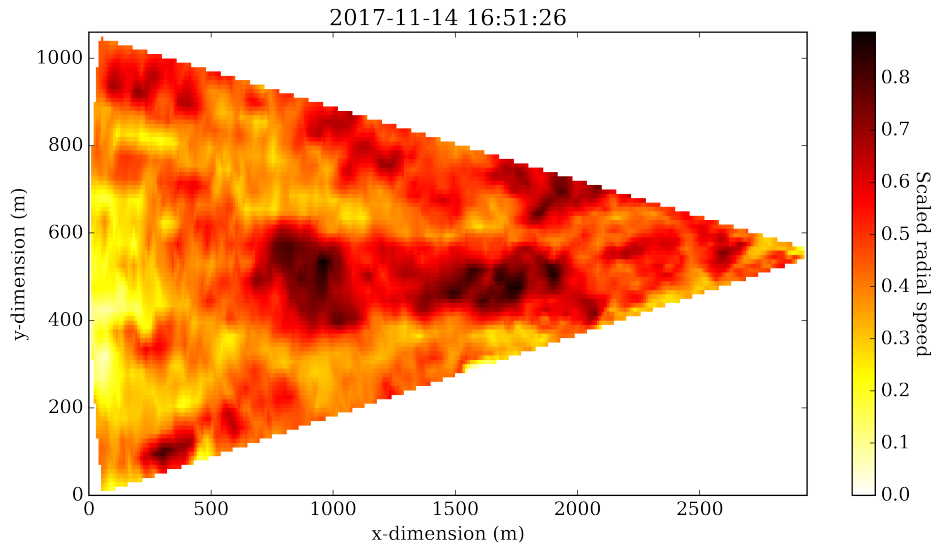


Figure 4. Example of processed scan image from a Sirocco PPI scan

To construct the data structure used for model training, processed scan images over the past input lag length at each scan-time were copied to a new dimension of the array. This represents the inputs fed to the forecasting model as each prediction and subsequent updated fit is made. The number of samples was then reduced at the beginning by the number of input lags, and at the end by the number of samples forecasted to remove periods with partial data on this axis. The final dataset structure is

- 5 5-dimensional with the shape (time, lags, x dimensions, y dimensions, channels), with radial speed being the only channel.

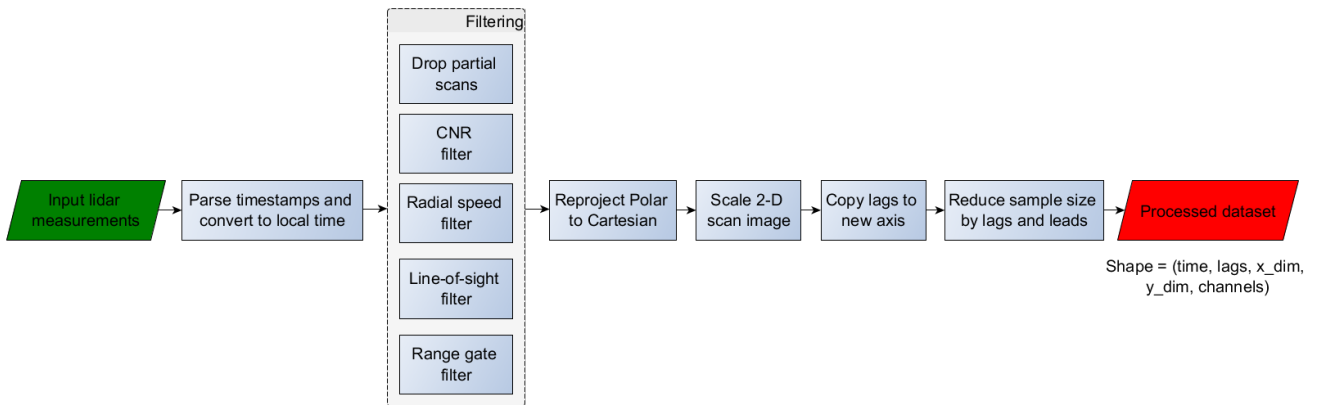


Figure 5. Flowchart of data processing for rooftop lidar (Sirocco)

3.3.2 Brise unit (DBS scans)

A flowchart overview of the data processing steps for Brise is presented in Fig. 6.

Processing of the DBS scans from Brise began similarly to Sirocco, with reading in the lidar measurements, parsing timestamps and removing partial scans at the boundary between scenario files. The same CNR filter thresholds as before were used to filter out observations with low signal quality or hard target contamination. Next, quality checks were performed which ensured that the beam positions were separated by index multiples of 5 (corresponding to the scan strategy outlined in Section 3.2.3).

The wind field reconstruction procedure was performed for all range gates following Section 3.4, and the lowest available height was chosen (50 m AGL). This corresponds to 42.2 m above the position of Sirocco. The reconstruction results in a sampling rate equal to the lidar’s LOS measurement speed, which was downsampled to match that of Sirocco (i.e. 13-second averaging).

Horizontal wind components u and v were used to compile the data structure for the reference measurement used in training the model and evaluating forecast errors.

Any undefined values as a result of filtering steps were set to zero. The forecast lead times were also copied to a new timestep axis. The same procedure was followed to reduce the number of samples at the beginning by the number of past lags and at the end by the length of the prediction interval. The final dataset structure is 3-dimensional with the shape (time, forecast leads, channels), where the two channels are reconstructed u and v components from the DBS measurements.

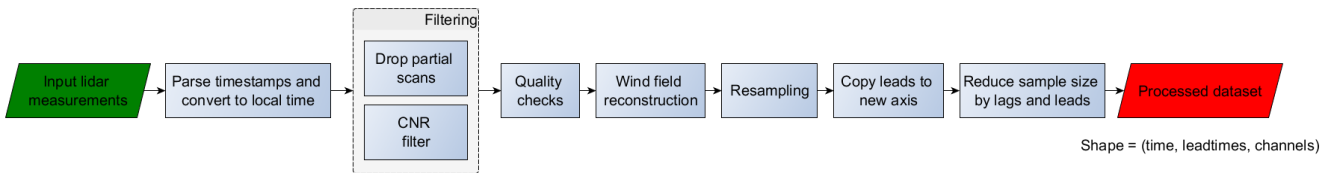


Figure 6. Flowchart of data processing for ground based lidar (Brise)

3.4 Wind field reconstruction (DBS measurements)

A flowchart of the DBS wind field reconstruction process is presented in Fig. 7. To perform the vertical profiling wind field reconstruction with the highest temporal resolution, a sliding window function is needed, which uses the latest available beam measurement to calculate the corresponding value at each timestep. The u and v horizontal wind components are each calculated from two orthogonal beam measurements, while w in this case is directly measured by the vertical beam. It is also possible to independently calculate w from the four orthogonal beams, as is done in the traditional four beam DBS configuration.

When implementing the reconstruction process, a vectorized approach was used. This avoids iterating through the entire dataset and results in a major computational speed advantage. The five line-of-sight (LOS) beams were split up accordingly by their azimuth and elevation angles. Quality controls were then performed to ensure that the beam index positions were separated by the correct LOS separation. Next, the measurements were interleaved along a new dimension according to the corresponding

5 beam-pairs. Finally, the reconstruction equations were applied across the entire dataset at once for each range gate.

$$u = \frac{U_{r_{west}} - U_{r_{east}}}{2 \sin \phi} \quad (3)$$

$$v = \frac{U_{r_{north}} - U_{r_{south}}}{2 \sin \phi} \quad (4)$$

$$w = U_{r_{vertical}} \quad (5)$$

$$w_{calc} = \frac{U_{r_{north}} + U_{r_{south}} + U_{r_{east}} + U_{r_{west}}}{4 \cos \phi} \quad (6)$$

$$10 \quad U_h = \sqrt{u^2 + v^2} \quad (7)$$

$$\psi = \arctan 2(v, u) + c \quad (8)$$

where U_r are the radial speed measurements, ϕ is the half cone angle, U_h is the scalar horizontal wind speed, ψ is the wind direction, and c represents a potential wind direction offset due to the lidar's orientation.

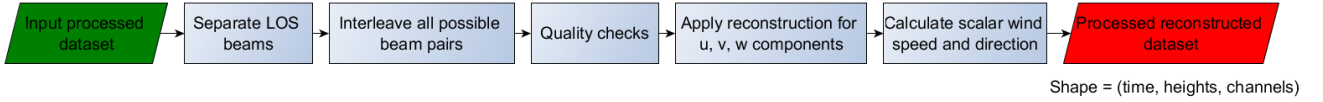


Figure 7. Flowchart of DBS wind field reconstruction from Brise

4 Forecasting methodology

15 4.1 Model training and prediction

4.1.1 Metrics

To evaluate performance of the forecast methods, the root-mean-square error (RMSE) between the predictions and reference values is used. This provides a single measure of predictive skill which penalizes larger errors relative to smaller ones. The RMSE metric is therefore sensitive to outliers which represent the largest potential impacts to the power grid and energy

markets.

$$RMSE = \sum_{i=1}^n \frac{(\hat{y}_i - y_i)^2}{n} \quad (9)$$

The predicted horizontal wind components u and v are similarly transformed to scalar wind speed and direction values using Eq. 7 and 8 for the purposes of the error analysis.

5 4.1.2 Forecast model implementation details

The lidar based forecast model utilizes the Keras framework in Python with Tensorflow backend. Training has taken place on a Google Cloud Compute instance equipped with one NVIDIA Tesla P100 GPU (graphics processing unit). The computation time for processing each batch (i.e. 13-second sample) is 32 ms, which is well within the time constraints for operational use. An overview of the training and prediction process is outlined in Fig. 8.

- 10 A walk-forward testing strategy was used, which emulates online learning of the model during real-time operation. This allows the model to be constantly updated with the latest available data when making out-of-sample predictions, as the samples are highly correlated in time. Therefore, the input layer has a batch size of one. The inputs are processed and scaled PPI images from Sirocco (i.e. rolling 5-minute window of upwind lidar observations), which are used to predict the u and v vector components reconstructed from DBS measurements by Brise across the 5-minute interval which follows.
- 15 Progressing chronologically through the dataset, each sample results in an updated model fit, and a forecast generated spanning 13-seconds to 5-minutes ahead. Subsequently, the dataset walks forward and the latest observations are assimilated resulting in an updated model and a new forecast. As properties of the target data would not be known ahead of time, it is necessary to perform feature scaling of the target signal (i.e. Brise reconstructed wind components) at every step using in-sample observations. This is achieved using Scikit-learn’s MinMaxScaler (Scikit-learn (2018)) to match the feature space of the processed PPI scan images.
- 20 scan images. This step is not applicable to Sirocco as the scaling has been applied across the image dimensions instead of time (Section 3.3.1).

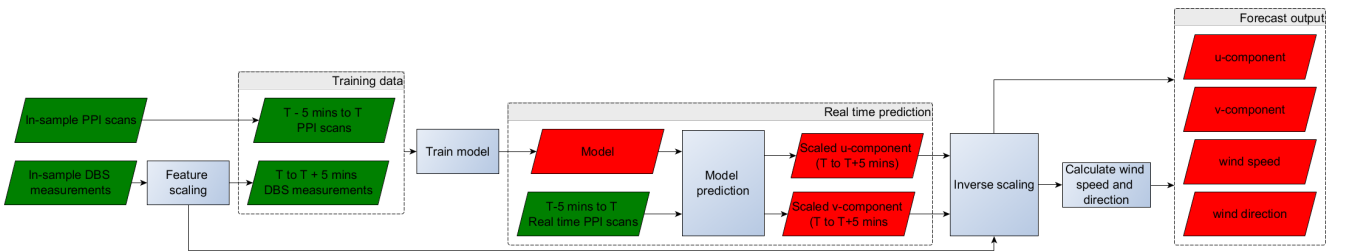


Figure 8. Flowchart of ANN-lidar forecast model operation

The neural network architecture is shown in Fig. 9. It is comprised of two sets of 2D convolutional LSTM layers (Tensorflow (2018)) which are downsampled using 2D MaxPooling (Keras (2018b)) layers before being flattened and then shaped using a fully connected (Dense) layer. Both ConvLSTM2D layers use ReLU (rectified linear unit) activation and neither dropout nor recurrent dropout was applied. As there are multiple stacked recurrent layers, it was necessary to return the entire hidden state output for each timestep so that the dimensionality for the next layer's input sequence is correct. In addition, the LSTM layers are stateful, meaning that the computed hidden states can be propagated between training batches. To preserve the time dimension of the multi-output model, TimeDistributed wrappers (Keras (2018a)) were applied to the non-recurrent layers. The model was compiled using the Adam optimizer (Kingma and Ba (2014)) and mean-squared-error (MSE) loss function. The model was then trained using the walk forward approach previously described, with one fitting epoch (training iteration) per batch (sample), and the model's internal states being reset following each epoch.

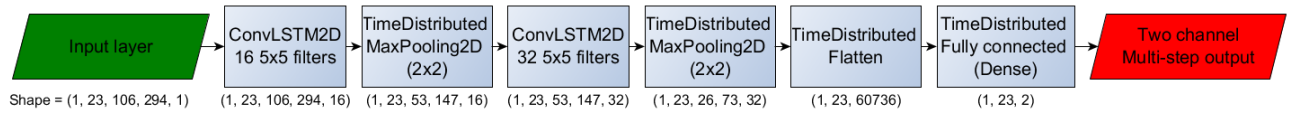


Figure 9. ANN-lidar model architecture

Following each forecast, the predicted values are inverse transformed into their (non-scaled) feature space for evaluation against the reference values.

4.1.3 Benchmarking (Persistence and ARIMA)

Two forecasting strategies based on standard methods applied within this timescale were carried out in order to benchmark the relative skill of the more neural network approach. These benchmark methods rely only on the univariate target signal, without any of the forward-looking information provided by the rooftop lidar (Sirocco). Scalar quantities of wind speed and direction are used in both cases. These are derived from the reconstructed horizontal winds of the DBS lidar (Brise) as outlined in Section 3.3.2.

The first benchmark is the persistence method, which forecasts future values to be the same as the most recent observation.

$$\hat{y}_{t+\Delta t} = y_t \quad (10)$$

where y is the reference signal and Δt is the forecast horizon.

The second benchmark is a time series modelling approach called ARIMA (autoregressive integrated moving average). This method utilizes past lags (AR) of the target variable and a moving average model (MA), along with differencing (I) of the series to transform it to a stationary process. Stationarity is determined through unit root testing, typically using the augmented Dickey–Fuller test. Seasonal adjustment here is not necessary, but would need to be applied for longer time series. The model

parameters ARIMA (p, d, q) represent the number of lags (p), the degree of differencing (d), and the order of the moving average model (q). The p parameter is determined through inspection of the autocorrelation function (ACF) and partial autocorrelation function (PACF), with consideration to increased computational demand for increasing number of lags (Fig. 10). The ACF describes the linear dependence of the signal with itself over a range of past values, while the PACF excludes the effects (indirect correlations) of intermediary lags. The d parameter is determined by performing an increasing number of differencing steps until the series becomes stationary (where the mean, variance, and probability distribution does not change with time). The final (q) (MA) component represents a weighted moving average of the past q error steps (exponential smoothing).

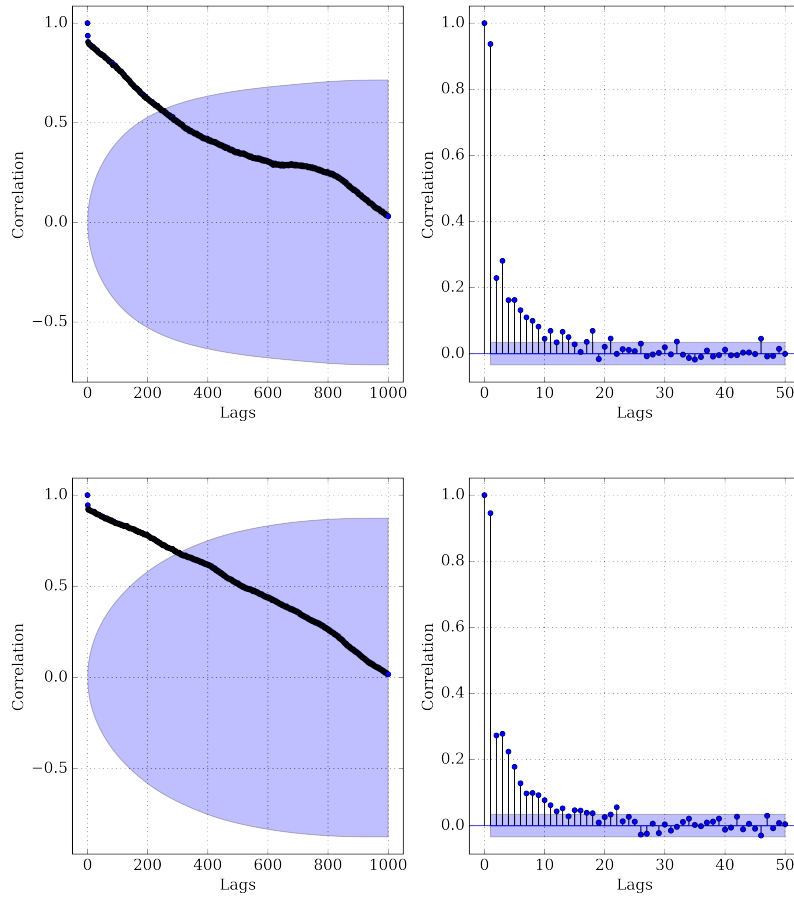


Figure 10. ACF (left) and PACF (right) plots (top: wind speed, bottom: wind direction) beginning from lag zero. The area outside the shaded region represents the 95% confidence interval where the correlation is non-zero (i.e. strong serial correlation)

The non-seasonal ARIMA formulation can be written as:

$$\hat{y}'_t = c + \phi_1 y'_{t-1} + \dots + \phi_p y'_{t-p} + \theta_1 \varepsilon_{t-1} + \dots + \theta_q \varepsilon_{t-q} + \varepsilon_t + c \quad (11)$$

Where y' is the arbitrarily d-differenced series, θ are parameters of the AR model, and ϵ are white noise error terms.

The ARIMA forecasts were generated in the same manner as the walk-forward training and prediction approach outlined in Section 4.1.2. The model was incrementally fit using in-sample data and predictions were made at each time step in a multi-output setup across the entire forecast length (i.e. every 13 s from 1 to 23 steps (5 minutes) ahead).

- 5 Two model formulations were tested, separately for wind speed and wind direction. Benchmark #1 is of order (5,1,0) which neglects the MA component and becomes a differenced fifth order AR model. Benchmark #2 is an ARIMA model of order (5,1,1). The parameters were fit using conditional sum-of-squares likelihood maximization.

Note that the wind direction signal over the time period chosen does not approach the boundary between 0 and 360 degrees, so it is not necessary to consider this when calculating the errors.

10 **5 Results**

5.1 Validation of wind field reconstruction method

To demonstrate the correct processing of the DBS measurements from Brise (according to Section 3.4), a validation has been included which compares the lidar obtained wind field to that measured at the nearby met-mast described in Section 3.2.4. The met-mast observations have been downsampled to match the sampling rate of the lidar. The data points have a time resolution
15 of 13-seconds and the sample size is 3220 observations.

The comparisons show generally good agreement between both independent instruments considering their spatial separation. The lidar reconstructed wind speeds from Brise indicate a small positive bias which increases with wind speed. The wind direction however is slightly underestimated relative to the met-mast. Nevertheless, the results confirm that there are no serious flaws in the source data or reconstruction methods.

20 **5.2 2D correlation of PPI scans**

A core assumption of the forecast model is that spatial patterns in the lidar scans are trackable as they advect downwind. An inspection of the cross-correlations between scan pairs has provided insight into this assumption. Six processed PPI scans from Sirocco are shown in Fig. 12, which are spaced in intervals of 3 scan-times (i.e. 40 s between each frame) for compactness. The darker structure with a higher radial speed visibly advects downwind while also transforming its properties due to turbulence.
25 The tail is centered at 2500 m upwind in the first frame, and 300 m in the last frame. This corresponds to an advection speed of 11 m/s, which closely matches the wind speed during the period (11.2 m/s).

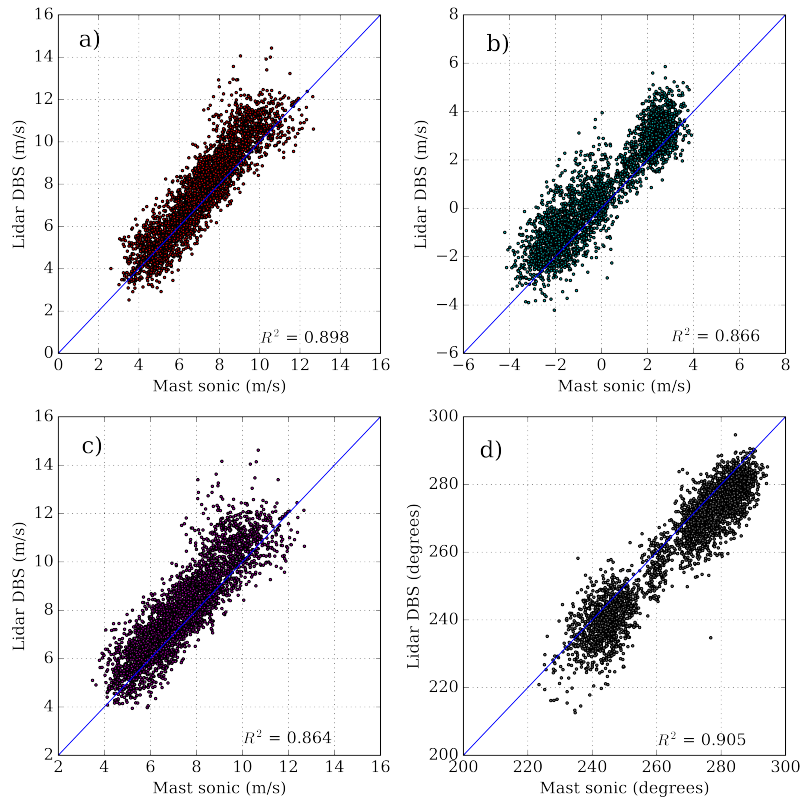


Figure 11. Validation of 50m lidar reconstructed DBS measurements (Brise) against 44m sonic measurements from nearby met-mast. a) u-component, b) v-component, c) wind speed, d) wind direction

Fig. 13 presents a 2D cross correlation result between one base image and the 1st to 8th scans which follow. This indicates the spatial distribution of correlations between the two images. The point where the maximum exists represents similar features appearing in both images. The advection rate of the structure from the correlation method (1km in 104 s = 9.6 m/s) also matches the average wind speed during the period (9.53 m/s). The 2D cross correlation was calculated using a 2D convolution function with the second image reversed along both axes.

5.3 Forecast results

Overall RMSE comparisons of the three forecast methods are presented in Fig. 14 both for wind speed and wind direction. This compares the RMSE performance by lead time of the various benchmarks together with the Lidar-ANN model.

The Lidar-ANN method outperforms two of the benchmarks (persistence and the integrated AR model) for the first 17 scan-times ahead (0.22-3.68 minutes). Following this and up to the maximum forecast length, the Lidar-ANN skill quickly deteriorates. The ARIMA(5,1,1) benchmark achieves the lowest RMSE across lead times, except for the first two forecast steps (13

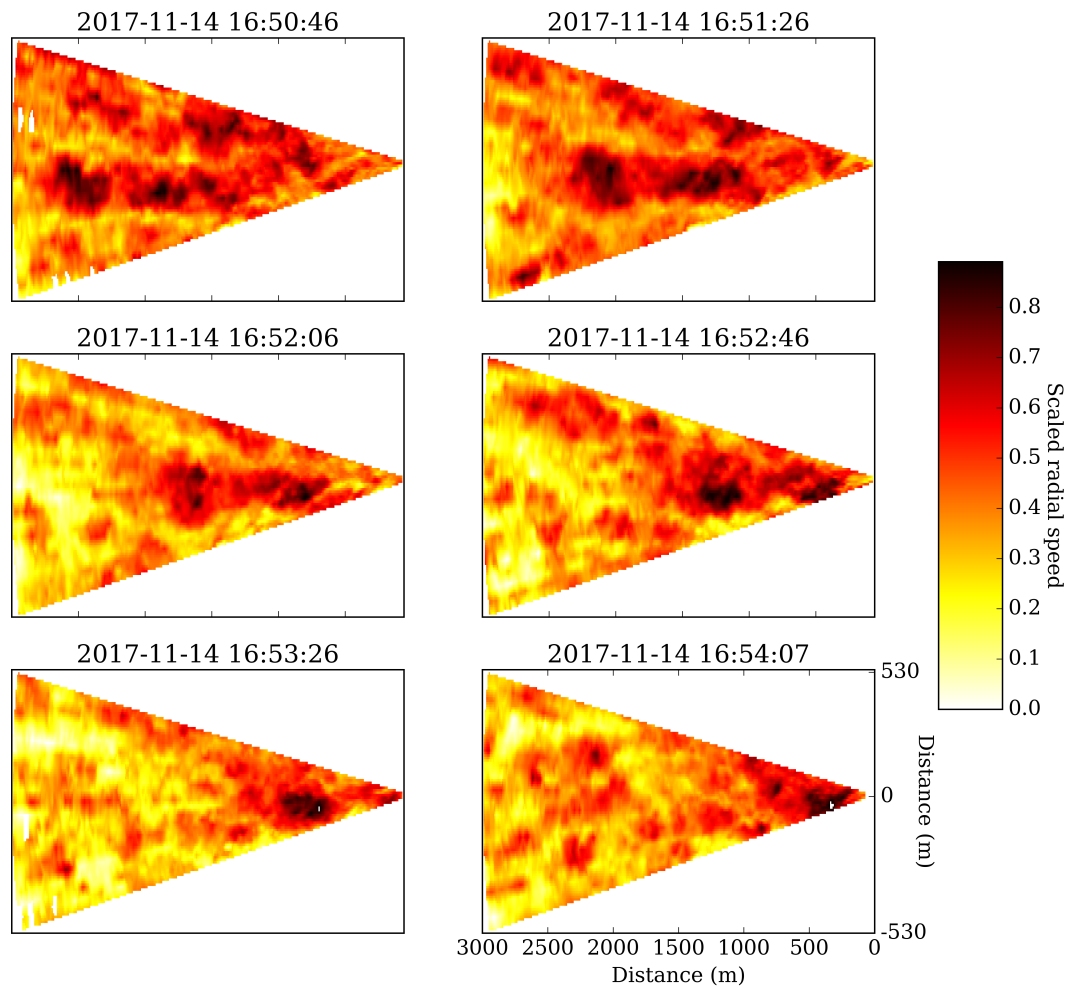


Figure 12. Example of PPI scan sequence (order: top-left to bottom-right) in intervals of 3 scans (i.e. 40 seconds between frames)

s and 26 s). Persistence performs well only at the shortest lead time (13 s ahead). Table 3 indicates the relative RMSE skill of the Lidar-ANN approach compared with the three benchmark methods.

The Lidar-ANN model predictions for the 1.08 minute ahead forecast horizon are shown in Fig. 15 and Fig. 16. Through inspection of the time series, it is clear that the model predictions follow the overall reference signal. However, they do not capture the fine variations (i.e. turbulence). This is shown as scatter around the $y=x$ line in 16.

Lidar-ANN model predictions exhibit larger amounts of scatter at higher wind speeds (> 10 m/s). The errors are also larger for wind directions where the inflow is not closely aligned with the center of the lidar scan (i.e. far from 270°).

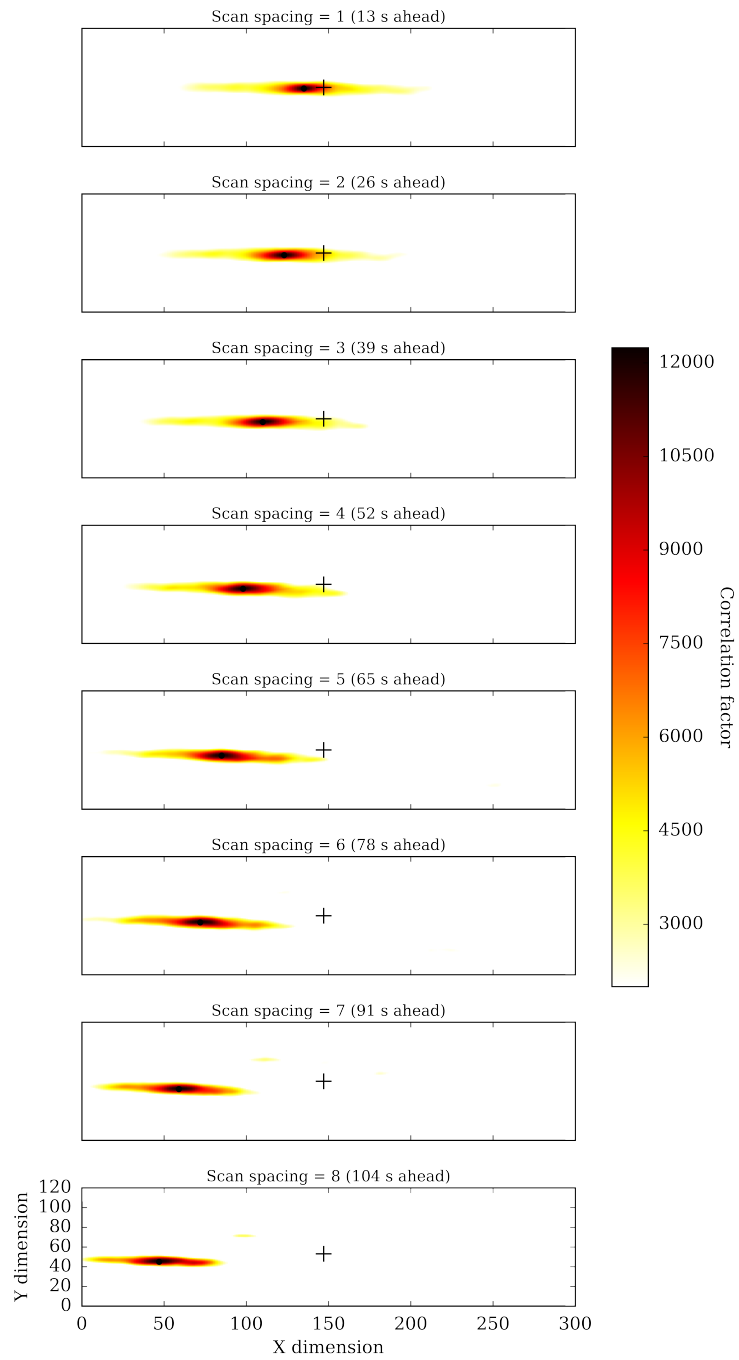


Figure 13. Example case of 2D cross-correlations between a base image and 1 to 8 scan-times (13-104 s) ahead. This period has a wind speed of 9.53 m/s and direction of 284 degrees. The center point of the images is denoted with a plus sign

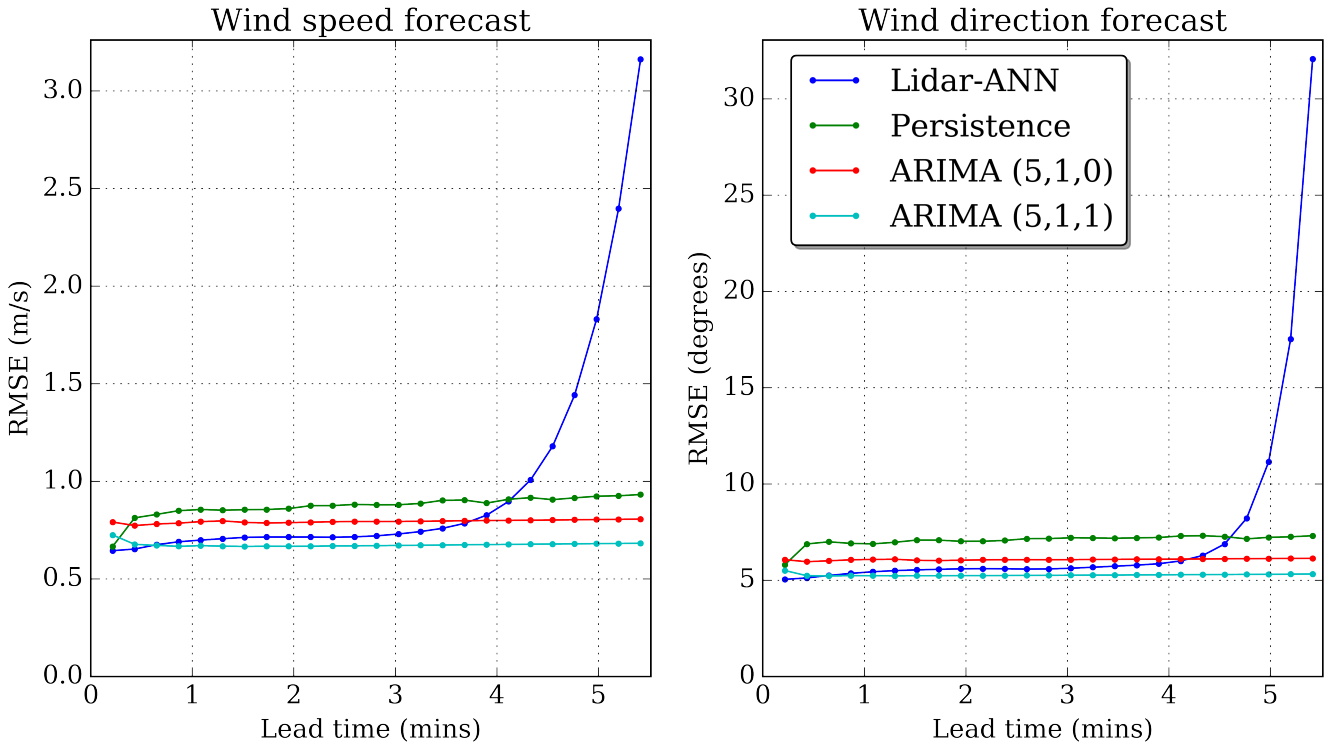


Figure 14. Forecast RMSE by lead time for all methods (left: wind speed, right: wind direction)

6 Discussion

There has been no tuning performed in the way of hyperparameter optimization, and the overall architecture of the model has been inspired from other frame prediction problems in the computer vision field. This suggests that the ANN-lidar model performance could be further improved through such changes, in combination with a sensitivity analysis. Other suitable methods which were explored early during this study but not prioritized include traditional image processing algorithms such as: the Sobel filter for separating gradients in the x and y direction, edge detection approaches including the Canny operator to define and track coherent structures, and dense optical flow methods for calculation the motion between frame pairs (Farneback (2003)).

A fact of the lidar PPI scans is that they do differ from the majority of image sources as they are not a snapshot in time, but rather acquired throughout the scanning period. As the scanner head motion sweeps through the scan area, features can be smeared or otherwise distorted. This limitation could be addressed with interpolation between neighboring scans. However, as the effect is largest with structures moving perpendicularly to the beam angle, this issue has been disregarded as the scan rate is fast (13 s) and the wind direction is generally aligned with the beam when measuring inflow.

Table 3. Results comparison of Lidar-ANN model to benchmarks by lead time. Improved skill is colored green while diminished skill is colored red

Lead time (mins)	Relative improvement of Lidar-ANN model compared with:					
	Wind speed			Wind direction		
	Persistence (%)	ARIMA (5,1,0) (%)	ARIMA (5,1,1) (%)	Persistence (%)	ARIMA (5,1,0) (%)	ARIMA (5,1,1) (%)
0.22	3.30	18.53	11.10	13.09	16.89	8.41
0.43	19.68	15.60	3.57	25.65	14.15	2.22
0.65	18.71	13.58	-0.57	25.05	12.71	-0.44
0.87	18.77	12.16	-3.47	22.56	11.66	-2.29
1.08	18.35	11.94	-4.26	21.05	10.54	-3.97
1.30	17.17	11.45	-5.70	21.13	9.70	-5.15
1.52	16.62	9.71	-6.97	21.88	8.24	-5.86
1.73	16.50	9.15	-7.07	21.41	7.54	-6.43
1.95	16.96	9.37	-7.12	20.42	7.45	-6.75
2.17	18.37	9.61	-7.05	20.28	7.53	-6.90
2.38	18.51	10.00	-6.67	20.87	7.78	-6.64
2.60	18.86	9.92	-6.90	22.09	8.04	-6.26
2.82	18.09	9.26	-7.54	22.05	7.88	-6.29
3.03	17.04	8.08	-8.73	21.97	7.35	-6.91
3.25	16.26	6.64	-10.45	21.18	6.64	-7.77
3.47	15.91	4.70	-12.75	20.27	5.85	-8.75
3.68	13.21	1.67	-16.27	19.73	5.07	-9.61
3.90	7.00	-3.43	-22.32	18.89	3.91	-10.93
4.12	1.20	-12.17	-32.62	17.80	1.61	-13.53
4.33	-9.94	-25.84	-48.69	14.10	-2.89	-18.77
4.55	-30.19	-47.14	-73.88	5.25	-12.62	-29.98
4.77	-57.58	-79.64	-112.31	-14.97	-34.33	-55.07
4.98	-98.38	-127.87	-169.25	-54.31	-82.12	-110.15

A necessary point of mention is that current commercial scanning lidar systems are expensive to purchase, require skilled technical staff to operate and maintain, and do not always provide sufficient signal across the entire measurement range. Therefore the added value must be large enough to justify its use. As shown in this and other minute-scale wind prediction studies, the “free” statistical approaches which utilize only historical data from existing instruments perform well on these time scales. However it is necessary to both have access to and store the high-frequency measurements for building and testing statistical time series models like ARIMA. This is highly suggested for operators who have an interest in improving their forecast performance.

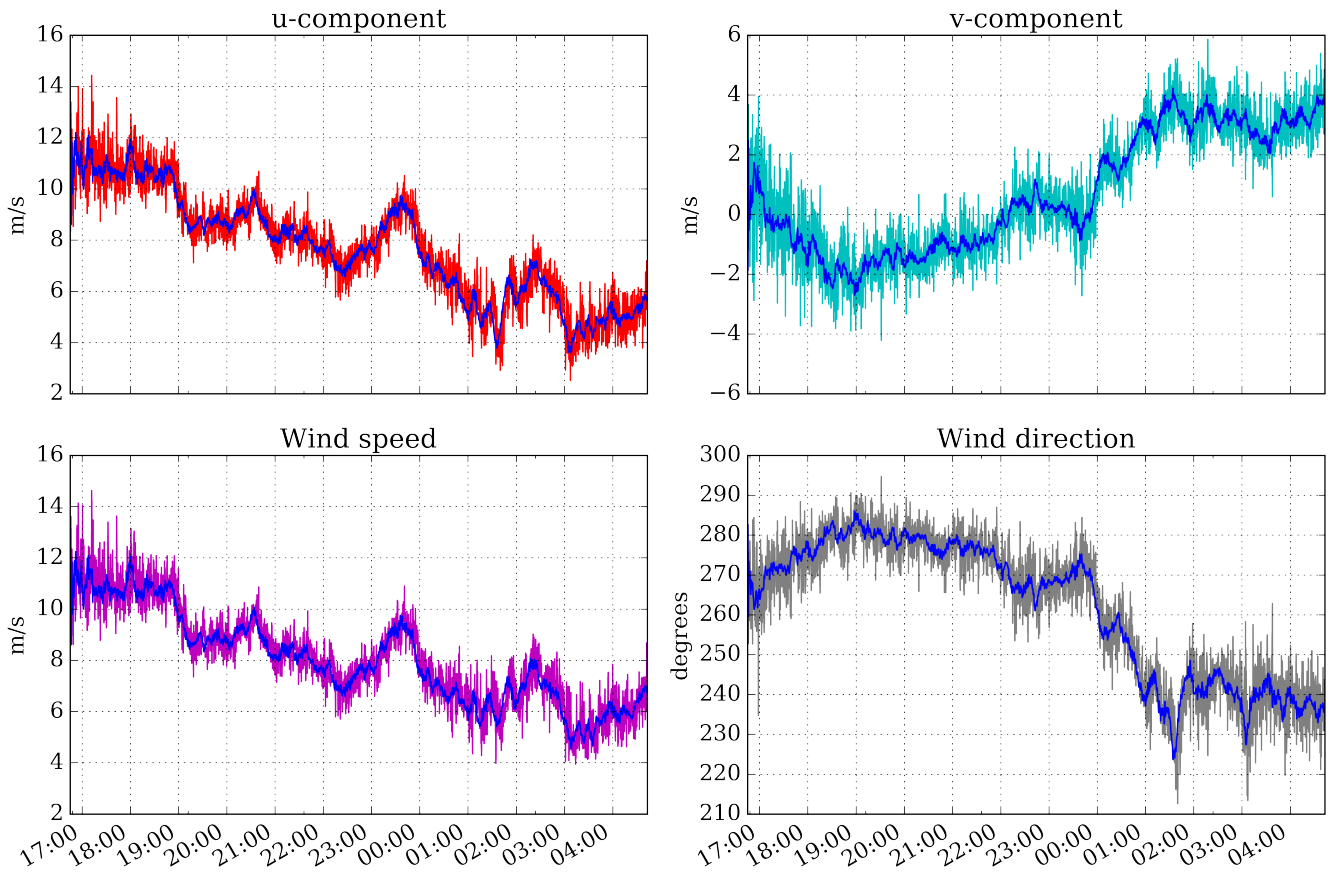


Figure 15. Time series of Lidar-ANN forecast (blue) with DBS reference signals at the 1.08-minute forecast interval. (top left: u-component, top right: v-component, bottom left: wind speed, bottom right: wind direction)

7 Conclusions

This study has demonstrated a groundwork introduction for utilizing ANN methods together with 2D upwind lidar scans for the purpose of minute-scale wind forecasting. The field experiment has successfully provided detailed measurements of the site inflow at large distances (3 km effective) upstream, together with high resolution wind profiles which constitute the downstream
5 reference.

Coherent wind structures present in the horizontal PPI scans from the rooftop scanning lidar have been shown to correlate strongly with scans taken in the range of up to 5-minutes apart. This enables the tracking of spatiotemporal features present in the scans on very-short timescales. A recently developed convolutional recurrent neural network cell (ConvLSTM) has been identified as appropriate for modelling the complex space-time relationships present in the scan image sequences. An ANN

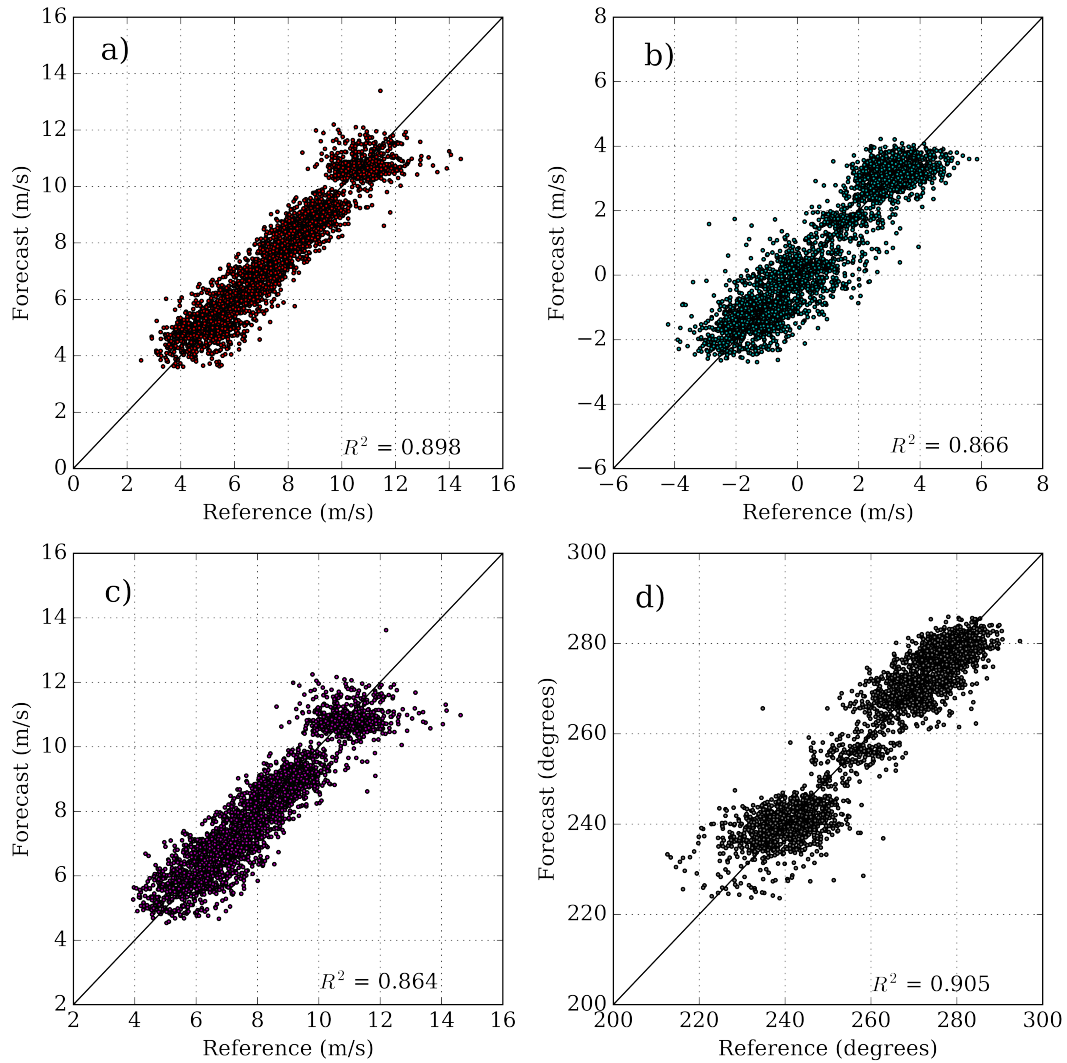


Figure 16. Scatterplot comparison between Lidar-ANN forecast and DBS references for the 1.08-minute forecast interval for: a) u-component, b) v-component, c) wind speed, d) wind direction

approach consisting of these cells and inspired by video frame prediction engines has been applied to create an online learning forecast model. The model inputs at each timestep consist of the past 5-minutes of upwind lidar scans, which are used to predict the horizontal wind vector at the downwind reference position with a forecast horizon spanning 13-seconds to 5-minutes ahead. The model has been designed to emulate real-time operation, and when utilizing hardware optimized for ANN operations (i.e. a GPU or AISC), the model is fully capable of producing forecasts which are usable for real-time decision making.

The horizontal wind vector components (u and v) have been utilized as the predictand in order to enable forecasts of both wind speed and direction. This allows for better integration into wind farm controllers and power curve models.

The ANN-lidar model has demonstrated a high degree of skill for predictions up to 4-minutes ahead. When comparing performance with other standard benchmarks, the ANN-lidar method outperforms persistence as well as the integrated AR model. However, the ARIMA benchmark has shown remarkable skill in achieving a lower RMSE than the ANN-lidar method following after the first two timesteps (i.e. from 39 s onwards). This signifies the challenge of demonstrating value with complex approaches over time series modelling which use already available historical data. Nevertheless, model refinements and tuning are recommended, in conjunction with training on a larger dataset to explore further prospects of the approach.

Data availability. The measurement data used in this study is publicly available under the CC BY 4.0 license. The dataset is available in Simon and Lea (2019)

Author contributions. E.S. conducted the research work, performed all data analysis, and composed the manuscript. E.S. designed the field experiment and conducted it together with Guillaume Lea. M.C. supervised the overall research work and made contributions to the scientific direction. All co-authors participated in discussing and revising the paper.

Competing interests. The authors declare that they have no conflicts of interest.

Acknowledgements. Guillaume Lea is recognized for his work in organizing and conducting the field campaign. Sue Ellen Haupt, David John Gagne II and the RAL group at NCAR are thanked for hosting the research stay where this study was conducted and for providing excellent mentorship. Tobias Ahsbals is thanked for his assistance with the vectorized DBS reconstruction code. Google is also acknowledged for providing free usage credits on their Cloud Compute platform.

References

- Ahsbahs, T., Badger, M., Karagali, I., and Larsén, X. G.: Validation of Sentinel-1A SAR Coastal Wind Speeds Against Scanning LiDAR, *Remote Sensing*, 9, 552, <https://doi.org/10.3390/rs9060552>, <https://www.mdpi.com/2072-4292/9/6/552>, 2017.
- Brower, M., ed.: *Wind resource assessment: a practical guide to developing a wind project*, Wiley, Hoboken, N.J, 2012.
- 5 Cariou, J.-P., Augere, B., and Valla, M.: Laser source requirements for coherent lidars based on fiber technology, *Comptes Rendus Physique*, 7, 213–223, <https://doi.org/10.1016/j.crhy.2006.03.012>, <http://www.sciencedirect.com/science/article/pii/S1631070506000818>, 2006.
- Carpenter, R. L.: Short-term Numerical Forecasts Using WindTracer Lidar Data, AMS, <https://ams.confex.com/ams/93Annual/webprogram/Paper216094.html>, 2013.
- EPEX SPOT: Intraday Lead Time, http://www.epexspot.com/en/product-info/intradaycontinuous/intraday_lead_time, 2019.
- 10 Farneböck, G.: Two-Frame Motion Estimation Based on Polynomial Expansion, in: *Image Analysis*, edited by Bigun, J., Gustavsson, T., Goos, G., Hartmanis, J., and van Leeuwen, J., vol. 2749, pp. 363–370, Springer Berlin Heidelberg, Berlin, Heidelberg, https://doi.org/10.1007/3-540-45103-X_50, http://link.springer.com/10.1007/3-540-45103-X_50, 2003.
- Giebel, G., Brownsword, R., Kariniotakis, G., Denhard, M., and Draxl, C.: The State-Of-The-Art in Short-Term Prediction of Wind Power, ANEMOS.plus, <https://doi.org/10.11581/DTU:00000017>, <https://doi.org/10.11581/DTU:00000017>, 2011.
- 15 Goodfellow, I., Bengio, Y., and Courville, A.: *Deep Learning*, MIT Press, 2016.
- Google Developers: *Machine Learning Crash Course*, <https://developers.google.com/machine-learning/crash-course/>, 2019.
- Greff, K., Srivastava, R. K., Koutník, J., Steunebrink, B. R., and Schmidhuber, J.: LSTM: A Search Space Odyssey, *IEEE Transactions on Neural Networks and Learning Systems*, 28, 2222–2232, <https://doi.org/10.1109/TNNLS.2016.2582924>, <http://arxiv.org/abs/1503.04069>, arXiv: 1503.04069, 2017.
- 20 Halo Photonics: Stream Line Doppler Lidar systems, http://www.halo-photonics.com/StreamLine-XR-Doppler_Lidar.htm, 2018.
- Hochreiter, S. and Schmidhuber, J.: Long Short-Term Memory, *Neural Computation*, 9, 1735–1780, <https://doi.org/10.1162/neco.1997.9.8.1735>, <https://www.mitpressjournals.org/doi/10.1162/neco.1997.9.8.1735>, 1997.
- Keras: Layer wrappers, <https://keras.io/layers/wrappers/>, 2018a.
- Keras: Pooling Layers, <https://keras.io/layers/pooling/>, 2018b.
- 25 Kim, Y.: Convolutional Neural Networks for Sentence Classification, arXiv:1408.5882 [cs], <http://arxiv.org/abs/1408.5882>, arXiv: 1408.5882, 2014.
- Kingma, D. P. and Ba, J.: Adam: A Method for Stochastic Optimization, arXiv:1412.6980 [cs], <http://arxiv.org/abs/1412.6980>, arXiv: 1412.6980, 2014.
- Laptev, N., Yosinski, J., Li, L. E., and Smyl, S.: Time-series extreme event forecasting with neural networks at uber, in: *International Conference on Machine Learning*, pp. 1–5, http://www.cs.columbia.edu/~lierranli/publications/TSW2017_paper.pdf, 2017.
- 30 Leica Geosystems: Leica Viva GNSS GS15 receiver Datasheet, https://w3.leica-geosystems.com/downloads123/zz/gpsgis/viva%20gnss/brochures-datasheet/leica_viva_gnss_gs15_receiver_ds_en.pdf, 2012.
- Leosphere: Scanning Windcube, <https://www.leosphere.com/products/scanning-wincube/>, 2018.
- Li, F.-F.: CS231n: Convolutional Neural Networks for Visual Recognition, <http://cs231n.stanford.edu/>, 2018.
- 35 Liang, X.: An Integrating Velocity–Azimuth Process Single-Doppler Radar Wind Retrieval Method, *Journal of Atmospheric and Oceanic Technology*, 24, 658–665, <https://doi.org/10.1175/JTECH2047.1>, <https://journals.ametsoc.org/doi/abs/10.1175/JTECH2047.1>, 2007.

- Magerman, B.: Short-Term Wind Power Forecasts using Doppler Lidar, Ph.D. Thesis, <http://adsabs.harvard.edu/abs/2014PhDT.....314M>, 2014.
- Mahoney, W. P., Parks, K., Wiener, G., Liu, Y., Myers, W. L., Sun, J., Monache, L. D., Hopson, T., Johnson, D., and Haupt, S. E.: A Wind Power Forecasting System to Optimize Grid Integration, *IEEE Transactions on Sustainable Energy*, 3, 670–682, <https://doi.org/10.1109/TSTE.2012.2201758>, 2012.
- 5 Mann, J., Menke, R., Vasiljević, N., Berg, J., and Troldborg, N.: Challenges in using scanning lidars to estimate wind resources in complex terrain, *Journal of Physics: Conference Series*, 1037, 072017, <https://doi.org/10.1088/1742-6596/1037/7/072017>, <http://stacks.iop.org/1742-6596/1037/i=7/a=072017>, 2018.
- Mislan, D. B. and Streich, P.: To the Sea! Sealand and Other Wannabe States, in: *Weird IR: Deviant Cases in International Relations*, edited by Mislan, D. B. and Streich, P., pp. 15–28, Springer International Publishing, Cham, https://doi.org/10.1007/978-3-319-75556-4_2, https://doi.org/10.1007/978-3-319-75556-4_2, 2019.
- Mitsubishi Electric: Ground based Long-range Doppler Lidar, <http://www.mitsubishielectric.com/bu/lidar/products/coherent/index.html>, 2018.
- Moehrlen, C.: Uncertainty in wind energy forecasting, <https://cora.ucc.ie/handle/10468/193>, 2004.
- 15 Ogunmolu, O., Gu, X., Jiang, S., and Gans, N.: Nonlinear Systems Identification Using Deep Dynamic Neural Networks, arXiv:1610.01439 [cs], <http://arxiv.org/abs/1610.01439>, arXiv: 1610.01439, 2016.
- Schlipf, D., Schlipf, D. J., and Kühn, M.: Nonlinear model predictive control of wind turbines using LIDAR, *Wind Energy*, 16, 1107–1129, <https://doi.org/10.1002/we.1533>, <https://onlinelibrary.wiley.com/doi/abs/10.1002/we.1533>, 2012.
- Scikit-learn: `sklearn.preprocessing.MinMaxScaler`, <https://scikit-learn.org/stable/modules/generated/sklearn.preprocessing.MinMaxScaler.html>, 2018.
- 20 Shi, X., Chen, Z., Wang, H., Yeung, D.-Y., Wong, W.-k., and Woo, W.-c.: Convolutional LSTM Network: A Machine Learning Approach for Precipitation Nowcasting, arXiv:1506.04214 [cs], <http://arxiv.org/abs/1506.04214>, arXiv: 1506.04214, 2015.
- Simon, E. and Lea, G.: LASCAR Experiment Dataset, <https://doi.org/10.11583/DTU.7321070>, 2019.
- Simon, E., Courtney, M., and Vasiljevic, N.: Minute-Scale Wind Speed Forecasting Using Scanning Lidar Inflow Measurements, *Wind Energy Science Discussions*, 2018, 1–30, <https://doi.org/10.5194/wes-2018-71>, <https://www.wind-energ-sci-discuss.net/wes-2018-71/>, 2018.
- 25 Strauch, R. G., Weber, B. L., Frisch, A. S., Little, C. G., Merritt, D. A., Moran, K. P., and Welsh, D. C.: The Precision and Relative Accuracy of Profiler Wind Measurements, *Journal of Atmospheric and Oceanic Technology*, 4, 563–571, [https://doi.org/10.1175/1520-0426\(1987\)004<0563:TPARAO>2.0.CO;2](https://doi.org/10.1175/1520-0426(1987)004<0563:TPARAO>2.0.CO;2), <https://journals.ametsoc.org/doi/10.1175/1520-0426%281987%29004%3C0563%3ATPARAO%3E2.0.CO%3B2>, 1987.
- 30 Taigman, Y., Yang, M., Ranzato, M., and Wolf, L.: DeepFace: Closing the Gap to Human-Level Performance in Face Verification, pp. 1701–1708, https://www.cv-foundation.org/openaccess/content_cvpr_2014/html/Taigman_DeepFace_Closing_the_2014_CVPR_paper.html, 2014.
- Tensorflow: `tf.keras.layers.ConvLSTM2D`, https://www.tensorflow.org/api_docs/python/tf/keras/layers/ConvLSTM2D, 2018.
- 35 Valldecabres, L., Peña, A., Courtney, M., Bremen, L. v., and Kühn, M.: Very short-term forecast of near-coastal flow using scanning lidars, *Wind Energy Science Discussions*, pp. 1–22, <https://doi.org/https://doi.org/10.5194/wes-2017-48>, <https://www.wind-energ-sci-discuss.net/wes-2017-48/>, 2017.

- Valldecabres, L., Nygaard, N., Vera-Tudela, L., von Bremen, L., Kühn, M., Valldecabres, L., Nygaard, N. G., Vera-Tudela, L., von Bremen, L., and Kühn, M.: On the Use of Dual-Doppler Radar Measurements for Very Short-Term Wind Power Forecasts, *Remote Sensing*, 10, 1701, <https://doi.org/10.3390/rs10111701>, <https://www.mdpi.com/2072-4292/10/11/1701>, 2018.
- Vasiljevic, N., Lea, G., Courtney, M., Cariou, J.-P., Mann, J., and Mikkelsen, T.: Long-Range WindScanner System, *Remote Sensing*, 8, 896, <https://doi.org/10.3390/rs8110896>, <https://www.mdpi.com/2072-4292/8/11/896>, 2016.
- 5 Veiga Rodrigues, C., Palma, J., Vasiljevic, N., Courtney, M., and Mann, J.: Coupled simulations and comparison with multi-lidar measurements of the wind flow over a double-ridge, *Journal of Physics: Conference Series (Online)*, 753, <https://doi.org/10.1088/1742-6596/753/3/032025>, 2016.
- Vollmer, L., Dooren, M. v., Trabucchi, D., Schneemann, J., Steinfeld, G., Witha, B., Trujillo, J., and Kühn, M.: First comparison of LES of an offshore wind turbine wake with dual-Doppler lidar measurements in a German offshore wind farm, *Journal of Physics: Conference Series*, 625, 012 001, <https://doi.org/10.1088/1742-6596/625/1/012001>, <http://stacks.iop.org/1742-6596/625/i=1/a=012001>, 2015.
- 10 Wagner, R., Pedersen, T. F., Courtney, M., Antoniou, I., Davoust, S., and Rivera, R. L.: Power curve measurement with a nacelle mounted lidar, *Wind Energy*, 17, 1441–1453, <https://doi.org/10.1002/we.1643>, <https://onlinelibrary.wiley.com/doi/abs/10.1002/we.1643>, 2014.

3.10 Addendum: Key results and lessons learned

- A field campaign was conducted which produced rapid high resolution inflow PPI scans and reference DBS measurements at the Risø test site.
- 2-Dimensional cross-correlations between pairs of scan images show the advection of coherent spatial features up to 3 km downwind and up to 5-minutes ahead.
- An appropriate machine learning algorithm (ConvLSTM) was identified which is able to learn spatiotemporal patterns from sequences of images.
- The ConvLSTM units were used to build an artificial neural network (ANN) which uses upwind lidar PPI scans to predict wind vectors at the position of the profiling lidar with a multi-step output up to 5-minutes ahead.
- Horizontal wind vector components (u and v) were predicted to enable both wind speed and direction forecasts.
- The ANN-lidar approach outperformed two of the three benchmarks up to 4-minutes ahead (persistence and integrated AR model).
- The ANN-lidar model scored the lowest RMSE against all benchmarks during the first two forecast periods (13 s and 26 s ahead).
- At the 1-minute ahead timestep, the ANN-lidar model outperformed persistence with 18% and 21% lower RMSE, and the integrated AR model by 12% and 11% for wind speed and wind direction respectively.
- ARIMA time series modelling has demonstrated superior skill from the third forecast period onwards leading to a diminished indication of the ANN-lidar method's worthiness.
- The ANN-lidar model is computationally capable of running in real time for advisory or automated decision input to other processes.
- This approach should be further refined (e.g. through model tuning and datasets with dissimilar conditions) to determine if the increased complexity and cost provides added value for industrial use.

CHAPTER 4

Discussion and outlook

4.1 What remote sensing can be used for in the context of minute-scale wind forecasting

Two approaches to remote sensing based forecasting have been demonstrated in this thesis work which indicate the usefulness of such a system.

The first is predicting the wind speed and direction minutes-ahead using upwind radial speed measurements together with a propagation model. The second is using the upwind observations to detect and track coherent structures advecting towards the site. These can include events such as weather fronts and wind ramps.

Various applications of operational forecasts on these timescales (i.e 0-60 minutes) have been identified, including the following:

- Wind farm control including induction control and wake steering/deflection.
- Trading in electricity markets with lead times below one-hour. Present day examples include Australia, and the EPEX Spot markets for national trades within Germany, France, Austria, Switzerland, Belgium and the Netherlands.
- Power grid balancing for voltage and frequency control by TSOs. This includes reserve capacity and regulating actions through ancillary service markets which are presently operating in the Spanish and German grids using wind power plants.
- Asset management by wind power owners and operators, including portfolio optimization and storage (e.g. battery) control.

Site measurements from remote sensing devices offer high-resolution information about local conditions which dominate the minute-scale wind variability. As the wind is fundamentally chaotic, it is arguable that numerical weather prediction (NWP) models on their own will continue to struggle considerably in the lasting future to correctly resolve these microscale turbulence features. Boundary conditions used for initializing NWP models may originate from remote sensing devices like Doppler lidar or radar (i.e. data assimilation), but present computational resources do not enable results to be available fast enough for real time operation on the minute scale.

In contrast, all forecast methods demonstrated in this body of work are capable of real time use. However it remains to be answered if any skill increase towards reducing forecast errors can be capitalized upon by the wind power industry. The lidar instrumentation used in the field experiments must be purchased, installed and maintained by skilled technical staff to provide accurate and reliable measurement data. These additional capital and operational expenses may not translate into a net benefit when compared with 'free' methods which use only existing data sources. That being said, as remote sensing device manufacturers mature and compete to improve product cost, and large wind farms approach and exceed the gigawatt scale of installed capacity, the business

case for installing and operating such a system may become feasible as even very small gains can result in significant economic impacts.

Within the minute-scale, all proposed methods must be benchmarked against statistical time series modelling approaches such as ARIMA which in surprisingly many cases outperforms the more complex lidar based methods examined here. The question as to whether or not ARIMA approaches can be consistently beaten using lidar propagation models also remains unanswered. The greatest opportunities for constructive impacts seem to lie in using the lidar system for detecting and tracking anomalies, either through a pure data driven approach or in a hybrid manner with existing NWP models. Although partly investigated, this was not the main theme addressed in the PhD project.

4.2 Recommended practical implementations

In this section, a number of practical suggestions are made towards an operational realization of a lidar based forecasting system.

Current commercially available pulsed scanning lidar systems are suitable tools, but are designed with excessive capabilities relative to the design requirements of propagation based and extreme event detection forecasting methods. Significant application specific simplifications can be made which would increase the robustness and reliability of the instruments as well as decrease their cost and maintenance demands. Fixed beam formulations similar to existing nacelle lidar models could be adapted for this purpose by increasing the power of the laser source and fibre amplifiers to achieve measurement ranges equal to the high-power scanning variants.

The significant added cost, complexity, and reliance on concurrent data availability using multiple systems in dual or triple Doppler configurations leads to the recommendation for deploying single units to scan at each region of interest upstream, and for obtaining wind field information either using the radial speed measurements directly, or through SDVR post-processing techniques to obtain the reconstructed horizontal wind vector components.

The field experiments have utilized two versions of publicly available scanning lidar hardware- the Leosphere Windcube 200S and 400S. The 400S has an expanded measurement range compared to the 200S system, and is preferred for this application in order to provide increased data availability at further distances. Ultimately, the scanning geometry of the WAFFLE experiment where the 400S was used led to a lack of success in capitalizing on the increased range. This was due to the ground based deployment where the instrument was not scanning horizontally. The experiments have also taught us that for feature tracking, it is preferable to trade detail (spatial resolution) for a higher scan rate (temporal resolution). The coherent structures naturally morph and transform as they advect. Increasing the scan rate allows for improved tracking, in addition to reducing distortion of the features due to the fact that the scans are not an instantaneous snapshot in time.

Although all field experiments performed during the project took place onshore, they have all attempted to emulate offshore conditions as much as possible (i.e. by reducing the effects of surface roughness and taking place in coastal environments). This is the recommended direction for any real world realization of such a system. The increased turbulence from terrain and surface effects, together with the possibility to deploy cheaper and simpler ground based instruments (e.g. masts and profiling lidars) around the site makes the idea better suited for the constraints of offshore locations.

A proposed framework for operating at a wind farm would be to install a simplified turbine mounted device within the first and/or last row (see Fig. 4.1), or several devices

placed at the corners of the turbine array to provide spatial coverage for all wind directions. Mounting the device at close to hub height (either atop the nacelle or fixed to the tower) will ensure that the horizontal wind measurements are not affected by wind shear or vertical wind motion (a lesson learned during the WAFFLE campaign). Similarly to traditional nacelle lidars, beam blockage by the turbine blades and tilting from trust loading of the rotor and structure are necessary considerations. An alternative setup would be to deploy a traditional ground based or tower mounted scanning lidar (onshore) or atop a substation platform in offshore environments. In this configuration, the scanning lidar would perform either continuous 360° PPI scans, or would perform an initial calibrating sector scan to determine the general wind direction, and then launch repeating scans centered in that direction.

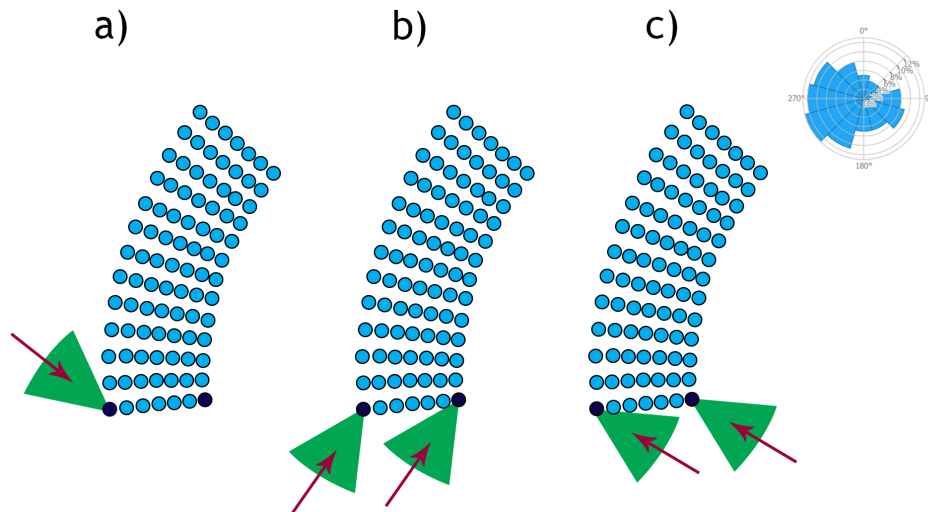


Figure 4.1: An example of a conceived operational system at the Horns Rev 2 offshore wind farm. The wind rose is shown in the top right corner, with data obtained using the Global Wind Atlas. Two lidar systems are mounted on the dark blue turbines and measure within a given angular width of the presiding wind direction (indicated with red arrows). This allows for coverage of the predominant climatology at the site: NW to SW winds (a-b), and S to E winds (c).

When processing measurement data, it is recommended to utilize advanced filtering techniques such as the dynamic method (Beck and Kühn, 2017) instead of a strict threshold filter to increase the effective measurement range. In cases where the lidar device does not provide sufficient data quality, a fall back approach should be included which instead relies on the persistence method within the first 30-seconds, and ARIMA time series modelling after that horizon. The level of sophistication required for processing lidar PPI measurements is lower for wind speed than direction. In the case of wind speed, the simple maximum-absolute-magnitude retrieval method is sufficient. However the high sensitivity and low resolution of this method for wind direction retrieval makes it

ill advised. In cases of needing accurate wind direction information, it is preferable to apply fitting algorithms such as IVAP.

In regards to forecast model formulation, two separate approaches are reviewed. The first being event detection, either for extreme events or for anticipated situations predicted by NWP models (i.e. a hybrid approach). This method utilizes real time measurements together with a static set of rules (i.e. model) to determine if an event is detected within close proximity to the site. Examples include monitoring the upstream wind speed or direction gradient to detect approaching weather regimes changes, or other highly localized meteorological phenomena. This is formulated as a classification problem and as such does not require any past information being time-independent by design. This method can however be optionally combined with a spatiotemporal advection model to predict the arrival timing of the event.

The second approach is based either on a simple time of flight shifting of upwind measurements, or on regression models which employ real time spatiotemporal correlations to predict wind vectors minutes-ahead. Due to the high temporal autocorrelation of the wind signals and the short stability of atmospheric conditions, model weights in the latter approach should be tuned as close to real time as possible. This can be done be incrementally re-fitting the existing model with new observations as they become available, or by training a new model on a rolling window of past observations or on the entire dataset at each timestep. It is also recommended to generate forecasts in a multi-output fashion (i.e. a vector forecast spanning a range of lead times) to ensure that all space time correlations can be extrapolated into the forecast.

4.3 Opportunities for extension of work

The limited duration of this project has imposed limits on the scope of the research and field work carried out. For future work on the subject, a number of possible continuations are suggested together with the open-ended questions presented earlier in this discussion section.

All forecasts in this body of work have been deterministic (single point predictions). Probabilistic forecasts are emerging as the new standard as they also contribute information about the range and distribution of uncertainties around the predicted values. This is useful for modelling sensitivities and in decision making, e.g. applying optimal bidding strategies to minimize risk when participating in the auction markets (P. Pinson, Chevallier, and Kariniotakis, 2007). Outputs from multiple deterministic models can be transformed into prediction intervals by methods including quantile regression averaging (Nowotarski and Weron, 2015), support vector quantile regression (He, 2017), or approaches based on logistic regression.

As discussed in Section 4.2, a suggestion for future field measurements is to define an adaptive scan trajectory which tracks the general wind direction, instead of repeating a fixed pattern which may not be focused upwind of the site. Other continuations of the measurement efforts include trials with large-scale Doppler lidars such as the Lockheed Martin WindTracer or Mitsubishi Diabrezza A which can measure at distances up to 30 km for increased look-ahead time. It is also suggested to explore beyond flat cross sections of the horizontal wind, by including e.g. vertical cross sections from RHI scans, or even 3-D volumetric trajectories to account for wind shear and the vertical structure of atmospheric motion.

State of the art wind farm models (e.g. PossPOW from DTU) have been recently applied for second-scale forecasting, using SCADA signals from within the wind farm to predict power production at downstream turbine rows during periods of normal and down-regulated operation (Göçmen et al., 2019). This system is envisioned to eventually interface with an operational wind farm controller and also enable grid support in the form of reserve power provisions. A coupling between one of the approaches outlined in this thesis which predicts for the first row, together with a wind farm model for the remaining turbines presents a natural combination which should be explored in future work.

CHAPTER 5

Conclusions

This PhD project has presented a framework for applications of minute-scale wind forecasts, and outlined various methods used to generate them in real time.

A collaborative workshop on the topic was convened through the IEA platform which brought together users and providers of wind power forecasts to exchange ideas and knowledge. The main outcomes have been reported in an open access journal article, which presents a broad overview of the field.

Applications of minute-scale wind forecasts mainly focus on three key areas: wind farm control, grid regulation and balancing, and trading in intrahour electricity markets.

In contrast to traditional closed-loop feedback control systems which adapt to immediate conditions at the turbine or wind farm, advanced control strategies using inputs from forecasts on the second and minute scale allow for preemptive optimization in anticipation of impending conditions. This acts to increase total production and decrease fatigue loads, leading to an expected extension of the turbine's lifetime and increased revenues for the owner. Short range nacelle lidars have become the standard for providing second-scale previews for individual wind turbine control, but lack the spatial coverage and measurement range needed for use in farm level control on the minute scale. Long range variants including high energy pulsed lidar or Doppler radar are however capable of measurement distances up to 5-30 km (design dependent) and are thus seen as suitable instruments for providing inputs to forecast models used for medium to long range control (i.e. in the range of 10-seconds to 10-minutes). The primary stakeholders for these applications are wind turbine manufacturers and plant operators.

The second major application lies within grid integration of wind power and is mainly applicable to national and regional transmission system operators (TSOs), balancing authorities (BA), and industrial participants in regulating roles (i.e. those supplying balancing capacity). The requirement of continuous physical balance between supply and demand in the electrical grid is strained by increased variability and production uncertainty introduced by the wind power generators. Imbalances between scheduled and realized production need to be accounted for by balancing controls which can occur either on the demand side (e.g. demand response or load shedding) or on the supply side (e.g. hydro or gas turbine governing, storage actions, wind power curtailment). Primary controls are normally automated actions on the seconds-scale and thus are not relevant in this context. However, secondary and tertiary balancing include both automated and manual actions with response times on the minute-scale. Improved wind power forecasts on the minute-scale can therefore reduce balancing costs and possibly enable wind power producers to participate in balancing roles in the future.

The third key application relates to the trading of power in wholesale electricity markets. Market operators such as NordPool and EPEX offer spot trading of electric power on day-ahead and intraday timescales with dispatch and pricing determined through an auction style bidding format. Participants in these markets are balance responsible for

their deviations between offered (accepted) supply and actual deliveries. For conventional power plants with controllable fuel resources, these imbalances are usually insignificant. However the variable non-controllable nature of the atmosphere combined with errors in the longer-term wind power forecasts can lead to large financial losses in cases where the direction of the imbalance is unfavourable to the grid. The forecasts for unsubsidized wind power players in day-ahead markets are normally generated by numerical weather prediction (NWP) models, with corrections being made through the intraday markets to reflect updated predictions about real production. The lead time to gate closure for these short term markets is arbitrarily chosen by the market operator. Traditionally power has been traded in 1-hour blocks, but is beginning to be reformulated into blocks of 5, 10, 15, or 30 minutes with gate closures also on the minute-scale as this reduces balancing costs and thus pricing to consumers. The utility of remote sensing based forecast models is therefore also applicable in this field, with the main stakeholders being plant operators, energy traders and energy asset managers.

The fundamental variability of the wind on very-short time scales justifies the need for real-time measurement inputs to minute-scale forecasting models. Physical-computational approaches are limited by their knowledge of boundary conditions and ability to deliver results with the required lead time. Alternatively, time series modelling approaches are able to exploit the strong temporal autocorrelation of the wind to demonstrate skill on the minute scale. However they are limited by their ability to only infer patterns from historical data. Therefore, a remote sensing based approach has been envisioned which can measure spatially distributed winds with a high sampling rate. The added value in this approach is that upwind measurements constitute the wind resource which is advecting towards the site. The local observations can then be used as inputs to a forecasting model.

To gather data for testing and evaluating the potential for remote sensing based forecasts, a series of field experiments were conducted using DTU's fleet of pulsed scanning Doppler lidars. The initial WAFFLE investigation (Section 3.2), which used a ground-based unit in plan position indicator (PPI) configuration to measure winds with a low elevation angle, saw a breakdown in correlations at distance of the horizontal winds due to the effect of wind shear and the natural vertical decorrelation of winds. This was rectified in the following Østerild Balconies field campaign (Section 3.4) by mounting the lidar alongside a meteorological mast at the desired height and scanning along a flat horizontal plane. The 1-D wind retrieval correlation results from the Balconies experiment demonstrated a sharp correlation peak with a spatiotemporal relationship extended out to 3 km upwind before significantly broadening. In the final LASCAR field trial (Section 3.8), a similar setup was used where the lidar was deployed on the roof of a building and performed flat, rapid PPI scans focusing up to 3 km upwind. 2-D correlations of this dataset were inspected, which show the ability to track coherent spatial features of the upstream wind field as they advect downstream in time, over a timescale of up to 5-minutes.

Two classes of remote sensing based forecasts have been identified. The first being classification based approaches which can be used to detect extreme events and warn of incidents expected to occur but at an unknown time. An example of such an event is the weather front passage with 180° direction change captured during the Balconies experiment at Østerild (Section 3.6). The boundary was first detected 2-hours before arrival to the site, and its propagation was tracked over the same period. Furthermore, the event was not contained in the NWP (WRF) forecasts yet would have a substantial impact on both the energy production and loads of the turbines. This type of forward information is invaluable as statistical models based on historical data have no skill in correctly predicting these types of events.

The second category represents regression based approaches which give a deterministic or probabilistic forecast output minutes-ahead. This has been the main area of focus in this body of work. The first technique, applied on the WAFFLE dataset, is a basic approach which shifts the IVAP reconstructed upstream wind speed signal by the time-of-flight distance to the downstream reference position. This method (at the 1-minute horizon) has achieved a 20% and 30% reduction in RMSE over persistence for wind speed and wind power respectively.

The following study, applied on the Østerild Balconies dataset, uses a wind direction aligned retrieval method to obtain upwind wind speeds which are fit to a linear model using stochastic gradient descent regression (SGDR). The model is incrementally fit following each newly available measurement, and a range of 1 to 60-minute ahead wind speeds are predicted. This method has achieved similar improvements over (10-minute average) persistence on the 1-minute scale (21%), 10.9% at the 5-minute scale, 9.2% at 10-minutes, 7.1% at 30-minutes, and 6.2% at 60-minutes.

The final and most complex technique was applied on the LASCAR dataset. The 2-D radial speeds were input into a convolutional-recurrent neural network (ConvLSTM) which exploits spatiotemporal patterns from sequences of lidar scan images to forecast wind vectors in a multi-output fashion up to 5-minutes ahead. The wind vector approach was used in order to extend the forecasts to include wind direction. This had not been incorporated into the previous studies because its importance for wind farm control had not yet been established. At the 1-minute ahead timestep, performance is similar to the first two lidar based techniques: 18% and 21% RMSE improvement over persistence for wind speed and wind direction respectively. However, the ARIMA time series model benchmark demonstrates statistically higher skill for time horizons greater than 30-seconds, leading to questions of the added value and justification of the resource requirements needed to deploy and operate the instrument for routine forecasting purposes (i.e. not extreme events).

Overall, remote sensing instruments including long-range pulsed Doppler lidars present a promising resource for inputs to generating minute-scale wind power forecasts. They provide spatial and temporal information with a high level of detail about impending

conditions and can detect changes in the wind resource before arrival to the site. This can take the shape of either an anomaly classification system for extreme events, or as a routine (continuous) forecasting tool which can be used in advanced control and trading algorithms. The former provides clearer added benefits, as there are no existing methods to attain this information on the minute scale with high accuracy (particularly the timing of such events). The latter has been applied to produce wind speed and wind vector (speed and direction) forecasts, with the vector approach preferable due to its usefulness in wind farm control and in the transformation of wind resources to wind farm power output. Derived products such as the wind direction variance (meandering) and wind speed variance (a measure of turbulence) are also available using this method, which are relevant for use in wind farm models. The worthiness of the continuous approach is highly dependent on a range of factors including; local meteorological and topographical conditions at the site (e.g. site specific weather patterns, on/off-shore deployment), the scale of the wind farm (e.g. spatial, layout, installed capacity), economic constraints (e.g. market mechanisms, balancing penalties, cost of instrumentation and maintenance), and technical characteristics (e.g. model formulation, data quality control, integration with other processes).

Ultimately, as the next generation of wind power forecasting methods are developed, the improved accuracy and widespread use of minute-scale practices will lead to the more efficient utilization of wind power and thereby a reduction in the levelized cost of electricity.

APPENDIX A

Coauthor statements

This appendix contains signed statements documenting the PhD student's contributions in the included manuscripts which are coauthored.

Declaration of co-authorship at DTU

If a PhD thesis contains articles (i.e. published journal and conference articles, unpublished manuscripts, chapters, etc.) written in collaboration with other researchers, a co-author statement verifying the PhD student's contribution to each article should be made.

If an article is written in collaboration with three or less researchers (including the PhD student), all researchers must sign the statement. However, if an article has more than three authors the statement may be signed by a representative sample, cf. article 12, section 4 and 5 of the Ministerial Order No. 1039, 27 August 2013. A representative sample consists of minimum three authors, which is comprised of the first author, the corresponding author, the senior author, and 1-2 authors (preferably international/non-supervisor authors).

DTU has implemented the Danish Code of Conduct for Research Integrity, which states the following regarding attribution of authorship:

"Attribution of authorship should in general be based on criteria a-d adopted from the Vancouver guidelines¹, and all individuals who meet these criteria should be recognized as authors:

- a. Substantial contributions to the conception or design of the work, or the acquisition, analysis, or interpretation of data for the work, *and*
- b. drafting the work or revising it critically for important intellectual content, *and*
- c. final approval of the version to be published, *and*
- d. agreement to be accountable for all aspects of the work in ensuring that questions related to the accuracy or integrity of any part of the work are appropriately investigated and resolved."²

For more information regarding definition of co-authorship and examples of authorship conflicts, we refer to DTU Code of Conduct for Research Integrity (pp. 19-22).

By signing this declaration, co-authors permit the PhD student to reuse whole or parts of co-authored articles in their PhD thesis, under the condition that co-authors are acknowledged in connection with the reused text or figure.

It is **important** to note that it is the responsibility of the PhD student to obtain permission from the publisher to use the article in the PhD thesis³





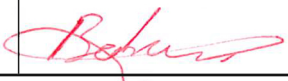
¹ International Committee of Medical Journal Editors – Recommendations for the Conduct, Reporting, Editing, and Publication of Scholarly Work in Medical Journals, updated December 2016

² DTU Code of Conduct for Research Integrity (E-book p. 19)

³ Many journals will allow you to use only the post-print version of your article, meaning the accepted version of the article, without the publisher's final formatting. In the event that your article is submitted, but still under review, you should of course use the latest submitted version of your article in your thesis. Always remember to check your publisher's guidelines on reuse of published articles. Most journals, unless open access, have an embargo period on published articles, meaning that within this period you cannot freely use the article. Check your publisher's rules on this issue.




Title of article		
Minute-Scale Forecasting of Wind Power – Results from the collaborative workshop of IEA Wind Task 32 and 36		
Journal/conference		
Energies (MDPI)		
Author(s)		
Würth, I., Valdecabres, L., Simon, E., Möhrten, C., Uzunoğlu, B., Gilbert, C., Giebel, G., Schlipf, D., and Kaifel, A.		
Name (capital letters) and signature of PhD student		
ELLIOT SIMON		
PhD student's date of birth		
March 13, 1990		
Declaration of the PhD student's contribution		
<i>For each type of work, please specify below the contribution as appropriate</i>		
	Minor contribution to the work <i>(please specify)</i>	Substantial contribution to the work <i>(please specify)</i>
Formulation of the conceptual framework and/or planning of the design of the study including scientific questions		<ul style="list-style-type: none"> • Co-organized the workshop which formed the basis of the paper • Involved in all working group meetings for planning the paper aims and scope
Carrying out of experiments/data collection and analysis/interpretation of results		<ul style="list-style-type: none"> • Hosted the workshop at Risø • Contributed own knowledge and experience to the direction of the work • Moderated workshop discussion sessions
Writing of the article/revising the manuscript for intellectual content	<ul style="list-style-type: none"> • Lesser contributions in other sections where overlap exists with own knowledge 	<ul style="list-style-type: none"> • Section writing contributions: <ul style="list-style-type: none"> ○ #2: Intrahour variability of wind generation ○ #5.1 and 5.1.1 on lidar/remote sensing approaches ○ #5.2 Statistical time series models ○ #5.5 overview/comparison of methods • Provided comprehensive reviews of all content in the paper • Article revisions during peer review stages

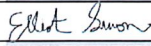
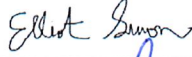

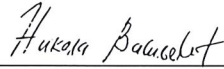
Title of article			
Minute-Scale Forecasting of Wind Power – Results from the collaborative workshop of IEA Wind Task 32 and 36			
Journal/conference			
Energies (MDPI)			
Author(s)			
Würth, I., Valdecabres, L., Simon, E., Möhrlen, C., Uzunoğlu, B., Gilbert, C., Giebel, G., Schlipf, D., and Kaifel, A.			
Name (capital letters) and signature of PhD student			
ELLIOT SIMON			
PhD student's date of birth			
March 13, 1990			
Signatures			
Date	Name	Title	Signature
Feb. 21, 2019	Elliot Simon	PhD Student	
Feb 21, 2019	Ines Würth	Research Fellow	
Feb 25, 2019	Gregor Giebel	Senior Scientist	
Feb. 26, 2019	David Schlipf	Professor	
Feb 22, 2019	Bahri Uzunoglu	Associate Professor	

Please note that by signing this declaration, co-authors permit the PhD student to reuse whole or parts of co-authored articles in their PhD thesis, under the condition that co-authors are acknowledged in connection with the reused text or figure.



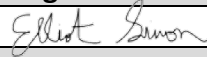
Title of article		
Minute-Scale Wind Speed Forecasting Using Scanning Lidar Inflow Measurements		
Journal/conference		
Wind Energy Science		
Author(s)		
Elliot Simon, Michael Courtney, Nikola Vasiljevic		
Name (capital letters) and signature of PhD student		
ELLIOT SIMON 		
PhD student's date of birth		
March 13, 1990		
Declaration of the PhD student's contribution		
<i>For each type of work, please specify below the contribution as appropriate</i>		
	Minor contribution to the work (please specify)	Substantial contribution to the work (please specify)
Formulation of the conceptual framework and/or planning of the design of the study including scientific questions		<ul style="list-style-type: none"> • Overall concept and design of the research work • Planning of field experiment
Carrying out of experiments/data collection and analysis/interpretation of results		<ul style="list-style-type: none"> • Preparation and repair of instruments prior to field campaign • Live monitoring, control and troubleshooting of systems during experiment • Data collection and processing • In-depth data analysis • Model formulation • Interpretation of results
Writing of the article/revising the manuscript for intellectual content		<ul style="list-style-type: none"> • Writing of manuscript • Creation of figures, plots, etc. • Revising manuscript with feedback from co-authors and reviewers



Title of article			
Minute-Scale Wind Speed Forecasting Using Scanning Lidar Inflow Measurements			
Journal/conference			
Wind Energy Science			
Author(s)			
Elliot Simon, Michael Courtney, Nikola Vasiljevic			
Name (capital letters) and signature of PhD student			
ELLIOT SIMON 			
PhD student's date of birth			
March 13, 1990			
Signatures			
Date	Name	Title	Signature
20 Dec, 2018	Elliot Simon	PhD Student	
14 Jan 2019	Michael Courtney	Senior Scientist	
21 Dec, 2018	Nikola Vasiljevic	Research Scientist	

Please note that by signing this declaration, co-authors permit the PhD student to reuse whole or parts of co-authored articles in their PhD thesis, under the condition that co-authors are acknowledged in connection with the reused text or figure.



Title of article		
Minute-Scale Wind Vector Forecasting Using Scanning Lidar Inputs to a Convolutional LSTM Neural Network		
Journal/conference		
Designated for Atmospheric Measurement Techniques (AMT)		
Author(s)		
Elliot Simon and Michael Courtney		
Name (capital letters) and signature of PhD student		
ELLIOT SIMON, ellsim 		
PhD student's date of birth		
13/03/1990		
Declaration of the PhD student's contribution		
<i>For each type of work, please specify below the contribution as appropriate</i>		
	Minor contribution to the work <i>(please specify)</i>	Substantial contribution to the work <i>(please specify)</i>
Formulation of the conceptual framework and/or planning of the design of the study including scientific questions		<ul style="list-style-type: none"> • Overall concept and formulation of the research work and objectives • Envisioning and planning the field experiment
Carrying out of experiments/data collection and analysis/interpretation of results		<ul style="list-style-type: none"> • Conducting (i.e. preparing, deploying, monitoring, decommissioning, etc.) the field experiment • Data collection and processing • Coding analysis tools • Interpreting results
Writing of the article/revising the manuscript for intellectual content		<ul style="list-style-type: none"> • Writing the manuscript • Revising the manuscript following feedback from coauthor



Title of article			
Minute-Scale Wind Vector Forecasting Using Scanning Lidar Inputs to a Convolutional LSTM Neural Network			
Journal/conference			
Designated for Atmospheric Measurement Techniques (AMT)			
Author(s)			
Elliot Simon and Michael Courtney			
Name (capital letters) and signature of PhD student			
ELLIOT SIMON, ellsim			
PhD student's date of birth			
13/03/1990			
Signatures			
Date	Name	Title	Signature
28/02/2019	Elliot Simon	PhD Student	
4/03/2019	Michael Courtney	Senior Scientist	

Please note that by signing this declaration, co-authors permit the PhD student to reuse whole or parts of co-authored articles in their PhD thesis, under the condition that co-authors are acknowledged in connection with the reused text or figure.

Bibliography for non-article texts

- AEMC (2017). *Five Minute Settlement*. en. URL: <https://www.aemc.gov.au/rule-changes/five-minute-settlement> (visited on March 11, 2019).
- Annoni, Jennifer et al. (2016). “Analysis of axial-induction-based wind plant control using an engineering and a high-order wind plant model”. en. In: *Wind Energy* 19.6, pages 1135–1150. ISSN: 1099-1824. DOI: 10.1002/we.1891. URL: <https://onlinelibrary.wiley.com/doi/abs/10.1002/we.1891> (visited on March 5, 2019).
- Bartl, J. and L. Sætran (2016). “Experimental testing of axial induction based control strategies for wake control and wind farm optimization”. en. In: *Journal of Physics: Conference Series* 753, page 032035. ISSN: 1742-6596. DOI: 10.1088/1742-6596/753/3/032035. URL: <https://doi.org/10.1088/1742-6596/753/3/032035> (visited on March 17, 2019).
- Bathurst, G. N., J. Weatherill, and G. Strbac (2002). “Trading wind generation in short term energy markets”. In: *IEEE Transactions on Power Systems* 17.3, pages 782–789. ISSN: 0885-8950. DOI: 10.1109/TPWRS.2002.800950.
- Beck, Hauke and Martin Kühn (2017). “Dynamic Data Filtering of Long-Range Doppler LiDAR Wind Speed Measurements”. en. In: *Remote Sensing* 9.6, page 561. DOI: 10.3390/rs9060561. URL: <https://www.mdpi.com/2072-4292/9/6/561> (visited on February 2, 2019).
- Bossanyi, E.A. (1985). “Short-Term Wind Prediction Using Kalman Filters”. In: *Wind Engineering* 9.1, pages 1–8. ISSN: 0309-524X. URL: <https://www.jstor.org/stable/43749025> (visited on October 2, 2018).
- Brunekreef, Bert and Stephen T Holgate (2002). “Air pollution and health”. In: *The Lancet* 360.9341, pages 1233–1242. ISSN: 0140-6736. DOI: 10.1016/S0140-6736(02)11274-8. URL: <http://www.sciencedirect.com/science/article/pii/S0140673602112748> (visited on January 12, 2019).
- Cariou, Jean-Pierre, Béatrice Augere, and Matthieu Valla (2006). “Laser source requirements for coherent lidars based on fiber technology”. In: *Comptes Rendus Physique. High power fiber lasers and amplifiers* Lasers et amplificateurs à fibre de puissance 7.2, pages 213–223. ISSN: 1631-0705. DOI: 10.1016/j.crhy.2006.03.012. URL: <http://www.sciencedirect.com/science/article/pii/S1631070506000818> (visited on August 31, 2015).
- Castronuovo, Edgardo D. et al. (2013). “An integrated approach for optimal coordination of wind power and hydro pumping storage”. In: *Wind Energy* 17.6, pages 829–852.

- ISSN: 1095-4244. DOI: 10.1002/we.1600. URL: <https://onlinelibrary.wiley.com/doi/full/10.1002/we.1600>.
- Charlson, R. J. et al. (1992). “Climate Forcing by Anthropogenic Aerosols”. en. In: *Science* 255.5043, pages 423–430. ISSN: 0036-8075, 1095-9203. DOI: 10.1126/science.255.5043.423. URL: <http://science.sciencemag.org/content/255/5043/423> (visited on January 12, 2019).
- Costa, Alexandre et al. (2008). “A review on the young history of the wind power short-term prediction”. In: *Renewable and Sustainable Energy Reviews* 12.6, pages 1725–1744. ISSN: 1364-0321. DOI: 10.1016/j.rser.2007.01.015. URL: <http://www.sciencedirect.com/science/article/pii/S1364032107000354>.
- Danmarks Klima- og Energiministeriet (2011). *Energistrategi 2050: fra kul, olie og gas til grøn energi : sammenfatning*. Danish. OCLC: 768656130. Klima- og Energiministeriet. ISBN: 978-87-92727-12-1.
- de la Fuente, Ignacio (2016). *Ancillary Services in Spain: dealing with High Penetration of RES*. URL: https://www.reshaping-res-policy.eu/downloads/topical%5C%20events/de-la-Fuente_Ancillary-Services-in-Spain1.pdf.
- Delle Monache, Luca et al. (2013). “Probabilistic Weather Prediction with an Analog Ensemble”. In: *Monthly Weather Review* 141.10, pages 3498–3516. ISSN: 0027-0644. DOI: 10.1175/MWR-D-12-00281.1. URL: <https://journals.ametsoc.org/doi/abs/10.1175/MWR-D-12-00281.1>.
- Doney, Scott C. et al. (2009). “Ocean Acidification: The Other CO₂ Problem”. In: *Annual Review of Marine Science* 1.1, pages 169–192. DOI: 10.1146/annurev.marine.010908.163834. URL: <https://doi.org/10.1146/annurev.marine.010908.163834> (visited on January 12, 2019).
- Drucker, Harris et al. (1996). “Support Vector Regression Machines”. In: *Proceedings of the 9th International Conference on Neural Information Processing Systems*. NIPS’96. Cambridge, MA, USA: MIT Press, pages 155–161. URL: <http://dl.acm.org/citation.cfm?id=2998981.2999003> (visited on January 9, 2019).
- DTU Wind Energy (2019). *The research wind turbine V52*. en. URL: <https://www.vindenergi.dtu.dk/english/research/research-facilities/the-research-wind-turbine-v52> (visited on January 3, 2019).
- Du, Yixing et al. (2016). “Air particulate matter and cardiovascular disease: the epidemiological, biomedical and clinical evidence”. In: *Journal of Thoracic Disease* 8.1, E8–E19. ISSN: 2072-1439. DOI: 10.3978/j.issn.2072-1439.2015.11.37. URL: <https://www.ncbi.nlm.nih.gov/pmc/articles/PMC4740122/> (visited on January 12, 2019).
- EPEX SPOT SE (2019). *Continuous Intraday Market*. URL: http://www.epexspot.com/en/product-info/intradaycontinuous/intraday_lead_time (visited on March 11, 2019).
- European Commission (2019). *Clean energy for all Europeans*. en. URL: </energy/en/topics/energy-strategy-and-energy-union/clean-energy-all-europeans> (visited on January 12, 2019).
- Fleming, Paul et al. (2017). “Field test of wake steering at an offshore wind farm”. English. In: *Wind Energy Science* 2.1, pages 229–239. ISSN: 2366-7443. DOI: <https://doi.org/>

- 10.5194/wes-2-229-2017. URL: <https://www.wind-energ-sci.net/2/229/2017/> (visited on March 6, 2019).
- Fleming, PA et al. (2014). “Evaluating techniques for redirecting turbine wakes using SOWFA”. English. In: *Renewable Energy* 70.October. harvest Available online 12-03-2014, pages 211–218. ISSN: 0960-1481. DOI: 10.1016/j.renene.2014.02.015.
- Floors, Rogier Ralph et al. (2016). *Report on RUNE’s coastal experiment and first inter-comparisons between measurements systems*. English. Denmark: DTU Wind Energy. ISBN: 978-87-93278-72-1.
- Gebraad, P. M. O. and J. W. van Wingerden (2015). “Maximum power-point tracking control for wind farms”. en. In: *Wind Energy* 18.3, pages 429–447. ISSN: 1099-1824. DOI: 10.1002/we.1706. URL: <https://onlinelibrary.wiley.com/doi/abs/10.1002/we.1706> (visited on March 6, 2019).
- Gebraad, Pieter et al. (2017). “Maximization of the annual energy production of wind power plants by optimization of layout and yaw-based wake control”. en. In: *Wind Energy* 20.1, pages 97–107. ISSN: 1099-1824. DOI: 10.1002/we.1993. URL: <https://onlinelibrary.wiley.com/doi/abs/10.1002/we.1993> (visited on March 5, 2019).
- Giebel, Gregor et al. (2011). “The State-Of-The-Art in Short-Term Prediction of Wind Power”. In: *ANEMOS.plus*. DOI: 10.11581/DTU:00000017. URL: <https://doi.org/10.11581/DTU:00000017>.
- Göçmen, Tuhfe (2016). “Possible Power Estimation of Down-Regulated Offshore Wind Power Plants.” 978-87-93278-53-0. PhD Thesis. DTU Wind Energy. URL: 978-87-93278-53-0.
- Göçmen, Tuhfe et al. (2019). “Possible power of down-regulated offshore wind power plants: The PossPOW algorithm”. en. In: *Wind Energy* 22.2, pages 205–218. ISSN: 1099-1824. DOI: 10.1002/we.2279. URL: <https://onlinelibrary.wiley.com/doi/abs/10.1002/we.2279> (visited on March 4, 2019).
- GWEC (2017). “Global Wind Report”. en-US. URL: <https://gwec.net/publications/global-wind-report-2/> (visited on January 12, 2019).
- Hamra, Ghassan B. et al. (2014). “Outdoor particulate matter exposure and lung cancer: a systematic review and meta-analysis”. eng. In: *Environmental Health Perspectives* 122.9, pages 906–911. ISSN: 1552-9924. DOI: 10.1289/ehp/1408092.
- Hansen, Anca D., Müfit Altin, and Florin Iov (2016). “Provision of enhanced ancillary services from wind power plants – Examples and challenges”. In: *Renewable Energy* 97, pages 8–18. ISSN: 0960-1481. DOI: 10.1016/j.renene.2016.05.063. URL: <http://www.sciencedirect.com/science/article/pii/S0960148116304736>.
- He, Yaoyao (2017). “Short-term power load probability density forecasting method using kernel-based support vector quantile regression and Copula theory”. In: *Applied Energy* 185, pages 254–266. ISSN: 03062619. DOI: 10.1016/j.apenergy.2016.10.079.
- Hirth, Brian D. et al. (2012). “Measuring a Utility-Scale Turbine Wake Using the TTUKa Mobile Research Radars”. In: *Journal of Atmospheric and Oceanic Technology* 29.6, pages 765–771. ISSN: 0739-0572. DOI: 10.1175/JTECH-D-12-00039.1. URL: <https://journals.ametsoc.org/doi/10.1175/JTECH-D-12-00039.1> (visited on March 17, 2019).

- Hodge, B. and M. Milligan (2011). “Wind power forecasting error distributions over multiple timescales”. In: *2011 IEEE Power and Energy Society General Meeting*, pages 1–8. DOI: 10.1109/PES.2011.6039388.
- Holttinen, Hannele et al. (2009). *Design and operation of power systems with large amounts of wind power: Final report, IEA WIND Task 25, Phase one 2006-2008*. English. VTT Technical Research Centre of Finland. ISBN: 978-951-38-7308-0.
- IEA Wind Task 36 (2018). *IEA Wind Forecasting - Video Archive*. URL: <https://www.youtube.com/channel/UCsP1rLoutSXP0ECZKicczXg> (visited on December 20, 2018).
- IRENA (2018). *Renewable Power Generation Costs*. en. URL: </publications/2018/Jan/Renewable-power-generation-costs-in-2017> (visited on January 12, 2019).
- Knudsen, Torben, Thomas Bak, and Mikael Svenstrup (2015). “Survey of wind farm control—power and fatigue optimization”. en. In: *Wind Energy* 18.8, pages 1333–1351. ISSN: 1099-1824. DOI: 10.1002/we.1760. URL: <https://onlinelibrary.wiley.com/doi/abs/10.1002/we.1760> (visited on March 5, 2019).
- Liang, Xudong (2007). “An Integrating Velocity–Azimuth Process Single-Doppler Radar Wind Retrieval Method”. In: *Journal of Atmospheric and Oceanic Technology* 24.4, pages 658–665. ISSN: 0739-0572. DOI: 10.1175/JTECH2047.1. URL: <https://journals.ametsoc.org/doi/abs/10.1175/JTECH2047.1>.
- Liu, Hui, Hong-qi Tian, and Yan-fei Li (2012). “Comparison of two new ARIMA-ANN and ARIMA-Kalman hybrid methods for wind speed prediction”. In: *Applied Energy* 98, pages 415–424. ISSN: 0306-2619. DOI: 10.1016/j.apenergy.2012.04.001. URL: <http://www.sciencedirect.com/science/article/pii/S0306261912002875>.
- Mackenzie, Dr Harley and Jonathon Dyson (2017). “Short-Term Forecasting of Wind Power Plant Generation for System Stability and Provision of Ancillary Services”. en. In: 1st International Conference on Large Scale Integration of Renewable Energy in India, page 6. URL: http://regridintegrationindia.org/wp-content/uploads/sites/3/2017/09/7B_3_GIZ17_053_paper_Harley_Mackenzie.pdf.
- Mahoney, W. P. et al. (2012). “A Wind Power Forecasting System to Optimize Grid Integration”. In: *IEEE Transactions on Sustainable Energy* 3.4, pages 670–682. ISSN: 1949-3029. DOI: 10.1109/TSTE.2012.2201758.
- Masdar (2019). *EDF Renewables-Masdar consortium awarded the Dumat Al Jandal (400 MW) wind project in Saudi Arabia*. en. URL: <http://masdar.ae/en/News%20and%20Events/News/2019/01/11/11/46/The%20EDF%20Renewables-Masdar%20consortium%20awarded%20the%20Dumat%20Al%20Jandal%20wind%20project%20in%20Saudi%20Arabia> (visited on February 21, 2019).
- Menke, Robert, Jakob Mann, and Nikola Vasiljevic (2018). “Perdigão-2017: multi-lidar flow mapping over the complex terrain site”. en. In: *figshare*. URL: https://data.dtu.dk/articles/Perdig_o-2017_multi-lidar_flow_mapping_over_the_complex_terrain_site/7228544 (visited on March 14, 2019).
- Niu, Tong et al. (2018). “Multi-step-ahead wind speed forecasting based on optimal feature selection and a modified bat algorithm with the cognition strategy”. In: *Renewable Energy* 118, pages 213–229. ISSN: 0960-1481. DOI: 10.1016/j.renene.

- 2017.10.075. URL: <http://www.sciencedirect.com/science/article/pii/S0960148117310364>.
- Nowotarski, Jakub and Rafał Weron (2015). “Computing electricity spot price prediction intervals using quantile regression and forecast averaging”. en. In: *Computational Statistics* 30.3, pages 791–803. ISSN: 1613-9658. DOI: 10.1007/s00180-014-0523-0. URL: <https://doi.org/10.1007/s00180-014-0523-0> (visited on February 3, 2019).
- Patel, Sonal (2018). *China Sets a New Renewable Portfolio Standard*. en-US. URL: <https://www.powermag.com/china-sets-a-new-renewable-portfolio-standard/> (visited on January 12, 2019).
- Peterson, Ernest W. and Joseph P. Hennessey (1978). “On the Use of Power Laws for Estimates of Wind Power Potential”. In: *Journal of Applied Meteorology* 17.3, pages 390–394. ISSN: 0021-8952. DOI: 10.1175/1520-0450(1978)017<0390:OTUOPL>2.0.CO;2. URL: [https://journals.ametsoc.org/doi/abs/10.1175/1520-0450\(1978\)017%3C0390:OTUOPL%3E2.0.CO%3B2](https://journals.ametsoc.org/doi/abs/10.1175/1520-0450(1978)017%3C0390:OTUOPL%3E2.0.CO%3B2) (visited on February 21, 2019).
- Pinson, P., C. Chevallier, and G. N. Kariniotakis (2007). “Trading Wind Generation From Short-Term Probabilistic Forecasts of Wind Power”. In: *IEEE Transactions on Power Systems* 22.3, pages 1148–1156. ISSN: 0885-8950. DOI: 10.1109/TPWRS.2007.901117.
- Pinson, Pierre (2012). “Very short-term probabilistic forecasting of wind power with generalized logit-Normal distributions”. In: *Journal of the Royal Statistical Society, Series C (Applied Statistics)* 61.4, pages 555–576. ISSN: 0035-9254. DOI: 10.1111/j.1467-9876.2011.01026.x.
- Potter, C. W. and M. Negnevitsky (2006). “Very short-term wind forecasting for Tasmanian power generation”. In: *IEEE Transactions on Power Systems* 21.2, pages 965–972. ISSN: 0885-8950. DOI: 10.1109/TPWRS.2006.873421.
- Regelleistung (2016). “Leitfaden zur Präqualifikation von Windenergieanlagen zur Erbringung von Minutenreserveleistung im Rahmen einer Pilotphase”. In: URL: <https://www.regelleistung.net/ext/download/pqWindkraft>.
- Schlipf, David, Dominik Johannes Schlipf, and Martin Kühn (2012). “Nonlinear model predictive control of wind turbines using LIDAR”. en. In: *Wind Energy* 16.7, pages 1107–1129. ISSN: 1099-1824. DOI: 10.1002/we.1533. URL: <https://onlinelibrary.wiley.com/doi/abs/10.1002/we.1533>.
- Scikit-learn (2018). *sklearn.svm.SVR — scikit-learn 0.20.2 documentation*. URL: <https://scikit-learn.org/stable/modules/generated/sklearn.svm.SVR.html> (visited on February 9, 2018).
- Simon, Elliot (2018). “Applied Workshop: Doppler Lidars for Wind Energy”. In: Brussels, Belgium. URL: <https://github.com/elliotsimon/2018-EAWE-lidar-workshop> (visited on September 20, 2018).
- Simon, Elliot I. et al. (2017). “Lidars Lifted: The Østerild Balconies Experiment”. English. In: AMS. URL: <https://ams.confex.com/ams/97Annual/webprogram/Paper314118.html> (visited on March 4, 2017).
- Simon, Elliot and Michael Courtney (2016). *A Comparison of sector-scan and dual Doppler wind measurements at Høvsøre Test Station – one lidar or two?* Technical Report. 978-87-93278-69-1. DTU Wind Energy. URL: <http://orbit.dtu.dk/>

- en/publications/a-comparison-of-sectorscan-and-dual-doppler-wind-measurements-at-hoevsoere-test-station--one-lidar-or-two(bfb41f11-ddac-474c-acca-6e79739faae8).html.
- Simon, Elliot and Guillaume Lea (2019a). *LASCAR Experiment Dataset*. DOI: 10.11583/DTU.7321070. URL: <http://doi.org/10.11583/DTU.7321070>.
- (2019b). *WAFFLE Experiment Dataset*. DOI: 10.11583/DTU.7321106. URL: <https://doi.org/10.11583/DTU.7321106>.
- Simon, Elliot and Nikola Vasiljevic (2018). *Østerild Balconies Experiment (Phase 2)*. DOI: 10.11583/DTU.7306802.
- Soman, S. S. et al. (2010). “A review of wind power and wind speed forecasting methods with different time horizons”. In: *North American Power Symposium 2010*, pages 1–8. DOI: 10.1109/NAPS.2010.5619586. URL: <http://ieeexplore.ieee.org/document/5619586>.
- Torres, J. L. et al. (2005). “Forecast of hourly average wind speed with ARMA models in Navarre (Spain)”. In: *Solar Energy* 79.1, pages 65–77. ISSN: 0038-092X. DOI: 10.1016/j.solener.2004.09.013. URL: <http://www.sciencedirect.com/science/article/pii/S0038092X04002877>.
- Trombe, Pierre-Julien, Pierre Pinson, and Henrik Madsen (2012). “A General Probabilistic Forecasting Framework for Offshore Wind Power Fluctuations”. en. In: *Energies* 5.3, pages 621–657. DOI: 10.3390/en5030621. URL: <https://www.mdpi.com/1996-1073/5/3/621> (visited on December 2, 2018).
- Vincent, Claire L. and Pierre-Julien Trombe (2017). “Forecasting intrahourly variability of wind generation”. In: *Renewable Energy Forecasting*. Edited by George Kariniotakis. Woodhead Publishing Series in Energy. Woodhead Publishing, pages 219–233. ISBN: 978-0-08-100504-0. DOI: 10.1016/B978-0-08-100504-0.00008-1. URL: <http://www.sciencedirect.com/science/article/pii/B9780081005040000081> (visited on October 17, 2018).
- Welch, P. (1967). “The use of fast Fourier transform for the estimation of power spectra: A method based on time averaging over short, modified periodograms”. In: *IEEE Transactions on Audio and Electroacoustics* 15.2, pages 70–73. ISSN: 0018-9278. DOI: 10.1109/TAU.1967.1161901.
- Wildmann, Norman, Nikola Vasiljevic, and Thomas Gerz (2018). “Wind turbine wake measurements with automatically adjusting scanning trajectories in a multi-Doppler lidar setup”. English. In: *Atmospheric Measurement Techniques* 11.6, pages 3801–3814. ISSN: 1867-1381. DOI: <https://doi.org/10.5194/amt-11-3801-2018>. URL: <https://www.atmos-meas-tech.net/11/3801/2018/> (visited on March 14, 2019).